MAINTAIN

Design Synthesis Exercise
AE3200

Group 18

Delft University of Technology

TU Delft

Final Report

AE3200: Design Synthesis Exercise

Group 18: MAINTAIN

July 3, 2018

B. van Beurden	4457595
B.C.D. De Bosscher	4429885
D.J.G. Cuppen	4488024
M.C. Hermans	4475038
A.M. Lammers	4395921
J. Maes	4453468
V.R. Meijer	4487338
W.J. Oosterom	4463250
S.I.R. Piera	4470370
M.S. Pouwels	4394151
Dr.ir. M. Pini	Tutor
Ir. A.E. Vieira	Coach
Ir. G. Mahapatra	Coach

TU Delft

Preface

The sparsity of geographical locations where mining natural gas and oil is possible, has led to an enormous network of gas pipelines across the world. Inspection of these pipelines is crucial for a successful and safe utilisation of the network, as well as avoiding environmental calamities. At this moment, manned inspection, by helicopter or ground vehicle, is the most widely applied inspection method. This is not only a very costly operation, but also exposes the staff to safety hazards. An alternative is the implementation of UAVs to monitor the pipelines. Current UAVs offering the required range and endurance are expensive and inefficient, and are therefore not suitable for replacing the means of inspection of these remote areas. In this project, MAINTAIN, a UAV was designed that is capable of satisfying long-range and -endurance requirements through the implementation of an innovative propulsion concept: the micro gas turbine. By using such an engine, the UAV will not only be of lower cost, but it will also be more sustainable.

The design team is composed of 10 aerospace students who are under the supervision of dr. ir. M. Pini. The team was brought together based on their mutual interest in propulsion and UAV technology. As micro gas turbines have not been implemented in the aircraft industry yet, this project is not only a long-range UAV design challenge, but also a proof of concept for the use of micro gas turbines. The project has a timeline of eleven weeks in which the preliminary design of MAINTAIN will be completed. It was started on the 23rd of April.

First and foremost, the team would like to thank tutor dr. ir. M. Pini and the coaches ir. A. Vieira and ir. G. Mahapatra for their guidance throughout the project. Furthermore, the team would like to thank ir. O. Stroosma and dr. ir. W. Visser who made themselves available to offer advice on their expertise. Additionally, the team would like to express their gratitude to the authors of the open-source software used within this project: SU2 by Stanford University and others, OpenVSP by NASA, AVL by professor Drela from MIT and OpenAeroStruct by J. Jasa from the University of Michigan. Lastly, the group wants to thank the Design Synthesis Exercise committee for the entire organisation of this project and the facilities offered.

Design Synthesis Exercise Group 18

Delft, July 2018

Executive Overview

The total length of all gas pipelines established worldwide is 3,030,691 kilometres, of which almost two million kilometres are situated in the United States. Only a selection of geographical locations feature large enough preserves of natural gas to make mining profitable. For this reason, a large network of pipelines is distributed over the world to make gas ubiquitously available. Underground pipelines are favourable due to the smaller temperature variations in the ground layer, leading to reduced expansion and contraction of the pipeline. However, in the presence of mountains or rivers, gas pipelines will usually be laid on the ground.

Adequate monitoring and inspection is an important aspect for gas pipelines due to the possibility of environmental contamination and economic losses. Currently, manned aircraft as well as ground vehicles carry out inspections on a daily basis, resulting in high operational costs. The primary cost driver is the amount of man-hours needed to inspect the entire network of pipelines. In addition, a large part of the network is located in remote areas due to which the travel time for most inspection workers is a significant waste of resources. For these reasons, the deployment of an Unmanned Aerial Vehicle (UAV) capable of monitoring gas pipelines will drastically reduce inspection costs and risk.

The need for such an Unmanned Aircraft System (UAS) for monitoring above-ground pipelines has sparked an initiative at Delft University of Technology for the design proposal of a micro gas turbine powered drone. As part of the Design Synthesis Exercise, ten Aerospace Engineering Bachelor students are dedicating eleven weeks to this initiative in the form of designing MAINTAIN: which is short for Un**m**anned **Ai**rcraft for Mo**ni**toring G**a**s Pipel**in**es. Besides being an alternative to current solutions for the inspection of gas pipelines, the design team aims to proof the concept of a micro gas turbine implemented on a UAV. This engine would replace the currently used reciprocating engines that, if properly designed, leads to higher fuel efficiency and lower engine vibrations. This implementation can address a niche in the global UAV market; the market of long-range, long-endurance UAVs.

Initially, 26 different concepts were established. After performing a trade-off, the five best concepts were analysed in greater detail. Subsequently, a second trade-off was performed with these five remaining configurations to select the final concept. This final concept was the flying wing, chosen for its high aerodynamic efficiency which is essential for a low altitude, long endurance UAV. Other concepts were the conventional wing-and-tail configuration and a VTOL UAV. Although several modern UAVs contain a tail, it was deemed to be a waste of wetted surface area; a proper design of the flying wing would lead to good stability characteristics by using the right amount of sweep. Conventional take-off and landing was also preferred over vertical take-off and landing due to the sufficient availability of runways in the vicinity of the pipeline network.

An exploratory study on both the UAV propulsion and payload technology was conducted in order to aid deciding upon the concept. A technological analysis of currently used UAVs has led to the conclusion that MAINTAIN would fill a gap in the market: the commercial need for low altitude long endurance drones. Regarding the propulsion system, it was found that currently, mostly electric and reciprocating engines are integrated in UAVs. The electrically powered UAVs are mostly for short range and endurance missions, since the energy density and specific energy of batteries are low compared to fuels. The advantage of a gas turbine, when compared to the reciprocating engine, is that it is an open-cycle, which means that it features less vibrations and increased performance at higher speeds. A gas turbine used within a turboprop is more suitable for lower speeds as it can capture more airflow for a given engine weight than the turbojet and turbofan. However, it was found that the transition to gas turbine engines for typical UAV power requirements was less ideal than expected. Simply downscaling an existing larger engine has its downsides. For example, the Reynolds number would significantly decrease and would deteriorate performance. Additionally, problems of heat transfer and tip clearances arise.

In order to properly monitor the pipeline network, the payload should be able to indicate corrosion threats and measure gas leakages. In the exploratory study of the payload, it was found that there are currently two techniques that are suitable: usage of a thermal camera or a **Li**ght **D**etection **A**nd **R**anging (LiDAR) system. Both use the infrared (IR) light spectrum. The thermal camera captures emitted IR radiation and can detect temperature differences. The LiDAR system integrates IR spectroscopy to determine the composure of the fluids from which it can detect methane. A LiDAR system can be used to measure corrosion indirectly by monitoring the displacement field of the pipeline and surrounding ground.

From an elaborate market analysis, it was concluded that the first market MAINTAIN is set to penetrate is the US gas pipeline market. This is because the US houses more than half of the global gas pipeline network and it has social-economical similarities to the Netherlands, which is the location of the MAINTAIN design team. It was estimated that

57 UAVs could be sold in the US based on the current market size. In a few years, the total length of gas pipelines will grow in the US which gives rise to an opportunity for selling more drones. In later stages, MAINTAIN also projects to expand its services world wide, both in gas pipeline monitoring as in other long range long endurance applications such as surface mapping. A frequently implemented monitoring method in the USA is the use of a helicopter. To compete with comparable UAVs and the current monitoring services, it was decided to sell one unit for 2 million USD, which would have a maximum cost of 20 USD per km.

The design and development process of an innovative project like MAINTAIN involves certain risks. Among the most severe risks identified, were the low possible thermal efficiency of the engine, inadequate stability, communication loss of the UAV with the ground segment and inadequate monitoring capabilities. As such, more technical resources have been assigned to the development of the micro gas turbine in order to optimise its quality. Stability of the design has also been assigned as a priority for the technical design. Moreover, adequate redundancy has been included within the communication system. Finally, the payload has been subjected to a careful selection process in order to satisfy the needs of the target group.

A next step was the analysis of the logistics and operations associated with MAINTAIN. The mission profile was determined to consist of take-off, monitoring of pipelines and landing. An algorithm was written to select an optimal amount of feasible airports in the US, which has led to 189 selected airports for refuelling and 10 airports for maintenance. Furthermore, constraints on the design resulting from regulations were investigated. It was found that, according to the *Code of Federal Regulations: 14. Aeronautics and Space*, there are no standard regulations that apply to a UAV with a take-off weight larger than 25 kg. Therefore, it is chosen to take the regulations of CFR 14, Part 23 which apply to aircraft heavier than 25 kg. The UAV will be supported in all its operations by the ground segment. The ground segment contains a control element which controls the aircraft and the airport operations that take care of the maintenance and refuelling of the aircraft. The control crew will require 2 people, which can be used for 2 UAVs simultaneously. For refuelling operations, if not available on the airport itself, will require 2 people. Maintenance activities shall be provided by a team of 5. The crew of the control segment was determined and its configuration decided upon. For the airport operations, the size of a crew for refuelling and flight checks and a crew for maintenance was established.

As the design evolved, different commercial entities were contacted in order to assess the feasibility of the corrosion detection system. A US based LiDAR developing company has revealed that they are developing a 68 kg LiDAR system suitable for UAVs. Such a relatively low weight LiDAR allows MAINTAIN to not only provide economic and sustainability benefits, but also corrosion detection capabilities beyond what is currently possible. The long endurance of the UAV allows it to gather sufficient data which can be mapped into surface strain information in order to indirectly find corrosion threats.

The design methodologies used for the development of the UAV are state of the art. The paradigm of Multi-disciplinary Design Optimisation (MDO) was utilised from the very start of the technical design. MDO allows for properly assessing the interaction of technical disciplines while optimising the overall design. As an example, the design of the wing planform is closely coupled to the design of the internal structure of the wing, and if one is preferred over the other, would lead to decreased design performance. Additionally, the principle of Object Oriented Programming was leveraged into a new design methodology: Object Oriented Design. This recognises the seemingly simple fact that any drone is simply a different combination of the same components. This principle permeated the development of the design software. As a result, the conceptual analysis was of high fidelity and ensured that the best concept passed the trade-off. Moreover, the design software can be used to create a derivative of MAINTAIN with different top-level requirements within minutes. This will be leveraged in expansion of the system to other market segments.

The performance of the UAV has been assessed using high-fidelity mission simulation which continuously updates the state parameters of the UAV. In the design mission, MAINTAIN will have a range of over 1600 kilometres when an endurance of 20 hours is required. Longer ranges can be achieved at the cost of reduced endurance. The flight altitude was optimised to be 300 metres above the instantaneous pipeline elevation to optimise payload performance. This 300 metres is the lower limit set by the system-level requirements. The UAV will cruise at 96 kilometres per hour, which is slightly below the maximum allowable speed for the LiDAR system to operate. Fuel burn has been determined to be 20 kilograms during the design mission.

The most design effort has been spent on the design of the propulsion system. The turboprop engine was considered the best gas turbine application due to its high performance at low speeds. Moreover, it was determined that the UAV shall only feature one engine, as multiple engines would lead to smaller individual units and an intensification of the disadvantages associated with downsizing a gas turbine. Both the compressor and the turbine were chosen to be of the radial type, in contrast to the axial type seen in most aircraft, in order to mitigate tip clearance losses. The turbine and compressor efficiencies were designed at 85% and 82% respectively. Although this is significantly lower than larger turboprop engines, the inclusion of a boundary layer ingesting inlet and highly efficient propeller (93%) allowed the engine to reach a low specific fuel consumption of 290 grams per kilowatt hours. The maximum propeller power is 3.75 kilowatts.

In order to analyse the aerodynamic performance of the UAV, an in-house computational fluid dynamics (CFD) software was developed. This CFD software solves the Laplace equation, describing incompressible and inviscid flow. This was selected because of the low flight speed of the UAV. Parasitic drag was assessed using a drag-buildup method. This analysis showed excellent results when validated with solutions of the full Navier-Stokes equation, which includes viscous effects. The final lift distribution closely approximates the elliptic one, hence minimising the amount of lift-induced drag. The final zero-lift drag coefficient was found to be approximately 0.01, which is close to half of that for current drones. The maximum lift-to-drag ratio was evaluated to be 33.2. The chosen airfoil is the reflexed PW75, used because of its positive aerodynamic moment generation which aids control of the UAV.

Next, the structural configuration of the UAV was determined. A typical wing-box structure is used which implements two spars in the wing to resist bending. By making this a box structure the wing has increased torsional resistance. Stringers were added to the upper and lower skins to promote bending resistance and avoid skin buckling. It was chosen to use J-stringers due to their good fail-safe characteristics. Subsequently, the materials were selected based on the loading to which a component is subject to. It was decided that the spars and ribs will be made from a carbon fibre reinforced polymer, the stringers from 7075-T6 aluminium and the skin from GLARE. Additionally, the landing gear struts will use steel because of its excellent strength.

Both static and dynamic stability were considered in the design of MAINTAIN. Longitudinal static stability required the aerodynamic centre of the wing to be aft of the centre of gravity, which was achieved by a combination of wing sweep and placing the payload and engine at the wing root. Lateral and directional stability was achieved by the dihedral, sweep and the winglets. The UAV's eigenmodes are all stable, except for the spiral mode. The onset of the spiral mode is slow enough for the autopilot to correct. The winglets have been designed mostly to provide stability for the Dutch Roll motion by inducing counter-acting yaw moments in case of directional disturbances. Their large size allows for better payload performance by mitigating the negative effects of the Dutch Roll. For control of the UAV, it was chosen to combine elevators and ailerons into elevons which are located at the outboard of the wing. In doing so, the moment arms of the control forces are increased which allows for lower weight solutions.

The disciplinary analyses were then integrated using MDO. This paradigm has allowed for fast optimisation of the entire UAV while meeting compliance between disciplines. In addition, an innovative design algorithm was developed to couple the aerodynamic and structural analysis of the UAV. By using the adjoint method, which can be viewed as lumping characteristics of the system that is analysed within some additional analysis, allows computation of design sensitivities at extremely low cost. These sensitivities are used to guide the design towards the best option. The design has been optimised with respect to fuel burn to minimise operational cost. The final design has a mere take-off weight of 160 kilograms, and only requires 20 kilograms of fuel for its mission. The effectiveness of the optimisation were clear when analysing the final design. It has a spanwise lift distribution that closely approximates the elliptic distribution, which is the absolute minimum for induced drag of a finite wing. Additionally, it has a relatively high cruise lift-to-drag ratio of 33. This has been achieved by the combination of the flying wing configuration, which minimises wetted area, and the slender wing, which minimises induced drag.

As the design is subject to a degree of uncertainty, both in materials and engine technology, an elaborate sensitivity analysis and uncertainty propagation was performed. By using the developed design software, a Monte-Carlo simulation was used in order to propagate uncertainties regarding design parameters into the performance metrics of the design. In order to decrease computational cost, the sensitivity analysis was leveraged to form a first derivative in the Monte-Carlo simulation. With 95% confidence, the maximum take-off weight will be between 158.95 and 171.6 kilograms. For the fuel weight, a 95% confidence interval yields that it will be between 17.38 and 28.0 kilograms.

Once the most important outer dimensions of the aircraft and the payload were known, the electrical system of the aircraft was designed. The μINS system of Inertial Sense was chosen for the navigation system as it combines an inertial reference unit, GPS and altimeter in a lightweight solution. The Sony FCB-EV7500 was chosen as camera for obstacle detection and pilot visibility. For communications, the Aviator UAV 200 from Inmarsat will be used due to its mature design.

After all the details of the design were finalised a cost analysis was made. The cost analysis is done with the use of a development and procurement cost of aircraft (DAPCA) model. Since this model is based on statistical data of general aviation some adjustments were made to apply it on a UAV. This has led to a unit cost of about 1.5 $\pm$ 0.75 million USD and operational costs of 1.62 $\pm$ 0.81 USD per flown kilometre. With a selling price of 2 million USD the break-even point will be reached after selling 18 UAVs.

In the resource allocation different technical resource parameters were analysed throughout the project. The parameters which were analysed are: cost, OEW, propulsive power, MTOW and fuel burn. Contingencies were implemented in the technical resource parameters to ensure a realistic estimate of the end product. The contingencies decrease with increasing time of development. The values of the technical resource parameters should be kept within the contingency ranges. Due to the use of an unsuitable regression and influence of the use of a micro gas turbine, this goal was not achieved

for every design stage in the project. However, this did not negatively affect the design, since most technical resource parameters decrease in value during the project, which is actually beneficial for the design.

To evaluate the reliability of MAINTAIN, a Fault Tree Analysis (FTA) of the system was performed and critical failure modes were made redundant. Next, the reliability of the total system was determined to be 0.998 per flight hour based on literature. Using the FTA, a maintenance planning was created. The UAV will be out of operation 66 days per year due to maintenance tasks. The availability of the UAV was determined by combining the reliability and maintenance planning of the UAV. It was determined that the availability is 0.8 on a yearly basis, which corresponds to 292 days per year. Finally, the safety of the UAV was assessed based on the reliability. It was determined that the chance of a fatality caused by each UAV is $\frac{1}{76}$ on a yearly basis.

The overall sustainability of MAINTAIN was assessed by evaluating five different sustainability indicators, which are: noise, safety, recyclability, emission and contamination. Next, the environmental footprint of a gas pipeline inspection mission performed by MAINTAIN was compared to the environmental footprint of a manned helicopter inspection mission, which is a currently used gas pipeline inspection method. A gas pipeline inspection mission performed by MAINTAIN reduces fuel burn with 96%, CO_2 emission with 99% and noise with 25% with respect to a manned helicopter mission.

The production process for MAINTAIN has also been developed. The skin will be made of GLARE composite and its production will use lay-up and roll bending. The aluminium stringers are to be manufactured using extrusion. The carbon fibre reinforced polymer ribs and spars are to be made using resin transfer moulding, which is preferred over the autoclave. The landing gear struts will also be produced by extrusion. Bonding of the skin and stringers will be performed using rivets. For the other rib and spar connections however, adhesive bonding will be used.

In conclusion, this Design Synthesis Exercise has proven that MAINTAIN is a viable alternative to current solutions. It outperforms modern pipeline inspection methods in every aspect: cost, efficiency, sustainability and quality. The UAV will feature a revolutionary mid-infrared LiDAR system that will grant it corrosion detection capabilities beyond what is currently possible. Additionally, MAINTAIN is an excellent proof of concept of the micro gas turbine implementation on a UAV. Albeit current component efficiencies are lower than those featured on large commercial airliners and its specific fuel consumption is higher than top of the line reciprocating engines, its higher power to weight ratio leads to a more fuel efficient UAV system. Additionally, reduced vibrations allow for significant payload performance improvement. It is expected that with modern high-fidelity shape optimisation techniques and innovative manufacturing procedures, the component efficiency will improve beyond the current design. Finally, the software developed for the design of MAINTAIN has been a prime example of the power of MDO and the efficiency of the adjoint method for gradient computations. The software can be used for the design of a complete MAINTAIN family of UAVs, satisfying the varying needs of commercial domains.

Contents

Nomenclature

List of Abbreviations

A	Availability
ADC	Attitude Determination and Control
AES	Aerodynamics and Stability
AHP	Analytic Hierarchy Process
AI	Almost Impossible
AP	Airframe and Powerplant
AP	Maintenance
At	Assume/Accept
ATC	Air Traffic Control
ATM	ATMOS
Av	Avoid
C	Cost
c.g.	Centre of Gravity
CA	Catastrophic
CAN	Canard
CERT	Certification
CF	Complex Flap System
CFD	Communication Flow Diagram
CFR	Code of Federal Regulations
CFRP	Carbon Fibre Reinforced Polymer
COMM	Telecommunications
COMP	Composite fraction
COMP	Ground Computer
CON	Conventional
CPI	Consumer Price Index
CPU	Central Processing Unit
CR	Critical
CS	Certification Specifications
CSTPROP	Constant Speed Propellers
Ct	Control
CTRL	Control
DAQ	Data AcQuisition
DC	Direct Current
DC	Distortion Coefficient
DEV	Development Support
DSE	Design Synthesis Exercise
EC	Electrical Component
ELEC	Electrical Subsystems
ENG	Engineering
FAR	Federal Aviation Regulation
FBS	Functional Breakdown Structure
FFBD	Functional Flow Block Diagram
FLW	Flying Wing
FML	Finite Element Method
FT	Flight Test Operations
FTA	Fault Tree Analysis
GC	Ground Control
GHG	Green House Gas
GLARE	Glass Reinforced Aluminium
GO	Ground Operations
GPS	Global Positioning System
GPU	Graphics Processing Unit
GS	Ground Segment
GWP	Global Warming Potential
IFR	Instrumental Flying Rules
INS	Inertial Navigation System
INS	Insurance
INSP	Inspection
IR	Infrared
L	Likely
LiDAR	Light Detection and Ranging
M	Marginal
MAINTAIN	Unmanned Aircraft for Monitoring Gas Pipelines
MAT	Materials
MDO	Multidisciplinary Optimisation
MFG	Manufacturing
MGT	Micro Gas Turbine Engine
Mo	Watch/Monitor
MON	Monitoring
MTN	MAINTAIN
MTOW	Maximum Take-Off Weight
N	Negligible
NAS	National Airspace System
NAV	Navgation
NPC	Navigation and Position Control
OEW	Operational Empty Weight
OOP	Object Oriented Programming
OPS	Operations
OVER	Overhaul
P	Probability
PCB	Printed Circuit Board
PL	Payload
PP	Power Plant
PRESS	Pressurised
PRF	Pressure Recovery Factor
PRO	Propulsion
PW	Power
QC	Quality Control
R	Reliability
RA	Rate of Labor in USD per Hour
RAM	Random-Access Memory
RCRA	Resource Conservation and Recovery Act
ref	Reference
RMS	Root Mean Square
ROC	Rate of Climb
ROI	Return On Investment
RTM	Resin Transfer Moulding
S	Severity
SFC	Specific Fuel Consumption
SHP	Shaft Horse Power
SL	Somewhat likely
SNR	Signal-to-Noise Ratio
SPL	Sound Pressure Level
SSM	Solid State Memory
STG	Storage
STOR	Storage
STR	Structures and Materials
SUB	Subsystem
SWOT	Strengths, Weaknesses, Opportunities and Threats
SYS	System
T	Temperature
T	Threats
Tf	Transfer
TIT	Turbine Inlet Temperature
TRL	Technology Readiness Level
U	Unlikely
UAS	Unmanned Aircraft System
UAV	Unmanned Aerial Vehicle
UDP	Uni-directional Propulsion
USA	United States of America
VFR	Visual Flying Rules
VL	Very Likely
VLM	Vortex Lattice Method
W	Weaknesses
WBS	Work-Breakdown Structure
WEEE	Waste Electrical and Electronic Equipment

WFD	Work-Flow Diagram

List of Symbols

%	Percentage
α	Angle of Attack
$\dot{m}$	Mass Flow
ϵ	Clearance
η	Efficiency
Γ	Circulation
γ	Dihedral
Λ	Sweep
λ	Taper Ratio
$\left(\frac{C_l}{C_d}\right)_{max}$	Maximum Lift-to-Drag Ratio of a 2D Shape
Ω	Angular Speed
ϕ	Flow Coefficient
ψ	Stage Loading Coefficient
ρ	Density
σ	Stress
τ	Shear Stress
N_p	Number of prototypes
Q_{FLGT}	Number of flight hours per year
Q_m	Estimated production rate in number of aircraft per month
θ	Twist
°	Degrees
C_m	Pitching Moment Coefficient of a 2D Shape
$C_{l_{max}}$	Maximum Lift Coefficient of a 2D Shape
$C_{m_{c/4}}$	Pitching Moment Coefficient at the Quarter Chord of a 2D Shape
$N_{a/c}$	Number of Aircraft Planned to be Produced over a 5-year Period
Q_m	Estimated Monthly Production Rate Aircraft
V_H	Maximum level of airspeed in KTAS
A	Area
AR	Aspect Ratio
B	Boom Area
B	Byte
b	Bit
b	Wing Span
C	Celcius
C	Coefficient
c	Chord
c_p	Specific Power Consumption
CH_4	Methane
CO_2	Carbon Dioxide
D	Diameter
D	Drag
dB	Decibel
E	Endurance
E	Young's Modulus
e	Oswald Factor
F	Factor
f	Friction Factor
ft	Foot
G	Shear Modulus
g	Acceleration of Gravity
h	Enthalpy
h/H	Hour
He	Helium
Hz	Hertz
I	Moment of Inertia
J	Bessel Function
J	Joule
J	Torsional Rigidity
K	Kelvin
K	Stiffness
kg	Kilogram
L	Lift
l	Length
l	Litre
lbs	Pounds
M	Mach
M	Moment
m	Metre
min	Minute
N	Newton
n	Safety Factor
NO_x	Nitrogen Oxides
P	Load
P	Power
p	Pressure
Pa	Pascal
pix	Pixel
psi	Pounds per Square Inch
q	Dynamic Pressure
q	Shear Flow
R	Range
r	Radius
R^2	Coefficient of Determination
R_{MF}	Maintenance man hours to flight hours ratio
RA	Rate of Labor in USD per Hour
RPM	Rounds per Minute
S	Shear Force
S	Surface
s	Second
T	Thrust
t	Thickness
U	Speed
USD	United States Dollar
V	Velocity
V	Voltage
W	Watt
W	Weight
€	Euro

1 Introduction

This report presents the final phase of group 18 in the Design Synthesis Exercise MAINTAIN, which is short for Un**m**anned **Ai**rcraft for Mo**n**i**t**oring G**a**s Pipel**in**es. It is estimated that 3.6 trillion cubic feet of natural gas escapes into the atmosphere yearly. Although methane, the chief component of natural gas, breaks down more quickly than carbon dioxide, it has a more planet-warming potential while it is present and is therefore a significant cause of global-warming[1]. Furthermore, these leakages are responsible for an average of 14 casualties and 50 wounded in the U.S[2]. The mission of this project is to design a UAV system capable of monitoring and inspecting gas pipelines, which is both economically and ecologically more attractive than current solutions. The existing solutions are manned aircraft surveillance and ground teams driving along the pipelines. Firstly, these existing solutions are found to be very expensive because it is extremely labour intensive and the operational cost of the aircraft is high. Moreover, it is hazardous for human safety as the vehicles have to drive, fly and land in challenging and potentially unsafe regions. The usage of UAVs could both reduce the cost and human risk, while increasing the quality and efficiency of the monitoring activities.

Traditionally, UAV designs implement electrical or reciprocating engines. However, the problem with these solutions is that they suffer from high noise emissions, excessive vibrations and relatively low endurance. Micro gas turbines have the advantage to be less affected by vibrations, which will increase the quality of the inspection activities. Moreover, they are known for their high power-to-weight ratio which will consequently increase the range capabilities of the UAV. Notwithstanding, there are some disadvantages as well, for which pioneering solutions have to be developed in order to make it feasible. An example is that the commercial implementation of micro gas turbines is a relatively new technology which has not been used before. This means that thorough research is necessary to make this design option a feasible concept that would be taken into account. The aim of this project is therefore to make micro gas turbines, running on bio-fuel, a feasible option as main engine for UAV designs with long-range and -endurance capabilities. This research is performed by a group of ten third year Aerospace Engineering students from Delft University of Technology during a period of eleven weeks.

This document represents the final report of the MAINTAIN project and thus serves as a summary of the eleven weeks of design efforts by the team. Firstly, in chapter 2, an exploration study is performed in order to obtain a clear overview of all the existing propulsion and payload solutions. Subsequently, in chapter 3, an extensive market analysis is outlined, since it is of utter importance to do research on the current market, its size, the competitors and other potential opportunities which were not considered yet. Thereafter, the technical risks associated with the different subsystems of MAINTAIN are assessed and the required mitigation plans are described in chapter 4. Then, the operations and logistics are elaborated upon in chapter 5, which is followed by the determination of the ground segment in chapter 6. Next, in chapter 7, a functional analysis is performed. In chapter 8, the communication flow is presented and in chapter 9 the concept evolution process is explained. This is followed by the payload selection as discussed in chapter 10. Thereafter, the different models which are used in the main optimisation are elaborated upon; in chapter 11-chapter 15, the performance, propulsion, aerodynamics, structures and materials, and the stability and control models are documented respectively. Subsequently, the electrical subsystem design is discussed in chapter 16. In chapter 17, the design optimisation with the final result is given. Then, one can find a documentation of the cost analysis in chapter 18 which is followed by the resource allocation and budget breakdown in chapter 19. After that, in chapter 20, the reliability, maintenance, availability and safety characteristics are incorporated. This is followed by the sustainability approach of the entirety of the project in chapter 21. Thereafter, the production plan is elaborated upon in chapter 22. In chapter 23, the requirements compliance matrix is stated and a feasibility analysis is executed. Following this, in chapter 24 the post-DSE activities that are to be performed are stressed in the post-DSE Gantt Chart. Lastly, the discussion of the results, future recommendations and conclusions which can be drawn are documented in chapter 25 and chapter 26.

[1] https://www.forbes.com/sites/tomzeller/2015/04/21/natural-gas-leaks-a-30-billion-opportunity-and-global-warming-menace/#13d7d2241632 [cited on: 25-06-2018]

[2] https://www.popsci.com/article/science/not-just-new-york-gas-leaks-are-problem-all-over-us [cited on: 25-06-2018]

2
Exploration of MAINTAIN Technologies

The MAINTAIN vehicle is an ambitious project, where a range of complex systems are combined to ensure successful implementation in both the pipeline maintenance industry and the general UAV market. This chapter presents the exploration of advanced technologies associated with the MAINTAIN project. The focus of this exploration study is on the propulsion and the monitoring system, which will be thoroughly investigated before the actual design of the UAV. First, the implementation of drone technology in society is elaborated upon in section 2.1. This is followed by section 2.2, where a broadening study into UAV-specific propulsion systems is performed. Thereafter, the monitoring techniques will be explored in section 2.3.

2.1. Exploration of UAV Technology

An Unmanned Aerial Vehicle (UAV), also known as a drone, is an aircraft replacing human crew members with computer systems. The development of UAVs has long been at the centre of military efforts to eliminate casualties of allies by removing the need of a pilot. More recently, the economically viable miniaturisation of the required technology has opened the doors to the commercial domain of the UAV concept. Within this domain, the combination of increased safety and economic reasons is what motivates the consumer to opt for an unmanned system to complete the mission in question.

The concept of a UAV provides a myriad of advantages over current technological solutions in different domains. The fact that they are unmanned means that they can operate in more dangerous environments than manned aircraft. Moreover, they are subject to less mistakes due to inability of computerised systems to become exhausted. Finally, replacement of a manned vehicle by an unmanned vehicle means cost reduction in two distinct ways: the vehicle itself can be smaller due to a reduction in payload, and the wage of the operator of the vehicle may be used elsewhere.

All of these benefits are applicable to a large range of industries and related companies. More specifically, Figure 2.1 displays the 5 largest commercial industries using drones. Note that the Drone Service Providers themselves also serve other industries.

Figure 2.1: The five largest industries for commercial drone use (*2017 Commercial Drone Industry Trends* n.d.).

It is convenient to classify UAVs according to their endurance and operation altitude. Such a classification is shown in Figure 2.2, based on (Gundlach 2014).
As can be seen, a large amount of the current UAV domain is still saturated with drones used for military applications. This is explained by the less stringent requirements on cost within this sector, allowing for more advanced technologies to be used. Also note how current commercial drones are lacking in both altitude and endurance, explained by the lack of fuel efficiency of commercially available drones which makes them infeasible for use from an economic perspective. **As such, the MAINTAIN UAV will be developed to satisfy the need for low altitude long endurance (LALE) UAVs as is the case for pipeline monitoring.**

2.2. Exploration of UAV Propulsion

A highly important technology in aircraft is the means of propelling the aircraft. Especially in the UAV research and development, the research on this system is far from saturated. To obtain an overview of the possible implementation of engines in a UAV, the propulsion system is explored. Currently, there are significant advancements in the propulsion

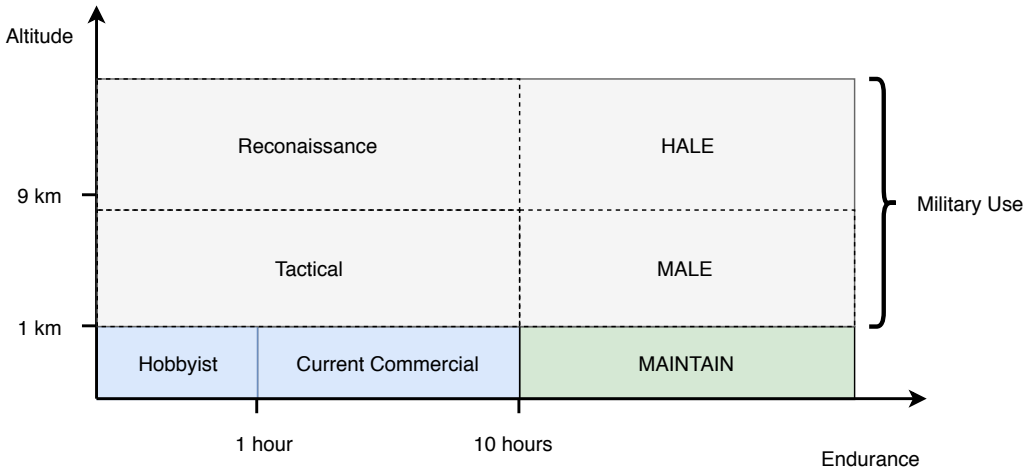

Figure 2.2: Classification of UAVs according to endurance and operation altitude. Abbreviations: MALE = Medium Altitude Long Endurance, HALE = High Altitude Long Endurance.

technology, opening new doors for the medium sized unmanned aircraft. First, the concept of a propulsion system is discussed, after which the implementation in UAVs is elaborated upon. Subsequently, the implementation of micro gas turbines is summarised, since the top level decision is made to include this technology in the system.

2.2.1. Propulsion System

All known vehicles feature a propulsion system, either internal or external, to overcome the resistance imposed by the environment on their inertia. Increasing propulsion efficiency is a topic that is always subject. This is because any such positive change results in lower power consumption, which may then lead to a multitude of other positive effects on the vehicle's design. From a systems point of view, a propulsion system is commonly decomposed in three parts: the energy source, the power conversion component and the thrust producing component. This view neglects the control of and regulations on the system, since it is momentarily not at the core of discussion. For each of these individual subsystems it is possible to find a set of alternative implementations of their functions. The choice of technology is determined by the specific vehicle's mission. Later in the report, the MAINTAIN design choices with regard to the propulsion system will become evident.

2.2.2. Propulsion Implementations Within UAVs

The UAV is always of smaller mass and size for a given mission than its manned counterpart due to the exclusion of human payload. For this reason, the use of propulsion technology within the UAV domain is not in one-to-one correspondence with manned aircraft. In general terms, the division between propulsion concepts for UAVs can be divided according to the manner of energy storage used: electric or thermal. Both energy sources can theoretically fulfil the role of energy source, yet in practice, this is not feasible due to the more cumbersome power extraction methods required for thermal energy storage.

Figure 2.3 shows the current composition of propulsion systems implemented in UAVs. One can see that electrical propulsion is implemented within a large share of the available UAVs. Interestingly, the UAV domain is one of the early adopters of electrical propulsion due to their less stringent requirements for range and endurance. When these constraints drive the design however, it is obedient to consider thermal engines due to the significantly higher specific energy and energy density.

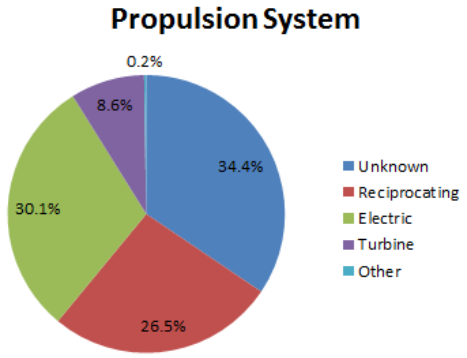

Figure 2.3: UAV propulsion system composition in 2013 (Marcellan 2015). Note that the unknown data is an indication of the fact that a large amount of UAVs are used within military applications and their engine specifications are proprietary.

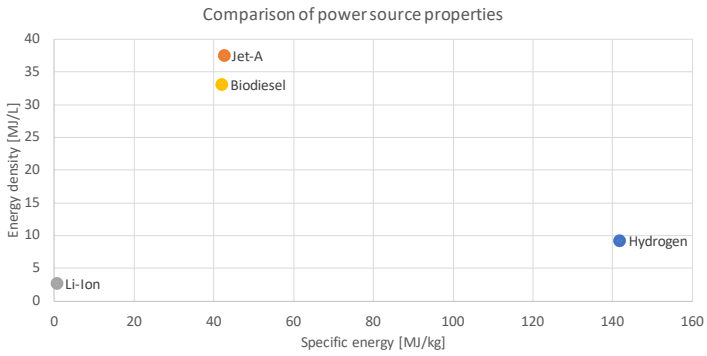

Figure 2.4: Specific energy and energy density for common energy sources.

A brief description of these engine types is given below:

- **Electric Motors**: These engines convert electrical energy to mechanical energy by the principal of magnetic induction. The power source can be batteries, fuel cells (using hydrogen) or solar cells. They are commonly used in hobbyist UAVs as they are cheap to produce.
- **Thermal Engines: Reciprocating** : Thermal engines convert the chemical energy within fuels into mechanical energy through expansion of a working fluid after combustion of the fuel. Reciprocating engines use pistons, which are connected to a rotating shaft which is used to drive some thrust-producing device such as a propeller. They are the most commonly used thermal engine type because of the availability of properly sized reciprocating engines (Gundlach 2014).
- **Thermal Engines: Gas Turbines**: Their working principle is very similar to the reciprocating engine. The gas turbine however, does not use a closed thermodynamic cycle. This allows these types of engines to be used in high-speed applications as the increase in mass flow aids engine performance. Additionally, gas turbines suffer from less vibrations than reciprocating engines and are therefore better for payload performance when this is integrated sufficiently close to the engine within a UAV.

2.2.3. Micro Gas Turbines

As elaborated upon above, there is a plethora of benefits associated with the gas turbine engine that justify further exploration of the concept. However, decreasing the size of a gas turbine engine in order to be implemented in a UAV comes with certain technical difficulties. Supposedly, if a large-scale, well-performing gas turbine engine is down-scaled and that engine intends to emulate the performance, the following phenomena would be encountered:

- **Lower Reynolds numbers**: This non-dimensional number is an indicator of the presence of viscous effects in the flow of a fluid over a solid object. By definition, this number decreases as the diameter of the engine decreases. Lower values indicate governing viscous effects, which in general decrease performance.
- **Increased energy transfer as heat**: The ratio of volume to surface is always proportional to the characteristic length of the device. As such, decreasing size decreases this ratio and consequently increases the amount of heat transferred. This represents an energy loss and therefore generally decreases the efficiency of the engine.
- **Manufacturing tolerances**: The tolerances of a manufacturing process are absolute. Therefore, production of a micro gas turbine becomes relatively inaccurate in comparison to larger gas turbines. Tip clearance is a significant contributor to losses in compressors and turbines (Dixon 2005).

Therefore, it may be concluded that designing an efficient micro gas turbine (MGT) for a UAV requires different design methodologies compared to the traditional gas turbine engine.

2.3. Exploration of Payload

A highly important aspect of the MAINTAIN mission is the payload that is monitoring the pipelines. This section explores the phenomena that have to be identified and the current equipment used to measure these. First, the pipeline defects that can be distinguished are identified. This is followed by an investigation into the techniques that are currently implemented in the monitoring process of gas pipelines. To conclude, the external factors influencing the measurements, primarily the weather conditions, are analysed.

2.3.1. Pipeline Defects

To ensure successful monitoring of gas pipelines, different types of damage and deterioration on pipelines need to be considered. Below, corrosion of pipelines and gas leakages are considered individually. These are the main divisions of failure modes in gas pipelines that need to be monitored. Additionally, the current monitoring techniques are explained for corrosion and gas leakages subsequently.

Corrosion and Rust

Corrosion is the deterioration of a material by reaction with its environment (Roberge 2012). In essence, it represents loss of valuable material due to the interaction with substances in direct contact. The functional degradation of the metal structure forms an enormous risk for the system it is a constituent to. Rust is one of the most commonly found forms of corrosion, as it pertains to iron, oxygen and water. Corrosion originates due to naturally occurring electrochemical potentials between substances.

Rather than discovering leakages in the pipelines, it is preferred to monitor defects before structural failure occurs. A significant amount of pipeline failures is due to excessive corrosion of the metal[3]. Normally, this is a gradual process where the anomaly develops over a certain time span until the very moment of fracture. Currently, there are electro-chemical and in-line methods to monitor corrosion. Next to that, methods using coupons that measure weight or potential change are being implemented (Orazem 2014). The problem with these technologies is that contact with the pipeline is necessary and therefore these methods are not suited for the airborne MAINTAIN vehicle.

Another solution could be to observe the land movements near the pipeline as this can be a good indicator for high-risk areas. At these areas, high stresses can be induced on the pipeline which will result in damages in the coating. If this damage is inflicted, the corrosion rate increases and should therefore be inspected using one of the current methods. Observing the land movements can be done using a LiDAR system, which maps the environment. Airborne LiDAR systems already exist with an accuracy of 2 cm, such as the RIEGL VQ-780i[4]. The problem with this method is that the navigation system has an accuracy of merely 2.5 m. This implies that comparing the two maps will not be possible based on data from the navigation system. An alternative is to map the consecutive measurements on top of each other based on similarities. Furthermore, visual beacons can be determined at an initial flight, after which subsequent measurements are compared. Note that this requires calibration, predicting that subsequent flight altitudes do not unconditionally coincide. A complex algorithm is required to use the described LiDAR mapping technique for finding corrosion threat areas, although undoubtedly possible.

Gas Leakage

Deteriorated pipelines or inflicted damage to pipelines can lead to gas leakages. This evidently has a negative effect on the environment and impedes the transportation of gas with optimal efficiency. It is essential that every substantial gas leak is detected and that maintenance operations are performed on short notice. Natural gas consists of several components. Table 2.1 shows the mole percentages of the different components where methane is clearly the largest share in the natural gas[5].

Table 2.1: Components of natural gas[5].

Component	Mole fraction [%]
Methane	93.9
Ethane	4.2
Nitrogen	1
Propane, Butane, Pentane, Carbon dioxide, Oxygen	<1

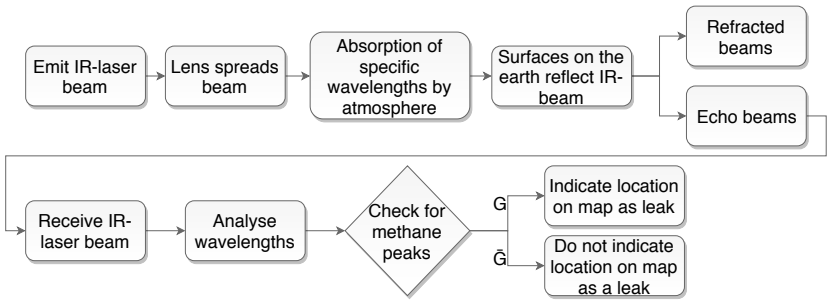

Figure 2.5: Use of a LiDAR system to detect gas leakages.

Detecting methane is thus an accurate indicator for gas leakages. The system must be able to detect gas leakages for both above- and underground pipelines. If a gas leak occurs underground, it is still detectable as the gas will rise and escape at the surface of the earth (Parvini and Gharagouzlou 2015). Even if the gas cannot escape, the surface temperature of the earth where the gas is trapped will be different and could therefore be detected. Underground leakages will therefore not pose an impeding problem for detection systems.

A technology that can be adopted for the monitoring of gas leakages is the usage of the infrared (IR) spectrum. Two common technological implementations of this spectrum are a thermal camera, which captures the emitted IR radiation

[3] http://www.materialsperformance.com/articles/chemical-treatment/2017/01/internal-corrosion-failures-are-we-learning-from-the-pa [cited on: 03-07-2018]

[4] riegl.com/uploads/tx_pxpriegldownloads/RIEGL_VQ-780i_Infosheet_2017-12-04_Preliminary.pdf [cited on: 18-06-2018]

[5] uniongas.com/about-us/about-natural-gas/chemical-composition-of-natural-gas [cited: on 08-05-2018]

of different surfaces, and a LiDAR system, integrating IR spectroscopy to determine the composure of the fluids through which it is measuring. IR spectroscopy is based on the fact that molecules have their own characteristic structure which absorb specific frequencies in the IR spectrum[6]. Thermal cameras can be used to differentiate the temperature of objects through the infrared spectrum. When a gas leak occurs, the leak has a temperature difference with respect to the pipeline. Using software, the temperature differences around the pipeline can be analysed in order to confirm the formation of a natural gas plume. Next to that, the received infrared signal can be filtered on a specific wavelength range. Using spectroscopy, the spectrum can then be analysed for the presence of methane. The problem imposed is that weather conditions will highly affect the detection accuracy of gas leaks. A more elaborate explanation on the weather conditions is stressed later in this chapter.

On the other hand, the LiDAR system emits a beam with a specific bandwidth of wavelengths, which reflects back to the system from a surface that it is pointed at. The detector measures the intensity of the wavelengths that are reflected, from which it can determine what gases are present in the atmosphere because some wavelengths are absorbed by the gases. This is a very accurate manner of detecting which gas is leaking from what location. The functional flow to detect gas leakages with a LiDAR system is shown in Figure 2.5. A LiDAR system, however, collects significant data sets which can result in a extensive data processing period[7].
Currently, for the inspection of gas leakages, the LaSen ALPIS (Airborne LiDAR Pipeline Inspection Service) is used to monitor pipelines using a helicopter. This system has proven to accurately find the location of cracks or holes . The complication with ALPIS is that the detection system has a weight of 113.4 kg. Implementing this system would not comply with the payload system's requirement which constrains the maximum payload weight at 50 kg. Furthermore, the weight of the system would render the UAV too expensive.

2.3.2. External Influences

To evaluate whether MAINTAIN will be operable during the entirety of the mission, the factors influencing the validity and quality of the measured data must be analysed. Therefore, first the effect of velocity, followed by the effect of weather conditions on the measurement data is discussed.

Flying Velocity

The operable velocity range of the payload can greatly affect the mission characteristics. In order to ensure sufficient quality of the acquired data, the effect of velocity on the observation accuracy is to be investigated. When images are taken at a relative motion with respect to an object, distortion of the image can be caused when the object in motion is captured by multiple photoreceptors during construction of the image (Choung, Shin, and Paik 1998). This is especially a problem for cameras with a rolling shutter, as not all pixels are collected simultaneously. Contrarily to this rolling option, it is possible to implement a global shutter. This shutter type electronically collects pixels simultaneously and, with that, it eliminates the possibility of objects being captured by multiple pixels, regardless of the relative velocity[8]. The shutter time can be adapted to the ground speed of the UAV, which is not imposing significant difficulties at the operating velocities that are considered. For this reason, the quality of the images does not depend on the chosen velocity range for the mission.

Weather Conditions

The operability of the UAV is dependent on the weather conditions as these effect the flight performance and the payload performance. The two monitoring methods which were discussed in subsection 2.3.1, a thermal camera or a LiDAR system, are both affected by weather conditions. Below, the effect of weather on the accuracy of these methods is investigated.

Atmosphere: Observing the leakages through thermal imagery proves to be more difficult with rain, snow, wind an high humidity(E. Bernard et al. 2014). The raindrops, dependent on their size, absorb or refract the infrared waves that are to be measured. Since MAINTAIN flies at a minimum altitude of 300 m, the radiation undoubtedly passes through the water amassments, compromising the signal. For that reason, a thermal camera is not able to detect gas leakages as well as it should if it is raining. Even light rain can make the signal unreadable. Furthermore, heavy winds will dissolve the gas plume which escapes through a leak quickly into the atmosphere. This decreases the likeliness of detection as well, since the volume of colder gas decreases quickly. Lastly, there are the events of the soil being more wet locally, or the air having a higher humidity, in excessive cases even mist. In all instances, there is more water in the monitoring path, which impedes the quality of the measurements, where severity is dependant on the concentration of the water particles. Detection using LiDAR is less sensitive to weather conditions, although it is still affected by it to some extent. Heavy rain or low clouds will affect the LiDAR system as some of the beams emitted will be refracted. Despite that, generally, the large collection of data can still be used for analysis[7]. Heavy wind, on the other hand, does affect the measurements of

[6] `ru.nl/systemschemistry/infrastructure/optical-spectroscopy/infrared/` [cited on: 15-05-2018]
[7] `http://www.lasen.com/technology.aspx` [cited on: 23-05-2018]
[7] `lasen.com/technology.aspx` [cited on: 23-05-2018]
[8] `http://pdf.aeroexpo.online/pdf/ascent-vision/cm202/175744-3989.html` [cited on: 16-5-2018]

the LiDAR techniques. This is due to the gas stream being dissolved quickly in the atmosphere, leaving the concentration of methane possibly too small to accurately measure.

Temperature: Regarding temperature, the thermal camera is more significantly affected than the LiDAR-assisted monitoring system. The thermal imaging procedure is based on the temperature difference between surfaces or objects. If the temperature difference between the pipeline exterior and the gases is substantial, one can easily recognise if there is gas escaping. On the other hand, if the temperature difference is not as evident as above, it is increasingly difficult to visualise that there is a gas leak. This should be taken into account, since the UAV is designed to cover a range of areas with different standard temperatures. A LiDAR system with the possibility to apply spectroscopy is not affected by temperature of the surroundings. The emitted infrared radiation is sent to the surface, where it reflects to the sensor. Regardless of the temperature, a range of the waves is absorbed by the gases, which provides information about the composition of the atmosphere.

Operating in The United States of America

Now that the thermal camera and the LIDAR system are compared with regard to their functionality in different weather conditions, the actual operating environment of the mission is to be analysed. The United States of America span such a significant part of the earth's surface, that a highly differing climate can be encountered. As can be seen in Figure 2.6, the average annual precipitation ranges from less then 150 mm to more than 4500 mm. Undoubtedly the largest part of the natural gas pipeline network lies in the Southern and Eastern part of the country. Evidently, these areas encounter an average annual precipitation in the range of 700 mm to 1800 mm. These conditions are comparable to averages of countries as the Netherlands and the United Kingdom. The average annual precipitation in the state Louisiana, which includes a significant part of the total pipeline network, is more than 1500 mm where it rains approximately 100 days per year [9]. For that reason, the system being designed is required to be capable of monitoring if it is raining, excessive situations excluded.

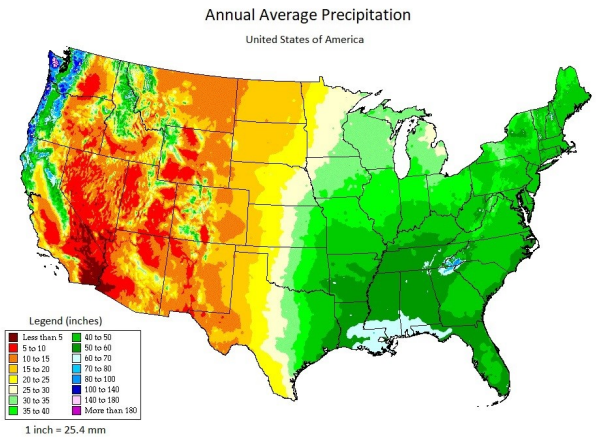

Figure 2.6: The average annual precipitation between 1961 and 1990 based on data provided by the Climate Prediction Center, NOAA.

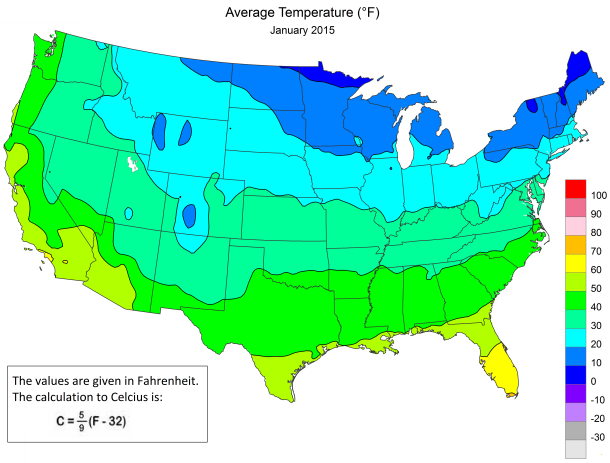

Figure 2.7: The average temperature measured in January 2015 provided by the Climate Prediction Center, NOAA.

Next to precipitation, there is the broad range of temperatures in which the system should be operable. Figure 2.7 shows the temperatures that can be expected throughout the United States. For illustration, the month January is selected to show that the temperature can range from 18 degrees Celcius below zero to 20 degrees Celcius above zero. Note that throughout the year, temperatures can become significantly lower and higher, meaning that the temperature of the surface covers a vast range. Generally, the gas within the pipelines ranges between 10 and 30 degrees Celcius[10]. Inevitably, there are moments where the temperature of the escaping gas is equal or close to that of its surroundings. Because of this, implicitly, a requirement arises that a monitoring technique is to be used which is not much affected by temperature differences.

For the climate analysis, precipitation and temperature have been quantitatively mapped at this stage. Other factors described earlier were wind velocities and accumulated water near pipelines. These parameters are varying more, which makes the mapping of the parameters less concrete. Note that the system should still be chosen to perform optimally when it encounters these phenomena. Later in the report, when the payload is selected, the weather conditions are taken into account in the trade-off.

[9] `https://www.usclimatedata.com/climate/louisiana/united-states/3188` [cited on: 23-06-2018]
[10] `https://pdfs.semanticscholar.org/5cf6/8603c31efecfcfe99c735e6eb64795b5be64.pdf` [cited on: 23-06-2018]

3
Market Analysis

After the exploration of the technologies that are implemented in the MAINTAIN mission, it is possible to initiate the realisation of the service. Before starting the design of a new product, a market analysis is conducted. This is in order to investigate where the system has the highest probability of succeeding and to evaluate its competitive position in the current market. The results of the market analysis are to be reviewed and it is decided whether the product is feasible from an economical perspective. First, MAINTAIN's market position is analysed by means of a SWOT analysis in section 3.1. Then, the involved parties in MAINTAIN will be identified in section 3.2. This is followed by a study of the market size, including the potential growth over the course of development, in section 3.3. With the knowledge of the market at hand, section 3.4 analyses the competition that the unmanned service encounters at the implementation of the system. In section 3.5 the future the market holds are described.

3.1. Market Position

In order to obtain insight in the market position of MAINTAIN, a SWOT analysis is conducted. In this analysis, strengths, weaknesses, opportunities and threats of the product are outlined in one figure. The representation of this SWOT analysis is displayed in Figure 3.1 and is used as a basis for all the further steps in the market analysis.

Figure 3.1: SWOT analysis of market position for a long-range and long-endurance UAV that monitors gas pipelines.

3.2. Stakeholders

To get an accurate view of all the parties that are involved with this project, the different stakeholders are mentioned and their relevance is explained:

- **Gas Companies:** As the gas companies will be the users of the product, they can be identified as stakeholders. The requirements from the gas companies will primarily drive the design.

- **Government:** The government is an important stakeholder because it is the primary legislation entity who will decide whether the UAV is allowed to fly in certain areas. The final design has to conform to the law in order to ensure a safe and legal operation.
- **Manufacturers:** The manufacturers must be taken into account as they determine the feasibility of the project. Especially the technical and economic feasibility of the project are dependent on the carefully chosen requirements with respect to the manufacturers.
- **Investor:** Without the investors, no funds are available for the design project which means that no further designing is possible.
- **Gas Users:** The success of the project will influence the gas users as the gas price will continue to fluctuate and the reliability of the gas delivery will improve after implementation of MAINTAIN. For them, the costs and risk of the project will be of primary concern.
- **Life near pipelines:** Humans and animals that live in the vicinity of pipelines should be taken in account. Important parameters are e.g. noise complaints, privacy concerns and safety measurements.
- **Delft University of Technology:** The Delft University of Technology is essentially the executor of the project. It is responsible for the supervision and availability of resources of the project and also finances part of the project.
- **Airports:** Airports are stakeholders because the drone will possibly be taking-off from and landing on their runways. Regulations will have to be made to ensure that efficient drone operations can be guaranteed next to the current air traffic operations without affecting them.
- **Bio-fuel suppliers:** The Bio-fuel suppliers have great interest in this project as they will benefit from the implementation of this UAV observation system which runs on a bio-fuel.

3.3. Market Size

The first step in the analysis of the market is determining the market size. Here, the maximum amount of products that can be sold will be evaluated. Often, the reason for failure of new products is an inadequate market size assessment. Especially in the technical startup phase, the focus is often on making the most efficient, innovative and creative solution, whereas the business-related aspect is neglected resulting in a high failure rate (Sander n.d.). If a hypothetical market size consists of 10 products and a company needs a minimum of a 1000 product sales to reach its break even point, this company is prone to bankruptcy if no alterations are made. This section elaborates on the total drone market, a prediction of market growth and the market segment that MAINTAIN is initially focusing on.

The MAINTAIN project is part of the global drone market. As the commercial application of UAVs has passed its proof of concept phase and is now being widely adopted, the growth of the market is substantial. The market size in the United States in 2016 has been estimated to be 2 billion USD with a compound annual growth rate of 25% (Global Market Insights 2004). Additionally, a combination of historical and forecasting data was collected by (Grand View Research 2016) and is shown in Figure 3.2. The global market growth based on 2015 forecasts is shown in Figure 3.3. It shows a 50% growth of drone usage in the energy sector from 2018 until 2022.

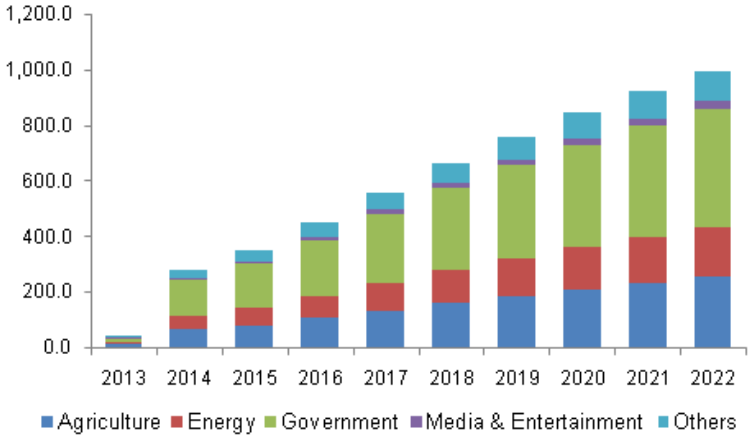

Figure 3.2: Growth of the US commercial drone market in millions USD (Grand View Research 2016).

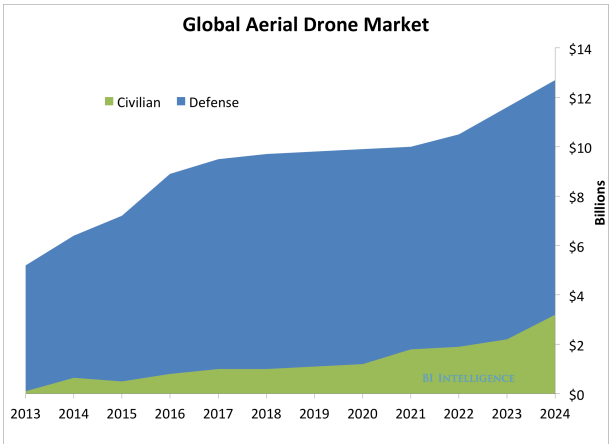

Figure 3.3: Global drone market growth in billions USD (Ballve 2015).

3.3.1. Market Segment

The previous section solely discussed the total drone market. The market segment that MAINTAIN is targeting is the inspection of gas pipelines, and more specifically, inspection by UAVs. To decide for which areas the product is going to be designed, information about the distribution of gas pipelines across the earth is needed. Furthermore, the niche market

size for inspecting gas pipelines needs to be determined. Table 3.1 displays the total length of gas pipelines per country. North America, i.e. the USA and Canada, and Russia provide the largest contribution to the total length of gas pipelines, which makes it a sensible choice to initially focus on these markets. However, the design process will generate a concept for a UAV, which is a product that has to comply with several airworthiness and legal regulations, which is differently specified per country. The advantages that the USA have over Russia is that the project group members all speak perfect English which is the spoken language in the USA. Furthermore, politically and economically, the Netherlands are more engaged with the USA in comparison with Russia (Bureau of European and Eurasian affairs 2018) (Lemmers, Smit, and Wijnen 2014). Finally, the USA have a more enterprising attitude, inhabiting regions like Silicon Valley. Therefore, **the initial market that the MAINTAIN design team is trying to penetrate is that of the USA.** After successful implementation in the USA expansion to Russian and Canadian markets will become a growth opportunity.

Table 3.1: Total length of gas pipelines per country[11].

Country	Gas pipelines [km]
USA	1,984,321
Russia	184,980
Canada	179,078
China	70,000
Other	612,312

In Table 3.1, the market size is expressed in kilometres of pipeline per country. The market size needs to be converted to the amount of required UAVs to cover the entire pipeline length. The approach used is based on the monitoring frequency imposed by the Code of Federal Regulations (U.S. government n.d.). The monitoring frequency corresponding to corrosion is defined to be 6 times per calender year and for gas leakage 4 times per calender year. Although MAINTAIN will not be able to detect corrosion directly, the corrosion threats will be checked. It is assumed that monitoring the corrosion threats should also be checked 6 times per calender year. Using this information, a calculation is made to determine the amount of drones that can saturate the gas pipeline surveillance market in the USA. Table 3.4 shows the inputs and outputs of the calculation, which is based on the regulations and the requirements as stated in (B. van Beurden et al. 2018a). It is found that **57 drones are needed to saturate the total gas pipeline surveillance market in the USA**. In section 3.5 possible future markets for MAINTAIN are discussed.

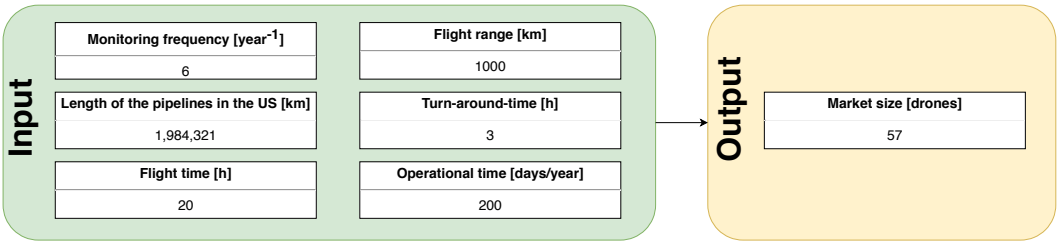

Figure 3.4: Current USA market size calculation.

3.3.2. Market Growth

Due to increased gas prices and development in gas extraction technology, the production of shale gas in the USA has become affordable. This new gas extraction technology opened possibilities to extract natural gas from shale formation. New gas reservoirs can be accessed using this technology. As a result, the gas production in the USA has rapidly increased over the last couple of years and is expected to keep growing. Figure 3.5, obtained from the U.S. Energy Information, Administration[12], shows the expected growth of the gas production in the USA over the next 22 years. In this time frame the gas production is expected to grow with 37%. Increased gas production will lead to the need for more gas pipelines. According to (Smith 2015) , plans to build more than 44200 kilometres of gas pipelines between 2015 and early in the next decade are in place. This is equivalent to a 2.23% increase in the total amount of gas pipelines installed in the USA.
Besides the expected increase in the market by direct growth of the amount of gas pipelines, the market is subject to safety and integrity regulations set by the USA government. The USA government is planning to increase the pressure on safety and integrity regulations concerning gas pipelines[13]. This could result in a need for a higher monitoring frequency and could therefore increase the market size. It would be appropriate to calculate the amount of drones in the market of 2020. However, information on future drone regulations is not yet available.

[11] `https://www.cia.gov/library/publications/the-world-factbook/fields/2117.html`[cited on: 01-05-2018]
[12] `https://www.eia.gov/energyexplained/index.cfm?page=natural_gas_where` [cited on: 01-05-2018]
[13] `http://www.materialsperformance.com/articles/material-selection-design/2017/02/proposed-changes-to-gas-\penalty\z@ transmission-pipeline-regulations-intended-to-increase-safety`[cited on: 01-05-2018]

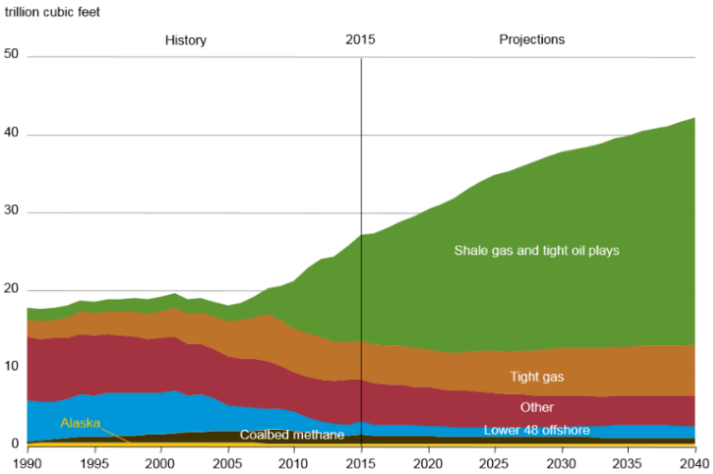

Figure 3.5: Growth of annual gas production in the USA in trillon ft^3.

3.4. Competitors

In North America, several different systems are used to monitor gas pipelines. The main division in inspection methods is between ground based and aerial inspection methods. This section will elaborate on both methods and compare them. Furthermore, a comparison will be made between MAINTAIN and other UAVs that can be applied in the gas pipeline inspection process. Finally, an initial price estimation for MAINTAIN is made which ensures a competitive position in the market.

3.4.1. Gas Pipeline Detection Systems

The aerial inspection systems consist of manned and unmanned inspection methods. A helicopter with measuring equipment is a system that is often used (Hausamann, Zirnig, and Schreier n.d.). For the inspection UAVs can be utilised. Ground inspection can be performed by car or by foot. Table 3.2 displays the different mechanisms with their key features. MAINTAIN is selected for the unmanned aerial inspection. Based on the table a target price for the cost per kilometre is estimated in subsection 3.4.2. The fuel consumption and CO_2 emission of MAINTAIN are the result of the final design. An elaboration on this characteristics can be found in chapter 12 and chapter 21 respectively.

Table 3.2: Characteristics of different pipeline inspections systems.

System	Unit price [USD][14]	Costs [USD/km]	Coverage per day [km]	Fuel consumption [l/km]	CO_2 emission [g/km]	Accessibility
Helicopter	1,800,000 [15]	83.33 (LaSen 2007)	580[16]	0.616[17]	1500[18]	High
MAINTAIN	TBD	TBD	1000	0.0205	11.8[18]	High
Walking detection	23,000	8[19]	16	-	-	Low
Ground vehicles	2,000 [20]	3 (Mohammadian 2006)	160	0.1337 [21]	305[22]	Low

Table 3.3 displays different UAVs configurations that have one or several similar characteristics as MAINTAIN. Purely based on performance, the MQ-1 Reaper is better than MAINTAIN, but the high price prevents it from being a real competitor. Although the Penguin C, Vanguard, Pegaz and RQ-7 Shadow have either similar payload capacities or endurance their range is much more limited than MAINTAIN. This feature is specifically important when inspecting gas pipelines. The Puma AE is already used by Britisch Petroleum (BP) for their Prudhoe Bayfield in Alaska, but it has lower endurance, range and payload weight[23]. Therefore, MAINTAIN is a UAV with unique features that has a strong competitive advantage over other UAVs.

[14] Unit price of the vehicle including the equipment
[15] `https://www.globalsecurity.org/military/systems/aircraft/b206.htm` [cited on: 25-06-2018]
[16] `http://www.lasen.com/services.aspx`[cited on: 01-04-2018]
[17] `http://www.deltahelicopters.com/bell206b.html`[cited on: 16-05-2018]
[18] See section 21.3
[19] `https://www.payscale.com/research/US/Job=Utility_Locator/Hourly_Rate`[cited on: 01-05-2018]
[20] `https://us.vwr.com/store/product/21468682/gas-leak-detection-systems` [cited on: 26-06-2018]
[21] `https://www.nrcan.gc.ca/sites/www.nrcan.gc.ca/files/oee/pdf/transportation/tools/fuelratings/2018FuelConsumptionGuide.pdf` [cited on: 16-08-2018]
[22] Calculations are made on the molecular combustion reaction.
[23] `https://www.bp.com/en/global/corporate/bp-magazine/innovations/drones-provide-bp-eyes-in-the-skies.html` [cited on: 01-05-2018]

Table 3.3: Characteristics of different UAVs.

UAV	Purchase price [USD]	Range [km]	Endurance [h]	Cruise altitude [m]	Payload weight [kg]
MAINTAIN	TBD	>1000	>20	>300	68
Penguin C [24] [25]	50,000	100	>20	4500	5
MQ-1 Reaper [26]	16,900,000	1850	14	7500	1700
Vanguard [27] [28]	45,000	35	1.57	4500	2
Pegaz [29]	600,000	100	12	3000	40
RQ-7 Shadow [30]	1,400,000	109	6	-	45
Puma AE [31]	-	20	3.5	152	<5.9

3.4.2. Target Price

The determination of a price per kilometre for the MAINTAIN system is not a very straightforward process. This is due to the different preferences of the clients. There are clients that attach great value to the accessibility whilst others purely look at cost. To penetrate the greatest part of the market, **the target price for MAINTAIN per kilometer is 20 USD**. This price includes the purchase price and operational cost. This attracts clients that usually hire a helicopter, and are now incentivised to use MAINTAIN, because of the lower price and higher range. Furthermore, clients that use ground based systems can be tempted to switch to MAINTAIN due to its relatively low cost, high speed and long-endurance. Other benefits of MAINTAIN are good accessibility, relatively low fuel consumption and relatively low CO_2 emission.

In order to estimate a selling price of MAINTAIN, data from Table 3.3 is used to generate a cost estimation function, taking into account the selling price of different UAVs having different payload masses and propulsive power. This function was set up using multivariable regression, leading to a unit **selling price estimation of 2 $\pm$ 1 million USD**. The entire process can be found in (B. van Beurden et al. 2018b) which is a separate chapter on multivariate regression analysis.

3.5. Future Markets

After the penetration of the gas pipelines surveillance market, the designed UAV could be used for different applications. Therefore different market segments can be entered. This section elaborates on an expansion in the current market segment and the penetration of other segments.

The first market segments that is accessed is the oil pipelines surveillance market in the USA. This market segment is closely related to the initial market segment. Since this market is subjected to the same UAV-regulations only minor adjustments, such as the payload, have to be made to the UAV and the marketing strategy to penetrate the oil pipeline inspection market. The size of this market can be evaluated using the total amount of oil pipelines in the USA. In the USA 240,711 km oil pipelines is installed. Using the same conversion as in section 3.3, oil pipeline inspection in the USA has a market size of 7 UAVs.

Furthermore, adjustments to the UAV can be made such that it obeys the legal and airworthiness regulations of countries other than the USA. Using Table 3.1, this will result in another potential market of 30 UAVs for monitoring gas pipelines world wide. As can be seen in Figure 3.2 and Figure 3.3, the global drone market will increase in size and will be worth more than 12 billion USD by 2024. The long-range and long-endurance characteristics are mostly applicable in the energy and government sector which also show steady growth until 2022, as shown in Figure 3.2. Therefore, entering the market segment of general long-range, long-endurance drones is a very interesting market. The proof of concept of the micro gas turbine drone in the pipeline inspection market will help in the transition to the general drone market. Additionally, after proof of concept, micro gas turbines can be useful in other applications like range extension for electrical vehicles, domestic heating that also produces electricity and as power unit and heater for trucks, as the battery capacity of trucks becomes insufficient as result of the increasing energy demand of the truck's electrical systems[32].

[24] http://www.uavfactory.com/product/74 [cited on: 30-04-2018]
[25] https://medium.com/@UAVLance/11-high-end-drone-models-46dafcf69aba [cited on: 30-04-2018]
[26] http://www.af.mil/About-Us/Fact-Sheets/Display/Article/104470/mq-9-reaper/ [cited on:30-04-2018]
[27] https://justdrones.com.au/vanguard-by-airborne-drones/ [cited on: 30-04-2018]
[28] https://www.airbornedrones.co/wp-content/uploads/2017/10/Vanguard_Brochure-1.pdf [cited on: 30-04-2018]
[29] https://www.airforce-technology.com/projects/pegaz-tactical-unmanned-aerial-vehicle-uav/ [cited on: 01-05-2018]
[30] https://www.army-technology.com/projects/shadow200uav/ [cited on: 01-05-2018]
[31] http://www.avinc.com/images/uploads/product_docs/PumaAE_Datasheet_2017_Web_v1.1.pdf [cited on: 01-05-2018]
[32] https://www.mtt-eu.com [cited on: 03-05-2018]

4
Risk Assessment

Although a market study gives insight in the economical feasibility of a project, there is always risk associated with the research and development of a system as MAINTAIN. Identifying risks and addressing them in the preliminary design phase can prevent major complications in further design phases. Such an assessment is based on the probability of occurrence and the severity of the consequences associated with each risk. Various risk analysis tools can be implemented to effectively mitigate risks. The midterm report focused on the general risks associated with a flying wing (B. van Beurden et al. 2018a). This chapter elaborates on the risks that originate from different subsystems that are part of MAINTAIN. section 4.1 identifies the risks of the individual subsystems of the MAINTAIN project. After the identification, the necessary risk mitigation procedures are described in section 4.2. For both the initial, as the posterior situation, a risk map is generated, which show the changes in probability and severity. These risk maps are documented in section 4.3.

4.1. Risk Identification

An effective manner of identifying the risks of a system is performing a SWOT analysis, after which the weaknesses and threats are reformulated as risks. The technical risks of the subsystems are defined as all possible events that can occur on a subsystem level that could jeopardise the mission. The mission of MAINTAIN is successful if all gas leakages are detected and this information is properly forwarded to the customer. Every risk is appointed a certain probability and severity as described in Table 4.1. Table 4.2 illustrates the different mitigation procedures that can be applied(Garvey 2008) after the probability and severity are determined.

In Table 4.3, the risks that result from the SWOT analysis are summarised with their accompanied probability, severity and risk mitigation procedure. To elaborate on Table 4.2; there are two types of mitigation procedures which have a direct effect on the probability and the severity. The avoid strategy mitigates the probability of occurrence and the control strategy minimises the impact of the risk. If desired, both methods can be applied simultaneously. The monitor mitigation procedure essentially means that extra precaution is taken in design decisions that affect a risk that is being monitored, but no concrete contingency plan is formulated. That extra precaution can express itself in for example extra safety margins, extensive analysing/testing or regular inspections. However, when during monitoring a risk increases in likelihood or the severity of consequences, an active risk mitigation plan can still be generated.

Table 4.1: Scale for different levels of probability and severity.

Probability	**Severity**
Almost impossible (AI)	Negligible (N), Non operational impact
Unlikely (U)	Marginal (M), Degradation of secondary mission
Somewhat likely (SL)	Critical (CR), Mission success questionable
Likely (L)	Catastrophic (CA), Mission failure
Very likely (VL)	

Table 4.2: Risk mitigation procedures with accompanied identifiers and definitions.

Risk Mitigation Procedure	**ID**	**Definition**
Assume/Accept	At	Risk is known, no effort to control it.
Avoid	Av	Adjust design constraints to reduce/eliminate risk.
Control	Ct	Implement actions for risk mitigation.
Transfer	Tf	Reassign risk to other stakeholder.
Watch/Monitor	Mo	Monitor environment risk.

Table 4.3: Identified concept-specific risks accompanied by their individual probability (P) and severity (S). A map ID is added to each risk to clearly indicate the risks in the risk map. A general risk mitigation procedure is appointed for each risk in the right column (RMP).

Risk	P	S	Map ID	RMP
Propulsion				
PRO-1 Insufficient power or thrust produced	SL	CR	A1	Mo
PRO-2 Thermal efficiency MGT engine insufficient	L	CR	A2	Av
PRO-3 Flow chokes in engine	U	CR	A3	Mo
PRO-4 Power transmission from shaft to propeller fails	U	CA	A4	Mo
PRO-5 Propeller efficiency below expectations	L	CR	A5	Av
PRO-6 Propulsion system experiences compressor stall or surge	U	CR	A6	Mo
PRO-7 Propulsion system turbine inlet temperature limit is exceeded	SL	CR	A7	Mo
PRO-8 Ambient conditions cause under performance of engine	L	M	A8	Mo
Structures and Materials				
STR-1 Skin of UAV buckles	SL	MA	B1	Mo
STR-2 The structure deforms and influences aerodynamics	VL	MA	B2	Mo
STR-3 The stringers fail under the bending load	UL	CA	B3	Mo
STR-4 Loads induced by in flight maneuvers cause the structure to fail	UL	CA	B4	Mo
STR-5 Materials cost exceed budget	SL	CR	B5	Tf
STR-6 Components cannot be assembled or formed	L	CR	B6	Av, Ct
STR-7 Skin fracture or delamination due to rivet spacing	L	CA	B7	Ct
STR-8 Cycle load leads to fatique failure during operations	L	CA	B8	Av,Ct
Telecommunications				
COMM-1 Connection with ATC or ground unit fails	VL	CR	C1	Av, Ct
COMM-2 Data downlink or uplink rate is insufficient	L	CR	C2	Av, Ct
COMM-3 Signal ambiguity due to noise	SL	CR	C3	Av, Ct
COMM-4 Ground system or UAV has power outage	L	CA	C4	Av, Ct
Payload				
PL-1 Gas leakage is not detected	VL	CA	D1	Av, Ct
PL-2 Payload weight exceeds payload carrying capacity	L	CA	D2	Av, Tf
PL-3 Payload destroyed due to impact	U	CA	D3	At
PL-4 Payload cost unfeasible	SL	CA	D4	Tf
PL-5 Weather imposes conditions in which the payload does not perform	L	CA	D5	Av
Aerodynamics and Stability				
AES-1 The eigenmotions are not stable	VL	CR	E1	At, Av
AES-2 High parasitic drag	U L	CR	E2	Mo
AES-3 Lift over drag ratio insufficient	SL	CR	E3	Mo
AES-4 Inaccurate estimation of aerodynamic properties due to software limitations	VL	MA	E4	Mo
AES-5 C.g. range yields instability	UL	CA	E5	Mo
AES-6 Wind gusts causes instability	SL	CA	E6	At/Ct
AES-7 Wing stall	UL	CA	E7	At
AES-8 Flutter and divergence instability	AI	CA	E8	At
Navigation and Position Control				
NPC-1 INS failure, position is not measured accurately	L	CR	F1	Av
NPC-2 Human pilot makes mistake while manually operating UAV	SL	CR	F2	At
NPC-3 Control surfaces become uncontrollable	UL	CA	F3	Mo
NPC-4 Miscommunication with ATC	SL	MA	F4	Mo
NPC-5 Wrong flight route is inputted to UAV	L	CA	F5	Av
Electrical Subsystems				
ELEC-1 CPU overheats	SL	CA	G1	Av, Ct
ELEC-2 Memory full due to long connectionless period and thus no data transfer	UL	CR	G2	Mo
ELEC-3 IR Camera failure	UL	CR	G3	Mo
ELEC-4 Imaging Camera failure	UL	CR	G4	Mo

4.2. Risk Mitigation

In the previous section, all risks have been assessed with regard to their probability and severity of occurrence. As can be seen, there is a variety of risks with either high severity, probability or a combination of both. These risks require active risk control and therefore the mitigation strategies to avoid or minimise the consequences of these risks are described in this section. For every high risk that is predicted, a brief explanation is provided and a mitigation procedure is proposed.

PRO-2 (A2) : The thermal efficiency of an engine is the ratio of work output over energy input. For the MAINTAIN vehicle, the output is the shaft power and the input is the fuel energy. Due to the limitations of a MGT engine described in chapter 2, the thermal efficiency of a MGT is generally lower than a regular size gas turbine. For that reason, it is desired to minimise the loss in thermal efficiency while the engine is being downscaled. The risk that the thermal efficiency is insufficient has to be mitigated by means of avoidance. This can for example be realised by research into new materials that can operate at a higher TIT, development of manufacturing tools with a smaller error margin and optimisation of compressor and turbine efficiency. However, after implementing these measures, it is still impossible to match the thermal efficiency of conventional size gas turbine engines. The severity of the reduction in thermal efficiency is not controllable, which means that the loss has to be primarily avoided.

PRO-5 (A5) : The MAINTAIN system has an integrated turboprop engine, thus a propeller has to be designed in addition to the gas turbine. If the propeller efficiency is not as excepted, more shaft power and hence more fuel is needed to produce the desired amount of thrust. This can result in mission failure if the fuel consumption is excessively higher than predicted. The mitigation strategy is again avoidance, so a reduction in the probability of occurrence. The best way to do this is to fully test and analyse each propeller, but since this is not very resource efficient, a quality control protocol can be established in which all important its parameters can be quickly checked. Once a propeller is attached to the UAV, nothing can be changed on its efficiency except replacing the old propeller with one that has the actual desired properties.

STR-6 (B6) : The structural framework of MAINTAIN will consist of a variety of components, of which all need to be compatible with each other to ensure a successful assembly. To reduce the risk of incompatibility of different components, communication is key. The lines of communication should be well defined and every individual working on a component knows to whom he or she should listen and report. Furthermore, an expert in the field of manufacturability should be hired and he should construct a manufacturing plan together with the heads of the other engineering department. This manufacturing engineer ensures that the chosen strategy and materials are feasible. Nonetheless, if incompatibility is discovered the expert should immediately be notified and a reflection on his miscalculation is to be made, together with a new manufacturing plan. Consequently, all other manufacturing processes are to be put on halt.

STR-7 (B7) : To assemble the various components of the UAV, the use of rivets is usually inevitable. The high loads on rivets can cause a fracture in the aircraft skin. For this risk, both the severity and the probability can be reduced. To prevent a fracture a safety factor of 1.5 is to be applied in the computation of the rivet spacing. Furthermore, inspection of the skin is to be performed to regularly monitor the fractures in the skin. If the crack size exceeds a specific limit, maintenance has to be performed.

STR-8 (B8) : Cycle load failure is perhaps a less obvious structural failure mode than the previously described risk. However, it is of utmost importance to take this into account. Failure occurs often due to the many load cycles applied to the structure. To prevent incidental fractures, a test rig can be prepared that can simulate loading cycles, which provides insight in the amount of loading cycles that the structure can bear. In order to monitor this event, an inspection interval can be computed at which investigation of cyclic load failure is to be performed. If cycle load failure occurs, there are no reasonable mitigation measures to control its impact, thus the above mentioned mitigation strategy is implemented to solely reduce the probability of occurrence.

COMM-1 (C1): The connection between the UAV and the ground unit is important for UAV control and data transfer. If this connection is lost, no data can be transferred and hence, the mission success is in jeopardy. Besides, contact with the ATC can be lost which would invoke a dangerous situation with regard to landing and take-off procedures. To prevent loss of communication with the UAV, the telecommunication subsystem has to use two separate communication channels. Initially, one channel is utilised for position control and the other for data transfer. In case of failure of one channel, there is still another channel available for control, so that the UAV can land as quickly as possible for inspection and maintenance. Having redundancy in communication lines means that the probability of this risk is mitigated. Finally, an autopilot system should be implemented in the UAV which can land the UAV completely autonomous based on the pre-programmed flight plan. In case of communication loss with the ATC while cruising towards the airport to land, the UAV has to loiter near the airport until connection is restored. If the connection cannot be restored, a subsidiary landing site has to be found by the ground crew and an emergency landing has to be conducted. To minimise the probability of occurrence, the ground crew has to perform pre-flight radio checks.

COMM-2 (C2) : Data transfer is a key element of the mission. An insufficient data rate results in a delay of data processing and can additionally result in loss of data. To prevent data loss, enough memory has to be available to ensure that all the

data acquired during one test flight can be stored and later extracted at the landing site. This is an extreme scenario which occurs if data transfer is near to fully impossible. To prevent an insufficient data rate, a safety margin of 1.5 has to be applied to the expected maximum data rate which would consist of data from payload and the data associated with the control of the UAV. Moreover, the data which is stored when peak data transfer occurs, can be transferred at later stage, if not the entire downlink or uplink rate is utilised. This is for example in the mission phase where the UAV is cruising back to the landing site from the gas pipelines.

COMM-3 (C3) : Next to the availability of data transfer and the data rate limitation, there is also the quality of the data that has to be taken into account. Data quality is dependent on the amount of noise that interferes with the data to be acquired. To minimise the influence of noise and thus the probability of low quality data, a high signal-to-noise ratio (SNR) has to be obtained for the MAINTAIN system. A high SNR is accomplished with for example an increment in antenna gain and power. Additionally, methods such as a Kalman filters can process and amplify the quality of the data before it is further analysed which minimises the severity and probability of this risk.

COMM-4 (C4) : Another important aspect for data transfer is the power available for transmission. Without power, no transmission would be possible. A battery is used for energy storage, which is charged during the flight by extracting power from the propulsion system. To avoid the problem of a power outage, the UAV battery has to be checked before every flight. Furthermore, to minimise the consequences, the UAV implements redundancy for its batteries meaning at least two units are integrated. So in case if failure of the first battery, the second battery will take over the role of the first battery. For the ground station, an emergency power generator has to be present in the control unit centre to overcome the event of a power outage.

PL-1 (D1) : The goal of MAINTAIN is to monitor gas pipelines and detect gas leakages, thus the inability to detect gas leakages results in direct mission failure. To minimise the probability, the payload has to produce data of the highest possible quality. This data quality is affected by the weather conditions, the stability of the camera and the measurement method of the payload itself. To improve the stability, a gimbal can be applied. If the payload has intrinsic stabilising components, the stability of the UAV itself can be improved by modifying the stability derivatives. Further mitigation will be done by future technical resource allocation in developing deep learning algorithms that can accurately extract the minor shifts in monitored strain fields. The consequences of this risk can be mitigated by inspecting each pipeline on a regular basis and therefore decreasing the period in which a gas leakage remains undetected.

PL-5 (D5) : As mentioned above, weather can severely affect the quality of the data. Since the gas pipeline network covers a large part of the United States, MAINTAIN has to operate in a variety of weather conditions, thus a payload with a large operable range of weather conditions is favourable. Besides the payload selection, flight routes are to be optimised with respect to weather conditions and payload capabilities. The severity of the consequences can again be minimised by performing inspections on a regular basis. Moreover, earlier obtained data can be analysed, which can be used to discover whether there is a relation between certain data elements and gas leakages. A ground crew can perform inspections in critical locations where the weather conditions cause inoperability of the payload.

AES-1 (E1) : Eigenmotions describe the reaction of an aircraft to an input while it is in a steady flight. Unstable eigenmotions yield intrinsic dynamic instability, which should therefore be avoided. The eigenmotion characteristics are found with the stability derivatives which follow from the aerodynamic analysis. The object oriented design method of MAINTAIN enables the possibility for extensive design iterations, so once a design is complete and the eigenmotions are not satisfactory stable, design variables have to be adapted until they yield a dynamically stable configuration. An unstable spiral eigenmotion, however, is very common and acceptable.

NPC-1 (F1) : The position of the UAV is a parameter which has to be known at all times. If the position is not measured accurately, incorrect data will be provided to the customers, possibly including faulty locations of gas leakages. To avoid these inconveniences, the position determination system is using decoupled sensors. On the one hand, the position of the system is determined by GPS and an altimeter, on the other, the starting position of the UAV in combination with inertial measurements compute the position. Both positions are compared and based on algorithms and statistics, the most accurate position is provided. It is complicated to mitigate the severity of an inaccurate position. However, it should be taken into account while computing error margins in the data for the customer.

NPC-5 (F5) : The UAV operates based on a flight plan that is programmed prior to the flight mission of the UAV. It is likely that during its operating life, an incorrect flight plan is assigned to a vehicle. This will directly yield a mission failure, since the wrong coordinates are inspected. Such circumstances can be avoided by having the flight plan inspected by multiple operators before take-off. The mitigation of the consequences of this risk is rather straightforward, as the ground crew has to assign the correct flight plan the the UAV.

ELEC-1 (G1) : The last risk for which a mitigation plan is described is the risk of the CPU overheating. Although this risk is qualified as somewhat likely and catastrophic and thus not situated in the red area, it seen as a critical combination of probability and severity. Failure of the CPU will result in failure of many other subsystems and therefore, it is decided upon to elaborate on the mitigation strategy. To prevent the CPU from overheating a cooling fan is installed near the CPU.

Furthermore, the required processing capabilities have to be thoroughly analysed and a safety margin is to be assigned. Furthermore, a watchdog timer is integrated in the CPU which resets the processor in case of overheating.

4.3. Risk Maps

At this stage, the risk is assessed on a subsystem level. A convenient tool for monitoring and adapting to the risk of a project is a risk map. The structure of the map is rather self-explanatory, where the top right corner indicates the risks that deserve most attention. If an avoidance mitigation measure is performed, the probability decreases and shifts the indicator downward. Conversely, using a control mitigation measure, one can shift the severity of the risk to the left. For an innovative project such as MAINTAIN, risks are generally high due to the complexity and design maturity of the the concept. For that reason, there remains a number of risks in a relatively high risk scale, which emphasises the importance of risk monitoring.

Initially, using the information from Table 4.3, a risk map is constructed. The results are showcased in Figure 4.1. Following this, a posterior risk map, which has integrated the above mitigation measures, can be generated. The posterior risk map is depicted in Figure 4.2. It is evident that after mitigation, risk of a gas leakage remaining undetected is still situated in the red area. The entire mission is based on the continuous inspection of pipelines. **Although the probability and severity of this event can be reduced to a certain extent, it is reasonable to assume that there are always gas leakages that are not detected with a single coverage**. Furthermore, even though risks decrease in likelihood and severity of consequences after mitigation, in some cases it is not enough to assign the risk to a different level in the scale.

Probability					
	Very Likely		B2, E4	C1, E1	D1
	Likely		A8	A2, A5, B6, B7, C2, C3, F1	B8, C4, D2, D5, F5
	Somewhat Likely		B1, F5	A1, A7, B5, E3, F2	D4, E6, F4, G1
	Unlikely			A3, A6, E2, G2, G3, G4	A4, B3, B4, D3, E5, E7
	Almost Impossible				E8
		Negligible	Marginal	Critical	Catastrophic
		Severity			

Figure 4.1: Risk map of the subsystems of MAINTAIN.

Probability					
	Very Likely		C1, B2, E1, E4		
	Likely		A2, A8, B8	D1	
	Somewhat Likely		B1, B7, C2, C3, F5	A1, A7, B5, E3, F1, F2, F6	D2, D4, D5, E6, F4, G1
	Unlikely		C4, B6	A3, A5, A6, E2, G2, G3, G4	A4, B3, B4, D3, E5, E7
	Almost Impossible				E8
		Negligible	Marginal	Critical	Catastrophic
		Severity			

Figure 4.2: Posterior risk map of the subsystems of MAINTAIN.

5
Operations and Logistics

So far, the feasibility of the project is studied, in combination with an early identification of the associated risk. In order to become acquainted with the structure of the mission to be performed, it is of utter importance to investigate the legislation and the logistical framework in which the system is operating. This analysis provides the design team with top level decisions, influencing the conceptual design of the vehicle. In this chapter, the operations and logistics that are relevant for MAINTAIN are discussed. The logistical and operational backbone of MAINTAIN significantly influence the return on investment and therefore the success of the project. In section 5.1, the operational flow of the UAV is explained. Then, the regulatory framework in which MAINTAIN operates is elaborated upon in section 5.2. Following the regulations, section 5.3 explains the logistics with regard to the airports.

5.1. Operational Flow

After the initiation of the system, an extensive part of the mission is continuously providing the service. The operation of MAINTAIN consists of several parts. Focusing on the operation types of the mission, a distinction can be made between the contributors. The flow diagram below visualises the activities that are part of the mission. Additionally, the different types of crew members are indicated in the figure.

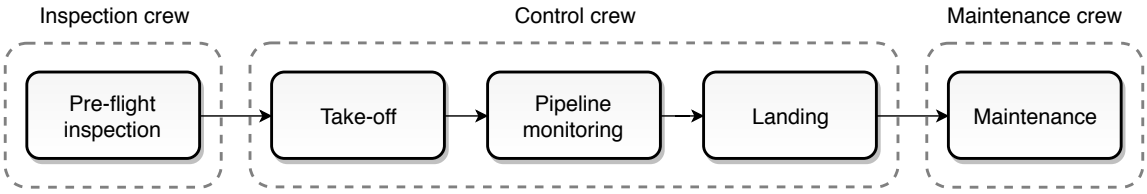

Figure 5.1: Overview of the operational life.

As can be seen in Figure 5.1, there is a division between the different operators. **The inspection crew is responsible for everything related to the pre-flight inspections, the control crew is responsible for everything between take-off and landing and lastly, the maintenance crew takes care of the maintenance activities.** At an earlier stage, in the Midterm Report (B. van Beurden et al. 2018a), each phase is elaborated upon in detail.

5.2. Regulations

The operation of an aircraft always has to be conform the regulations that are provided by authorities. A regulatory framework is necessary to ensure the safe operation of UAVs. To do this, UAVs are classified based on their mass. There are three classes relating to weight as discussed in the Midterm Report (B. van Beurden et al. 2018a). From the Midterm Report (B. van Beurden et al. 2018b), an MTOW of 191 kg is expected; thus classifying MAINTAIN in the highest class (MTOW > 25kg).

At the moment, regulations are continuously changing and are not standardised per country, not even per state level. This fact makes it quite challenging for MAINTAIN to be operable in all states of the United States. The problem with being situated in the highest weight class is that the certification procedure is not yet established. After doing an investigation into the FAA regulation, it was found that MAINTAIN will fall under the part 23 regulation, which is also used for the certification of small aircraft. In Figure 5.2, one can find the certificates which are required before MAINTAIN can start its activities.

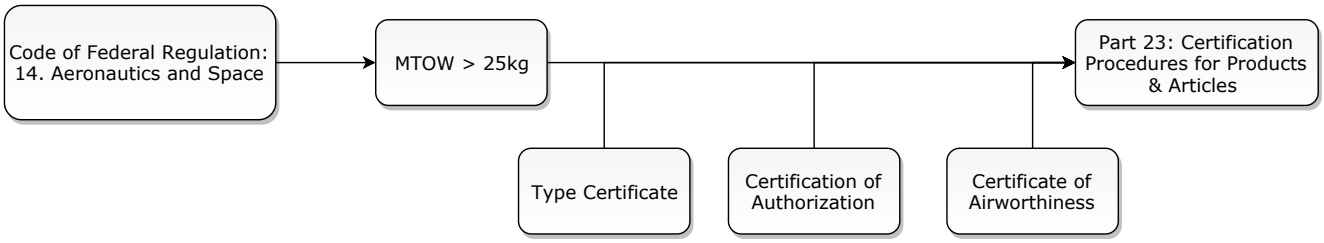

Figure 5.2: Regulatory framework in the United States.

5.2.1. Part 23: Normal, Utility, Acrobatic and Commuter Airplanes

From Figure 5.2, it is clear that within the Code of Federal Regulation (CFR), Chapter 14 is addressing the regulations on Aeronautics and Space. Within these Chapter 14 regulations, Part 23 specifies the regulations for normal category aircraft. The definition of a part 23[33] aircraft is as follows:

Certification in the normal category applies to airplanes with a passenger-seating configuration of 19 or less and a maximum certificated take-off weight of 19,000 pounds or less.

It is expected the the final UAV regulations will be very similar with this Part 23, that is why it is decided to base the current design on these regulations.

5.3. Airport Logistics

Narrowly related to the operations of the system are the logistic affairs that are part of the usage of airports. In this section, the airport logistics is discussed. Since The United States consist of more than 14,000 airports, it logically follows that not all airports will be provided with fuel and a ground crew for maintenance in order to reduce operational costs. An analysis is performed using several algorithms to generate a selection of these airports, minimising the multiplicity while still guaranteeing smooth operations. The first algorithm eliminated a range of airports, for which the reasons are stated below.

- Airports that are not illuminated, since the UAV should be able to land during nighttime.
- Airports that are not in use anymore.
- Airports that have a runway length shorter than 1374 feet, as determined in the Midterm Report(B. van Beurden et al. 2018a).
- Airports that have a runway width smaller than 50 feet, since this should be bigger than the wing span multiplied by a safety factor of 1.5.
- Airports that are not small or medium sized by definition.
- Airports that do not have a concrete or asphalt runway surface.
- Airports that do have a scheduled service.
- Airports that have an elevation higher than 9000 feet, since the pipelines are not installed above that.

This reduces the amount of feasible airports to 3076, which is still too much. Hence, another algorithm was created to select an optimal amount of airports out of those feasible ones. Essentially, this algorithm placed a mesh of 200 km by 200 km over the United States and only kept the most central airport per cell if there was an airport in that specific mesh. That way, it was guaranteed that the airports were enough spread out across the US. **After this, 189 airports were kept.** The remaining airports are visualised in Figure 5.3.

[33] `https://www.ecfr.gov/cgi-bin/text-idx?SID=685dc1ae97ae3f5e5569e47880fab01e&mc=true&node=pt14.1.23#se14.1.23_12000` [cited on: 24-05-18]

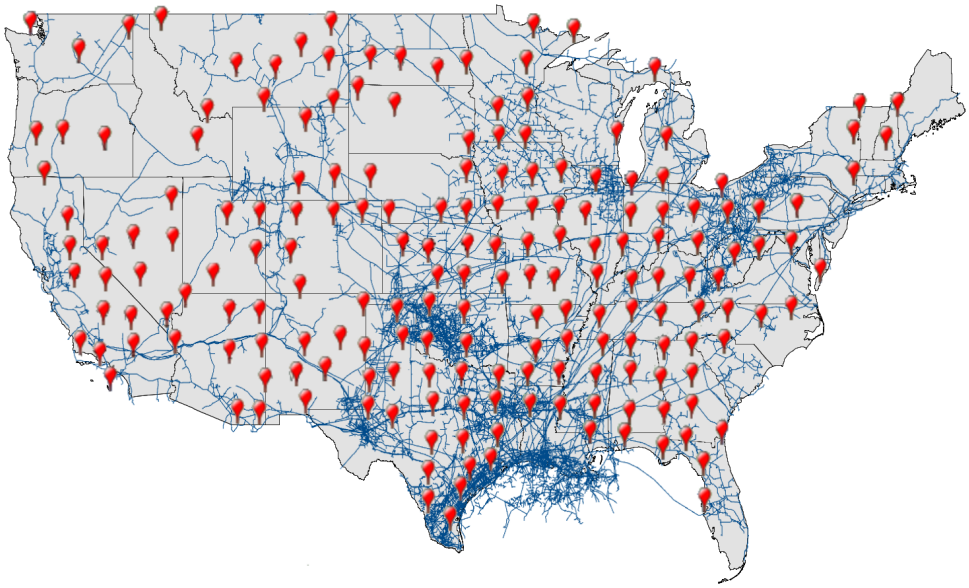

Figure 5.3: Feasible airports.

From Figure 5.3, it is clear that the airports are well spread out across the US mainland. It is remarkable that the airport density in the North-West corner is less than at the rest of the country. However, this will not cause operational problems as in that area there are much less pipelines because of the Rocky Mountains range. Therefore less airports are situated and needed in that region.

Now that the operational airports are determined, the logic behind the mission planning for refuelling and maintenance can be set up:

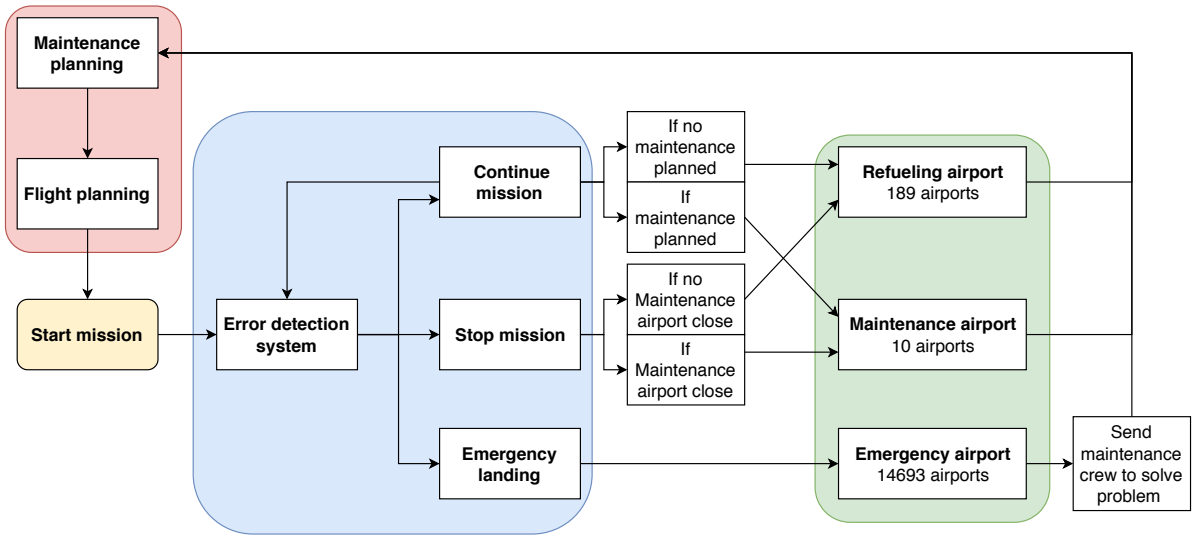

Figure 5.4: Mission planning logic.

From Figure 5.4, one can see that the maintenance and flight planning are of utter importance before the start of the mission. The flight planning should be optimised such that the landing airfield is chosen which covers the most amount of pipelines while minimising the distance between the airport and the pipelines. Furthermore, the maintenance planning should be kept in mind as there will be only 10 airports across the US which have a ground crew available for maintenance, to reduce operational cost. If there would be an emergency, the UAV is capable to land on any runway which is closest by. A ground crew will be sent to that airport to repair, recover and refuel the drone. If the problem would be too severe such that it cannot be repaired at that airport, a carrier will be available to transport the UAV to the closest maintenance airport.

6 Ground Segment

When visualising an unmanned aerial system, one often envisions the vehicle itself. The ground segment however, is a major and vital component of the system. The function of the ground segment is to support the vehicle in all its operations. The ground segment will be divided in a control element and airport operations. The control of the vehicle in mainly performed during operation of the vehicle and is performed remotely from the vehicle. The airport operations will be executed before and after flight and concern the hands-on work that needs to be performed on the vehicle. The data analysis will also be performed remotely of the vehicle and is therefore executed in the control element. The control element of the unmanned aerial system is presented in section 6.1. Additionally, in section 6.2, the airport ground operations are discussed.

6.1. Control Element

The control element of the ground segment is involved in the direct control of the unmanned aerial vehicle when it is operational. It should be noted that the control element can be capable of controlling multiple drones simultaneously. This section discusses the different aspects of the control element that will be considered for the design of the control element. First, the crew of the ground element will be determined and afterwards the configuration of the control element will be discussed.

6.1.1. Control Element Crew

The size of the control element crew required to perform the mission is dependent on the tasks that need to be satisfied to operate the aerial vehicle. Several functions of the control element that are of importance for the mission are found to be(Gundlach 2014):

- **Vehicle operation:** This concerns giving commands to the vehicle during take-off, flight operations, landing and ground operation. The operation of the vehicle also includes anticipating on the current weather conditions by adapting the route or aborting the mission and landing at the closest airport.
- **Mission planning:** This involves creating a mission plan prior to the launch of the vehicle. A mission plan consists of a planned route that uses a number of waypoints. This requires making estimates of the capabilities of the vehicle at different stages of the mission such as remaining fuel, maximum available rate of climb and descent and minimum turn radius. Furthermore, mission planning also involves having knowledge about the operation environment, such as weather, elevation, political boundaries or restricted airspace. When the mission planning is done, the planned route will be communicated to air traffic control.
- **Communication:** This involves processing information from outside the system boundaries and anticipating by e.g. diverting from the planned route. Another important part of this function is communicating with air traffic control during take-off and landing.
- **Payload control:** Payload control concerns supervision of the operation of the payload during flight and real time processing and storage of the data. Furthermore, the payload control includes forwarding relevant data to the customer.

The vehicle operation and communication take place during the operational stage of the vehicle. The mission planning will happen before operation of the vehicle. Furthermore, the payload will be operated during flight.

Looking at the tasks that need to be performed, one can see that when multiple drones need to be operated the most critical stage of the operation for determining the size of the control element crew will be the operation of the vehicle. During this stage of the mission most functions of the control element need to be performed, namely the vehicle operation, communication and payload control shall be performed. Since the predominant task of the communication is consulting air traffic control and the predominant task of the payload control is the operation of the payload, these functions can be performed simultaneously by a single person as these tasks are not performed simultaneously during a mission. **For this reason it is determined that the control element crew will consist of two persons.** During flight one person will be in charge of vehicle operations and one person will be in charge of communications and payload control. Both before and after the flight, the two manned crew can work together on the mission planning and data processing. It

should be noted that since the system should perform approximately 20 hours each day and the control element shall be capable of operating the vehicle at any hour of the day, the operation of the vehicle shall be performed in multiple shifts where a similarly configured crew shall alternate between different time slots. On every day of operation, four eight hour long shifts will be sufficient to provide a crew at any hour of the day and leave enough time to prepare the mission and process the data.

6.1.2. Control Element Configuration

The configuration of the ground element can be different for different types of unmanned aerial systems. Small vehicles can be operated by a portable device and line of sight control, whereas vehicles with a larger range require a more elaborate control element to guide the vehicle with more subsystems. Below, possible configurations for the control element are listed(Gundlach 2014).

- **Remote viewing terminal:** A portable device that allows the operator to view the payload data and provides the ability to control the vehicle.
- **Portable ground control element:** A portable device that allows the operator to view payload data and a display with the view from the vehicle. Furthermore does this control element allow for control of the vehicle.
- **Forward ground control element:** Is usually part of a hub and spoke network. This control element operates the vehicle within a specific region outside of the hub, but does not provide take-off and landing operations in the hub region.
- **Line-of-sight ground control element:** Does not provide information to the operator, but only provides the ability to control the vehicle. The decisions made by the controller shall be purely based on their own observation of the vehicle.
- **Launch and recovery element:** These primarily provide take-off and landing operations. Often launch and recovery elements are used in a hub and spoke system in combination with a forward ground control element. Usually these control elements are situated near airports and use line of sight communication.
- **Mission control element:** A mission control element is a station that provides control of the vehicle by using satellite connections. This is typically a workstation located outside of the operational event. This simplifies the logistics of the control elements compared to line of sight control elements.
- **Tasking, processing, exploitation, and dissemination element:** This is a collection of the tasks performed by the mission control element and the processing of the data of the payload of multiple vehicles. This type of control element is generally used in combat situations where a multitude of ground stations is used and where all available information needs to be combined instantaneously to determine the advancements in the mission. This configuration of the control element uses multiple mission control elements and a combined air operations centre.

Aside from these configurations, options exist to place a control element in a moving vehicle such as a submarine or ground carriage. However, these are not considered for this mission as the velocity and large range of the vehicle make it impossible to keep the control element in close proximity to the vehicle. Furthermore do these mobile control elements require more personnel and do they also induce more cost compared to a grounded control system.

Due to the nature of the mission, some of the above mentioned control element configurations can be deemed to be unsuited for the MAINTAIN project. The remote viewing terminal and line-of-sight ground control element cannot be used as a line of sight cannot be provided during the entire mission. The forward ground control element and the launch and recovery element will not be suited for the mission as this will require a control element at each available airport driving the cost of the operations to an unrealistic extent. Reason for this is that emergency landings also need to be accounted for meaning that a temporary control element at both the take-off and landing locations is not sufficient. Furthermore, the tasking, processing, exploitation, and dissemination element will also drive the cost to a higher extent than necessary. This is due to the increased number of required stations for this configuration. Furthermore, real time processing of the data is not required for the mission as the mission plan is predetermined ruling out any advantages of this configuration.

The previous reasoning leaves two possible options for the control element: a portable ground control element and a mission control element. As the crew of the control element will be two-manned and a division between payload control and vehicle operation is made, a sophisticated system would be required. Besides the control of the vehicle other systems are required to perform communication, plan missions and monitor the weather. Furthermore, the communication to the vehicle will be performed using a satellite connection. Therefore, a portable control element will not yield any advantages. **For this reason, the mission control element is chosen as the configuration of the control element.** An overview of the flow of information within the control segment as well as the communication flow between the control segment and other parts of the unmanned aerial system can be found in chapter 8. A list of the required systems of the control segment based on the flow of communication is provided in Table 6.1.

Table 6.1: List of required systems implemented in the control segment.

System	Function
Communication system	Receiving, providing and processing data from and to the vehicle and the payload
Control system	Processing input of the operator and providing the vehicle with commands
Back-up control system	Providing redundancy for the control of the vehicle
Navigation communication system	Receiving and displaying the location of the vehicle
Data handling system	Processing and saving the mission data and providing it to the customer
Weather system	Forecasting the weather on the planned mission route

The communication of the ground segment will have a single channel for the vehicle and the payload since the vehicle only has a single communication channel. Furthermore, since the communication link between the vehicle and the ground segment is established through satellites, the required operational range of at least 5000 km will be met. Lastly, the data storage shall provide storage of the data of one week of monitoring. With a maximum data rate of 200 kb per second as explained in chapter 16, a storage of $200 \cdot 3600 \cdot 20 \cdot 7 = 101 Gb$ will be required to provide storage of a full week of monitoring data. Converting this to bytes will lead to a required storage capacity of 13 GB. Modern computers can easily store this amount of data several times, so this requirement will easily be met.

6.1.3. Integration of the Control Element

A single control element can be used to operate multiple vehicles simultaneously. Furthermore, operating a large number of vehicles will inevitably lead to the need of division of the workload over multiple control elements. When control elements will be present, planning and assessment of the overall mission will become more complicated. For this reason an assessment of the required personnel is made based on an evaluation of the tasks performed by the control segment. All the personnel involved in operating the control segment and their restrictions in terms of number of vehicles to be operated is listed below.

- **Control segment operators:** This consists of a two-manned crew as described above. This crew is able to simultaneously operate a maximum of four vehicles. When the unmanned aerial system exceeds the capacity of four vehicles per control segment crew, another crew shall be added to the system and consequently the capacity of the control segment shall be expanded.
- **Mission manager:** If more than two control segment crews are required to operate the vehicles, a mission manager shall be appointed to keep an overview of the project and control the quality of the mission. The mission manager will be responsible for meeting the mission requirements.

6.2. Airport Ground Operations

In this section, there will be elaborated on the airport logistics which are discussed in chapter 5. In total, 189 airports across the United States will be provided with bio-fuel tanks of at least 300 litres as stated in the requirements. From these 189 airports, 10 well-spread out airports will be serving as maintenance airports. First, the ground operations of the refuelling airports will be discussed and then the ground operations of the maintenance airports.

6.2.1. Refuelling Airports

As mentioned above, 189 airports will serve as refuelling sites. In Figure 6.1, an overview of the ground operations of such an airport can be found:

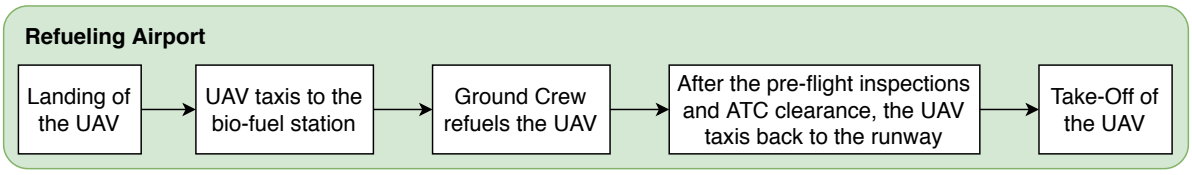

Figure 6.1: Ground operations of a refuelling airport.

It is important to point out that there is no necessity of a ground control group at the airports. The control group has as a matter of fact nothing to do with the airport operations groups. Since the UAV is remotely controlled, all the control operations (including the airport manoeuvres such as the taxiing for example) can be executed from the control station. So only a ground crew to refuel the UAV is needed as this cannot be done remotely yet. If there is an active refuelling service available on the airport, there is no need to send an extra crew to that concerned airport. The only thing to be kept in mind is that the bio-fuel stocks do not run out of supplies. If there is no active refuelling service available on the airport, MAINTAIN will provide a crew consisting of 2 persons per airport.

6.2.2. Maintenance Airports

Next, there are the maintenance airports. If an aircraft lands at a maintenance airport, either it is for maintenance or just for refuelling as these airports also serve as refuelling airports. These airports will be manned with a support crew that will ensure the maintenance activities of the several UAVs. It is important to mention that it is not required to conduct maintenance after every flight but only after a certain amount of flying hours or take-off and landing cycles as described in the Code of Federal Regulations, chapter 14 part 23 (U.S. government n.d.). A maintenance schedule will be made in order to make sure that the flying planning of the UAVs is such that the MAINTAIN UAV is close to a maintenance airport when the aircraft should have its maintenance. Also, it will be avoided that too much UAVs will need maintenance at the same time as this would be very inefficient because of long waiting lines.

The logical flow behind a maintenance airport is illustrated in Figure 6.2:

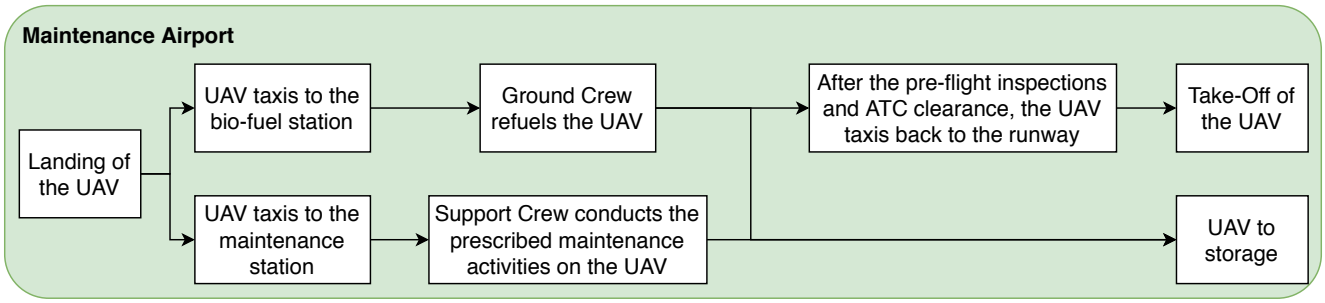

Figure 6.2: Ground operations of a maintenance airport.

The support crews responsible for the maintenance activities are estimated to consist of 5 persons per maintenance airport. However, this might change conform the maintenance schedule depending on the needs. MAINTAIN will provide the specialised crews on the airports in order to guarantee a safe operation. The maintenance airports are able to store the UAVs for a longer time if they won't be necessary for a while. The storage place should be kept as dry as possible in order to avoid corrosion. Hangars will be provided on these airports to store at least five UAVs. At refuelling airports, the UAVs are only able to stay for shorter periods.

7
Functional Analysis

The complexity of the MAINTAIN project requires the design to be performed methodically. In order to understand what the system should look like, all its functions should be clearly defined beforehand. This chapter contains a functional analysis of the system to be designed. This is relevant in order to decompose the overall system mission in sufficiently small functions as to enable subsystem design. Additionally, a proper functional analysis allows the designer to specify requirements in a more accurate manner. As (Romli 2013) alleges:"*Exploring the product's functional space provides more design freedom and appears to promote more innovative ideas*". Two systems engineering tools are employed to support the functional analysis, namely the functional breakdown structure, which is elaborated on in section 7.1, and the functional flow block diagram, which is explained in section 7.2. This is followed by a more in depth analysis of functions which need clarification in section 7.3.

7.1. Functional Breakdown Structure

It is convenient to start the functional analysis of the system constructing a Functional Breakdown Structure (FBS). This is an AND-tree, containing all functions the system has to perform to a certain level of accuracy. The sequence of the different functions is not visualised in the FBS. The main use of the FBS is "to create an exhaustive list of potential requirements which the architecture designers can use to evaluate the completeness of their designs" (Dehoff, Levack, and Rhodes 2009). Furthermore, after an architecture has been selected it "will allow the systems engineering activities to totally integrate each discipline to the maximum extent possible and optimise at the total system level, thus avoiding optimising at the element level" (Dehoff, Levack, and Rhodes 2009). In addition, for aircraft the required functions at system level determine to a large extent what subsystems are required; unnecessary subsystems should be avoided, mainly due to their added weight. The subsystems feed back into the system introducing constraints to the system level (Romli 2013). The FBS is shown in Figure 7.1. Six different main phases are distinguished: Setting up the system, turning it on, operation, checking the system's performance, turning off the system and maintenance. All phases are further explored in a second-level, and some functions are even broken down into third-level functions. In addition, a seventh phase is included which shows all functions that are independent from time, which can be included in a FBS but not in the functional flow block diagram.

7.2. Functional Flow Block Diagram

The Functional Flow Block Diagram (FFBD) is a flow block diagram visualising functions and their time sequence. Different levels of different accuracy can be observed, and relations between functions are clearly indicated with arrows. The FFBD therefore complements the FBS, and is shown in Figure 7.2. Note that the decision blocks are followed by G or $\bar{G}$, indicating a positive and negative result respectively. Any other loop means that the process is continuously running. Furthermore, the different main phases and breakdown structure can be found as in the FBS, using the same numbering system for convenience. Some functions which are independent from time are not included in the FBS.

7.3. Elaboration on Selection of Functions

In the initial version of the functional flow analysis in (B. van Beurden et al. 2018b), several functions were listed which were to be analysed in detail. All of these functions are included in more detail in the presented diagrams, but some functions require some explanation.

- **3.0: Check weather**. The weather will not be actively checked by the UAV, but the ground segment will perform a weather investigation beforehand and change the flight plan accordingly. In addition, it will monitor the weather during flight and adjust the flight plan whenever necessary.
- **3.2: Flight to assigned coordinates**. A specific flight plan will be uploaded to the UAV, and the flight controller will make sure that the UAV follows the flight plan continuously.
- **3.3: Fly along pipeline**. The UAV will constantly compare its own position with the flight plan and adjust its path accordingly, using inputs to the elevons and propulsion system.

- **3.3.2: Determine position w.r.t. pipeline**. This will be done using the μINS system and comparing it to the flight plan. The first is explained in more detail in section 16.1.
- **3.4.3, 3.4.4: Data transmission**. During flight, the UAV will try to send its data immediately to the ground station. However, connection might be lost and the UAV needs to store its data until connection is re-established. The 'Check communication link' check-box is an ongoing process.
- **3.4: Type of data to be transmitted or read out**. The results of the visual inspection of the pipelines will be the detected irregularities and their respective location.

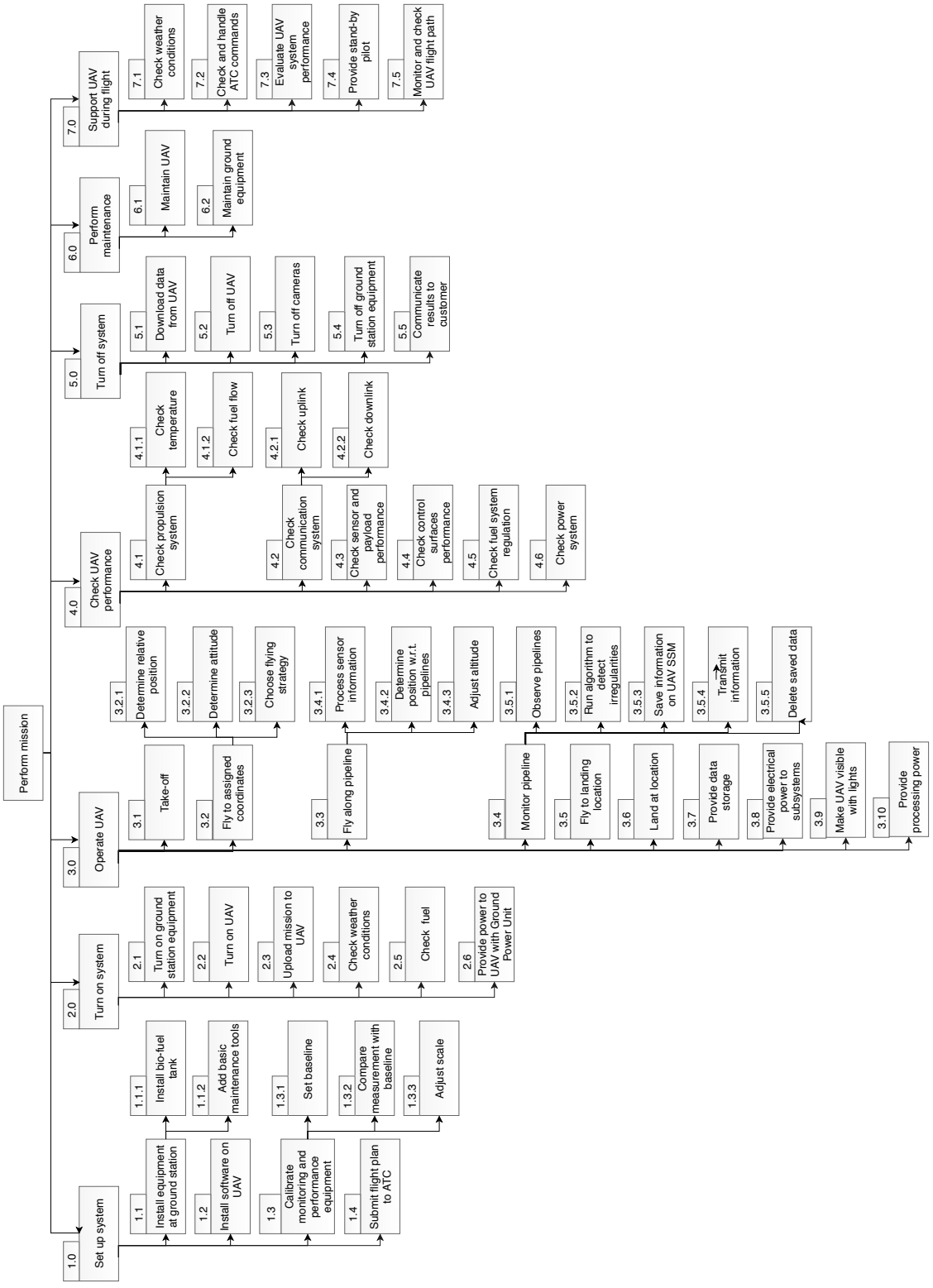

Figure 7.1: Functional breakdown structure for the MAINTAIN system.

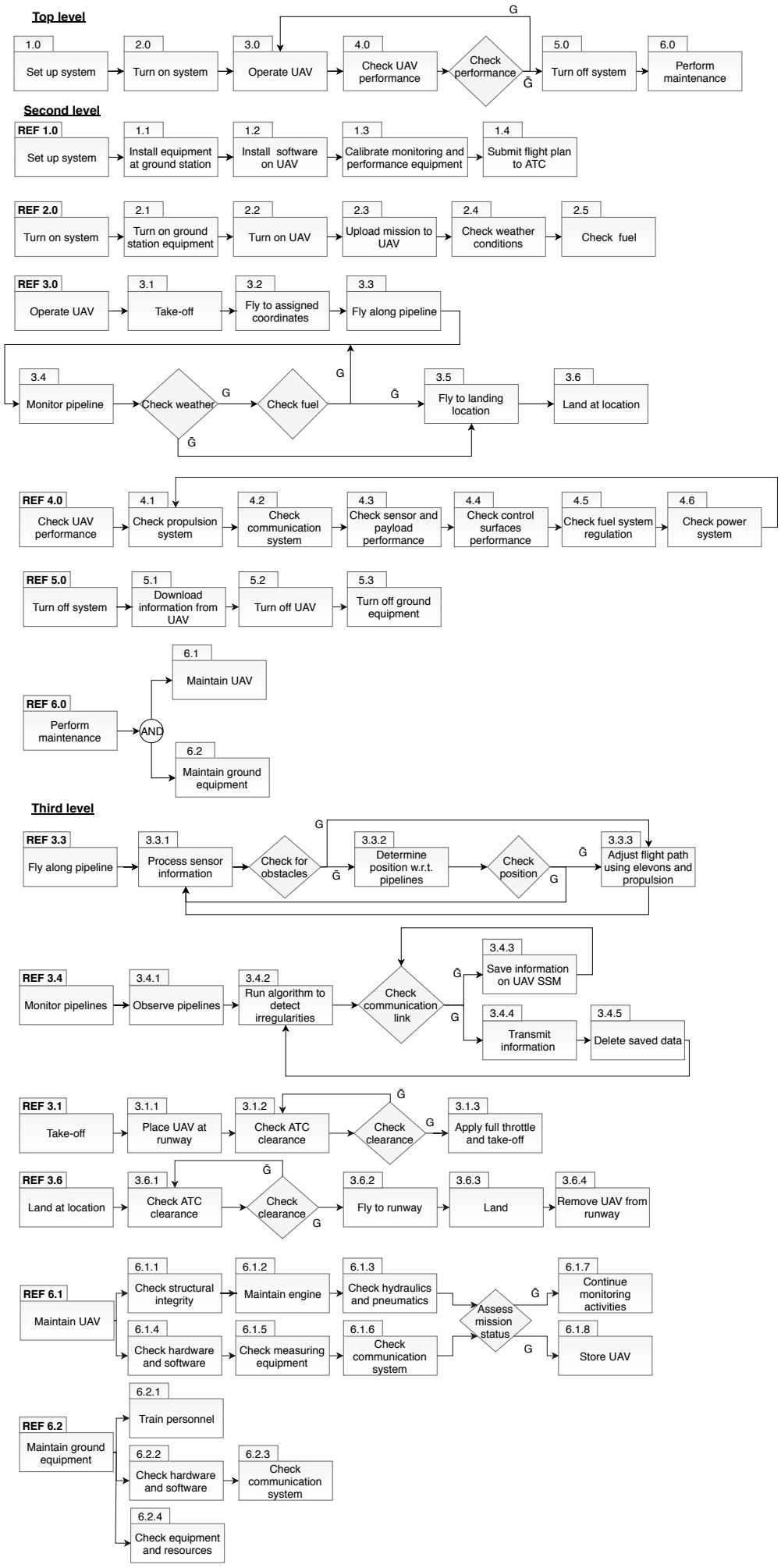

Figure 7.2: Functional flow bock diagram for the MAINTAIN system.

8 Communication Flow

Now that the functions of the MAINTAIN system are defined, it is possible to elaborate on the manner how the information is interchanged between the different mission components. Proper communication of data within the whole system of MAINTAIN is of paramount importance, hence all communication flows present in the system are visualised using a Communication Flow Diagram (CFD). Figure 8.1 shows the CFD for the system at hand and will serve as a guideline in discussing the communication flows within the system. In addition, Table 8.1 explains the communication flows in the system.

Analysing external components interacting with the system, three different sources can be distinguished. First of all, a gas pipeline company defines the mission to be performed and communicates that to the ground segment which provides flight commands to the vehicle. Secondly, Air Traffic Control (ATC) controls the airspace and will approve or disapprove with flight paths flown and provide information about other aircraft in the surroundings of the UAV. Lastly, external forces and moments are acting on the UAV, which will be measured by different sensors on the vehicle. All data will be gathered by the Data AcQuisition (DAQ) module, communicating the necessary parameters to different subsystems. The visual processing module will analyse the visually tracked data to detect pipelines, defects and obstacles. A finite state machine (FSM) will be needed in order to convert the current state of the vehicles and sensor data to the final required state of the system. This state is communicated via the attitude controller and position controller to the propulsion system and control surfaces. An example of such an application in a UAV can be found in (Freitas et al. 2013) or (Eriksen, Ming, and Dodds 2014).

The means of communication between the vehicle and ground segment is explained in section 16.2, as is the observation module in subsection 16.1.2. Using the observation module, the vehicle will detect obstacles and actively avoid them. An elaboration on this process can be found in the same section. Monitoring the pipelines is done with the payload, as discussed in chapter 10. Following the pipelines will be done using the navigation system, which is investigated in section 16.1; this section contains an explanation on the sensors used. Like stated in (B. van Beurden et al. 2018a), the pilot's role remains uncertain. The regulations are constantly changing and the hence it is difficult to predict how often the pilot will be involved in the process and how the ATC will communicate with the system in the future. As (Kamienski and Semanek 2015) alleges: "There is a need to better understand the impacts unmanned aircraft systems (UAS) have on air traffic control (ATC) when they are integrated into the National Airspace System (NAS) in controlled airspace."

Table 8.1: Legenda communication flow diagram.

Number	Description	Number	Description
0	Mission specification	19	Estimation of state
1	Mission data	20	System state
2	Health data	21	Detected defects
3	Drone location	22	Emergency manoeuvres
4	Drone data	23	Attitude and altitude commands
5	Calculated path	24	Computed state
6	Path given by pilot	25	Pipeline locations
7	ATC commands	26	Obstacle locations
8	Drone location	27	Visual map
9	Path commands	28	Control surfaces commands
10	Drone status and detections	29	Propulsion commands
11	Detected defects and location	30	Propulsion system status
12	External forces and moments and GPS data	31	Engine status
13	Environment	32	Emergency status
14	Flight data	33	Detected defects
15	Payload data	34	Inspection results
16	Flight commands	35	Environment
17	Location, flight path and parameters	36	Observed environment
18	Sensor and payload data	37	Requests to ATC

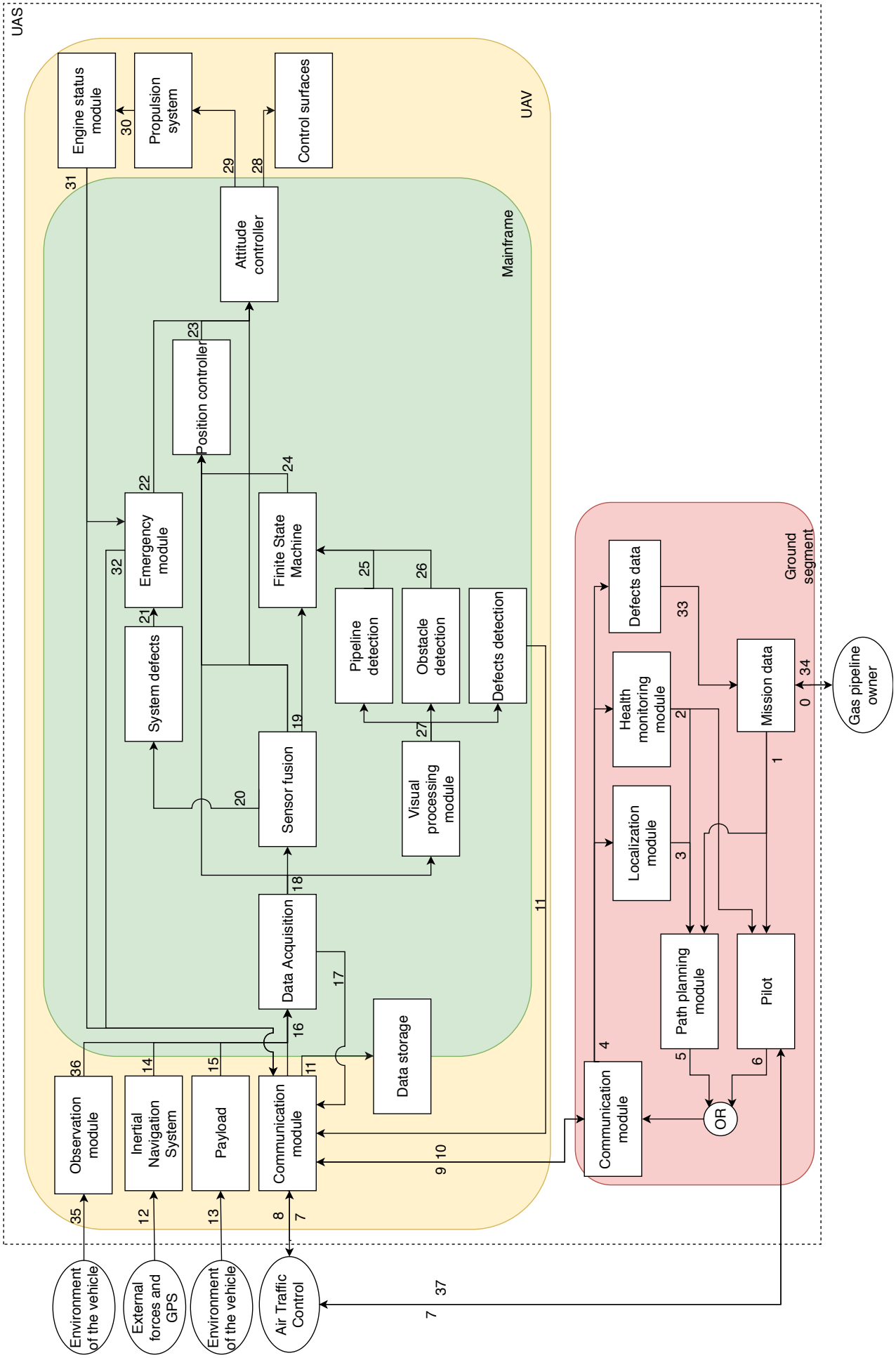

Figure 8.1: Communication Flow Diagram for MAINTAIN.

9 Conceptual Design Summary

At this stage, one has an insight in the implementation of the MAINTAIN system. It is analysed based on its operations and functionality. The actual design of the vehicle is yet to be determined. Before the final design is established, the process followed to end up with this choice of concept should be made clear. The design is separated in multiple design phases: the conceptual, preliminary and detailed design phase. This chapter elaborates on all the actions that have been performed as preparation for the preliminary design and actions yet to be finished in order to realise the MAINTAIN UAV section 9.1 and section 9.2 summarise the concept evolution of the conceptual and preliminary design, respectively.

9.1. Conceptual Design

First, during the conceptual design phase a variety of concepts was assessed on cost, technical risk, performance and sustainability in order to end up with 5 concepts to enter the preliminary design phase. These concepts are visualised in Figure 9.1[34] [35] [36] [37] [38] [39]. A more elaborate discussion on the trade-off performed during the conceptual design phase can be found in the Baseline Report (B. van Beurden et al. 2018b).

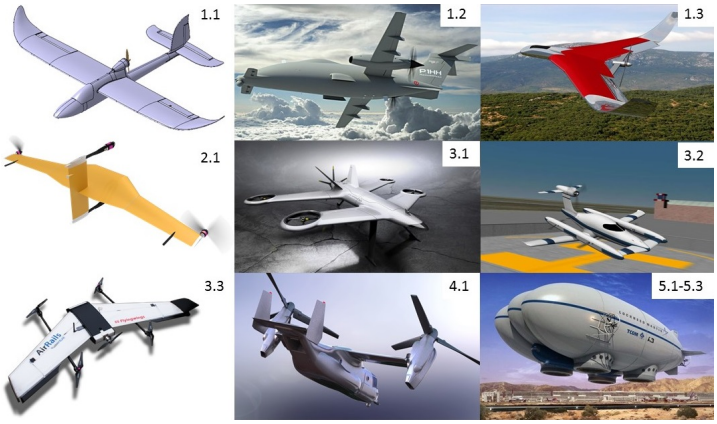

Figure 9.1: Design options.

9.2. Preliminary Design

In the preliminary design phase, it is key to identify the parameters which determine the performance of the design in order to easily differentiate between concepts. Trade-off criteria will be used to asses the different concepts and rank them on suitability for the mission. All criteria will be qualitative, except for the fuel burn which is already analysed quantitatively. Using the Analytics Hierarchy Process (AHP) (Saaty 1987), the complex decision to be made was structured. To reach the goal, choosing the optimal design for the detailed design phase, all criteria are ranked assessing their relative importance and all design concepts are compared to each other on all criteria. In the following, all criteria will be discussed. Note that there were found no subsystems which differ per concept and influence the project at a system level.

Before discussing the various trade-off criteria, an example result of sizing and optimising the different concepts using the multidisciplinary analysis software is shown in Figure 9.2. Note the large vertical wing it requires for stability. It would land on all four of its wing tips. The optimisation results are presented in the form of a parameter sweep for aspect ratio AR and taper ratio λ which were taken as design variables at this stage. The Lighter Than Air concept was analysed in the Midterm Report (B. van Beurden et al. 2018a) and deemed unfeasible due to its incredibly high fuel weight of 671 kilograms. For this reason, it will not be part of the trade-off.

[34] https://www.mentor.com/products/mechanical/engineering-edge/volume4/issue2/ [cited on: 21-06-2018]
[35] http://www.janes.com/images/assets/614/23614/p1513123.jpg [cited on: 21-06-2018]
[36] https://www.deingenieur.nl/artikel/draaiende-drone-doet-inspecties [cited on: 21-06-2018]
[37] http://www.tuvie.com/fedex-autonomous-cargo-drone-concept-by-raphael-doukhan/ [cited on: 21-06-2018]
[38] https://www.uasvision.com/2017/02/22/affordable-ready-to-fly-hybrid-vtol-drone/ [cited on: 21-06-2018]
[39] https://grabcad.com/library/osprey-v-22-1 [cited on: 21-06-2018]

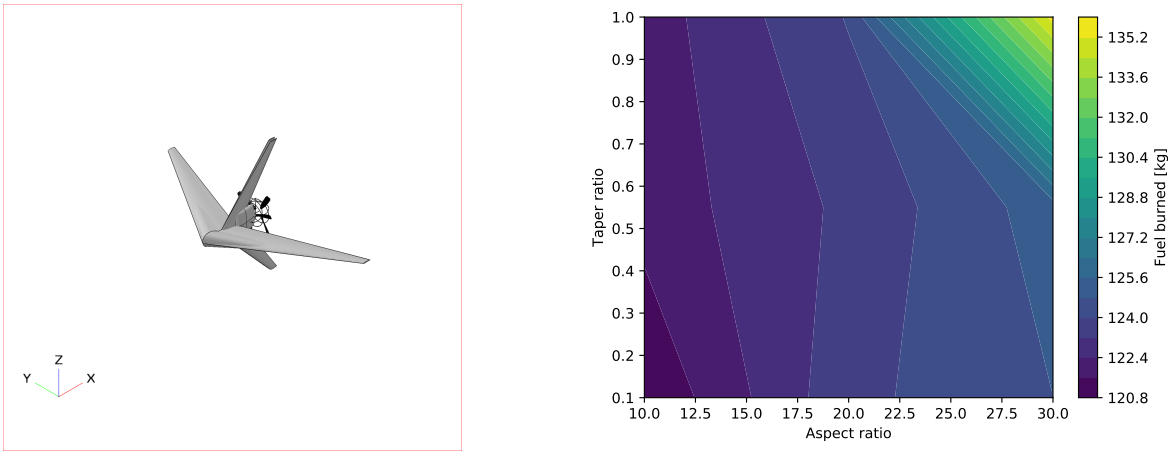

Figure 9.2: Results for the ATM-FLW configuration.

9.2.1. Criteria

In this subsection, the various criteria used to assess the five preliminary concepts are discussed.

Technical Performance

Considering the driving requirements, the UAV should have a minimum range of 1000 km and a minimum endurance of 20 hours. Furthermore, the cruise altitude should be higher than 300 m. The fuel burn, lift-to-drag polar and stability and controllability were considered when assessing the technical performance of a design.

Cost Performance

In order to make the project feasible, the accompanied costs should be predicted and monitored accurately. To implement the cost differences in the trade-off between the concepts, a set of cost criteria has to be defined. The cost can divided up over three subdivisions: production, infrastructure and disposal cost. The fuel burn is not included in the cost even though it is probable that it will be the main contributor to the operational cost. This is because it is already assessed in another criterion. In addition, development costs are not included since this is largely covered by the technical risks which is a separate criterion.

Sustainability

With respect to sustainability, the guidelines which are elaborated in the sustainability approach are applied and a qualitative measure is given to the three different sustainability pillars: economic, environmental and social sustainability. This analysis is performed with the information that is already available in the conceptual design phase. The outcome of this will be taken into account during the trade-off procedure. Characteristics that provide an indication on how well the system is performing with respect to sustainability are noise, safety, contamination, recyclability and emission.

Risk

Risk relates to the maturity of the design in this case and the probability of an unsuccessful design . If a specific concept is applied more often than another, it will encompass less risk.

9.2.2. Criteria Weighting

Using the AHP method (Saaty 1987), all weights are compared to each other following the scores indicated on the right of Table 9.1. The results are shown on the left of the table, clearly visualising the importance of a criterion with respect to another.

Table 9.1: Criteria comparison and corresponding score explanation.

	Fuel burn	Lift-drag polar	S & C	Sustainability	Cost	Risk
Fuel burn	1	7	5	3	3	5
Lift-drag polar	1/7	1	1/3	1/5	1/5	1/5
S & C	1/5	3	1	3	1/3	1
Sustainability	1/3	5	1/3	1	1/3	3
Cost	1/3	5	3	3	1	5
Risk	1/5	5	1	1/3	1/5	1

1	X is of equal importance as Y
3	X is slightly more important than Y
5	X is more important than Y
7	X is much more important than Y
9	X is extremely more important than Y

Transforming the weights to fractions summing up to 100%, the weights as shown in Table 9.2 are found for the different trade-off criteria. Note that only technical performance criteria are assessed separately, since the UAVs performance is

deemed most important and has a close relation with the other criteria. For example fuel burn is closely related to the operation cost of the UAV, and is therefore separately assessed. Within sustainability, safety is deemed most important, followed by noise, recyclability and emission. Contamination is considered the least important aspect, which is also the hardest aspect to assess. With respect to cost, infrastructure cost is given priority over production and disposal cost since this is a life-long cost and therefore will be largest.

Table 9.2: Summary of trade-off criteria.

Trade-off criterion	**Weight (%)**	**Trade-off criterion**	**Weight (%)**
Fuel burn [kg]	39.9	Sustainability	12.2
Lift-to-drag polar	3.4	Cost	23.9
Stability and controllability	11.9	Technical risk	8.6

The weights are representing the importance of the different criteria quite well. Since fuel burn not only drives the design to a large extent but also influences the emission and operational cost of the UAV, it is of huge importance. In addition, cost are quite important being of big importance for the customer. Lift-to-drag polar is included in order to have to possibility to eliminate a design due to e.g. poor stalling characteristics, but is not a driving criterion.

9.2.3. Trade-Off

Now that the trade-off criteria and their respective weights are known, the trade-off is performed. Following the Analytic Hierarchy Process method, all design options are compared on each criterion. The different concepts are visualised in Figure 9.1, in which the UPD-CON concept is subfigure 1.1, UDP-CAN is subfigure 1.2, UDP-FLW is subfigure 1.3 and ATM-FLW is subfigure 2.1.
Considering all design options, certain characteristics with respect to the criteria can be observed which are summarised in Table 9.4.

Table 9.3: Color legend.

Excellent	Good	Average	Worse	Terrible

Table 9.4: Rationale used during the trade-off process. Note that the width of the columns does not indicate anything about the importance of the corresponding criterion.

	Fuel burn [kg]	$C_L - C_D$ **polar**	**S & C**	**Sustainability**	**Cost**	**Risk**
UDP-CON	95.6	Baseline	Baseline	Baseline	Baseline	Baseline
UDP-CAN	86.4	Better due to reduced trim drag	Slightly less stable, more controllable due to canard	Similar to baseline	Similar to baseline	Slightly more risk: less proven concept
UDP-FLW	60.0	Better due to reduced friction drag	Naturally less stable and controllable due to absence of stabilisers and associated control surfaces	More safe due to smaller MTOW	Similar to baseline	More risk, not often applied technique
ATM-FLW	120.8	Better due to reduced friction drag but larger wetted area with respect to flying wing	Less stable due to absence of stabiliser, similar controllability as baseline	Less safe due to vertical take-off, more noise involved during take-off due to larger propeller	Less operational cost due to less required infrastructure, but large production cost due to larger engine	Involves a lot of risk: based on recent developments, not a proven concept

Giving a score similar to the scoring process used during the criteria weight determination procedure, most favourable concepts with respect to different criteria are found. An example is shown in Table 9.5, in which the stability and control of the concepts are compared.

Table 9.5: AHP concept comparison on stability and control.

	UDP-CON	UDP-CAN	UDP-FLW	ATM-FLW	Sum	Average
UDP-CON	1	3	5	7	16	0.51
UDP-CAN	1/3	1	3	5	9.33	0.30
UDP-FLW	1/5	1/3	1	3	4.5	0.14
ATM-FLW	1/7	1/5	1/3	1	1.68	0.05

1	X performs similar to Y
3	X is slightly performing better than Y
5	X is performing better than Y
7	X is performing much better than Y
9	X is performing outstanding compared to Y

Multiplying the scores of all concepts with their respective criteria weights yields Table 9.6. As can be observed, **the UDP-FLW concept scores better than the other concepts and is the chosen concept to enter the detailed design phase.**

Table 9.6: Scores of concepts on all criteria and the total score resulting from multiplication with the criteria weight.

	UDP-CON		**UDP-CAN**		**UDP-FLW**		**ATM-FLW**	
	Score	***Total***	***Score***	***Total***	***Score***	***Total***	***Score***	***Total***
Fuel	0.120	0.048	0.247	0.098	0.589	0.235	0.044	0.018
C_L-C_D polar	0.066	0.002	0.379	0.013	0.379	0.013	0.177	0.006
S & C	0.507	0.061	0.296	0.035	0.143	0.017	0.053	0.006
Sustainability	0.278	0.034	0.278	0.034	0.379	0.046	0.066	0.008
Cost	0.167	0.040	0.167	0.040	0.167	0.040	0.500	0.120
Risk	0.507	0.043	0.296	0.025	0.144	0.012	0.053	0.005
Total		**0.228**		**0.246**		**0.364**		**0.162**

9.2.4. Trade-Off Sensitivity Analysis

The sensitivity of the trade-off just presented with regards to the criteria and criteria weights needs to be investigated in order to ensure the chosen concept is the most optimal one. When a criterion weight is set to zero, the flying wing remains the chosen concept for all criteria except for the fuel burn. Varying the weights of the criteria also provides valuable insight into the sensitivity of the trade-off to the criteria. Each criterion is compared to all other criteria as explained in subsection 9.2.2, and studying the sensitivity all these comparison results are slightly changed. Changing the relative importance of a criterion with respect to all other criteria one step, e.g. a change in importance from '3' to '5', the most optimal concept is noted down. Doing so with multiple steps until the maximum score of 9 is reached on some comparison, Figure 9.3a results. A more thorough explaination of the sensitivity analysis can be found in (B. van Beurden et al. 2018a). As can be seen from the figure, the flying wing configuration is a stable outcome of the trade-off. Only a drastic change in the importance of the fuel weight criterion would yield another concept. Note that varying a combination of criteria is not assessed in this figure, but can be implicitly determined. The preliminary design resulting is visualised in Figure 9.3b.

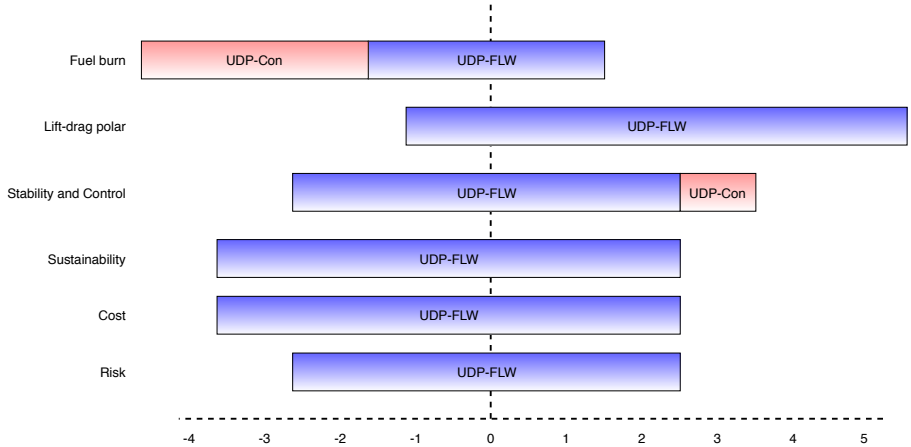

(a) Sensitivity of design trade-off.

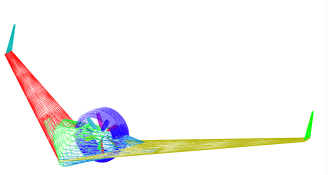

(b) Preliminary design result.

10 Payload Selection

A very thorough payload analysis is performed to ensure all customer requirements are met. Thereafter, the suitable payload is selected. This chapter elaborates on the process of the payload selection. First, in section 10.1, the capabilities and disadvantages with regard to mission performance are outlined. A preliminary camera selection is performed that complies with the initial requirements of the mission in section 10.2. When the set of cameras is chosen, it is evaluated in section 10.3 whether the solution has a competitive position in the current market. After that, section 10.4 concludes with the updated payload selection to provide a system that is optimally implemented as an alternative to current solutions.

10.1. Monitoring System Types

For current airborne platform methane leakages can be detected by thermal cameras and Light Detection and Ranging (LiDAR) systems which depend on the principle of spectroscopy. Below, the implementation of these systems with respect to gas pipeline monitoring is elaborated upon.

Thermal Camera

The fundamental concept of the thermal camera is explained in section 2.3. A thermal camera can assist the monitoring system based on the temperature difference between the gas that is escaping and the environment. Furthermore, if the system's sensitivity is specifically calibrated for the absorption spectrum of methane, it can to a certain extent provide information about the atmosphere that the UAV is flying above. Do note that the system effectively provides a representation of the temperature of surfaces. This technique introduces several factors that can impede the quality of the images and that can make the results ambiguous. For clarity, the following bullets explain in what situations the system is less effective.

- In the scenario of rain in the atmosphere, the water droplets absorb or refract a substantial part of the emitted infrared radiation of the surface to be monitored. This will give less readable output to the detection system.
- Normally, the gas within the pipelines is colder than the surroundings of the pipelines. Then, the gas is visualised by providing a relatively dark silhouette in the images, from which is extrapolated that there is a gas leakage. Two situations induce erroneous readings. One is if the gas that escapes from the pipelines is the same temperature as its surroundings, and with that, the leakage stays undetected. The other is if the system detects a colder region which is not necessarily caused by natural gas, it is still read off as a gas leak.

LiDAR System

As elaborated upon in section 2.3, a LiDAR system emits a certain range of wavelengths in the infrared spectrum. These electromagnetic waves propagate towards a surface where it either refracts or reflects. A selection of these signals follows a path back to the sensor of the LiDAR system. Often, the altitude of a certain terrain is mapped, based on the time interval between the sending and receiving of an electromagnetic signal. Also, note that some wavelengths are absorbed by specific gases. If the LiDAR system keeps track of the relative intensity of different wavelengths when sending and when receiving, spectroscopy can be applied to discover the composition of the atmosphere. Because of this characteristic, it can be verified that the reading is correctly indicating methane. The absorption band of methane is clearly visible from 2.8 to 3.5 μm, which is part of the mid-wavelength infrared spectrum ranging from 2.5 to 25 μm.

The resolution of the LiDAR system will determine in what degree it can detect small gas leaks. Regarding a LiDAR system, there are three types of resolutions. First of all, there is a time measurement resolution. This type of resolution is especially of importance when mapping areas to identify corrosion threats. Secondly, there is a resolution based on the emitted light beams, which is most often expressed in light beam pulses per square metre and is dependent on the following aspects:

- Field of view (FOV): area which can be observed by the LiDAR system.
- light beam pulse repetition rate (PRR): rate with which light beam pulses are emitted.
- Scan speed: dependent on the light beam pulse repetition rate and the amount of pulses for each scan.
- Angular step width: angular step size between emitted light beams.

Thirdly, the spatial resolution of the sensor is of importance. This type of resolution is dependent on the monitoring height, the detector's resolution and the field of view and can be calculated using Equation 10.1. As the resolution of the emitted light beam is often very high, LiDAR systems are equipped with a high resolution detector. For this reason, solid state photodetectors are most commonly used[40].

$$\text{spatial resolution} = \frac{\frac{h}{sin(\frac{1}{2} * FOV)}}{\frac{1}{2} \cdot \text{amount of pixels in width}} \tag{10.1}$$

Furthermore, the light beam system is sensitive to bad weather conditions to a smaller extent, since it receives higher intensity signals than a thermal camera. Nonetheless, there are problem areas, which are stated below.

- If one requires to discover whether the vehicle is flying over a gas leak, the emitted wavelength spectrum should be within a range where methane absorbs the electromagnetic waves. Most LiDAR systems are designed for mapping of surfaces and their altitude. The spectral range is often in the near infrared spectrum, which is absorbed to lesser extent than mid-infrared waves by methane.
- The mid-infrared LiDAR systems are heavier, larger and more power consuming than near infrared systems. Furthermore, these mid-infrared LiDAR systems are not as commercially available as their near infrared counterparts. With the initial requirement of the payload not exceeding 50 kg, it is difficult to integrate a mid-infrared camera. As they are possibly essential for the mission's success, they are still considered to be integrated in the MAINTAIN system.

10.2. Preliminary Camera Selection

Before the actual selection of the camera, a study has been performed into the different options that can be integrated in MAINTAIN. First, the thermal cameras are addressed. A choice is made, based on a set of essential characteristics of the cameras. If there is decided upon the thermal camera, it is evaluated how much value is added to the UAV with the integration of a LiDAR system. Thereafter, again, a selection procedure is performed to decide upon which LiDAR system is best suited for the mission.

Thermal Camera

As explained above, a thermal camera can monitor the temperature of surfaces, provided that the temperatures correspond to the wavelengths that the system is calibrated for. A thermal camera, ideally in combination with an electro-optical camera for validation, is well-suited for monitoring areas where the gas is significantly colder than the surrounding surfaces. The driving parameters for the selection of the thermal cameras are mass, dimensions, resolution plus possible optical zoom, sensitivity and price. Voltage and power usage are not considered as driving, since the generator is connected to a gas turbine engine that provides adequate power for the systems. Furthermore, the free spectral range is not considered in the trade-off, since the cameras are all in the same specific range for optimal methane detection. That was a criterion to be considered an option.

Table 10.1: Specifications of a selection of thermal cameras.

Thermal Camera	**Mass [kg]**	**Dim. [mm^3]**	**Sens. [mK]**	**Resolution [pix]**	**Price [USD]**
Trade-off weight	4/5	2/5	2/5	3/5	5/5
FLIR A8200sc [41]	3.73	226x117x135	20	1024x1024	[-]
FLIR A8300sc [42]	3.73	227x209x129	20	1280x720	[-]
FLIR Star Safire III [43, 44]	44	450x380x380	unknown	640x512 (71x)	500 K >
FLIR Star Safire III 380HDc [3, 45]	45	475x380x380	unknown	1080x720 (120x)	750 K >
Ascent Vision CM202G [3, 46]	3.5	295x190x190	10[47]	640x512	160 K >

Aided by the above parameters, it is possible to perform a trade-off. In contrast with the trade-off procedure performed earlier in the conceptual design phase, a conventional trade-off process is used to decide upon the thermal camera. This is because the amount of options are not extensive, and the reasoning is directly coupled to the requirements. The individual weights can be found in Table 10.1. After the trade-off, one should bear in mind that the outcome has to be realistic

[40] `https://www.hamamatsu.com/resources/pdf/ssd/Photodetector_lidar_kapd0005e.pdf` [cited on 03-07-2018]
[41] `flirmedia.com/MMC/THG/Brochures/RND_090/RND_090_US.pdf` [cited on 20-06-2018]
[42] `flirmedia.com/MMC/THG/Brochures/RND_035/RND_035_US.pdf` [cited on 20-06-2018]
[43] These systems are provided as a combination of a gimball, an electro-optical camera and an infrared camera
[44] `flir.com/globalassets/imported-assets/document/flir-star-safire-iii-airborne-datasheet-ltr.pdf` [cited on 20-06-2018]
[45] `flir.com/globalassets/imported-assets/document/flir-star-safire-iii-airborne-datasheet-ltr.pdf` [cited on 20-06-2018]
[46] `ascentvision.com/cm202g-gimbal.html` [cited on 20-06-2018]
[47] This is valid in the methane absorption band (3.2-3.5 μ m) [cited on 20-06-2018]

with regard to price and mass. Since it is attempted to meet the mass requirement for the total payload, this parameter is assigned a high weight factor. The FLIR A8200sc, FLIR A8300sc and Ascent Vision CM202G had a comparable score after the trade-off. **It is decided the CM202G is the best option, because it is integrated in a gimball with an additional electro-optical camera and the sensitivity is calibrated to be optimal in the spectral range of methane.**

LiDAR System

At this stage, the best thermal camera is selected, which ensures that the system is able to detect gas leakages by means of the temperature differences between the gas and its surroundings. With solely a thermal camera, some difficulties arise. These difficulties are already stated in the first section of this chapter. With the thermal camera already selected, it is evaluated whether the integration of a LiDAR system is a contribution to the vehicle. Inclusion of an additional LiDAR system yields better performance when rain is involved and can assist the detection of methane when the temperature difference is less significant. This is only valid for sensors that apply the spectrometry technique in the mid-wave infrared spectrum. If spectrometry in the mid-wave infrared spectrum is not possible, only the corrosion threats can be mapped by means of covering the area around the pipelines multiple times. Below, a table can be found with essential parameters for the trade-off.

Table 10.2: Specifications of a selection of light detection and ranging cameras.

LiDAR Camera	**Mass [kg]**	**Dim. [mm^3]**	**Spectroscopy** [−]	**Accuracy [mm]**[48]
Trade-off weight	5/5	2/5	4/5	2/5
RIEGL VQ-780i [49]	20	425x212x331	No	24
RIEGL VUX-1LR [50]	3.75	227x209x129	No	30
Ball Aerospace sensor [51]	108	Unknown	Yes	600
LaSen ALPIS sensor [52]	113	1219x762x305	Yes	300

Before entering a trade-off comparable to the selection of the thermal camera, rationale is applied to evaluate whether the available LiDAR systems add value to the project. By complying with the initial requirements, the total subsystem weight should not exceed 50 kg. This requirement restricts the implementation of systems that can successfully apply spectroscopy or the analysis of the atmosphere. The only LiDAR systems remaining are capable of mapping the the surface over which the vehicle is flying. This cannot give a quantitative visualisation of gas leaks. It can detect threat areas for the formation of corrosion. After assessing whether this would add sufficient value to the system, **it was decided to not implement a near infrared LiDAR system.**

10.3. Competitive Position Evaluation

For MAINTAIN to be competitive, it should be a less costly solution for inspecting pipelines than current missions. Furthermore, the quality should be comparable or better than the services that are provided at the moment. Then it holds that there should not be a more affordable solution on the market which can be adapted in order to fulfil the same functions as the MAINTAIN project is to perform. Looking at existing pipeline inspection services, in general, two solutions exist. On the one hand, pipelines are inspected by manned aircraft using the spectroscopy analysis of mid-infrared LiDAR systems. This can be done by either a fixed wing or rotorcraft configuration flying at an altitude that is safe for the personnel flying above the pipelines. Companies providing these services are e.g. LaSen Inc. and Ball Aerospace. On the other hand, inspection can be performed by light UAVs carrying thermal cameras to distinguish potential leakages. For these configurations, there are two possible disadvantages. First, it is not possible yet to integrate mid-infrared LiDAR technology, and with that spectroscopy. Second, the flying velocity or altitude or a combination of the two is relatively low. Companies providing these services are Sharper Shape Ltd. and UAVE Ltd. by means of small unmanned vehicles. The following conclusions can be drawn from the evaluation:

- Either thermal cameras or near infrared LiDAR systems are already being implemented in small UAVs to inspect gas pipelines.
- Mid-infrared LiDAR systems are succesfully being integrated in manned inspection flights, either with priority on accuracy and sensitivity or on high velocity.

To be both revolutionary and financially more attractive, the system should be accurate and quick while it is able to monitor the gas pipelines with high sensitivity. **That is why an unmanned, fixed wing UAV, including a LiDAR system**

[48] This is based on the maximum measuring error in locating at an altitude of 300 meters. Note that this is not related to the design altitude in this table. E.g. the VUX-1LR is designed for lower altitudes, and the accuracy is scaled with the altitude change. It is not taken into account in the table that the signal strength is lower.

[49] `riegl.com/uploads/tx_pxpriegldownloads/RIEGL_VQ-780i_DataSheet_2018-04-12_Preliminary.pdf` [cited on 20-06-2018]

[50] `riegl.com/uploads/tx_pxpriegldownloads/RIEGL_VUX-1LR_Datasheet_2017-09-01.pdf` [cited on 20-06-2018]

[51] `ball.com/aerospace/Aerospace/media/Aerospace/Downloads/D3242-Methane-Monitor_0518.pdf?ext=.pdf` [cited on 20-06-2018]

[52] `lasen.com/technology.aspx`

capable of applying spectroscopy, is the most optimal solution. In direct relation with this optimum, this means that the weight requirement of the payload cannot be met. In the next section, one can find an updated camera selection with an alleviated payload mass restriction.

10.4. Updated Camera Selection

After the analysis on where the implementation of an unmanned gas leakage detection is most viable, the payload selection is reassessed. It is decided that the UAV shall include a mid-IR LiDAR system, so that spectroscopy can be applied. This has the advantage that it is less prone to weather interference and that it can be implemented in all atmosphere temperatures that the system encounters. Undoubtedly the most significant difficulty is that these LiDAR systems capable of detecting gas leakages prove to be heavy (Table 10.2). The LaSen ALPIS sensor is suitable for the application. However, the weight is more than a factor 2 higher than the maximum set in the requirements. Currently, a new system, provided by LaSen, is in the last stage of development. This system is specifically designed for UAVs and has comparable performance to the current ALPIS sensor, at a mass of 68 kg. It includes global shutter, which makes the system suitable for MAINTAIN's flying velocity, as discussed in the exploration of the payload. Since the product is developed and manufactured by LaSen Inc., the LiDAR system is not directly commercially available. It is important that agreements are made with the company regarding the implementation of the system. The main reasons of implementing this system over the initial choice are summarised below:

- This is the segment of the aerial gas leakage detection that has not been automated. The long-range, long-endurance fixed wing aircraft carrying a spectroscopy LiDAR system is a cheaper and more sustainable than the current comparable manned inspections. The detection is of higher accuracy than the light drones using thermal cameras.
- The mid-infrared LiDAR system proved to perform better in bad weather conditions[53]. This makes the system highly suitable for service in The United States of America, where a wide range of weather conditions is encountered.
- An innovative system in the MAINTAIN aircraft is the micro gas turbine. There is a limit to the extent that the turbomachinery can be downscaled currently. The advantage of increased efficiency is lost when the gas turbine becomes too small. If little weight is required, there are more feasible carrying solutions. A vehicle with a carrying capacity of 70 kg creates a platform for the prove of concept of the micro gas turbine, while it is applied in an unsaturated market.
- The implementation of new systems is stimulated in The United States. The gas detection company LaSen Inc. was provided funding of 2.2 million USD by the PHMSA (Pipeline and Hazardous Materials Safety Administration) for their gas leak monitoring service. The same technology can be implemented in a fixed wing UAV, which provides a more sustainable and feasible solution.

Implementing this new technique of LaSen means that the payload mass requirement is to be reevaluated. However, the focus is on making the system comply with the mission need statement. This focus, in combination with the above positive effects, justifies that the mass requirement is exceeded. The final camera system characteristics can be found in the table below. These were obtained by means of email correspondence with the founder and president of the company. The resolution specifications of the LiDAR system remain disclosed as well, but the company ensured detection of natural gas leaks would be possible from a 300 m cruise altitude.

Table 10.3: Specifications of the recently developed updated ALPIS system by LaSen Inc.

Final System	**Mass [kg]**	**Dim. [mm^3]**	**Spectroscopy [−]**	**Accuracy [%]**[54]	**Price [USD]**	**Resolution**
LaSen ALPIS X sensor	68	<TBD>	Yes	98	<TBD>	<TBD>

Momentarily, the dimensions and the price are to be determined, since they are not released by the commercial company. However, it is possible to make a decent estimations. For the dimensions, it is assumed that the system lengths shift linearly with the weight. As for the cost, a safety factor of 1.2 was applied to the price of a highly advanced military reconnaissance camera; the FLIR Star Safire III, as described above. This camera costs in the range of 500,000 USD, which renders the preliminary cost of the monitoring system at 600,000 USD.

These parameters are taken into consideration for the modelling of the vehicle and the mission. This concludes the preparatory phase of the project. The following part of the report describes the design phase, where all models are elaborated upon. Moreover, the results obtained from the converged solution of the models and a detailed design of how the payload is integrated are presented.

[53] This information was obtained from a technology data sheet, provided by LaSen Inc.

[54] In this instance, the accuracy is given as the statistical amount of correct leakage identifications at an altitude of 150 meters. In the previous table, accuracy was explained differently, since near infrared was compared with mid-infrared, where the first is not yet capable of detecting methane in the atmosphere.

11 Performance

The first model to be described is the analysis of the system performance. If one is acquainted with how the system should perform, it is eventually possible to converge to a detailed design. This chapter addresses that performance of the designed UAV. In section 11.1, a representative mission to be flown in described. Subsequently, the performance at a specific wing loading and power loading is analysed in section 11.2. This is followed by a model for the fuel burn in section 11.3. In section 11.4, the equations to optimise the flight velocity are outlined, after which the flight envelope is stressed in section 11.5. To conclude, the verification and validation of the models is summarised in section 11.6.

11.1. Mission Analysis

Before sizing for performance, the flight mission should be analysed in more detail. A typical mission is determined, which covers the entire range of 1000 km as specified in the top-level requirements, inspecting pipelines across North Carolina, Virginia, Georgia and Tennessee. Since this covers both the Blue Ridge mountains as well as large areas of flat land, this is a somewhat more difficult mission than the average mission flown, as discussed in (B. van Beurden et al. 2018a). All airports used during this sample mission follow from the selected airports as discussed in section 5.3. Taking off from Tri-County Airport in Aulander, North Carolina, the UAV flies to the pipeline to be inspected near Roanoke in Virginia. Following the pipeline towards Tom B. David Airport in Calhoun, Georgia, 625 km of pipeline is inspected. At a flown distance of 875 km, the UAV lands at Tom B. David Airport. When this is not possible due to an unforeseen complication, the UAV should divert to a nearby airport, which is R.G. LeTourneau Airport in Toccoa, Georgia, which is also one of the selected airports as discussed in section 5.3. The mission ground track is visualised in Figure 11.1a, in which the map is retrieved from Google Earth[55]. The mission profile follows from the altitude the pipelines are at, above which the UAV should fly at approximately 300 m. Dividing the mission into multiple climb and range segments yields Figure 11.1b, which is discussed in more detail in the following sections. Note that the endurance requirement of 20 hours is met and verified by the design software, but is not found to be a driving mission requirement and hence is not part of the sample mission.

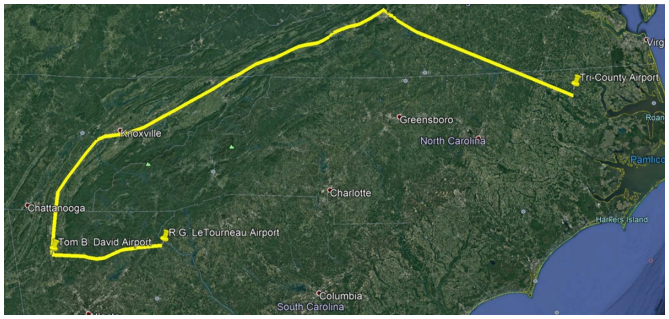

(a) Mission ground track for MAINTAIN UAV.

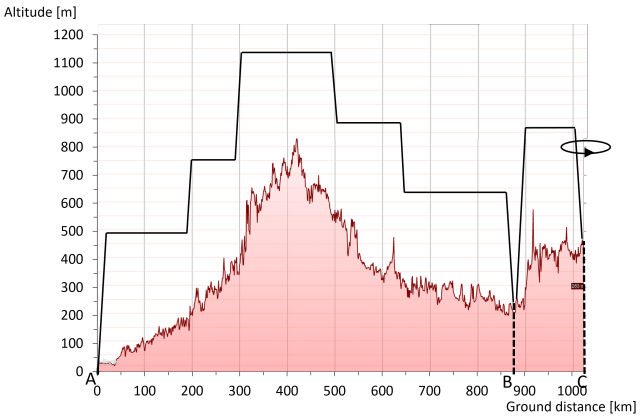

(b) Mission profile for MAINTAIN UAV, with A: Tri-County Airport, B: Tom B. David Airport and C: R.G. LeTourneau Airport. The altitude profile follows from Google Earth.

Manoeuvring to Site

Firstly, the UAV should fly to the inspection site. This involves starting the engines, taxiing, if necessary for a horizontal take-off, taking off and climbing to cruise altitude. According to (Raymer 2012), fuel weight consumed during the above mission segments can be estimated using statistical data. The weight fraction for starting the engine, taxiing and taking

[55] https://www.google.com/intl/nl/earth/ [cited on: 21-06-2018]

off is typically 0.970. How to calculate the fuel burned during the climbing phase of the mission is explained at later stage in the report, in section 11.3.

Inspection
Flying across the inspection site and performing the inspection is the next mission segment. It is assumed that the aircraft continuously flies along the pipelines for inspection and does not need to loiter during inspection. At any time, a pilot can take over control of the UAV and decide to briefly loiter, but this affects the range of the drone. Flying the maximum range of 1000 km burns a significant amount of fuel which is calculated as explained in section 11.3. During the inspection phase, the UAV needs to climb once in a while to remain an almost constant altitude with respect to the pipelines, as shown in Figure 11.1b.

Returning to Base
Eventually, the UAV lands at one of the selected airports as discussed in chapter 5, where it possibly loiters shortly before it is allowed to land, lands and taxis back to where it is stored. In addition, it should be able to divert to an alternative airport when landing is not possible at the desired airport. Abortion of the landing at point B, Tom B. David Airport, is clearly visualised in Figure 11.1b. Back at cruise altitude the aircraft will fly to an alternative airport, which in case of the sample mission is point C, R.G. LeTourneau Airport. Prior to each mission a plan should be written investigating the required diverging range based on available nearby chosen airports, as discussed in section 5.3. In regions having many airports, diverging ranges will be considerably smaller than in regions with a lower airport density. Furthermore, it can be assumed that the aircraft needs to loiter for 45 minutes and fuel burned is calculated as explained in section 11.3. The loiter time holds for domestic flights according to (Vos, Melkert, and Zandbergen 2017). (Raymer 2012) provides weight fractions for descending and landing combined with taxiing based on statistics, which are 0.990 and 0.992 respectively.

11.2. Wing Loading and Power Loading

Following from the mission profile and various design parameters, power loading (W/P) and wing loading (W/S) can be calculated as inputs to the propulsion model and aerodynamic model. These figures are of importance to relate the power and surface area of the aircraft to the weight and thus to provide a clear relation between the various analyses in aircraft design. In (B. van Beurden et al. 2018a) a method to find the optimal combination of wing loading and power loading following several imposed requirements was established. No specific requirements on performance of UAVs exist, however, often FAR23 regulations are imposed on UAVs too (Gundlach 2014). Since the UAV to be designed will weigh less than 6000 lbs and uses a turboprop engine, CS/FAR 23 is taken as the regulations to comply with, in correspondence with chapter 5. It is assumed that following this legislation will provide the UAV with sufficient performance to meet potential future regulations posed. The requirements taken into consideration can be found in the following list (Raymer 2012):

- **Stall speed**: The stall speed shall not be higher than 113 km/h.
- **Take-off and Landing**: The obstacle height is 50 ft.
- **Approach speed**: The approach speed should be equal to or greater than 1.3 times the stall velocity.
- **Rate of Climb**: The rate of climb should not be less than 300 ft/min.
- **Climb Gradient**: The climb gradient should be 0.083 minimum.
- **Limit manoeuvrability load factor**: the positive limit manoeuvring load factor n may not be less than 2.1 + (24,000/(W+10,000)) for normal and commuter category airplanes, where W is the design maximum take-off weight in lbs, except that n need not be more than 3.8.
- **Limit manoeuvring load factor**: the negative limit manoeuvring load factor may not be less than 0.4 times the positive load factor for the normal utility and commuter categories.

The chosen design point complies with all listed requirements, leading to a wing loading of $167.3 N/m^2$ **and a power loading of** $0.419 N/W$**.**

11.3. Fuel Burn

During all mission segments, fuel is burned. The mission segments discussed in section 11.1 can also be found in Table 11.1, visualising the fuel fractions at each mission segment. Segments 1-3, 10 and 11 follow from statistics in (Raymer 2012), whilst others refer to an equation discussed below.

Table 11.1: Fuel fractions during the mission for different phases following from Figure 11.1a.

Mission phase	Start engine, taxi, take-off	Climb	Cruise	Loiter	Descend	Land, taxi
Weight fraction	0.970	Eq. 11.7	Eq. 11.2	Eq. 11.4	0.990	0.992

In the following, fuel burn during range, endurance or climb segments is investigated. Note that in all equations in this section, η_p is used to indicate propeller efficiency instead of $\eta_{\text{propeller}}$ for reasons of brevity. For all mission segments, the distance covered is the found optimal velocity multiplied by the time the segment takes.

Range
Most of the time, the UAV has to fly long distances and hence requires the best performance possible regarding range. The range equation from Breguet[56] is used in this section, given by Equation 11.1. This equation is valid assuming steady flight. Rewriting to predict the fuel weight consumed during a given range segment yields Equation 11.2.

$$R = \frac{\eta_p C_L}{c_p C_D g} \cdot \ln\left(\frac{W_i}{W_f}\right) \tag{11.1}$$

$$W_{\text{fuel}} = W_i \left(1 - e^{-\frac{R c_p C_D g}{\eta_p C_L}}\right) \tag{11.2}$$

Endurance
Endurance, the possibility of staying in the air for a certain period of time, is obtained by dividing the range covered by the velocity at which that distance is flown. This can be rewritten in the form represented in Equation 11.3. Rewriting to find the weight difference during the endurance mission segment yields Equation 11.4.

$$E = \frac{\eta_p C_L}{c_p C_D V g} \cdot \ln\left(\frac{W_i}{W_f}\right) \tag{11.3}$$

$$W_{\text{fuel}} = W_i \left(1 - e^{-\frac{E c_p C_D V g}{\eta_p C_L}}\right) \tag{11.4}$$

Climbing
Climbing to the determined cruise altitude requires a certain rate of climb. The achieved rate of climb differs per altitude and is calculated using Equation 11.5, which is the power required subtracted from the power available. Assuming a linear relationship between the rate of climb at two different altitudes, Equation 11.6 is established. Using the above equations in Equation 11.7, results in the fuel required to climb a certain height.

$$ROC = \frac{P\eta_p}{W} - \frac{DV}{W} = \frac{P}{W}\frac{W}{V} - \frac{1/2\rho V^3 C_D}{W/S} \tag{11.5}$$

$$a = \frac{ROC_2 - ROC_1}{h_2 - h_1} \tag{11.6}$$

$$W_{\text{fuel}} = -c_p \frac{P}{Wg} W \frac{1}{a} \ln\left(\frac{ROC_1}{ROC_2}\right) \tag{11.7}$$

11.4. Velocity Optimisation

For a given climb, range or endurance mission segment, the optimal velocity can be found using an iterative procedure. Maximising the range, endurance or climb distance over the fuel weight consumed during the segment studied yields the optimal speed (Gundlach 2014). For example, calculating the velocity required for a certain range segment, Equation 11.2 can be used to calculate the fuel weight consumed during the mission segment. The figure of merit (FOM) in Equation 11.8 should be maximised for a given range segment. Calculating the FOM at a finite number of velocities evenly distributed between the maximum and minimum possible velocities, and iterating until sufficient convergence, yields the optimal velocity for the given flight segment. The minimum velocity will be the stall velocity, calculated using Equation 11.11. The maximum velocity is given by Equation 11.12.

$$FOM = \frac{R_{\text{segment}}}{W_i - W_f} \tag{11.8}$$

$$FOM = \frac{E_{\text{segment}}}{W_i - W_f} \tag{11.9}$$

$$FOM = \frac{\Delta h_{\text{segment}}}{W_i - W_f} \tag{11.10}$$

$$V_{\text{min}} = \sqrt{\frac{W}{S}\frac{2}{\rho}\frac{1}{C_{L_{\text{max}}}}} \tag{11.11}$$

$$\frac{W}{P} = \eta_{\text{propeller}} \left(\frac{\rho}{\rho_0}\right)^{\frac{3}{4}} \left[\frac{C_{D_0}\frac{1}{2}\rho V_{\text{max}}^3}{W/S} + \left(\frac{W}{S}\right)\frac{1}{\pi A e \frac{1}{2}\rho V_{\text{max}}}\right]^{-1} \tag{11.12}$$

11.5. Flight Envelope

Studying the performance of the aircraft at different flight phases, the performance can be visualised in different flight envelopes. First, the relation between altitude and velocity will be discussed, whereafter the load factor will be related to the velocity.

11.5.1. Altitude Velocity

Relating the maximum altitude of the aircraft to the velocity it can fly at, a flight envelope is constructed visualising all constraints present on the aircraft. The result is shown in Figure 11.2. The service ceiling is visualised by the horizontal line in the plot, meaning the aircraft can fly at a maximum of 5226 m. The service ceiling is defined as the altitude at which the aircraft cannot perform a climb rate of more than 100 feet per minute anymore (Gundlach 2014). Furthermore, the minimum and maximum velocity constraints are presented by the mainly vertical lines in the figure. Due to the relatively

[56] `http://web.mit.edu/16.unified/www/FALL/thermodynamics/notes/node98.html` [cited on: 22-06-2018]

low velocity, there is no maximum Mach number influencing the flight envelope; only below Mach 0.1 this parameter would influence the maximum velocity possible.

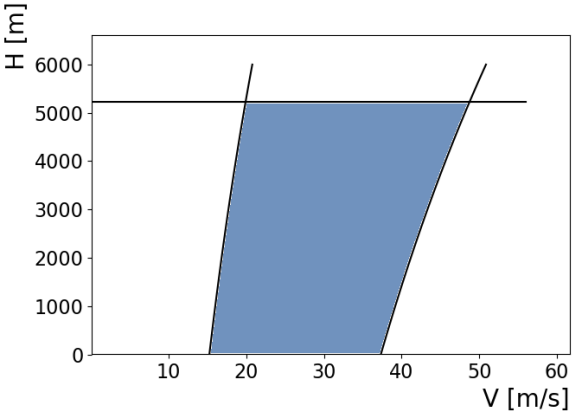

Figure 11.2: Altitude velocity diagram of the UAV.

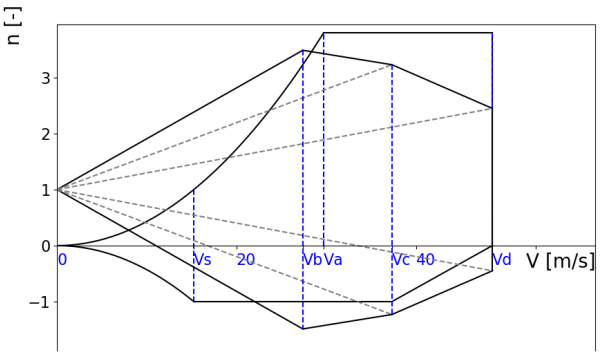

Figure 11.3: Load factor n - velocity V diagram of the UAV.

11.5.2. Load Factor Velocity

Not only altitude and velocity constraints are present on the aircraft, but also the maximum positive and negative load factors are of importance. Figure 11.3 shows the relation between the load factor and velocity of the aircraft at cruise condition, normalised to sea level, transforming true airspeed to equivalent airspeed. Clearly, the maximum positive and negative load factors are 3.8 and -1 respectively. Multiplying by a safety factor of 1.5 yields the ultimate load factors of 5.7 and -2.2. Initially the requirements stated that the aircraft should be able to cope with a load factor of 3, which means that this requirement is easily met.

11.6. Verification and Validation

Verification of the performance model regarding power to weight loading is done by visual inspection of the resulting plot and checking the relative orientation of the different constraints in them. The fuel burn model is verified by checking the fuel to weight ratio for various flight phases with statistics. Finally, the flight envelopes are checked visually by inspecting the plot and checking the order of magnitude of the results. The Fokker 27 is a relatively small turboprop passenger aircraft and since there is a lot of data available on this aircraft, it will be used for validation of the performance model. Calculating the fuel burn and optimal velocities for a complete mission on its maximum range of 1550 kilometres, the code can be validated. The results are shown in Table 11.2.

Table 11.2: Validation of performance model with Fokker 27.

Parameter	**Fokker 27 data (G. Whiley 2016) (Green. 1970)**	**Model**	**Deviation [%]**
Climb speed [m/s]	82.3	72.2	12.3
Rate of climb [m/s]	7.37	7.96	8.0
Cruise speed [m/s]	115.7	114.6	1.0
Loiter speed [m/s]	99.4	83.6	15.9
Fuel used [kg]	4112	4065	1.1
Wing loading[kg/m^2]	282	273	3.2
Power loading[kg/W]	0.071	0.065	7.8
Service ceiling[m]	8992	8024	10.0
Maximum speed at cruise altitude[m]	128.6	134.7	4.7

As can be seen from this table, the performance model is within 10% accurate on all results except for the climb speed and the loiter speed. Especially the latter is difficult to obtain for different aircraft, and for now the aircraft is assumed to loiter at Mach 0.3[57]. Of course, this number is not really accurate and a general specification for loiter speed is not as accurate as an aircraft specific number. The deviation in climb speed can be partly explained by the lack of knowledge about the lift coefficient at this flight phase as well as the exact power setting during climb. Looking at the service ceiling of the aircraft, the importance of the propeller efficiency and drag coefficient has to be stressed. Using an assumed propeller efficiency of 0.8, which is average for general aviation (Roskam 2000) and a parasitic drag coefficient of 0.02, the above values are found. Changing the parasitic drag coefficient to e.g. 0.015 would increase the service ceiling to 8406 m, which is only a 6.5% deviation of the given ceiling. Finally, the remaining flight envelope is only checked qualitatively since there is no sufficient data available to validate this method quantitatively.

[57] `http://nptel.ac.in/courses/101106035/011_Chapter%203_L8_(02-10-2013).pdf` [cited on: 21-06-2018]

12 Propulsion System

This chapter discusses the design and performance of the propulsion system used on the MAINTAIN UAV. The chapter starts with selection of the fuel used for propulsion in section 12.1. Next, high-level decisions on the propulsion system are presented in section 12.2. section 12.3 describes the characteristics of the thermodynamic cycle of the engine. Finally, in section 12.4, the overall engine performance is analysed and its components are designed in greater detail.

12.1. Fuel Selection

In order to improve the sustainability of MAINTAIN, the micro gas turbine that propels the UAV will run on a bio fuel. In this chapter the fuel for the micro gas turbine is chosen by means of a trade-off process.

12.1.1. Exploring Bio Fuels

A bio fuel is defined as any fuel that is derived from biomass[58]. Nowadays a variety of bio fuels are known, which are not all included in the trade-off since some types of bio fuel are not suitable for aircraft applications. Therefore, first a pre-selection is done in order to focus the trade-off procedure on suitable candidates for this application. Bio fuels are distinguished by 4 different generations. The first generation contains bio fuels that are produced with food crops as feed stock. Sequentially, the second generation is produced using non food crops or food crops that have already served their purpose. The third and fourth generations are characterised by respectively algae feed stock and the conversion of solar energy into fuel (Aro 2016). Since the 3rd and 4rd generation do both not exceed a Technology Readiness Level (TRL) of 7[59] [60], which means they are still in the pilot and demonstration phase, these are not considered in the trade-off.

The UAV designed in this project uses a micro gas turbine as propulsion system, therefore the fuel should be suited for gas turbines. A consequence is that only liquid and gaseous bio fuels are considered. Both hydrogen (not a real bio fuel but renewable if produced from renewable electricity) and bio gas are also not included in the trade-off because the requirement of cryogenic or pressurised storage makes them unsuitable. As found in (Nascimento and Santos 2011), both ethanol and bio diesel are convenient as fuel for gas turbines, due to reasons like availability and physical-chemical characteristics similar to fuels like kerosene and diesel. In practice, bio fuels are often mixed with fossil fuels. Therefore, in the rest of this section a bio fuel refers to a mixture of at least 50 volume % fuel derived from biomass. As a result, in this trade-off different types and blends of bio ethanol and bio diesel are considered. The types of fuels that are included in the trade-off are presented in Table 12.1

Table 12.1: Bio fuels included in the trade-off.

Fuel	Description
E85	Blend of 85% bio ethanol and 15% gasoline
E100	100% bio ethanol
B50	Blend of 50 % Fatty acid methyl ester (FAME) and 50% diesel
B100	100 % Fatty acid methyl ester (FAME)
Green Diesel	hydrotreated vegetable oil (HVO)

12.1.2. Trade-Off Criteria

To select the most feasible bio fuel, important characteristics the fuel of the UAV should possess are determined. In the trade-off these characteristics are used as the trade-off criteria. The trade-off criteria are as follows:

- **Specific Energy:** The amount of MJ contained by a kg fuel. Important to keep the fuel weight to a acceptable level.
- **Cost:** The cost in USD per litre fuel. Relevant to keep the operational cost of the UAV as low as possible.
- **Energy Density:** The energy stored per litre fuel. This criterion is important to keep the required size of the fuel tank acceptable.

[58] `https://www.britannica.com/technology/biofuel` [cited on: 24-06-2018]
[59] `https://www.wider.unu.edu/sites/default/files/wp2017-87.pdf` [cited on: 23-05-2018]
[60] `https://www.ncbi.nlm.nih.gov/pmc/articles/PMC4678123/` [cited on: 03-06-2018]

- **CO_2 emission:** The amount of CO_2 emitted per mega joule extracted from the fuel. Fuels which use renewable hydrocarbons (carbons extracted from the atmosphere before being used as a fuel) are considered to have no contribution to the CO_2 increase in the atmosphere.
- **Freezing/cloud point:** The temperature at which the fuel starts to freeze or gets a cloudy appearance. Operational temperatures equal or below the freezing/cloud point cause problems in the engine since the thickened fuel might clog fuel filters and injectors in the gas turbine.

The trade-off is performed using the Analytic Hierarchy Process (AHP), as fully explained in (B. van Beurden et al. 2018a). The AHP process compares all trade-off criteria with respect to each other to determine their relative importance. Next, all bio fuels are compared with respect to each other for each trade-off criterion. Combining this with the relative importance of each criterion a trade-off result is generated. The relative importance of the trade-off criteria as determined using the AHP method are: specific energy (36%), cost (34%), CO_2 emission (13%), energy density (12%), and freezing/cloud point (5%). The availability and feasibility are not considered in the trade-off because all fuels considered in the trade-off were checked to be commercially available and feasible for a gas turbine. Although the trade-off criteria are measured quantitative, the trade-off is performed using qualitative scores. The quantitative values on which the trade-off is based are shown in Table 12.2

Table 12.2: Quantitative scores of the bio fuels in the trade-off.

	Specific Energy[MJ/kg]	**Cost[USD]**	**Energy Density[MJ/L]**	**CO_2 emission[kg/MJ]**	**Freezing/Cloud point[°C]**
E85	32.8[61]	0.58[62]	25.59[70]	13.35[63]	-97[64]
E100	29.7[62]	0.53[63 65]	24[70]	0[64]	-115[66]
B50	41.28[62 69]	0.87[66 67]	34.6[70]	35.09[64]	-13(Heck et al. n.d.)
B100	37.2[68]	0.90[68]	30.53[69]	0[64]	-2.44 (Demirbas 2008)
Green Diesel	44[70]	0.94[71]	34.32[71]	0[64]	-25 (T. J. Hilbers et al. 2015)(Aatola, Larmi, and Sarjovaara 2008)

12.1.3. Trade-Off Result

From the trade-off process it is decided that Green diesel (HVO) is the most suitable fuel for the micro gas turbine of MAINTAIN. The main reasons are the high specific energy, high energy density and the fact that is completely produced using renewable hydrocarbons. The largest drawback of green diesel is the cost of the fuel. Table 12.3 contains the most important properties of green diesel.

Table 12.3: Characteristics of green diesel (Aatola, Larmi, and Sarjovaara 2008)(NESTE 2016)(T. J. Hilbers et al. 2015).

Characteristic	**Value**
LHV [MJ/L]	34.4
Density[kg/m^3]	780 (T. J. Hilbers et al. 2015)
Viscosity (@ 40 °C) [mm^2/s]	3.0
Cloud point [°C]	-25
Flash point [°C]	>61
Auto-ignition temperature [°C]	204

Green diesel obtains its good properties through the production process, which significantly different from the production process of biodiesel (FAME). During the production of green diesel hydro cracking and isomerisation are performed. These two processes control the length of the chains of the fuel and rearrangement of the atoms within a fuel molecule, respectively. These adjustments cause the fuel to obtain high quality (T. J. Hilbers et al. 2015). Although green diesel is

[62] https://neutrium.net/properties/specific-energy-and-energy-density-of-fuels/ [cited on: 17-06-2018]
[63] https://www.worleyobetz.com/commercial/wholesale-fuels-transport/e85-ethanol [cited on: 17-06-2018]
[64] Based on calculation made on the molecular combustion reaction. Only non-renewable hydrocarbons are considered to add CO_2 emission to the atmosphere
[65] Estimate based on ethanol/gasoline fractions.
[66] https://www.globalpetrolprices.com/ [cited on: 17-06-2018]
[67] https://www.engineeringtoolbox.com/ethanol-water-d_989.html [cited on:17-06-2018]
[68] https://www.afdc.energy.gov/fuels/prices.html [cited on: 17-06-2018]
[69] https://ec.europa.eu/energy/intelligent/projects/sites/iee-projects/files/projects/documents/biomotion_biodiesel_and_plant_oil_leaflet_en.pdf [cited on: 17-06-2018]
[70] http://www.energy-101.org/renewable-energy/biofuelsbiomass-facts/biofuel/biofuel-ethanol-basics [cited on: 17-06-2018]
[71] https://advancedbiofuelsusa.info/wp-content/uploads/2011/03/11-0307-Biodiesel-vs-Renewable_Final-_3_-JJY-formatting-FINAL.pdf [cited on: 17-06-2018]

completely produced using renewable hydrocarbons, the production process itself consumes some energy. **Considering the complete life-cycle of green diesel it provides a 80% decrease in greenhouse gas emissions with respect to fossil diesel**[72]. The high quality of green diesel makes it possible to use green diesel without making alterations to the diesel engine[73]. However in MAINTAIN HVO is used as fuel for a micro gas turbine. No data is available on the alterations required to the gas turbine to achieve efficient combustion of HVO. Therefore, the combustion properties of HVO should be examined and if needed, alteration to the gas turbine should be made. Table 12.4 presents parameters which affect the processes inside the micro gas turbine. The values of Jet-A, a fuel frequently used in aerospace gas turbine application, are compared to those of Green Diesel. By examining the data in Table 12.4 the following conclusions were drawn:

- The slightly higher LHV of green diesel with respect to kerosene can cause high flame temperatures, therefore attention must be paid to make sure the temperatures inside the gas turbine stay within an acceptable range (K. Sugiyama et al. 2011). A possible measure is adding more primary air than needed for combustion.
- Significant difference exists between the viscosity of kerosene and green diesel. Therefore, the automization of the fuel should be adjusted to the viscosity, and also the density and surface tension of green diesel.
- The amount of solid particles in green diesel are less than in kerosene: therefore no additional erosion problems with the material inside the turbine are expected (Kallenberg 2013).
- The pressurisation pumps in the fuel tanks should be adjusted to the density and kinematic viscosity of HVO.

Table 12.4: Characteristics comparison of HVO and Jet A-1.

Characteristic	**Jet A-1**	**Green diesel (HVO)**
LHV [MJ/kg]	42.8	44
Density [kg/m^3]	810	780
Kin. viscosity @ 40°C [$cSt(mm^2/s)$]	1.5	3.01
Solids [wt%]	0.001	<0.001

12.1.4. Logistic Aspects

Green diesel is not available at or near most airports in the US. Therefore, the supply of green diesel must be arranged by the operator of MAINTAIN. Well arranged shipping possibilities for green diesel are available[74]. Combined with the fact that green diesel is suitable for storing makes it possible to use it during the operations of MAINTAIN. There are several reasons why green diesel is suitable for storing. First of all, green diesel is not classified as a hazardous material like diesel and hence permits for storage facilities should be obtainable within acceptable timeframes[74]. Secondly, if available, green diesel can be stored in existing diesel tanks without any alterations[75]. Furthermore, green diesel does not have the storage stability problems that FAME has and can be stored without effects on fuel quality[76]. Consequently, large amounts of green diesel can be stored for long periods of time which provides freedom in the optimisation of the distribution of green diesel to all airports from which MAINTAIN is operating.

12.2. System Level Decisions

Before performing the more detailed design of the propulsion system, some characteristics are constrained beforehand. These are high-level decisions that will not be adapted during the optimisation process. This section discusses these decisions.

12.2.1. Engine Type

A high-level constraint for the project was that the UAV needs to feature a micro gas turbine (MGT). Such a gas turbine engine usually comes in the form of a turbojet, turbofan or turboprop within aerospace applications. **The turboprop type was selected as it is the only engine type which performs well at lower flight speeds, because its propeller allows sufficient mass flow for thrust generation.**

12.2.2. Engine Number

The engine number was chosen to be one. This was because the MGT suffers decreased performance due to its smaller size. Higher viscosity, lower control of temperature and manufacturing tolerances all decrease its efficiency. Choosing for multiple engines, although offering redundancy, would decrease size and efficiency. Additionally, the required emergency landing system mitigates the severity associated with the risk of engine failure.

[72] https://www.honeywell.com/newsroom/pressreleases/2017/03/diamond-green-diesel-to-expand-renewable-fuel-capacity\-using-ecofining-technology-from-honeywell-uop [cited on: 03-06-2018]
[73] https://www.neste.com/customers/renewable-products/neste-my-renewable-diesel [cited on: 16-06-2018]
[74] http://gosunshinebiofuel.com/renewable-biofuel-diesel-fuel-delivery/[cited on: 03-06-2018]
[75] http://onbio.co.uk/fuels/eco-renewable-diesel/ [cited on: 03-06-2018]
[76] https://www.neste.us/customers/products/renewable-products/nexbtl-renewable-diesel/key-benefits [cited on: 03-06-2018]

12.2.3. Engine Placement

For reasons of lateral stability, the single engine will be placed in the symmetry plane of the UAV. As such, the choice of placement is between a tractor propeller in front of the body and a pusher propeller aft of the body. A set of factors that affect the choice between the two are the following:

- Centre of gravity location (stability)
- Engine performance
- Noise
- Aerodynamic interference
- Ground clearance
- Payload performance

After the trade-off, the pusher configuration proved to be the best option. Critical was its small effect on payload performance whereas the tractor configuration would cause significant swirl aft of the propeller which would cause turbulence on the part of the wing in which the payload will be stored, negatively affecting its performance.

12.2.4. Propeller Type

The most basic propeller is a fixed pitch propeller. A fixed pitch propeller has a pitch which is fixed by the manufacturer and the power output is regulated by varying the Round Per Minute (RPM). Consequently, this type of propeller is the propeller type with the lowest life cycle cost. However, this cost advantage is reached at the expense of another important design parameter, namely efficiency. Since the pitch of this type of propeller is fixed, a compromise between performance and efficiency is made. The propeller can be designed for either one flight condition or the design is a comprise between the optimal designs for different flight conditions. To increase efficiency, several options are considered. All of the efficiency increasing measurements increase the weight of the propeller. Therefore, to ensure stability, the amount of efficiency increasing measurements is set to one. The different efficiency increasing measurements entering the trade-off are displayed in Table 12.5.

Table 12.5: Efficiency increasing measures with respect to fixed pitch propeller.

Propeller Type	**Way of increasing efficiency**
Contra-rotating propeller	Recovery of the swirl energy (E. Bradley et al. 1982) Torque exerted on the airplane cancels out
Ducted propeller	Reduce induced drag at propeller tips (Longbottom 2006)
Constant speed propeller	Varying pitch to optimise efficiency at each mission segment[77]

Subsequently, a trade-off is performed between the different measures stated in Table 12.5. The options are evaluated based on their Technical Risk, Cost, Weight, Sustainability and Efficiency Increase. The trade-off is performed qualitatively and presented in Table 12.6.

Table 12.6: Trade-off between efficiency increasing measurements.

	Technical Risk	**Sustainability**	**Cost**	**Weight**	**Efficiency increase**
Contra-rotating propeller	Not often seen on HTOL UAV	Increased Noise (Vanderover and K. D. Visser n.d.)	Complex inner structure (Stefanov-Wagner 2006)	Increased weight	No side effects
Ducted propeller	Not often used on HTOL UAV or general aviation	Reduced noise(when using liners)[78], More safe (Mason 2003)	High production costs due to small tolerances, high design costs[79] (Mei and Zhou 2015)	Increased weight	Increased drag during cruise (Recks 1977)
Constant speed propeller	Often used in HTOL UAV[80]	No major effects	Hydraulic/Electric system included[81]	Increased weight	No side effects

From the trade-off it is decided to use a constant speed propeller. Main reasons are the low technical risk and the fact that, compared to the other options, no major side effects are induced by the implementation of a constant speed propeller.

12.2.5. Number Of Propeller Blades

The propeller design optimisation is not able to design all parameters describing the propeller. Therefore, some parameters are set before starting the optimisation. Here the basic geometry of the propeller, e.g. the number of blades of the propeller, is selected. In theory a single bladed propeller is aerodynamically most efficient, this is caused by the fact that the interference between the blades and tip losses are minimised (Martinez 2018). However due to stability reasons the number of blades is set to two. To support this decision a study was done on the propellers of reference UAVs as found in (B. van Beurden et al. 2018b). It was found that 77.5% of the reference aircraft is equipped with a two bladed propeller, most of them having a higher power than the maximum power required. **Therefore the decision to use a double bladed propeller is considered reasonable.** However, if ground clearance or tip speed of propeller blades due to large diameter of the blades becomes a problem, the number of blades can be increased to overcome this problem.

12.2.6. Propeller Airfoil

Airfoils suitable for the wings of the UAV are not efficient for the propeller, because the local velocity of on propeller sections is higher than the speed of the aircraft. The local velocities on propeller sections can approach the speed of sound. General wing airfoil sections would become very inefficient at these speeds, therefore the NACA 16-series was developed to overcome this problem. The NACA 16-series is designed to prevent thrust losses and increased drag due to shock formation in high speed regions. For now, the airfoil selection will not be optimised and a NACA 16 series airfoil with a relatively high L/D ration for High Reynolds numbers is used. The selected airfoil is the NACA 16-012 and is shown in Figure 12.1.

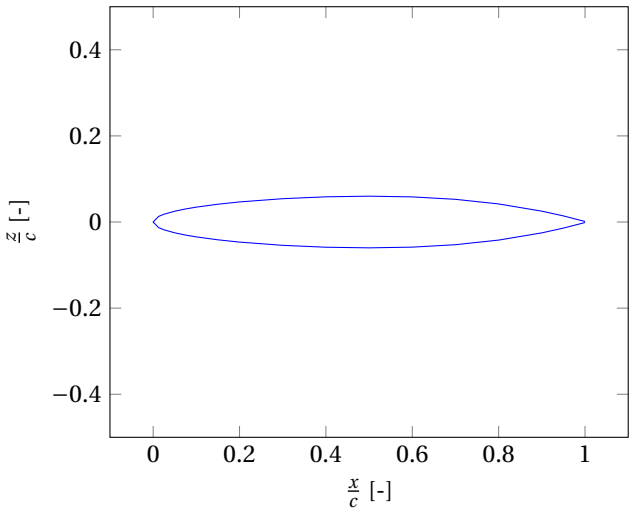

Figure 12.1: Plot of the NACA 16-012 airfoil used for the propeller blades.

12.3. Engine Thermodynamic Cycle Characteristics

The design of the turbo machinery is greatly dependent on the engine characteristics. The parameters related to the compressor, combustor and turbine influence the engine performance. The required shaft power, turbine inlet temperature (TIT), mass flow and compressor pressure ratio are additional parameters utilised in the engine design. The engine is sized based on the design point, which is chosen to be standard atmospheric conditions at sea level during take-off. A performance analysis of the engine during cruise conditions, an off-design condition, is subsequently conducted.

First, a scaling factor (SF) is determined based on power output ratio of the MAINTAIN engine and a reference gas turbine engine: the Capstone C30. This is depicted in Equation 12.1. The specifications of the Capstone C30 can be found in Table 12.7. The mass flow is estimated based on a correlation between mass flow in a gas turbine engine and the scaling factor as can be seen in Equation 12.2.

$$SF = \frac{PW_{des}}{PW_{ref}} \tag{12.1}$$

$$\dot{m}_{air} = \dot{m}_{air,ref} \cdot SF \tag{12.2}$$

From the performance analysis, a required engine power of 3.75 kW can be extracted. Using Equation 12.2 and data from Table 12.7 (*Capstone Turbine Corporation* 2018) the mass flow for the MAINTAIN engine can be estimated. Table 12.8 shows the other engine specifications necessary to perform a design point analysis in GSP which is a gas turbine simulator program. The propeller efficiency in Table 12.8 is the result of the propeller design performed in subsection 12.4.4. To further design and optimise the engine design, it is chosen to perform a design point sweep by varying compressor pressure ratio and TIT. This results in the carpet plot found in Figure 12.2. Reference micro gas turbine engines have pressure ratios between 3 and 4 (Nascimento, Oliveira Rodrigues, et al. 2013) (Steyn 2006) and since the engine utilises a single stage centrifugal compressor that is capable of achieving a pressure ratio up to 10 (Pini 2018), the pressure ratio range is verified. With advanced materials such as MAR-M247 (W. P. J. Visser, Shakariyants, and Oostveen 2011), the TIT can be raised up to 1300 K. Therefore a TIT range of 1100-1300 K is chosen to see the influence of the TIT on the engine performance.

Table 12.7: Engine specifications C30 Capstone micro gas turbine.

Parameter	Value	Unit
Power	30	kW
Inlet air flow	0.31	kg/s

Table 12.8: Micro Gas Turbine Engine Specifications Utilised in Design Point Sweep.

Symbol	Parameter	Value	Unit
η_m	Mechanical Efficiency (Oppung et al. 2017)	0.98	[-]
Π	Pressure Ratio (Nascimento, Oliveira Rodrigues, et al. 2013) (Steyn 2006)	3-8	[-]
η_c	Compressor Isentropic Efficiency (Oppung et al. 2017)	0.82	[-]
η_t	Turbine Isentropic Efficiency (Oppung et al. 2017)	0.85	[-]
η_{cc}	Combustor Isentropic Efficiency (Oppung et al. 2017)	0.9	[-]
η_p	Propeller Efficiency	0.93	[-]
TIT	Temperature Inlet Turbine	1100-1300	K

Taking the propeller efficiency of 93 % into account which followed from the propeller design, the required shaft power is approximately 4 kilowatts. **According to Figure 12.3, a compressor pressure ratio of 6 and a TIT of 1210 K provide this power with a minimised TSFC.**

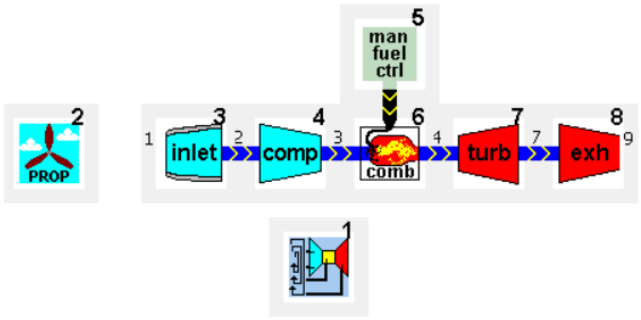

Figure 12.2: GSP model of single spool turboprop configuration.

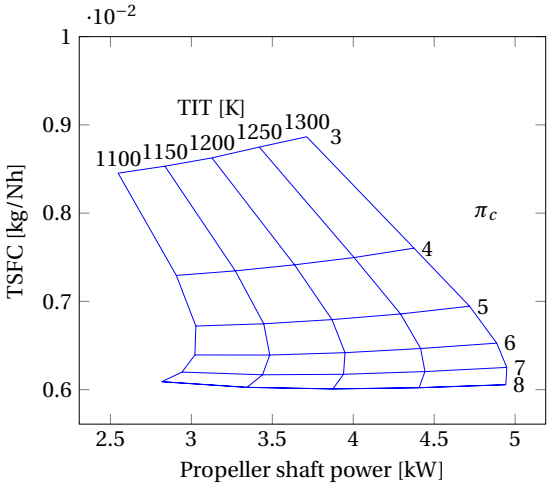

Figure 12.3: Carpet plot of engine design points for varying pressure ratio and TIT.

12.4. Engine Component Design

This section elaborates upon the design of the compressor, turbine and propeller. **Both the compressor and turbine are of the radial type as this mitigates part of the increased tip losses for a micro gas turbine.** This is because axial flow turbomachinery requires higher tip clearances (Dixon 2005).

12.4.1. Inlet Design

The inlet will be designed as to accommodate the mass flow required for sufficient engine performance throughout the flight envelope. Boundary layer ingestion (BLI) will be used to increase the efficiency of the propulsion system. The boundary layer has a slower velocity than the undisturbed freestream flow. Denoting the airspeed with U, the thrust for a podded engine is equal to:

$$T = \dot{m}(U_j - U_\infty) \tag{12.3}$$

With power input required as:

$$P_{\text{in}} = \frac{\dot{m}}{2}(U_j^2 - U_\infty^2) = \frac{T}{2}(U_j + U_\infty) \tag{12.4}$$

Now, if one assumes that for a BLI system, the inlet air speed U_w is less than U_∞, which is caused by viscous effects, it is clear that for a given thrust level, the power input required with BLI is:

$$P_{\text{in}_{\text{BLI}}} = \frac{T}{2}(U_w + U_\infty) \tag{12.5}$$

Hence $P_{\text{in}_{\text{BLI}}} < P_{\text{in}}$. The BLI effect does not come without penalties however. The flow is commonly turbulent and thus may cause stability issues within the engine. However, small passive flow control devices can already have large positive effects (Allan, Owens, and Berrier 2004) on this distortion.

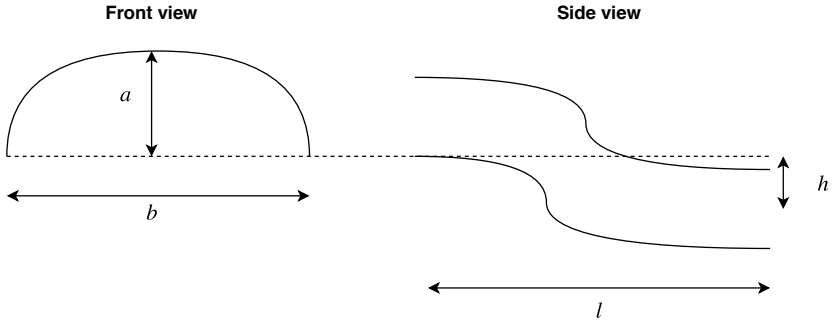

Figure 12.4: Parametrisation of engine n.

A parametrisation of such a BLI inlet is shown in Figure 12.4. Note that the side curves are parametrised as well in some form of spline. Two key performance metrics are defined for BLI inlets as in Equation 12.6 and Equation 12.7.

$$DC_{60} = \frac{P_{t,m} - P_{60,\min}}{q_\infty} \tag{12.6}$$

$$PRF = \frac{P_{t2}}{P_{t0}} \tag{12.7}$$

The Distortion Coefficient is a measure of the pressure variation over the inlet face of the engine, whereas the pressure recovery factor is a measure of the total efficiency of the inlet. It is desired to have PRF as close to unity as possible, and to have DC_{60} as low as possible. From parametric analysis in (Rao, Sharma, and Dijk 2017) it is apparent that for given flow conditions, an optimum for the aspect ratio of the inlet will exist. The suggested aspect ratio, $\frac{b}{a}$ based on this work for the inlet is 1.25. The height and length are made as small as possible. Using the aspect ratio AR_{inlet} the mass flow at a given flight condition is found as:

$$\dot{m} = \frac{\pi}{2} AR_{\text{inlet}} a^2 U_{\text{inlet}} \tag{12.8}$$

Where $U < U_\infty$. From Equation 12.8 it is found that:

$$a = \min_{\dot{m}, U_{\text{inlet}}} \sqrt{\frac{2\dot{m}}{\pi AR_{\text{inlet}} U_{\text{inlet}}}} \tag{12.9}$$

With $\dot{m}, U$ varying over the flight envelope of the UAV.

12.4.2. Compressor Design

Before the design of the compressor stage can start, a high-level decision has to be made regarding the nature of the compressor; centrifugal or axial. According to (Olivero 2012) radial-flow components are usually selected for the compressor stage of turbine engines since radial-flow components offer minimum surface and end-wall losses and provide the highest efficiency. Furthermore, centrifugal compressors can offer high pressure ratio per stage and are less expensive to manufacture compared to their axial counterpart. Therefore, MAINTAIN utilises a centrifugal compressor. 12.5 displays a sketch of such a compressor with the accompanying velocity triangles at the inlet and outlet of the impeller. The preliminary design is computed with a method of (Dixon 2005).

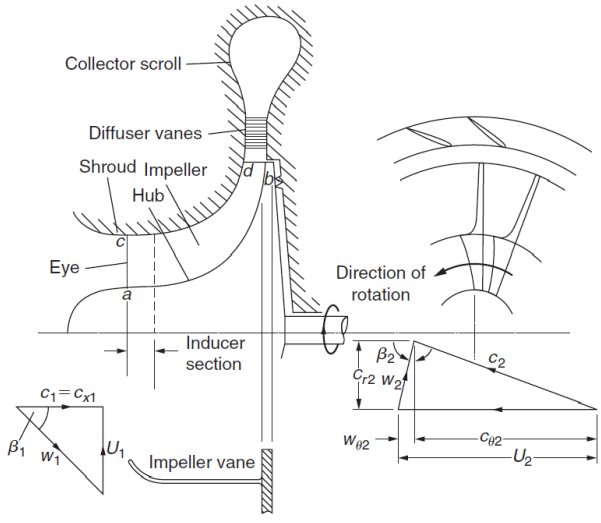

Figure 12.5: A sketch of a radial compressor with the accompanying velocity triangles at the inlet and exit of the impeller (Dixon 2005).

The governing equations used in the compressor design are the ideal gas law and the continuity equation.

The design start with the determination of the blade speed and impeller radius. This radius is found by using the Stanitz expression for the slip factor (Equation 12.10) and together with the specific work results in the blade speed as specified in Equation 12.11. Finally the impeller radius can be computed with Equation 12.12.

$$\sigma = 1 - 0.63\frac{\pi}{Z} \quad (12.10) \qquad U_2 = \sqrt{\frac{\Delta W}{\sigma}} \quad (12.11) \qquad r_2 = \frac{U_2}{\Omega} \quad (12.12)$$

Subsequently, the design of the impeller inlet performed. The first step is to choose a suitable choice of relative Mach inlet number at the shroud. The optimum angle of the incoming flow, β_{s1}, occurs when Equation 12.13 is maximum. To find this optimum, Equation 12.13 is differentiated with respect to $\beta s1$ resulting in Equation 12.14.

$$f(M_{1,rel}) = \frac{\Omega^2 \dot{m}}{\pi k p_{01} \gamma a_{01}} = \frac{M_{1,rel}^3 \sin(\beta_{s1})^2 \cos(\beta_{s1})}{(1+0.2M_{1,rel}^2 \cos(\beta_{s1})^2)^4} \quad (12.13) \qquad \cos(\beta_{s1})^2 = 0.7 + \frac{1.5}{M_{1,rel}^2} - \sqrt{0.7 + (\frac{1.5}{M_{1,rel}})^2 - \frac{1}{M_{1,rel}^2}} \quad (12.14)$$

Using the definition of k given in 12.16, the value of $f(M_{1,rel})$ at optimum β_{s1}, the continuity equation as displayed in Equation 12.15 and isentropic relations, the values for the inlet shroud radius r_{s1} and inlet hub radius r_{h1} can be computed.

$$\dot{m} = \rho_1 A_1 c_{x1} \quad (12.15) \qquad k = 1 - \left(\frac{r_{h1}}{r_{s1}})^2\right) \quad (12.16)$$

For the vanes on the impellers, an impeller efficiency η_i of 92% is assumed (Dixon 2005). For simplicity reasons and lower manufacturing costs radial vanes are applied on the impeller. Furthermore, a common assumption is to take the radial velocity at impeller exit c_{r2} equal to the axial velocity c_{r1} at the inlet. The angular velocity out outlet $c_{\theta 2}$ can be calculated with Equation 12.17. Thereafter, the total velocity at outlet c_2 follows from addition of radial and angular velocity as can be seen in Equation 12.18. The angle of the flow α_2 measured from radial direction is constructed according to Equation 12.19

$$c_{\theta 2} = U_2 \sigma \quad (12.17) \qquad c_2 = \sqrt{c_{\theta 2}^2 + c_{r2}^2} \quad (12.18) \qquad \alpha_2 = \arctan\left(\frac{c_{\theta 2}}{c_{r2}}\right) \quad (12.19)$$

Using Equation 12.20 and Equation 12.21 the ratio of $\frac{T_{02s}}{T_{01}}$ can be obtained. The subscript 's' denotes a process with no entropy increase. With this ratio, $\frac{p_{02}}{p_{01}}$ can be computed and subsequently p_{01}. The value of T_2 results from an energy balance, isentropic relations and the ideal gas law, values for p_2 and ρ_2 are found.

$$\eta_i = \frac{\frac{T_{02s}}{T_{01}} - 1}{\frac{T_{02}}{T_{01}} - 1} \quad (12.20) \qquad \frac{T_{02}}{T_{01}} = \frac{\Delta W}{C_p T_{01}} + 1 \quad (12.21)$$

By applying Equation 12.15 in which the area A_2 is defined by Equation 12.22 and the impeller exit radius r_2 by Equation 12.23, Equation 12.24 is constructed and the width of flow exit passage b_2 can be calculated.

$$A_2 = 2\pi r_2 b_2 \quad (12.22) \qquad r_2 = \frac{U_2}{\Omega} \quad (12.23) \qquad b_2 = \frac{\dot{m}}{2\pi \rho_2 c_{r2} r_2} \quad (12.24)$$

The next step is to analyse the flow in the vaneless space. This space is defined as the spatial difference between the impeller exit radius r_2 and the start of the diffuser vanes r_{2d}. According to (Dixon 2005) the minimum value of the ratio $\left(\frac{r_{2d}}{r_2}\right)$ is 1.1, it is also assumed that the width of the vaneless space b_2 remains constant. Furthermore, flow that enters the vaneless space is assumed to be smooth, frictionless and incompressible. The tangential velocity at start of diffuser vanes $c_{\theta 2d}$ can be computed with Equation 12.25 and the radial velocity c_{r2d} with Equation 12.26. T_{2d} follows from an energy balance and subsequently M_{2d} can be computed.

$$c_{\theta 2d} = \frac{r_2 c_{\theta 2}}{r_{2d}} \quad (12.25) \qquad c_{r2d} = \frac{r_2}{r_{2d}} c_{r2} \quad (12.26)$$

For the vaned diffuser a conical shape is adopted with a C_p of 0.8 and a $C_{p,id}$ of 0.949. The static pressure at diffuser exit p_3 and exit velocity c_3 are calculated with Equation 12.27 and Equation 12.28 respectively. The number of diffuser exit nozzles is to a certain extend an arbitrary number and for the design of MAINTAIN 12 nozzles will be taken which corresponds with common manufacturing standards (Dixon 2005).

$$p_3 = p_{2d} + C_p q_{2d} \quad (12.27) \qquad c_3 = c_{2d}(1 - C_{p,id}) \quad (12.28)$$

The last component of the centrifugal compressor is the volute which main role is to guide the flow to the engine intake. A good assumption is to state that half of the dynamic pressure is lost in the volute part. First calculate the exit temperature T_{03} with an energy balance, thereafter calculate the density with the ideal gas law and compute the dynamic pressure. Equation 12.29 displays the total pressure p_3 as a function of static and dynamic pressure.

$$p_{03} = p_3 + q_3 \tag{12.29}$$

Finally, the total efficiency of the compressor is found by Equation 12.30 in which $\frac{T_{03ss}}{T_{01}}$ follows from Equation 12.31.

$$\eta_c = C_p T_{01} \frac{(\frac{T_{03ss}}{T_{01}} - 1)}{\Delta W} \tag{12.30}$$

$$\frac{T_{03ss}}{T_{01}} = \left(\frac{p_{03'}}{p_{01}}\right)^{\frac{1}{3.5}} \tag{12.31}$$

12.4.3. Turbine Design

The radial turbine is analysed in greater detail by employing a mean-line flow analysis. This analysis assumes axi-symmetry of the flow in the turbine. It also neglects the fundamental physical phenomena responsible for energy transfer and instead focuses more on a higher-level approach. The method is a combination of several previous methods (Glassman 1972)(Whitfield and Baines 2002)(Ventura et al. 2012)(Rahbar et al. 2015).

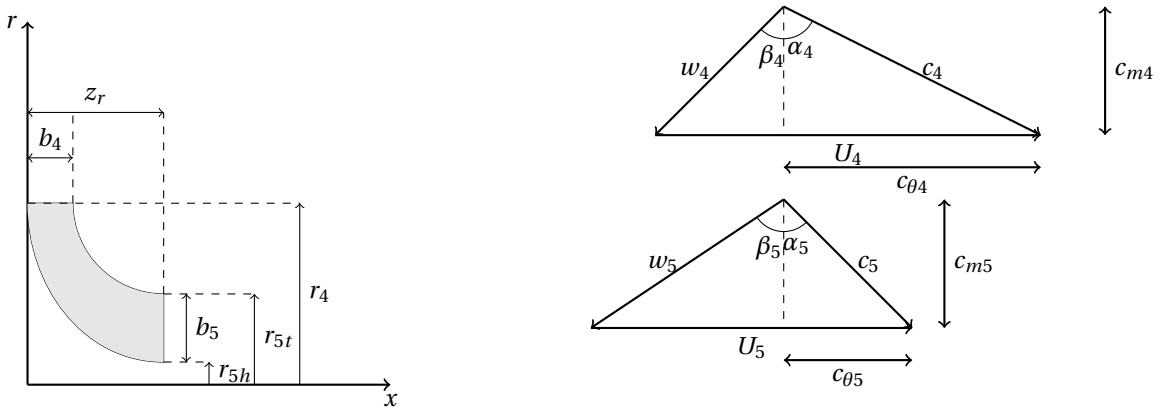

Figure 12.6: Geometrical definition of the rotor part of the radial turbine and the associated velocity triangles.

The geometry of the rotor part of the turbine and the associated velocity triangles are shown in Figure 12.6. The following two fundamental nondimensional numbers for a radial turbine stage are defined to simplify its analysis. The flow coefficient ϕ Equation 12.32 can be seen as as measure of the flow angles within the stage. The stage loading coefficient ψ in Equation 12.33 is the ratio of stagnation enthalpy change to the blade kinetic energy.

$$\phi = \frac{c_{m4}}{U_4} \tag{12.32}$$

$$\psi = \frac{\Delta h_0}{U_4^2} \tag{12.33}$$

Additionally, the analysis assumes that a decision is made on the radius ratio, $\frac{r_{5h}}{r_4}$, a priori. Then, the following analysis can be used to asses the turbine performance. An efficiency, η, is assumed a priori and is to be confirmed after analysis. The blade velocity at the rotor inlet and the accompanying radius can be determined using Equation 12.34 and Equation 12.35.

$$U_4 = \psi \eta \frac{\dot{W}}{\dot{m}} \tag{12.34}$$

$$r_4 = \frac{U_4}{\Omega} \tag{12.35}$$

Looking at Figure 12.6 and using Equation 12.36 and Equation 12.37, the remaining velocities which are needed are found.

$$C_{m4} = C_{m5} = \phi U_1 \tag{12.36}$$

$$C_{\theta 4} = \eta \frac{\dot{W}}{\dot{m} U_4} \tag{12.37}$$

This last step has fixed the velocity triangles. Consequently, the relative velocities w_4, w_5 can be found. Using the previously assumed efficiency η and the inlet state of the rotor, which is related to the inlet state of the stator by the adiabatic assumption, it is possible to find the outlet state. From a mass balance, b_4, b_5, r_{5t}, r_{5h} are found. Next, the stator exit radius, r_3, is found with Equation 12.38.

$$r_3 = r_4 + 2 b_4 \cos(\alpha_3) \tag{12.38}$$

The stator inlet radius is found with the specified ratio of $\frac{r_3}{r_2}$. The number of stator vanes is found using Equation 12.39, where $\sigma_s = 1.35$ is the solidity and set based on (Glassman 1972).

$$Z_{\text{rotor}} = \frac{2\pi r_2}{\sigma_s} \tag{12.39}$$

The loss model used is mostly based on empirical observations and can be found using Equation 12.40. It is quantified as loss in enthalpy.

$$\Delta h_{\text{loss}} = \Delta h_{\text{incidence}} + \Delta h_{\text{friction}} + \Delta h_{\text{secondary}} \Delta h_{\text{exit}} + \Delta h_{\text{clearance}} \tag{12.40}$$

These loss sources are quantified using Equation 12.41 up until Equation 12.46. One can refer to Table 12.9 for an explanation of undefined parameters and their values.

Table 12.9: Constant in the analysis of the radial turbine.

Parameter	Symbol	Value
Radial clearance	ϵ_r	$1.2 \cdot 10^{-3} m$ (Ventura et al. 2012)
Axial clearance	ϵ_x	$1.2 \cdot 10^{-3} m$ (Ventura et al. 2012)

$$\Delta h_{\text{incidence}} = \frac{w_{\theta 4}^2}{2} \tag{12.41}$$

$$\Delta h_{\text{friction}} = f_t \frac{L_h}{D_h} \bar{w}^2 \tag{12.42}$$

$$\Delta h_{\text{secondary}} = \frac{2(c_{\theta 4}^2 + c_{m4}^2) r_4}{Z_{\text{rotor}} r_c} \tag{12.43}$$

$$\Delta h_{\text{exit}} = \left(\frac{c_{m5}^2}{2} \right) \tag{12.44}$$

$$\Delta h_{\text{clearance}} = \frac{U_4^3 Z_{\text{rotor}}}{8\pi} \Gamma_{\text{clearance}} \tag{12.45}$$

$$\Delta h_{\text{nozzle, friction}} = 4 f \bar{c}^2 \frac{L_h}{D_h} \tag{12.46}$$

The hydraulic length and diameter are in this case defined as:

$$L_h = \frac{\pi}{4} \left(\left(z_r - \frac{b_4}{2} \right) + \left(r_4 - r_5 - \frac{b_5}{2} \right) \right) \tag{12.47}$$

$$D_h = \frac{1}{2} \left(\left(\frac{4\pi r_4 b_4}{2\pi r_4 + Z_r b_4} \right) + \left(\frac{2\pi (r_{5t}^2 - r_{5h}^2)}{\pi (r_{5t} - r_{5h}) - Z_{\text{rotor}} b_5} \right) \right) \tag{12.48}$$

The mean relative velocity is defined as in Equation 12.49. The clearance factor $\Gamma_{\text{clearance}}$ can be found as in Equation 12.50.

$$\bar{w} = \frac{w_4 + \left(\frac{w_{5t} + w_{5h}}{2} \right)}{2} \tag{12.49}$$

$$\Gamma_{\text{clearance}} = 0.5 \epsilon_x C_x + 0.75 \epsilon_r C_r - 0.3 \sqrt{\epsilon_x \epsilon_r C_x C_r} \tag{12.50}$$

The relevant friction factor f_t is found by use of Equation 12.53, in which f_c is defined in Equation 12.51 and f in Equation 12.52.

$$f_c = f \left(1 + 0.075 \text{Re}^{0.25} \sqrt{\frac{D_h}{2 r_c}} \right) \tag{12.51}$$

$$f = \frac{16}{\text{Re}} \tag{12.52}$$

$$f_t = f_c \left(\text{Re} \frac{r_4}{r_c}^2 \right)^{0.05} \tag{12.53}$$

After all losses are quantified, it is possible to find the new efficiency value using Equation 12.54. A flowchart of the turbine design process is shown in Figure 12.7.

$$\eta = \frac{\Delta h_0}{\Delta h_0 + \Delta h_{\text{loss}}} \tag{12.54}$$

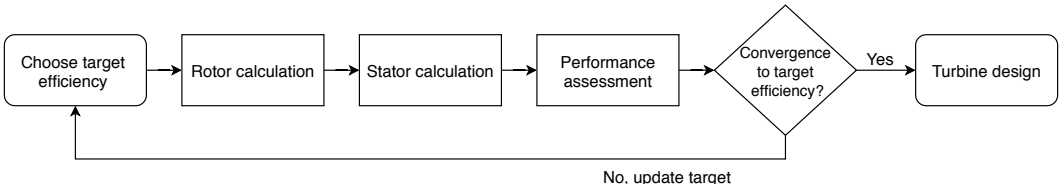

Figure 12.7: Flowchart of the turbine design process indicating the iterative nature of the scheme.

12.4.4. Propeller Design

After specification of hub and tip radii, number of blades and blade airfoil it is possible to optimise the remaining propeller parameters using a condition of minimum energy loss. The presented method is a slight adjustment of that presented in (Adkins and Liebeck 1983). The Betz condition, named after its founder, requires the vortex sheet shed from the propeller to be a regular screw surface (Betz 1958). Such a surface is simply a helicoid with a pitch that is invariant in the radius. This argument is based on the fact that a second identical propeller may always be placed in the wake of the first propeller and that this second propeller's efficiency may always be raised by adjusting the circulation distribution (i.e. the helicoid) unless it is a regular screw surface (Ribner and Foster 1990). A visualisation of this concept of a shed vortex sheet is given in Figure 12.8. Additionally, the geometric conventions of the propeller design are shown in Figure 12.9. A visual explanation of the induced velocity can be found in Figure 12.10

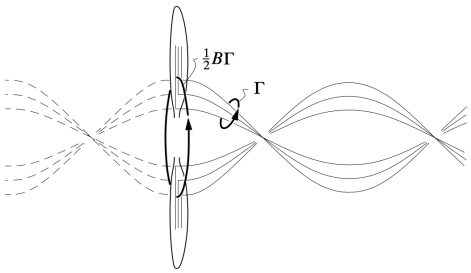

Figure 12.8: A propeller and the associated vortex sheets shed from the blades as they generate lift (Drela 2006).

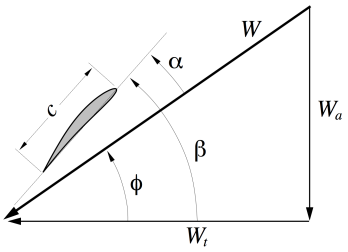

Figure 12.9: Illustration of a propeller blade cross-section and relevant angles for analysis (Drela 2006).

The displacement velocity ratio is introduced in Equation 12.55 with v' the local axial vortex sheet velocity and V_∞ the free-stream velocity. Evident from the Betz condition is that ζ must be constant along the propeller radius. The local flow angle ϕ is related to the flow angle at the tip ϕ_t by Equation 12.56 with $\xi = \frac{r}{R}$ which is the normalised radial coordinate.

$$\zeta = \frac{v'}{V_\infty} \tag{12.55}$$

$$\tan(\phi) = \frac{\tan(\phi_t)}{\xi} \tag{12.56}$$

The relation in Equation 12.56 is a consequence of $\zeta = 0$.The Prandtl tip loss effect is quantified through Equation 12.57, Equation 12.58 and Equation 12.59.

$$f = \frac{B}{2}\frac{1-\xi}{\sin(\phi_t)} \tag{12.57}$$

$$F = \frac{2}{\pi}\arccos(e^{-f}) \tag{12.58}$$

$$G = F\cos(\phi)\sin(\phi) \tag{12.59}$$

$$\tan(\phi_t) = \frac{V_\infty}{\Omega R}(1+\frac{\zeta}{2}) \tag{12.60}$$

Additionally Equation 12.60 is introduced to quantify the flow angle at the tip.

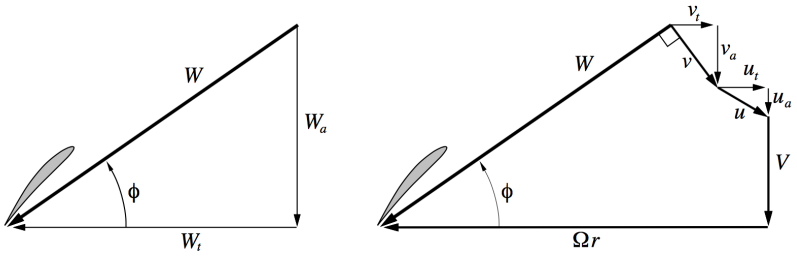

Figure 12.10: Illustration of a propeller blade cross-section and the velocity composition (Drela 2006).

Now the efficiency may be quantified by first defining the dimensionless forms of thrust and power as in Equation 12.61 and Equation 12.62. These may then be cast in a derivative form with respect to dimensionless coordinate ξ as in Equation 12.63 and Equation 12.64.

$$T_c = \frac{2T}{\rho V^2 \pi R^2} \tag{12.61}$$

$$P_c = \frac{2Q\Omega}{\rho V^3 \pi R^2} \tag{12.62}$$

$$T_c' = I_1'\zeta - I_2'\zeta^2 \tag{12.63}$$

$$P_c' = J_1'\zeta + J_2'\zeta^2 \tag{12.64}$$

The four derivatives are defined in the equations below.

$$I_1' = 4\xi G(1-\epsilon\tan(\phi)) \tag{12.65}$$

$$I_2' = \lambda(\frac{I_1'}{2\xi})(1+\frac{\epsilon}{\tan(\phi)})\sin(\phi)\cos(\phi) \tag{12.66}$$

$$J_1' = 4\xi G(1+\epsilon\tan(\phi)) \tag{12.67}$$

$$J_2' = \frac{J_1'}{2}(1-\epsilon\tan(\phi))\cos^2(\phi) \tag{12.68}$$

Additionally, it is required to link the circulation theorem of lift to the general lifting formula as in Equation 12.69 which may then be used to express the product Wc as in Equation 12.70.

$$\frac{1}{2}\rho W^2 c C_l = \rho W\Gamma \tag{12.69}$$

$$Wc = \frac{4\pi\lambda G V R\zeta}{C_l B} \tag{12.70}$$

The following procedure is then performed to generate the optimum propeller design.

1. Provide an initial estimate for ζ.
2. Determine the values for F and ϕ at each radial station.
3. Determine the product Wc at each radial station.
4. Determine ϵ and α from airfoil data at each radial station.
5. Find the relative velocities W through application of momentum theory.
6. Determine the blade twist and chord at each radial station.
7. Determine the four derivatives for finding the radial dimensionless power and thrust.
8. Determine ζ.
9. If not sufficiently close to the initial estimate, repeat step 1 to 9.
10. Find the propeller efficiency $\eta_{\text{propeller}}$.

12.4.5. Off-Design Performance of Propeller

Now the propeller is designed, the off-design performance is determined. A flowchart of the off-design performance model is presented in Figure 12.11. The performance of the propeller in off-design conditions is determined using a Blade Element Theorem (BET). In this theorem, the propeller blade is divided into non-interacting sections along the radius of the propeller (step 2). It is assumed that each blade section acts as a two dimensional airfoil. Secondly, the total velocity on each blade and the velocity angle are determined using respectively Equation 12.71 and Equation 12.72.

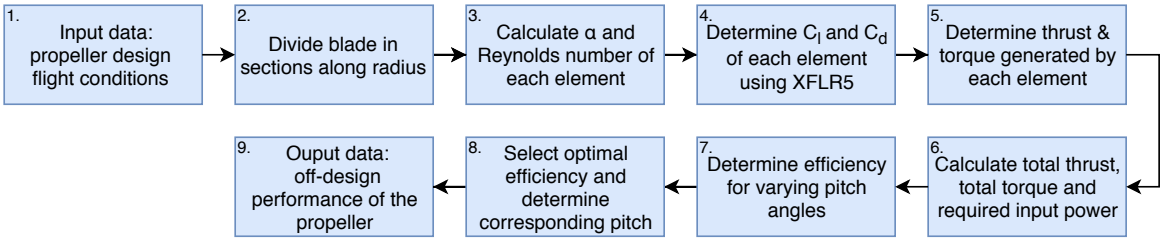

Figure 12.11: Flow chart of the propeller off-design performance model.

$$V_{total} = \sqrt{V_0^2 + (2\pi r_i \Omega)^2} \quad (12.71) \qquad \phi = \arctan\left(\frac{V_0}{2\pi r_i \Omega}\right) \quad (12.72)$$

In step 3, the angle of attack is then calculated by Equation 12.73. Since a constant speed propeller is considered, the pitch will be varied in order to find the optimal, and corresponding efficiency, for a certain flight condition. In addition, the Reynolds number of each blade element is determined using Equation 12.74. Subsequently, an XFLR5 analysis can be performed to determine C_l and C_d of each blade element for different pitch angles.

$$\alpha = \beta_{pitch} - \phi + \theta_i \quad (12.73) \qquad Re = \frac{\rho c_i V_{total}}{\mu} \quad (12.74)$$

Now, in step 5, the forces on the blade elements are determined. Equation 12.75 and Equation 12.76 calculate the lift and drag contribution of each blade element. Thereafter, based on the lift and drag contribution, the thrust, torque and power input contribution are determined using Equation 12.77, Equation 12.78 and Equation 12.79 .

$$dL = \frac{1}{2}\rho V_{\text{total}}^2 C_l c_i dr \quad (12.75) \qquad dD = \frac{1}{2}\rho V_{\text{total}}^2 C_d c_i dr \quad (12.76)$$

$$dT = dL\cdot\cos\phi - dD\cdot\sin\phi \quad (12.77) \qquad dQ = dL\cdot\sin\phi + dD\cdot\sin\phi \quad (12.78) \qquad dP_{in} = dQ\cdot 2\pi r_i\Omega\cdot\sin\phi \quad (12.79)$$

In step 6, the total thrust and drag are calculated by summing the contributions of all elements and multiplying the number of blades in Equation 12.80 and Equation 12.81. The required input power of the propeller is determined in Equation 12.82.

$$T = N_b\cdot\sum dT \quad (12.80) \qquad Q = N_b\cdot\sum dQ \quad (12.81) \qquad P_{in} = N_b\cdot\sum dP_{\text{in}} \quad (12.82)$$

Next, using Equation 12.83, the efficiency of the propeller is determined in step 7. In order to be able to create a performance graph, the advance ratio is determined in Equation 12.84. Finally, the pitch angle corresponding to the highest efficiency is selected (step 8).

$$\eta_{prop} = \frac{TV_0}{P_{\text{in}}} \quad (12.83) \qquad J = \frac{V_0}{\Omega D_{\text{prop}}} \quad (12.84)$$

12.4.6. Structural Analysis of Components

In order to properly size the rotational components of the engine, a structural analysis method is developed. The compressor and turbine are modelled as a rotating disk, for which a differential ring can be analysed as in Equation 12.85.

$$d\sigma(r) = \frac{dF}{dA} = \frac{2\pi\rho\Omega^2 r^2 t dr}{2\pi r t} = \rho\Omega^2 r dr \tag{12.85}$$

Next, Equation 12.85 may be integrated to yield the stress at any radial location as in Equation 12.86.

$$\sigma(r) = \frac{\rho}{2}\Omega^2 r^2 \tag{12.86}$$

Evident from Equation 12.86 is that the maximum stress always occurs at maximum radius and therefore only this is assessed. For the propeller blades, a slightly different analysis is performed yielding:

$$\sigma(r) = \int_{r_h}^{r} \rho\Omega^2 c(r)^2 dr \tag{12.87}$$

Which is evaluated numerically.

12.5. Engine Vibrations

Engine vibrations are assessed using a lumped mass model of the main shaft. The propeller is modelled as a forcing function on the main shaft. The compressor and turbine are modelled as rigid disks, whereas the shaft may deform slightly. Note that the displacement coordinate θ is relative to the equilibrium position in a frame rotating with the compressor and turbine. Hence the final motion of the engine can be seen as the superposition of a constant rotational velocity and a smaller harmonic rotary oscillation. The model is illustrated in Figure 12.12.

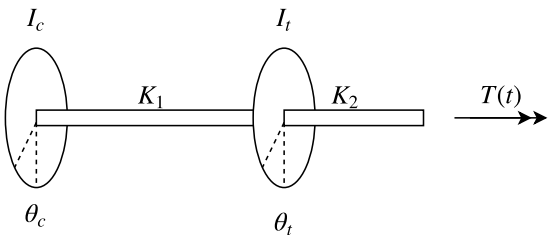

Figure 12.12: Illustration of the lumped mass model used for assessing the engine vibrations.

Damping is neglected as its effect is expected to be small ("Gas Turbine Engine Components" n.d.). As such, the system of ordinary differential equations describing the system becomes:

$$I_c\ddot{\theta}_c + K_1(\theta_c - \theta_t) = 0 \tag{12.88}$$

$$I_t\ddot{\theta}_t + K_1(\theta_t - \theta_c) + K_2\theta_t = T(t) \tag{12.89}$$

Hence the system may be written as:

$$\underbrace{\begin{bmatrix} I_c & 0 \\ 0 & I_t \end{bmatrix}}_{I}\ddot{\boldsymbol{\theta}} + \underbrace{\begin{bmatrix} K_1 & -K_1 \\ -K_1 & K_1+K_2 \end{bmatrix}}_{K}\boldsymbol{\theta} = \begin{bmatrix} 0 \\ T(t) \end{bmatrix} \tag{12.90}$$

Thus if the solution takes the form $\boldsymbol{\theta} = \boldsymbol{x}e^{\lambda t}$ the following must be true:

$$|\lambda^2 I + K| = 0. \tag{12.91}$$

Solving above equation for the eigenvalues λ allows quantification of the frequency response to propeller inputs. Note that these propeller input torques are easily determined as Equation 12.92. This equation is a result from a simple energy balance.

$$T = \frac{\Omega_{\text{propeller}}}{\Omega_{\text{turbine}}} \frac{P_{\text{propeller}}}{\eta_{\text{propeller}}\Omega_{\text{propeller}}} \tag{12.92}$$

The results of a frequency analysis are presented in Figure 12.13.

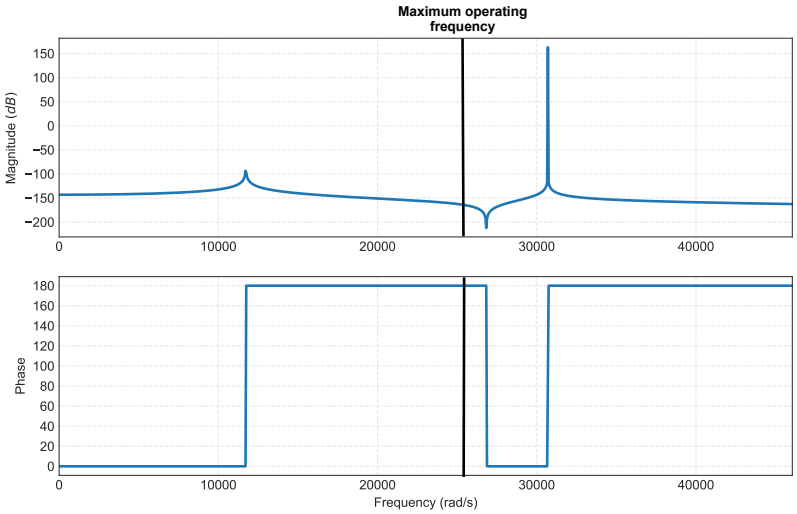

Figure 12.13: Frequency domain response of the system to excitations. Note that one must translate the forcing input to the frequency domain an decibel scale before the results are relevant.

From Figure 12.13 it is clear that for maximum propeller power at the operating speed regime of the engine (below 200,000 rpm) does not create vibrations exceeding a magnitude of -70 dB. This is lower than reciprocating engines in this power range, typically quoted at vibration magnitudes of -45 dB (“Gas Turbine Engine Components” n.d.).

12.6. Component Integration and Optimisation

For preliminary sizing of the engine, a 0D thermodynamic cycle model was developed in (B. van Beurden et al. 2018a) to quantify engine size, fuel consumption and mass flow based on a required power number. This model already requires specification of the component efficiencies, pressure ratios and the turbine inlet temperature. The models for component design presented in this chapter are used to size the engine in greater detail. This design is formulated as an optimisation problem with respect to weight as

$$\min_{\boldsymbol{x}_{\text{engine}}} W_{\text{engine}}(\boldsymbol{x}_{\text{engine}}) \tag{12.93}$$

subject to the following constraints

$$\Omega_{\text{compressor}} - \Omega_{\text{turbine}} = 0 \tag{12.94}$$
$$\eta_{\text{compressor}} - \bar{\eta}_{\text{compressor}} = 0 \tag{12.95}$$
$$\eta_{\text{turbine}} - \bar{\eta}_{\text{turbine}} = 0 \tag{12.96}$$
$$\max(M_{\text{compressor}}) - M_{\text{limit}} \leq 0 \tag{12.97}$$
$$\max(M_{\text{turbine}}) - M_{\text{limit}} \leq 0 \tag{12.98}$$
$$\max(\sigma_{\text{compressor}}) - \sigma_{\text{yield}_{\text{compressor}}} \leq 0 \tag{12.99}$$
$$\max(\sigma_{\text{turbine}}) - \sigma_{\text{yield}_{\text{turbine}}} \leq 0 \tag{12.100}$$

where variables as $\bar{\eta}$ represent problem parameters specified on a higher design level. Note that Equation 12.94 represents the fact that the turbine and compressor will be connected to the same shaft. The other constraints are either to form compliance or to prevent transonic flow and structural failure. The design vector is presented in the next section in the form of results. Note that the material used is unknown at this point but chosen to have a yield stress of 500 MPa and capable of resisting temperatures of 1300 K as suggested in (Dixon 2005).

As an example of the engine optimisation, one can refer to Figure 12.14 which shows a subset of the design space for the radial turbine efficiency and the chosen design point. It also serves as a means of validation as the trend illustrated is in accordance with literature (Dixon 2005).

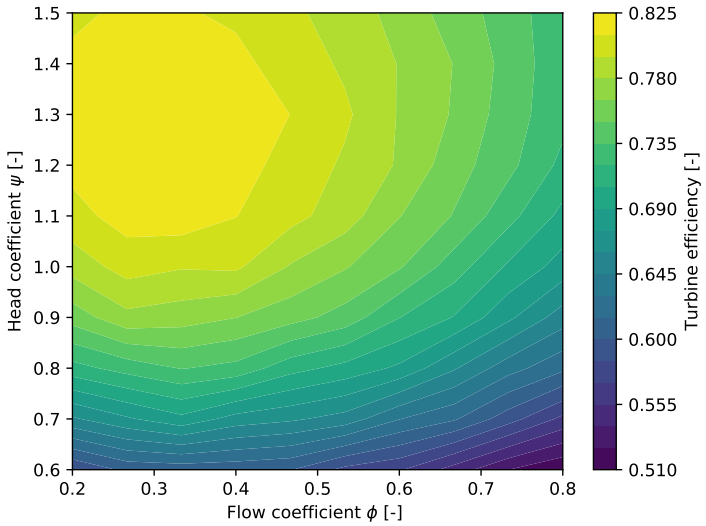

Figure 12.14: Visualisation of the design space for the turbine illustrating the effects of flow and head coefficient on the turbine efficiency.

12.7. Results

Overall cycle parameters for the engine are shown in Table 12.10 along with a Mollier diagram of the cycle in Figure 12.16. A three-dimensional exploded view of the engine is shown in Figure 12.15.

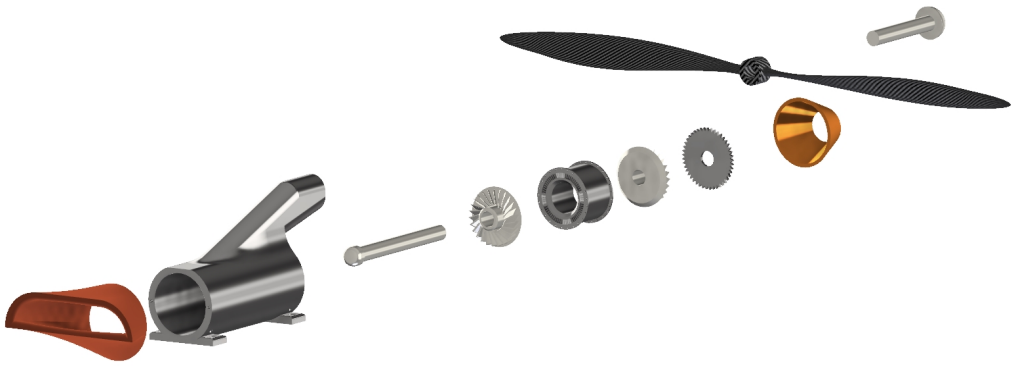

Figure 12.15: Exploded view of the engine showing the radial compressor and turbine as well as the combustor, gearbox and propeller.

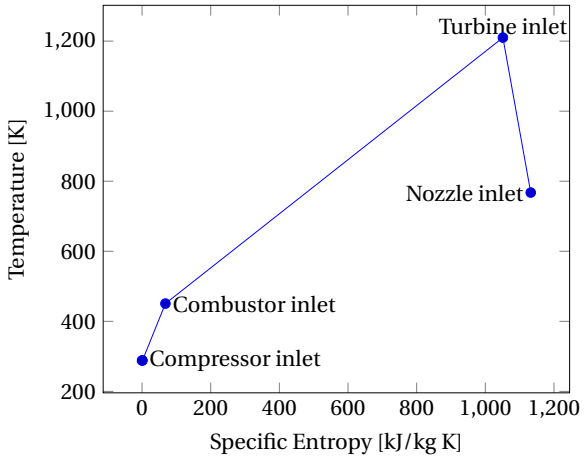

Figure 12.16: Mollier diagram of the gas turbine in the turboprop engine.

Table 12.10: Main design values for the engine

Parameter	Value
Pressure ratio compressor	6
Isentropic efficiency compressor	0.82
Efficiency of combustion	0.9
Turbine Inlet Temperature	1210 K
Isentropic efficiency turbine	0.85
Mechanical efficiency	0.99
Gearbox efficiency	0.99
Specific Fuel Consumption	290 g/kWh

Moreover, engine performance as a function of velocity and altitude is shown in Figure 12.17. The power margin is defined as the amount of power of the engine that is left for other use when in steady flight. **Hence, throughout the entire flight envelope the engine has sufficient power to propel the UAV.** Additionally, sufficient power is available to power all subsystems for 20 hours, as the fuel mass is designed for the regions of higher specific fuel consumption within the flight envelope as seen in Figure 12.18.

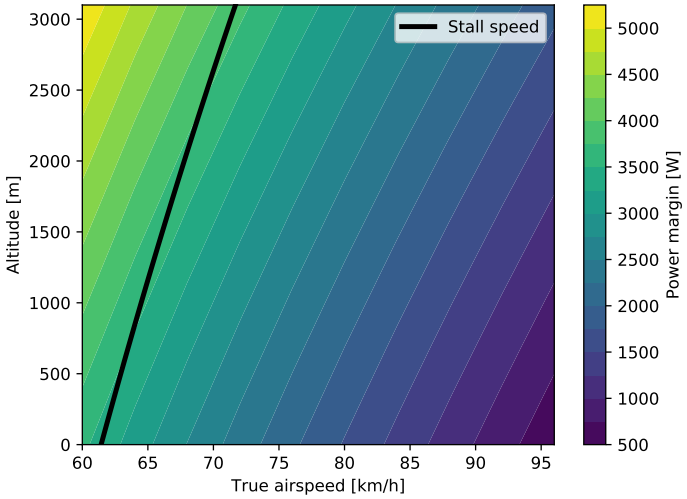

Figure 12.17: Engine performance as a function of altitude and flight speed. Note that the stall speed constraint is included and hence any power margin to the left of this line is infeasible.

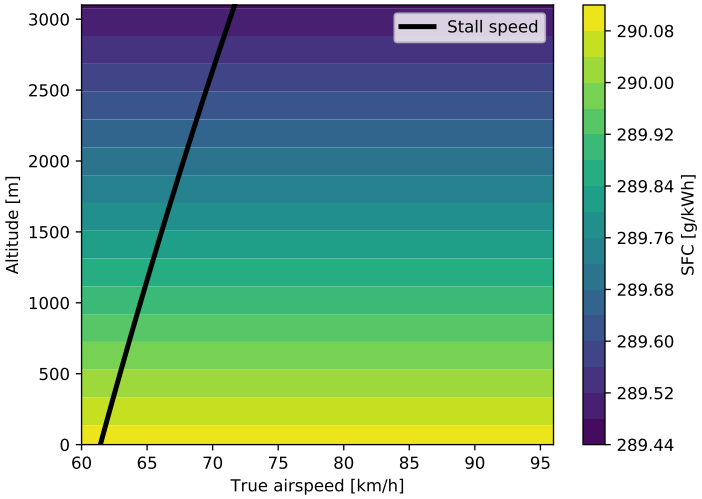

Figure 12.18: Specific fuel consumption as a function of altitude and true airspeed. Note that it is only a function of altitude as the thermodynamic performance of the engine depends only on intensive variables such as temperature.

12.7.1. Propeller

The radial distribution of twist and chord for the propeller are shown in Figure 12.19. Other design parameters are shown in Table 12.11.

Table 12.11: Design parameters for the propeller design.

Parameter	Value
Number of blades	2
Diameter	1.85 m
Hub diameter	0.2 m
Rotational speed	2400 rpm
Airfoil	NACA 16-012
Propeller efficiency	93 %

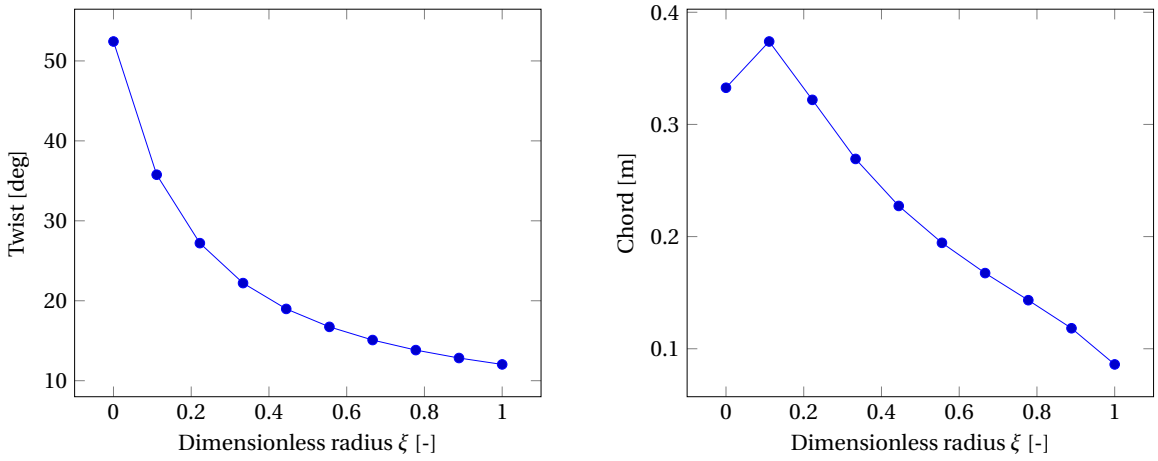

Figure 12.19: Twist and chord distributions of the propeller design.

12.7.2. Turbomachinery

Drawings of the radial compressor and turbine are shown in Figure 12.20. Design variables of the radial turbine are shown in Table 12.12. Design variables of the compressor are shown in Table 12.13.

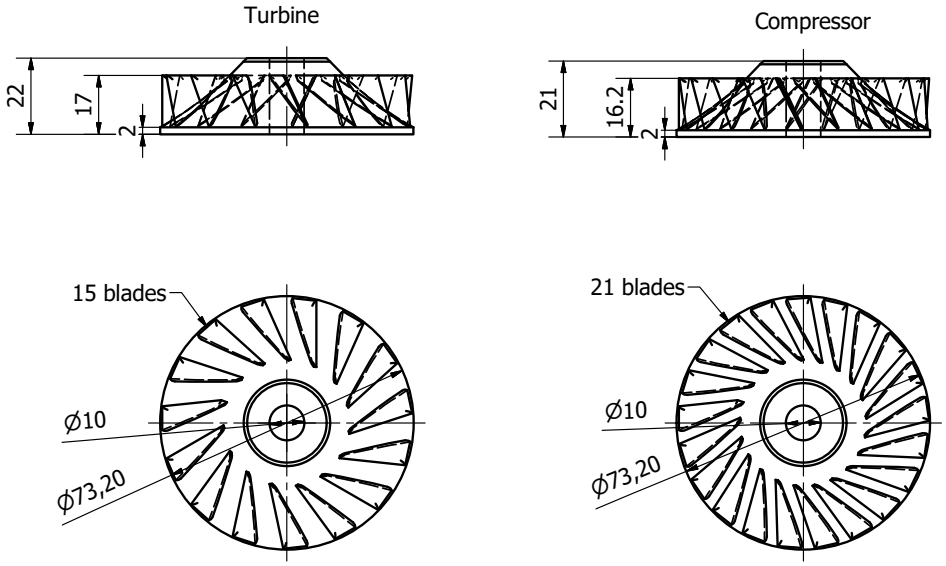

Figure 12.20: Drawing of the turbine and compressor rotors illustrating the main dimensions and the number of blades. Dimensions are in millimeters. Note that the stators are omitted as they have not yet been fully designed for the compressor. Additionally, the blade design itself is not finalised.

Table 12.12: Design values for the radial turbine.

Parameter	Value
Number of rotor blades	15
Number of stator blades	36
Flow coefficient ϕ	0.3
Head coefficient ψ	1.31
Rotational speed	200,000 rpm
Efficiency	84.7 %

Table 12.13: Design values for the compressor.

Parameter	Value
Number of blades	21
Rotational speed	200,000 rpm
Efficiency	82.1 %

12.8. Verification and Validation

This section presents the verification and validation efforts for the analysis of the engine cycle and its components.

12.8.1. Thermodynamic Cycle

The thermodynamic cycle model used within the design software has been validated in (B. van Beurden et al. 2018a) against the GSP software and showed a maximum deviation of 3.8% in power and specific fuel consumption prediction.

12.8.2. Compressor

This method is verified with an example given in Appendix B of (Dixon 2005) and deviations do not exceed 1%.

12.8.3. Turbine

The turbine design process has been validated against experimental results for a turbine (Jones 1994). The results are summarised in Table 12.14. Deviations do not exceed 14% in the turbine dimensions. The efficiency deviates only by 0.6%.

Table 12.14: Validation results of the turbine design process.

Parameter	**Real turbine** (Jones 1994)	**Model**	**Deviation**
Rotor			
Inlet radius r_4	$58.2 \cdot 10^{-3}$ m	$58.96 \cdot 10^{-3}$ m	1.3 %
Inlet blade height b_5	$6.36 \cdot 10^{-3}$ m	$5.47 \cdot 10^{-3}$ m	14 %
Inlet absolute flow angle α_4	76.8 deg	76.6 deg	0.26 %
Inlet relative flow angle β_4	-31.8 deg	-36.87 deg	13.75%
Axial clearance ϵ_x	$0.4 \cdot 10^{-3}$ m	$0.4 \cdot 10^{-3}$ m	0 % (Input)
Radial clearance ϵ_r	$0.23 \cdot 10^{-3}$ m	$0.23 \cdot 10^{-3}$ m	0 % (Input)
Number of Rotor Blades Z_r	16	16	0 %
Outer hub radius	$15.20 \cdot 10^{-3}$ m	$17.2 \cdot 10^{-3}$ m	13.1 %
Outlet shroud radius	$36.8 \cdot 10^{-3}$ m	$40.2 \cdot 10^{-3}$ m	9.4 %
Outer blade height	$21.6 \cdot 10^{-3}$ m	$24.2 \cdot 10^{-3}$ m	10.74 %
Outlet Absolute flow angle	-0.03 deg	0.00 deg	(Model assumption)
Outlet relative flow angle	-57.4 deg	-63 deg	9.8 %
Chord	$45.70 \cdot 10^{-3}$ m	$43.3 \cdot 10^{-3}$	5.3 %
Stator			
Inlet radius	$74.00 \cdot 10^{-3}$ m	$73.4 \cdot 10^{-3}$ m	0.81 %
Average blade height	$6.18 \cdot 10^{-3}$ m	$5.98 \cdot 10^{-3}$ m	3.1 %
Outlet radius	$63.5 \cdot 10^{-3}$ m	$61.4 \cdot 10^{-3}$ m	3.3 %
Outlet absolute flow angle	77.8 deg	76.9 deg	1.02 %
Chord	$22.9 \cdot 10^{-3}$ m	$25.2 \cdot 10^{-3}$ m	9.1 %
Number of nozzle vanes Z_s	19	19	0 %
Efficiency	0.860	0.854	0.6 %

12.8.4. Propeller

The propeller design algorithm has been validated against experimental results from (Reid 1949) for a commercially available propeller. This propeller has been chosen as it has been designed with a predecessor of the works on which the design method is based on. Data for this propeller is shown in Table 12.15. A geometric description can be found in (Reid 1949).

Table 12.15: Data for a commercially available propeller (Reid 1949).

Parameter	**Value**
Number of blades	2
Diameter	5.75 ft
Hub diameter	1 ft
Rotational speed	2400 rpm
Airfoil	NACA 16-012
Propeller efficiency	86.9 %

The found efficiency for the propeller is 86.7%, indicating a deviation of 0.23%. This is deemed an excellent result.

13 Aerodynamics

A topic in close relation with many other models is aerodynamics. The planform of the flying wing can be optimised in order to achieve best aerodynamic performance at as little cost as possible of the other departments. This chapter discusses the aerodynamic analysis methods used to design the UAV in section 13.1 as well as the procedure for airfoil selection in section 13.2. The results and its verification and validation are summarised in section 13.3 and section 13.4, respectively.

13.1. Aerodynamic Analysis

This section elaborates upon the methods conceived to assess the aerodynamic performance of the UAV. First, the force decomposition is explained, followed by a brief explanation of the vortex lattice method and the drag buildup method.

13.1.1. Decomposition of Forces

The aerodynamic forces on the wing originate from the pressure and friction forces exerted by the air on the wing skin. Multiple decompositions of these forces exists which are all statically equivalent. In the design of the UAV, it was chosen to employ the widely used lift-drag decomposition, which aligns a force perpendicular to the flight direction (lift) and one along it (drag). This decomposition is shown in Figure 13.1.

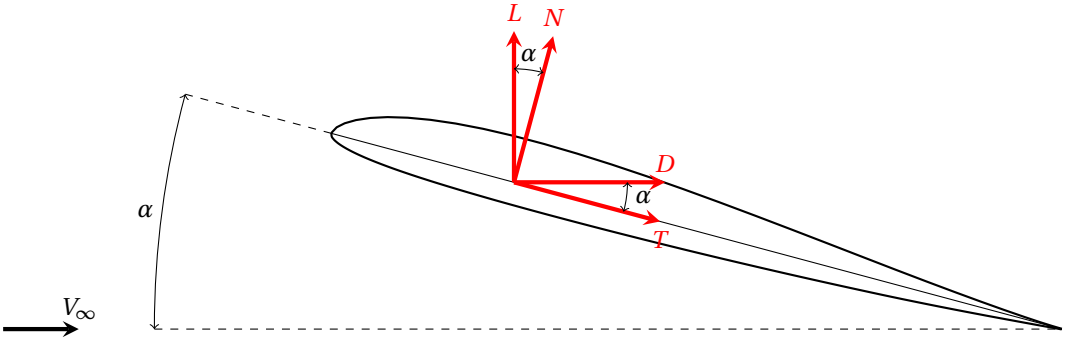

Figure 13.1: The PW75 airfoil exposed to a given freestream velocity V. The forces acting on the airfoil are shown decomposed orthogonally in the local airfoil coordinate system and in the system aligned with the freestream velocity.

Application of the Buckingham-Pi theorem (J. D. Anderson 2010) has lead to equations for these forces as shown in Equation 13.1 and Equation 13.2.

$$L = 0.5\rho V^2 S C_L \tag{13.1}$$

$$D = 0.5\rho V^2 S C_D \tag{13.2}$$

The coefficients C_L and C_D are the crux of these relationships, as they are measures of the aerodynamic performance of the wing design (all other variables depend on flight conditions or extensiveness of the wing). Consequently, the remainder of this section will focus on obtaining these coefficients.

13.1.2. Vortex Lattice Method

As the flight regime of the UAV can be assumed incompressible by the Prandtl-Glauert correction factor (J. D. Anderson 2010), it was chosen to use a vortex lattice method (VLM) for analysis of the design. A VLM was preferred over lifting line theories as it is capable of assessing a wider range of wing planforms. An in-house VLM was developed and implemented in the design workflow. The VLM is a numerical solution method to the Laplace equation defined in Equation 13.3. This is a consequence of the irrotational and incompressible assumptions, hence making the model inviscid.

$$\nabla^2 \phi = 0 \quad \text{s.t.} \quad \frac{\partial \phi}{\partial n_i} = 0 \quad \forall n_i \in \partial\Omega \tag{13.3}$$

The function sought is $\phi(\boldsymbol{x})$ with $\boldsymbol{r}$ the position vector. This function is the potential function and its gradient is defined to be the velocity field. The VLM approach for solving this partial differential equation is by introducing source functions such as the vortex filament, which is in itself a solution to Equation 13.3 and hence by the linearity of the PDE any arbitrary sum is as well. Thus the VLM places vortex filaments on the wing to approximate the flow field around the body. The induced velocity by a segment of such a vortex filament is given by the Biot-Savart law:

$$d\boldsymbol{V} = \frac{\Gamma}{4\pi}\frac{d\boldsymbol{l}\times\boldsymbol{r}}{|\boldsymbol{r}|^3} \tag{13.4}$$

With Γ the circulation strength of the filament. As such, one places n horseshoe vortex filaments over the wing with n associated but unknown circulation strengths. Then, the flow tangency condition is imposed at n control points in order to form the linear system:

$$A\boldsymbol{\Gamma} = \boldsymbol{b} \tag{13.5}$$

Where A contains the influence coefficients of the horseshoe vortices and vector $\boldsymbol{b}$ contains information of the upwind flow field. By construction, Equation 13.5 is always uniquely solvable.

Using $\boldsymbol{\Gamma}$ the flow field is reconstructed and the pressure distribution over the wing is found by application of the incompressible inviscid Navier-Stokes equations. The pressure field is integrated to yield information of the lift and induced drag coefficients C_L and C_{D_i}. A resulting pressure field and VLM mesh are shown in Figure 13.2.

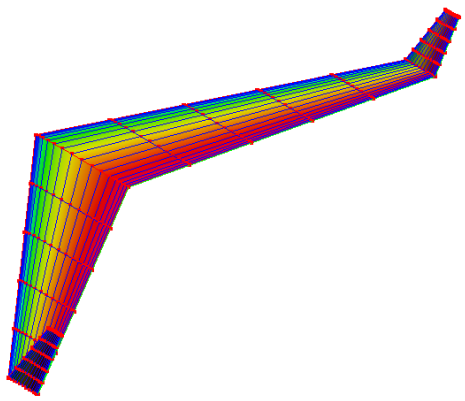

Figure 13.2: Illustration of a VLM mesh and results at angle of attack of 5 degrees at a mach number of 0.077 which correspond to cruise conditions.

13.1.3. Drag Buildup Method

As the VLM only predicts the induced drag, the parasitic drag is found by the drag-buildup method. This parasitic drag coefficient consists of friction, form and interference factors as:

$$C_{D_0} = \sum_{i=1}^{n} C_{f_i} FF_i Q_i \frac{S_{\text{wet}_i}}{S_{\text{ref}}} \tag{13.6}$$

With C_{f_i} the skin friction coefficient, FF the form factor and Q_i the interference factor. All relevant equations for evaluating these factors are derived from literature (Raymer 2012)(Torenbeek 1982).

13.2. Airfoil Selection

During the initial aerodynamic sizing, an airfoil was chosen where the maximum lift to drag ratio and multiplicity of implementation were driving factors (B. van Beurden et al. 2018a). Now, the selection is revisited where a more elaborate analysis is performed on a larger set of reflex airfoils. By means of AVL, a selection of performance indicators is presented for the different airfoils at a fixed angle of attack. The values that are constrained in the analysis are presented in Table 13.1 and the performance indicators can be found in Table 13.2. The reason that these parameters are fixed, is that now all differences in performance are due to a change in the airfoil. The values of these parameters are based on the conceptual design (B. van Beurden et al. 2018a). This ensures that conclusions drawn are not interchanged with other contributors than the airfoil.

Table 13.1: Parameters that are fixed for the analysis of the different airfoils using AVL.

Parameter	Value	Unit
Surface area (S)	13.1	m
Aspect ration (AR)	11	-
Taper ratio (λ)	0.2	-
Dihedral (γ)	0.0	deg
Sweep (Λ)	0.0	deg
Angle of attack (α)	3.0	deg

Table 13.2: Aerodynamic performance indicators obtained from AVL, with merely the airfoil varying.

Airfoil	C_L [-]	C_D [-]	C_m [-]	L/D [-]
MH45	0.2958	0.00261	0.00685	113.33
MH61	0.2497	0.00185	0.01901	134.97
MH83	0.6043	0.01084	-0.0646	55.747
MH104	0.3042	0.00276	0.00829	110.22
PW75	0.2794	0.00233	0.01399	119.91
PW106	0.3345	0.00333	0.00072	100.45

Looking at Table 13.2, one can choose the most optimal airfoil for the specific design point. A high lift coefficient is advantageous with regard to the flying velocity and surface area of the UAV. A low drag coefficient is superior, since it provides the possibility to integrate lighter engines. A moment coefficient of approximately zero, preferably slightly positive, renders a structure of much lower complexity, since no twist needs to be included(Nickel and Wohlfahrt 1994). Although the initially selected MH61 airfoil has the highest lift over drag, the lift coefficient is considered too low to perform the mission. The highest lift coefficient is found for the MH83 airfoil. Unfortunately, the lift over drag value is significantly lower than the other airfoils. The remaining profiles are assessed with respect to their compatibility with applying sweep and dihedral. This is included to assist the stability of the aircraft. AVL proves that raising the dihedral and the sweep, particularly the last, both decrease the moment coefficient. For this reason, a higher zero-dihedral-zero-sweep moment coefficient renders more possibility for dihedral and sweep, which is preferred for the stability of the flying wing. **The fact that the airfoil has a value which allows for more dihedral and sweep, is why the PW75 airfoil is considered the best option for the MAINTAIN mission.** A final comparison between the PW75 and MH61 airfoil can be seen in Figure 13.3.

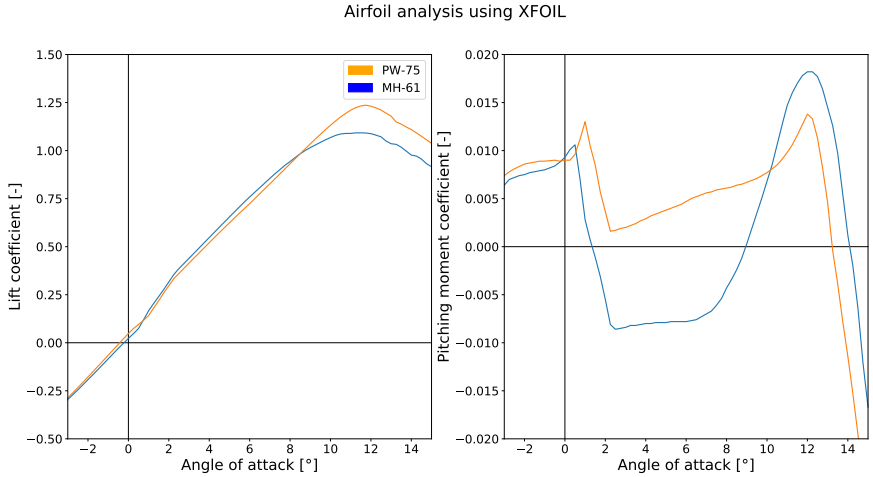

Figure 13.3: Airfoil comparison based on lift coefficient and pitching moment coefficient.

13.3. Results

This section presents the aerodynamic performance characteristics of the final design. The chosen airfoil, PW75, is shown in Figure 13.1. The final wing planform is shown in Figure 13.4.

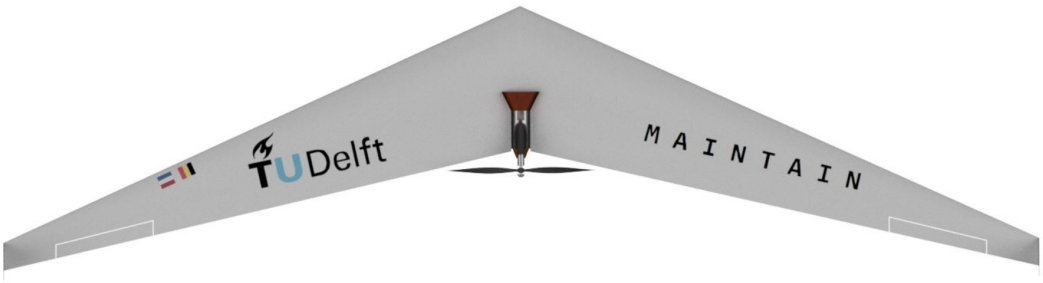

Figure 13.4: Top view of final design, illustrating the wing planform.

The aerodynamic coefficients are shown in Figure 13.5 and Table 13.3. This information has been gathered by several solutions of the Navier-Stokes equations using SU2 for a mach number of 0.077 and a Reynolds number of 200,000. **The flying wing has an incredibly low parasitic drag coefficient which yields high lift to drag ratios at a wide angle of attack range.** The reflexed airfoil does not feature a high maximum lift coefficient which causes the wing to stall at smaller lift coefficients than conventional configurations. However, the stall is 'flat' in the sense that entering the region of the maximum lift coefficient does not necessarily mean that the UAV will stall.

Table 13.3: Aerodynamic characteristics of the MAINTAIN UAV as generated by SU2.

Parameter	Symbol	Value
Zero-lift drag coefficient	C_{D_0}	0.00943
Maximum lift coefficient	$C_{L_{\max}}$	1.15
Zero-lift moment coefficient	C_{M_0}	0.13
Maximum lift over drag ratio	$(\frac{L}{D})_{\max}$	33.2

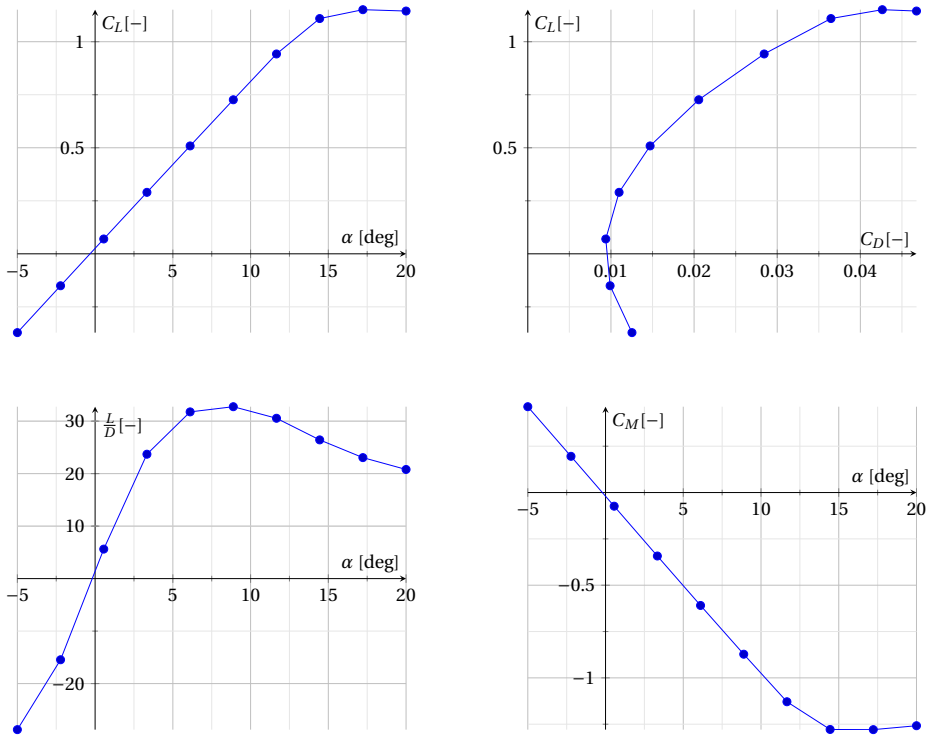

Figure 13.5: Aerodynamic characteristics of the MAINTAIN UAV. Top left: the lift coefficient as a function of angle of attack. Top right: the lift-drag polar. Bottom left: the lift to drag ratio as a function of angle of attack. Bottom right: The longitudinal moment coefficient as a function of angle of attack.

The spanwise lift distribution is shown in Figure 13.6 for the cruise angle of attack. This has also been obtained using the SU2 software. **One can see that the lift distribution closely approximates the optimal elliptic lift distribution as a result of the slender wing design and large winglets.**

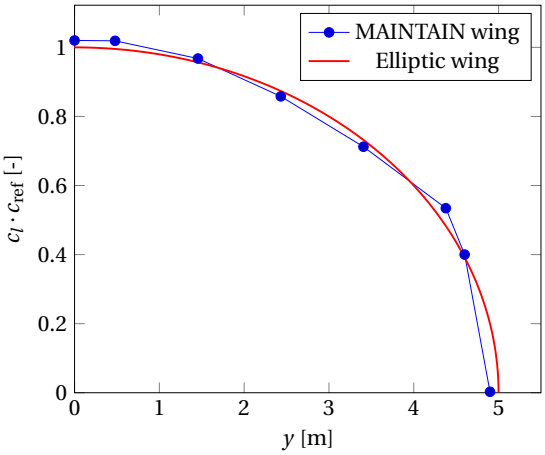

Figure 13.6: Spanwise lift distribution at the cruise angle of attack of 5 degrees, mach number 0.077 and Reynolds number 200,000. The elliptic lift distribution, which minimises the induced drag, is plotted for comparison.

13.4. Verification and Validation

The in-house VLM has been validated against both the OpenVSP and AVL software and showed errors only in the order of the machine epsilon (10^{-16}) . However, it did not have the capability to asses the effects of winglets and stability derivatives and hence AVL was integrated in the design workflow. Additionally, as all aerodynamic assessment has been done through the incompressible inviscid vortex lattice method and a drag-buildup method during design, a final validation of the design was performed using computational fluid dynamics software. The results in the previous section have also been generated using this CFD analysis. The mesh used is shown in Figure 13.7. The mesh consists of 100,438 3D elements and uses a symmetry plane in order to reduce computational time.

The lift-drag polar of the UAV is shown in Figure 13.8 as generated by both SU2 and the in-house aerodynamic analysis. It is clear that below an angle of attack of 12 degrees the discrepancy does not exceed 5%. These results are excellent, especially considering that the design software does not directly sample from the in-house VLM above an angle of attack of 10 degrees.

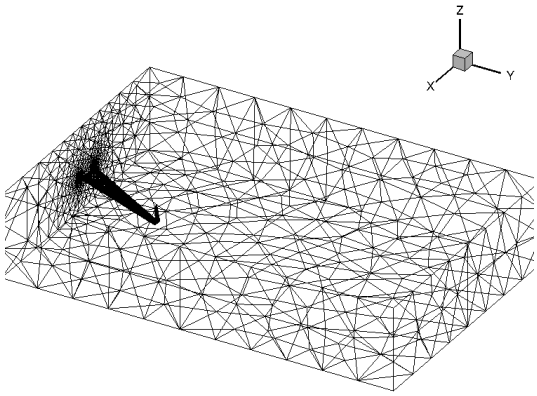

Figure 13.7: Isometric view of the mesh used for the CFD analysis of the wing.

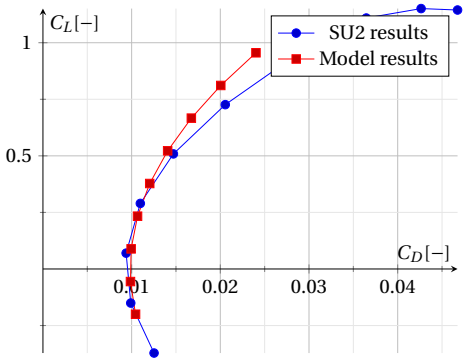

Figure 13.8: Validation of the lift-drag polar comparing the results of the design software and the CFD software SU2.

14
Structures and Materials

The structural weight is an important parameter for every aspect in the design of an aerial vehicle. In order to make sure that the structure is capable of sustaining all the loads acting on the UAV, a structural analysis of the aircraft is performed in this chapter. In the end, the goal is to optimise the weight of the structure to a minimum while still being able to guarantee the load carrying capacities. First, the entire structural analysis logic and algorithm is outlined in section 14.1. This is followed by section 14.2, where the selection of the materials is elaborated upon. After that, a detailed sizing and analysis of the landing gear is described in section 14.3. Also part of the structural design of the vehicle, is the structural dynamics, which is described in section 14.4. This chapter concludes with section 14.5 with the verification and validation of the structures simulation software.

14.1. Structural Analysis

In the Structural Analysis, first a coordinate system is established. After that, the assumptions made during the analysis to simplify the calculations are presented. Then, the external loads which are acting on the structure are analysed after which the internal stresses are documented. Next, the simulation program is elaborated upon.

14.1.1. Coordinate System

In the following picture, the coordinate system which was used during the analysis is visualised. As one can see, a right-handed coordinate system was established with the z-axis pointing downwards to the nadir direction, the y-axis goes along the wing and the x-axis along the chord.

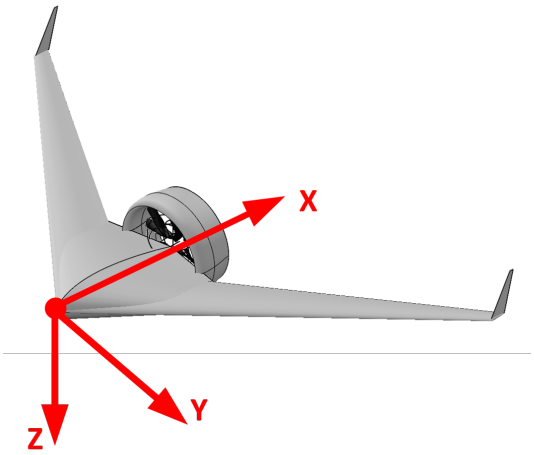

Figure 14.1: Coordinate system used during the analysis.

14.1.2. Assumptions and Effects

Before continuing with the analysis, it is important to discuss the limitations of the structural model. It will never be possible to simulate a model without any limitations. Therefore, it is important to identify these limitations which are introduced because of certain assumptions and analyse what they affect. The main assumptions which are made to simplify the calculations and their effects are the following.

Table 14.1: Assumption made during the calculations and their effects.

Assumptions	Effects
The drag distribution is assumed to be a point load acting on the centre of gravity.	Due to this assumption, a torque around the z-axis is neglected.
The mass is assumed to be a point load acting on the centre of gravity.	The UAV will be overdesigned as the weight distribution induces bending relief to counter the lifting forces.
The control surfaces are neglected.	Extra moments around the x-axis are neglected when the control surfaces are being used.
In order to simplify cross-section calculations, structural idealisation and boom theory is used.	This theory assumes that the skin is only effective for carrying shear forces and that the normal stresses are carried by the stringers.
The UAV is discretised in different sections.	A discretisation error will be introduced.
The aerodynamic centre is assumed to be at the quarter chord.	The torque across the sections will be different, which means that the actual cross-sectional shear stress will be different as well. It can either be increased or decreased depending on the flight condition.
The lift distribution is assumed to act on the aerodynamic centre (so quarter chord length).	The lift is not distributed over the whole wing. This means that the actual bending moment will be different.
The skin thickness will not vary across the cross-section and neither along the span.	The skin at the wing tips will be overdesigned.
The skin is assumed to be thin-walled	Simplifications are made in the equations, leaving out the thickness terms which are of higher order.

From Table 14.1, one can read that because of some assumptions, there will be both overestimation and underestimation of the forces acting on the structure. This means that the effect of the various assumptions can cancel each other out to a certain extent. Next to these assumptions, the structure shall be designed for a maximum loading condition of 3g which follows from the requirements. Keeping in mind that the structure is designed for the maximum loading condition, which is determined in subsection 11.5.2 and together with the introduction of a safety factor of typically 1.5, it can be guaranteed that the structure will be able to withstand the loads acting on it.

14.1.3. External Loads

Now it is time to discuss the external loads which are acting on the UAV. Along the z-direction, there is a lift force and a weight which should be considered. In chapter 13, the lift distribution along the wing span was given. The weight is assumed to be a point force, as elaborated on in subsection 14.1.2. Keep in mind that the lift is actually a negative force and the weight positive due to the coordinate system convention which was discussed earlier. In Figure 14.2, the shear force diagram is given. From the shear force diagram, the moment diagram can be derived which is displayed in Figure 14.3.

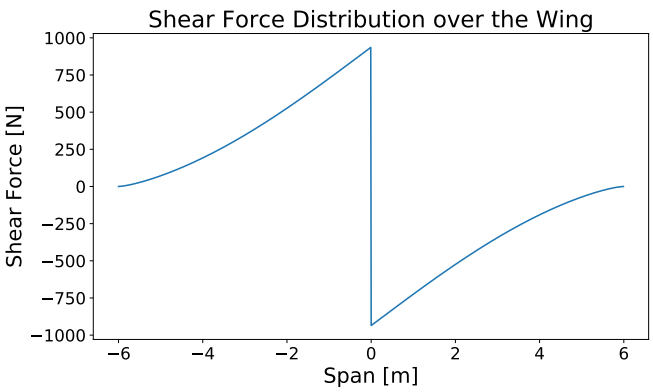

Figure 14.2: Shear force diagram.

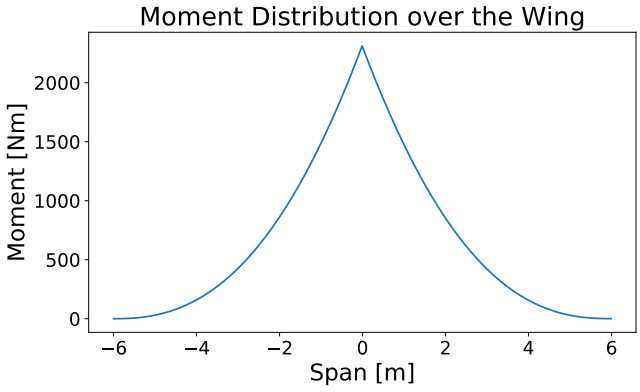

Figure 14.3: Moment diagram.

From the two diagrams, it is clear that the maximum shear force and moment are located at the wing root (at which y = 0m). **The maximum shear force is equal to 936 N and the maximum bending moment equals 2312 Nm.** This location will be critical to keep in mind during the further sizing of the different wing elements.

14.1.4. Stringers

Stringers are designed to have a high bending capacity, which is dependent on the shape of the stringer. The two most popular stringers which are used in aerospace industry nowadays are the J- and Z-stringer, shown in Figure 14.4 and Figure 14.5 respectively. The Z-stringer is structurally slightly more efficient in bending capacity than the J-stringer. However, the J-stringer has good fail-safe characteristics due to double-riveting opportunities. Therefore it is chosen to **use the J-stringer** as safety and reliability is highly valued in MAINTAIN.

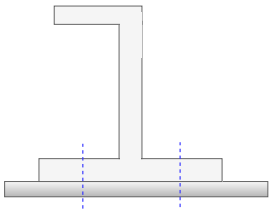

Figure 14.4: J-stringer.

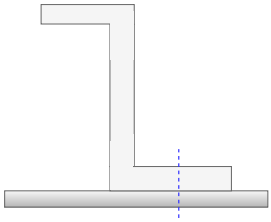

Figure 14.5: Z-stringer.

14.1.5. Ribs

The rib spacing is important to prevent buckling. As structural idealisation and boom theory are used, the direct stresses on the skin are zero and the stringers take-up all the stresses. Therefore the stringers will buckle before the skin. The Euler critical load can be calculated using Equation 14.1. In this equation, K is the column effective length factor, which has a theoretical value of 0.5 in this case, in which the column is fixed at both ends. However, a value of 0.65 proves to be more realistic in a practical design which is why this value was used (Megson 2007). E is Young's modulus of the stringer material and I is the cross-sectional moment of inertia.

$$P_{cr} = \frac{\pi^2 \cdot E \cdot I}{(K \cdot L)^2} \tag{14.1}$$

Buckling is a form of yielding and shall therefore be prevented. The ribs are be designed for the critical yielding load. The critical load can be calculated with Equation 14.2, in which σ_{yield} is the yield stress of the stringers. A safety factor of 1.5 is incorporated to take manufacturing imperfections and deterioration of the material into account. A_i is the cross-sectional area of a stringer.

$$P_{cr} = \sigma_{\text{yield}} \cdot A_i \cdot n_{\text{safety}} \tag{14.2}$$

The rib spacing, L, can be found by combining Equation 14.1 with Equation 14.2.

14.1.6. Stresses

The structure must be able to resist the stresses acting on it. Therefore, these stresses will determine the amount of material needed and thus consequently the weight of the structure. The Von-Mises stress incorporates both the direct stresses and shear stresses and must not exceed the yield stress of the material at any point in the cross-section. That way, there can be guaranteed that the structure is able to withstand the loads without yielding.

Normal Stress

The most significant normal stresses in the structure are the one introduced due to bending forces by the lift and weight over the wing. The normal stresses were calculated using following equation:

$$\sigma_y = \frac{M_x \cdot (I_{zz} \cdot z - I_{xz} \cdot x)}{I_{xx} \cdot I_{zz} - I_{xz}^2} + \frac{M_z \cdot (I_{xx} \cdot x - I_{xz} \cdot z)}{I_{xx} \cdot I_{zz} - I_{xz}^2} \tag{14.3}$$

In Equation 14.3, one can see that the the moments around the x-axis and z-axis play the biggest role. Due to the assumptions mentioned in subsection 14.1.2, the bending moments around the z-axis and y-axis are equal to zero. This means that only the most significant bending moment around the x-axis is taken in account. This consequently implies that σ_x equals zero because it depends on the moments around y and z which are both zero. Although σ_z also depends on M_x (meaning that this stress will not be zero), it is still safe to neglect its contribution. That is because thin-walled assumptions were made, which implies that the in-plane shear stresses are of much more importance than the rather small normal stress acting on it.

Shear Stress

To evaluate the shear stress, use was made of the idealised cross-section. Shear stresses are induced on the airfoil by a shear force and a torsion around the shear centre due to this shear force. The translation needed to compute the corresponding torsion can be found in Figure 14.6. Therefore, the shear centre at every cross-section has to be located in

order to calculate the torsion. Solely the x-location of the shear centre has to be obtained as the shear force throughout the wing points in z-direction, resulting in a torsion around the y-axis.

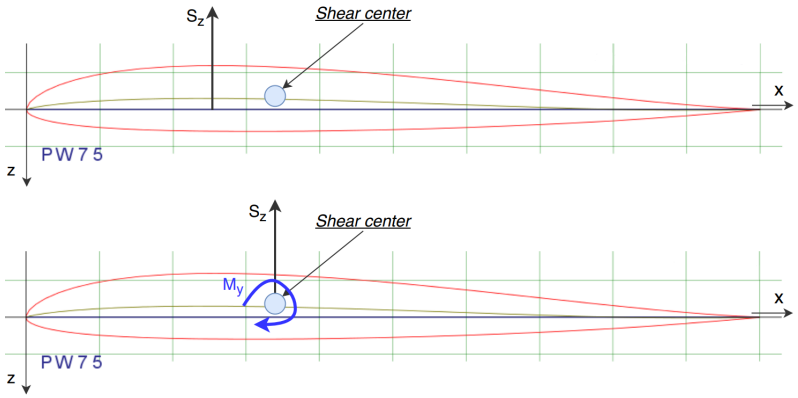

Figure 14.6: Translation of shear force to the shear centre.

The shear centre is the point on the cross-section through which shear loads do not produce any twisting. Therefore the angle of twist needs to be zero, which can be calculated using Equation 14.4.

$$\frac{d\theta}{dz} = \frac{1}{2A}\oint \frac{qds}{Gt} \tag{14.4}$$

As can be seen from 14.5, the shear flow is composed of the base and redundant shear flow. Using Equation 14.6, the base shear flow for an idealised section can be calculated. In this equation, the effective direct stress carrying thickness, t_D, equals zero as it is assumed that the skin is only effective in carrying shear stresses.

$$q_i = q_{b_i} + q_{s0_1} \tag{14.5}$$

$$q_{b_i} = -\left(\frac{S_x I_{xx} - S_z I_{xz}}{I_{xx} I_{zz} - I_{xz}^2}\right)\cdot\left(\int_0^s t_D x ds + \sum_{r=1}^{n} B_r x_r\right) - \left(\frac{S_z I_{zz} - S_x I_{xz}}{I_{xx} I_{zz} - I_{xz}^2}\right)\cdot\left(\int_0^s t_D z ds + \sum_{r=1}^{n} B_r z_r\right) + q_{i-1} \tag{14.6}$$

Combining Equation 14.4, Equation 14.5 and Equation 14.6, the shear flow induced on the airfoil by the shear force acting through the shear centre can be calculated. The shear flow due to the torque can be found by using Equation 14.7 and Equation 14.4. Carefully performing this integration and incorporating the fact that the angle of twist of the individual cells is equal results in n+1 equation and n+1 unknowns. Fusing the shear stress due to the shear force and torque results in the overall shear stress.

$$T = \sum 2Aq_i \tag{14.7}$$

Von-Mises Stress

Now that the most significant stresses are evaluated, it is possible to determine the Von-Mises stress. This stress predicts the yielding limitations of the material under different loading conditions along multiple axes. The Von-Mises stress is calculated using following formula:

$$\sigma_v = \sqrt{\frac{(\sigma_{xx} - \sigma_{yy})^2 + (\sigma_{yy} - \sigma_{zz})^2 + (\sigma_{zz} - \sigma_{xx})^2 + 6(\tau_{xz}^2 + \tau_{yz}^2 + \tau_{xy}^2)}{2}} \tag{14.8}$$

As can be seen from Equation 14.8, the Von-Mises stress is composed of the direct stresses and the shear stresses. The shear stress acting on the xz-plane and the direct stress acting on the y-plane, τ_{xz} and σ_{yy}, can be determined. The remaining stresses in Equation 14.8 are incorporated by the safety factor. The material selection and sizing parameters which is elaborated upon in subsection 14.1.7 are done based on the Von-Mises stress. That is because this stress incorporates all the relevant stresses which should be taken into account.

14.1.7. Simulation

In following flowchart, one can find the logical flow behind the structures program which analyses and sizes the structural components of the MAINTAIN UAV. The components to be sized are the thickness, location and amount of the skin, spars and the stringers. The stringers are idealised to booms using structural idealisation and boom theory.

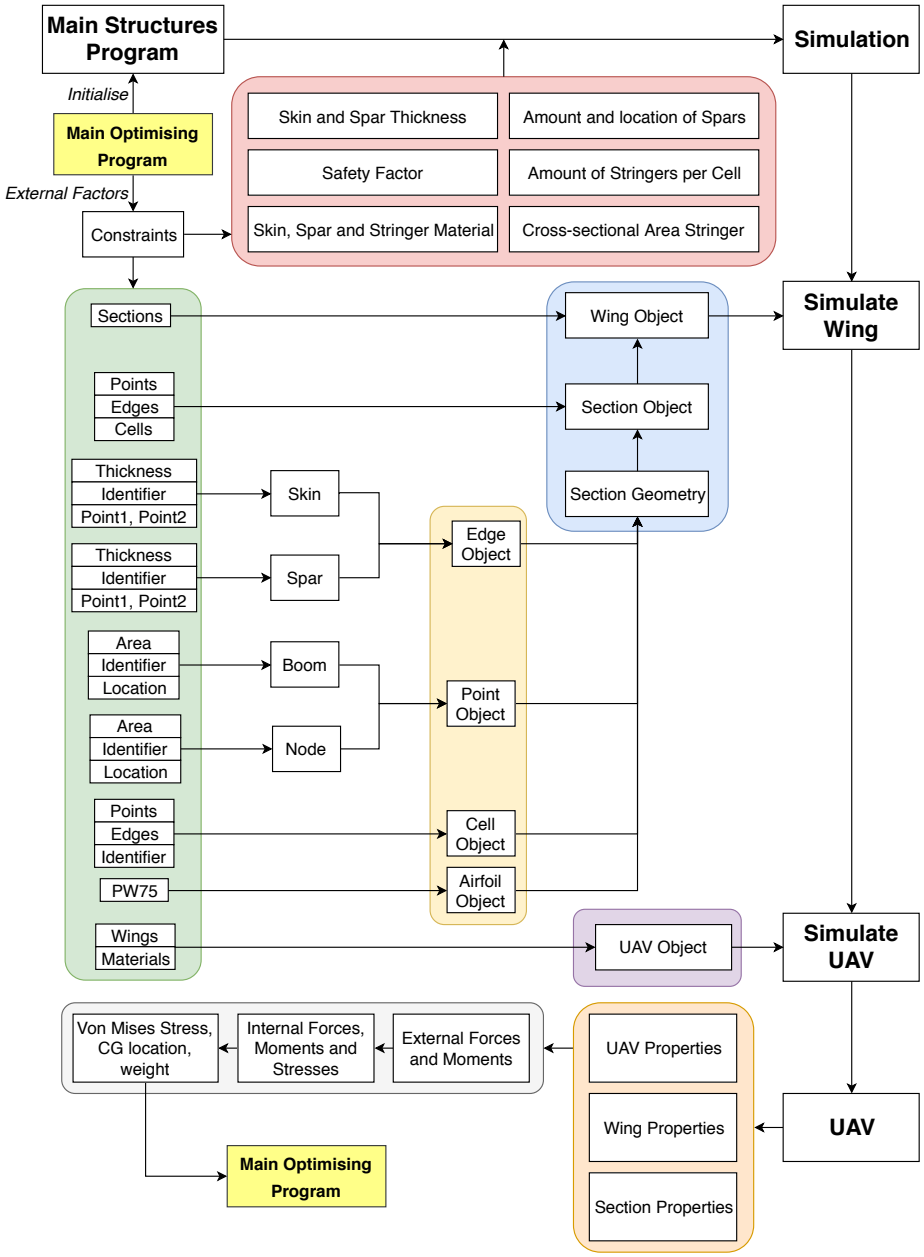

Figure 14.7: Logical flow of the structural analysis program.

14.2. Selection of the Materials

The material selection is dependent on the stresses resulting from the Von-Misses stress. Next to that, manufacturability, density and cost are key parameters. Overall, two specific classes of materials are considered. On one hand, there is the metal group which is commonly used and proven in the aerospace industry. Four different types of aluminium are considered as one can see inTable 14.2 [82].

Table 14.2: Properties of different metals.

Metals	E-modulus [GPa]	Shear modulus [GPa]	Tensile yield strength [MPa]	Tensile ultimate strength [MPa]	Mass density [kg/m^3]
Al 7475-T7651	71.7	27	462	531	2810
Al 7075-T6	71.7	26.9	503	572	2810
Al 2024-T86	72.4	28	440	515	2780
Al 6061-T913	69.0	26	455	620	2700

On the other hand, the composite material group is considered. Composites give more flexibility than other materials; they can be composed as one wishes. It is thus quite difficult to give exact values for the different properties. It should

[82] http://www.aerospacemetals.com/aluminum-distributor.html [cited on: 13/06/2018]

also be mentioned that composite materials have directional properties, this means that the properties are different for every direction. Therefore, an estimation range is given of the tensile ultimate strength and tensile Young's Modules in Table 14.3 (Callister 1985). After that, in Table 14.4 and in Table 14.5 the density is discussed of different fibre and matrix materials respectively. Note that only Fibre Reinforced Polymers (FRP) are discussed. That is because other composite alternatives such as sandwich structures, composite woods or concretes are no efficient options for this UAV design. Note that in Table 14.5, UP stands for Unsaturated Polyester Resin and EP stands for Epoxy Resin. Lastly, a good way to differentiate composite materials is by making a qualitative comparison between them as shown in Table 14.6.

Table 14.3: Quantitative comparison of FRP Composites.

Composite	Tensile ultimate strength [MPa]	Tensile E-modulus [GPa]
Glass FRP	517 - 1207	30 - 55
Carbon FRP	1200 - 2410	147 - 165
Aramid FRP	1200 - 2068	50-74
GLARE	620	58

Table 14.4: Density of fibres.

Fibre	Density [kg/m^3]
Glass	2550
Carbon	1700 - 1900
Aramid	1440

Table 14.5: Densities of matrix materials.

Matrix	Density [kg/m^3]
UP	1200
EP	1200
Al 2024-T3	2780

Table 14.6: Qualitative comparison of FRP Composites.

Criterion	Carbon FRP	Glass FRP	Aramid FRP	GLARE
Tensile Strength	Very Good	Good	Very Good	Good
Modulus of Elasticity	Very Good	Adequate	Good	Good
Long Term Behaviour	Very Good	Adequate	Good	Good
Fatigue Behaviour	Excellent	Adequate	Good	Adequate
Bulk Density	Good	Adequate	Excellent	Adequate
Cost	Adequate	Very Good	Adequate	Adequate

From the above tables, it is clear that the CFRP (Carbon Fibre Reinforced Polymer) is the composite with the highest strength and E-modulus. The density is also significantly lower compared to metals. The only drawback could be that the cost is higher compared to other options, although the benefits of the CFRP properties outweigh its disadvantages.

14.2.1. Material Selection of the Spars and the Ribs

With the above information, it is decided that MAINTAIN its **spars and ribs will be made of Carbon Fibre Reinforced Polymer**. This is an efficient design choice as the forces on these elements are directional, meaning that the composite can be designed for the specific load case. In the following two pictures, Figure 14.8 and Figure 14.9, the main relevant loads are visualised with their corresponding fibre orientation to withstand the loads.

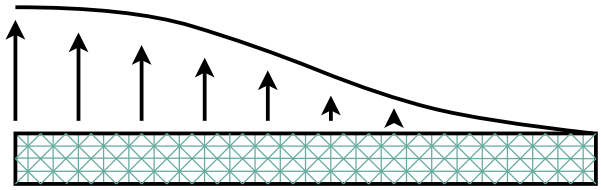

Figure 14.8: Fibre orientation for the spars.

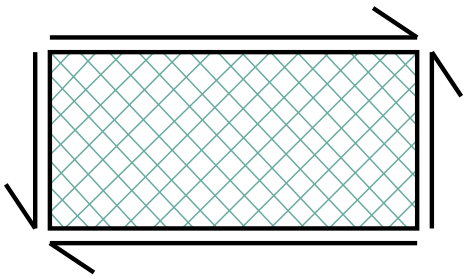

Figure 14.9: Fibre orientation for the ribs.

In Figure 14.8, it is visualised that the lift force is the main force acting on the spar. The lifting force will induce normal forces due to the bending moment it creates. However, that is not the only force. Spars play a really important role in the so called wing box. The wing box is also subject to shear and torsional forces. That is why the spar has fibres in both the normal directions (0° and 90°) and the shear directions (-45° and +45°). Next, in Figure 14.9 the rib is visualised. As the rib is mostly only subject to shear forces, it is sufficient to only lay fibres in the shear directions (-45° and +45°).

14.2.2. Material Selection of the Skin

The skin is of utter importance as everything is connected to the skin. The skin also defines the outer shape of the wings and should protect the inside. When there would be an impact, the skin should be able to minimise the impact damage. Therefore, a more ductile material with a high-fracture toughness is desirable. This means that aluminium would be an option. However, if the whole skin would be only of aluminium, the structural weight would increase. Therefore, **GLARE is chosen as the material of the skin** since it would be a better option as it consists partially of aluminium. When using GLARE (which stands for Glass Reinforced aluminium), it remains possible to adapt the material to the load case the skin

encounters. This will make the material more efficient and thus lighter. In following picture, the top view of the wing is visualised with the fibre direction. Once again, there are fibres in the shear directions (-45° and +45°) and along the span to take on the bending induced normal stresses (90°).

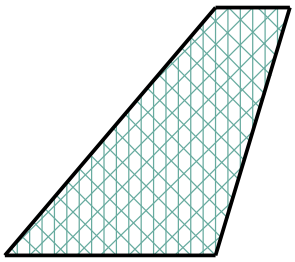

Figure 14.10: Fibre orientation for the skin.

14.2.3. Material Selection of the Stringers

The stringers play a really important role in taking up the normal stresses which are induced because of the lift. Also, when the UAV is landed, there will be normal stresses acting on the structure as the structural weight will induce bending. Therefore, the stringers should be able to withstand both compressive and tensile stresses; which is why it is decided to use an aluminium for the stringers. This aluminium should be a stiff material (a high E-modulus), should have a high yield strength, as yielding is highly undesired, and should have a low density in order to reduce the weight. From Table 14.2, **it is decided to use 7075-T6 aluminium**. That is because the tensile yield strength is significantly higher than the other options. The fact is that the density of 7075-T6 is slightly higher and that it is a little bit less stiff than the 2024-T86 option but because of the big different in yield strength, it is decided to make use of the 7000 series aluminium.

14.3. Landing Gear

During take-off and landing of the UAV, a landing gear should handle the huge loads on the structure that occurs in these operational phases. Sizing a landing gear is really important, as (Raymer 2012) alleges: "Landing gear will ruin your layout more than anything else, so plan ahead." In this section, the landing gear will be designed in detail. The landing gear will be designed to handle landing on various types of surfaces, since a requirement is posed stating that the UAV should be able to land autonomously whenever the propulsion system fails. To comply with this requirement, the landing gear is designed to land on soft, loose desert sand as well as on asphalt, and all surfaces in between. This is of huge influence on the maximum tire pressure, which is the lowest, 30 psi, for the soft loose desert sand.

14.3.1. Configuration

First of all, a proper landing gear configuration should be chosen. Several configurations exist, which will be discussed shortly before a choice is made.

- **Single main**: used mainly for sailplanes, hence this option is eliminated.
- **Bicycle**: the bicycle configuration, featuring two main wheels, has to take-off and land in a flat attitude, which means the aircraft should generate much lift at low angles of attack. This will not be the case for the UAV, and hence this option is discarded.
- **Taildragger**: the taildragger configuration is used mainly in aircraft featuring a propeller at the front of the aircraft. As explained in section 12.2, a pusher propeller aft of the body will be used, meaning that the taildragger configuration loses its biggest advantage and will be discarded as well.
- **Quadricycle**: this configuration is a special version of the bicycle configuration and is eliminated for the same reason.
- **Tricycle**: the tricycle configuration features one nose wheel in front of the c.g. and two main wheels aft of the c.g., and is the most common configuration in modern aviation. When designed properly, enough tip clearance is present and it will allow for an aft propeller.

From the listed configurations, the **tricycle configuration** is the most convenient one for the design. Taking off will be done at an angle, providing enough lift, and the main struts should be designed accounting for the aft propeller. Providing the required **tip-back angle of 15 degrees** in static configuration (Raymer 2012), the landing gear is located as visualised in Figure 14.11. The exact location of the gear can be found in Table 14.8. The small rake angle of the nose wheel will increase steering capabilities (Raymer 2012).

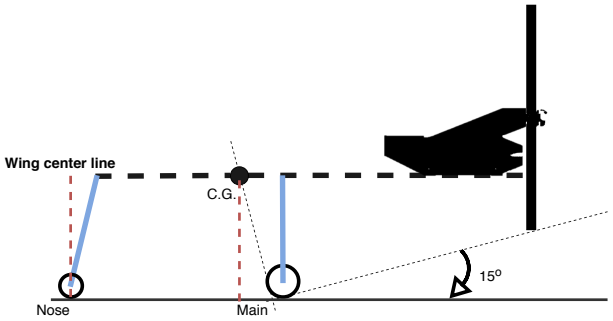

Figure 14.11: Landing gear configuration layout. Note that the wing centre line and turboprop engine are also drawn.

Providing lateral clearance, (Roskam 2000) provides Equation 14.9, to calculate the lateral distance between the two main wheels, in which ϕ should be no less than 63 degrees (Raymer 2012).

$$y_{\text{mlg}} = \frac{l_n + l_m}{\sqrt{\frac{l_n^2 tan^2\phi}{z_{c.g.}} - 1}} \tag{14.9}$$

14.3.2. Wheel and Tire Design

Sizing the wheels and tires of the landing gear as well as the brakes involved, is the next step in the design of a landing gear. The maximum static load on all struts is calculated, as well as the dynamic load on the nose landing gear as given in (Raymer 2012).

When the aircraft is on the ground, the tires are loaded and the so-called loaded radius (R_r) will be smaller than the maximum tire radius. Following from Equation 14.10(Raymer 2012), the area of the tire resting on the ground is calculated. Dividing the load on the tire by this area yields the tire pressure. Note that a lower tire pressure will increase the life of the tire significantly(Raymer 2012).

$$A_p = 2.3\sqrt{wd}\left(\frac{d}{2} - R_r\right) \tag{14.10}$$

$$KE_{\text{braking}} = \frac{1}{2}\frac{W_{\text{landing}} V_{\text{stall}}^2}{g N_{\text{wheels}}} \tag{14.11}$$

Based on those loads and on the maximum defined pressure due to landing at rough surfaces, proper tires are selected for both gears. The most important dimensions are listed in Table 14.7.

Table 14.7: Tire and wheel specifications.

	Nose wheel	**Main wheel**
Tire	280/250 X 4 SAWTOOTH TIRE, 4 PLY	Goodyear type III 5.00-5, 4 PLY
Outer diameter [m]	0.223	0.361
Tire width [m]	0.0711	0.107
Loaded radius [m]	0.107	0.145
Pressure [psi]	29.5	7.71

Sizing the brakes, the kinetic energy per brake is calculated with Equation 14.11. Following from statistics in (Raymer 2012), the brake diameter will be approximately 0.19 m. Note that only the main gear wheels are used to brake.

14.3.3. Strut and Shock-Absorber Sizing

Now that the tires are sized, the struts and shock-absorbers should be sized. Again, the kinetic energy to be absorbed is calculated, equated to the energy absorbed by the tires and shock-absorbers, resulting in Equation 14.12. Rewriting yields Equation 14.13, used to calculate the stroke of the shock-absorber. The total length of the shock-absorber will be approximately 2.5 times this size (Raymer 2012). N_{gear} is equal to 3 for general aviation, and the efficiency of an oleopneumatic shock absorber, η, is 0.7 whilst that of tires, η_t, is 0.47 (Raymer 2012).

$$\frac{1}{2}\frac{W_{\text{landing}} V_{\text{vertical}}^2}{g} = (\eta L S)_{\text{shock absorber}} + (\eta_t L S_t)_{\text{tire}} \tag{14.12}$$

$$S = \frac{V_{\text{vertical}}^2}{2g\eta N_{\text{gear}}} - \frac{\eta_t}{\eta} S_t \tag{14.13}$$

The common mechanism to absorb the shocks is an oleopneumatic shock absorber, which has a high internal pressure of typically 12,415 kPa (Raymer 2012). Relating pressure and force to area, the diameter of the shock absorber can be calculated using Equation 14.14, in which L_{oleo} is the load on the oleo, which equals the load on the strut.

$$D_{\text{oleo}} = 1.3\sqrt{\frac{4L_{\text{oleo}}}{P\pi}} \tag{14.14}$$

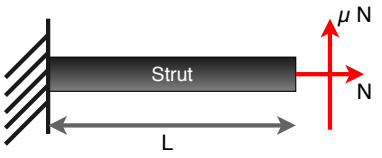

Figure 14.12: Forces on the landing gear strut during braking.

The selected material for the strut is steel, alloy 4340, a commonly used material in landing gears (Jeevanantham, Vadivelu, and Manigandan 2017). Featuring a yield strength of 472.3 MPa, this material will mean the struts can have a relatively low thickness and diameter. Setting the inner diameter to the oleo diameter just determined, the outer diameter is calculated using normal bending theory, as visualised in Figure 14.12. The friction coefficient of a wheel with full brakes applied is assumed to be 0.4 (Roskam 2000). As such, the outer diameter of the strut can be calculated.

Now that the landing gear is fully sized, its layout and most important dimensions can be found in Figure 14.11 and Table 14.8.

Table 14.8: Landing gear dimensions.

	Nose landing gear	**Main landing gear (per strut)**
Strut length [m]	0.60	0.67
Strut diameter [m]	0.018	0.022
Shock absorber stroke [m]	0.19	0.19
Shock absorber diameter [m]	0.0093	0.012
Wheel casing width [m]	0.12	0.16
Ground distance to centre of gravity [m]	0.75	0.13
Design load [N]	300	852
Track width [m]	-	0.63

14.4. Structural Dynamics

Essential to the design of a structural wing is the assessment of dynamic phenomena such as flutter and buffeting. Buffeting is disregarded in this analysis due to the low flight speeds of the UAV.

Flutter is defined as the dynamic instability of a structure within a fluid flow caused by positive feedback between aerodynamic forces and structural deformation. A typical example is an airfoil pitching up due to a torsional load, hence causing more lift due to a higher angle of attack, which further increases deformation. This is clearly a diverging phenomenon. Assessment of flutter is typically one of high computational complexity for that it requires detailed assessment of both aerodynamic properties and structural deformation. Currently, two-dimensional assessment of flutter is best practice. This relevant section is selected a priori by knowledge on the structural properties of the wing.

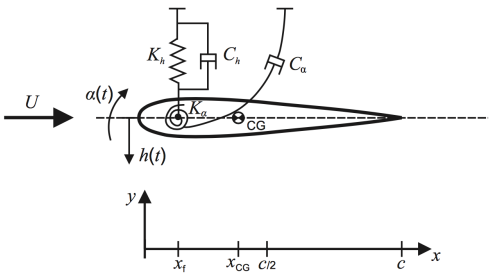

Figure 14.13: Representation of the wing as a two-dimensional dynamic system in order to perform analysis of flutter (Sanchez et al. 2016).

The implemented model is a coupled system of second order ordinary differential equations. The dynamics of the wing are decomposed in a pitching and plunging mode as shown in Figure 14.13. Now, the equations of motion become as in Equation 14.15.

$$m\ddot{h} + S\ddot{\alpha} + C_h\dot{h} + K_h h = -L \tag{14.15}$$

$$S\ddot{h} + I_f\ddot{\alpha} + C_\alpha\dot{\alpha} + K_\alpha\alpha = M \tag{14.16}$$

The subscript f denotes the flexural axis is the wing (which is the curve formed by connection of the sectional shear centres) and S indicates the distance between this axis and the local centre of gravity location. Note however that the coefficients in Equation 14.15 are dynamic in nature, they change with the deformation of the system. As such, the aerostructural capabilities of SU2 are used to assess the flutter of the wing. The used mesh is shown in Figure 14.14 Only the highest possible mach number is assessed, as flutter itself is a limit oscillation cycle (Fung 2008). The chosen location to assess flutter is the wing tip, as is common for conventional wings (Fung 2008). Results of this analysis are shown in Figure 14.15. The initial condition complies with a gust as specified in subsection 11.5.2. **Thus, the wing will not suffer from flutter within its flight envelope.**

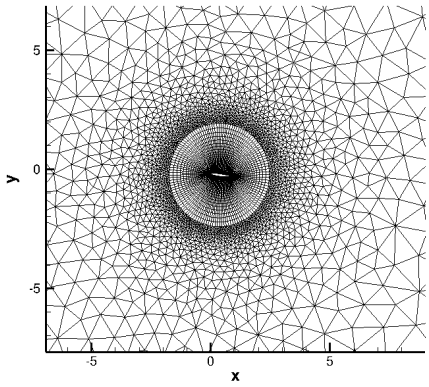

Figure 14.14: The mesh of the PW75 airfoil used in the analysis of flutter.

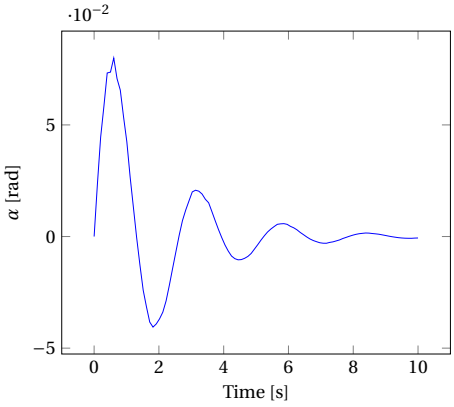

Figure 14.15: Response of angle of attack to a gust speed of 8 m/s (at time zero) at a mach number of 0.1 with Reynolds number 200,000.

14.5. Verification and Validation

The verification of the structural analysis is performed by implementing a simplified wing, a box, in the program. The skin thickness is 1mm and is equal for all the edges. The results of the program are then compared with a manual analysis of the box in Table 14.9. The simplified problem is visualised in Figure 14.16. A uniform lift distribution of 100 N/m and point weight force of 200 N acts on the box. Just as in the simulation of the UAV, the lift acts at the quarter-chord location.

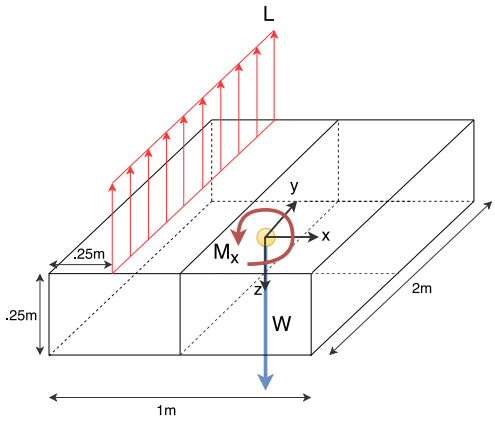

Figure 14.16: Verification model for the wing.

Table 14.9: Verification results.

Parameters	Simulation	Manual Analysis
$x_{\text{shear centre}}$	0.5	0.5
Maximum cross-sectional shear stress	133 $\frac{N}{m^2}$	133 $\frac{N}{m^2}$
Maximum M_y	49.95	50
Maximum normal stress $\left[\frac{N}{m^2}\right]$	6.60	6.67
I_{zz}	10	10
I_{xx}	0.9375	.9375
I_{xz}	0	0

Validation of the structural properties obtained using the method described later in subsection 17.2.2 has been done through a finite element analysis (FEM) solution of the entire wing. The software used is AutoDesk Inventor (*AutoDesk Inventor* n.d.). The loading used was the lift distribution from Figure 13.6 scaled by the maximum load factor obtained in subsection 11.5.2. The results in Figure 14.17 show that the maximum Von Mises stress of 376 MPa does not exceed any of the material yield stresses.

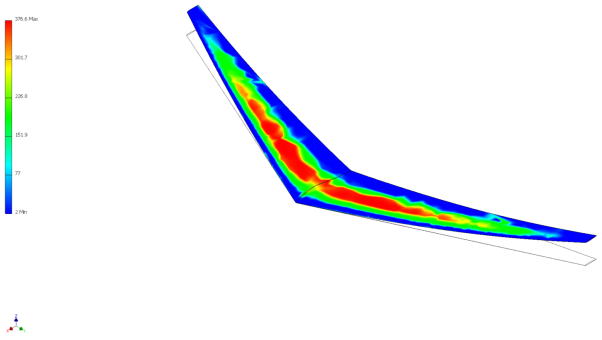

Figure 14.17: Contour plot of the Von Mises stress in the wing under its maximum loading.

15
Stability and Control

The stability and control are important aspects with regard to the flight dynamics of the aircraft. The two are closely related, where an optimum has to be obtained combining the best parts of both. This chapter discusses the approach used for the design of control surfaces and the manner in which the stability characteristics of the UAV are assessed. First, the stability analysis, including both the static and dynamic stability and their verification and validation, is explained in section 15.1. Subsequently, an analysis and sizing procedure of the control surfaces is outlined in section 15.2. In section 15.3 and section 15.4, the results and their verification and validation can be found, respectively.

15.1. Stability Analysis

The Stability Analysis will start with stating the requirement(s) related to stability. Hereafter, the procedure to obtain the stability derivatives will be explained, followed by the assessment of static and dynamic stability, making up the stability model. Finally, this model will be verified and validated.

15.1.1. Requirements for Certification

Requirement -MTN.SYS.UAV-17- states that the UAV shall be stable (B. van Beurden et al. 2018a). This requirement originates from FAR part 23, regulation 23.2145.

FAR 23.2145 [83]: *"Aircraft, not certified for aerobatics, must have static longitudinal, lateral, and directional stability in normal operations. Furthermore, they must have dynamic short period and Dutch roll stability in normal operations."*

15.1.2. Calculation of the Stability Derivatives

In order to assess both the static and dynamic stability of the UAV it is crucial to obtain the system's stability derivatives. Such a stability derivative is in general defined as

$$C_{X_\alpha} = \frac{\partial C_X}{\partial \alpha} = \frac{\partial X}{\partial \alpha} \frac{1}{\frac{1}{2}\rho V^2 S} \tag{15.1}$$

Where X is an aerodynamic force, α is the independent variable and S is the reference area. Note that for aerodynamic moments the reference area is multiplied with some reference length for ensuring that the coefficient is dimensionless.

[83] https://www.ecfr.gov/cgi-bin/text-idx?SID=685dc1ae97ae3f5e5569e47880fab01e&mc=true&node=pt14.1.23#se14.1.23_12145 cited on: 11-06-2018

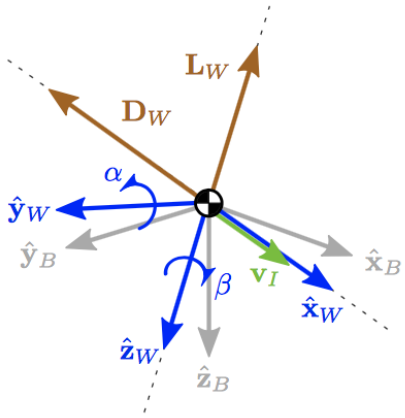

Figure 15.1: Relation between the body and wind frame (Macdonald et al. 2017).

The Stability derivatives for a given configuration have been obtained by making use of the Athena Vortice Lattice method (AVL)(Drela 2006). In contrast to the aerodynamic analysis of the wing, the in-house developed vortex lattice method (VLM) was not capable of assessing the wing stability. This is because it was concluded that efficient implementation of this capability would have required more time than is saved by its computation. In general, the VLM is adjusted by a velocity field perturbation which would appear on the right-hand side of Equation 13.5. The inlet flow field is adjusted if rotation of the body is present as in Equation 15.2. The rotation vector is $\boldsymbol{\Omega} = [p, q, r]^T$ and the position vector $\boldsymbol{r}$ extends from the vehicle's centre of gravity.

$$\boldsymbol{V}' = \boldsymbol{V}_\infty + \boldsymbol{\Omega} \times \boldsymbol{r} \tag{15.2}$$

In case of a stability derivative with respect to an angular displacement between the body frame B and wind frame A the adjusted velocity field is found as in Equation 15.3 with $\mathbf{T}_{BA}$ the transformation matrix. This relation is illustrated in Figure 15.1.

$$\boldsymbol{V}' = \mathbf{T}_{BA}\boldsymbol{V}_\infty \tag{15.3}$$

Changes in the flow field due to a change in velocity are simply found by vector addition. Finally, AVL computes the partial derivative in Equation 15.1 by means of a central difference scheme Equation 15.4.

$$\frac{\partial X}{\partial \alpha} = \frac{X(\alpha + \Delta\alpha) - X(\alpha - \Delta\alpha)}{2\Delta\alpha} + \mathcal{O}(\Delta\alpha^2) \tag{15.4}$$

15.1.3. Assessing Static Stability

The static stability behaviour of an aircraft can be observed by giving an increase in pitching moment -pitch up-, leading to a change in angle of attack when flying at the trim condition. If the nose pitches up, the aircraft is considered longitudinally unstable, whereas a pitch down would imply that it is stable. Mathematically, this would mean that Equation 15.5 is satisfied for a particular flight condition.

$$\frac{dC_m}{d\alpha} < 0 \tag{15.5}$$

$$C_m = C_{m_0} + C_{L_h} + C_{LA-h} \cdot \frac{S_h V_h}{SV}(x_{cg} - x_{np}) \tag{15.6}$$

Combining Equation 15.5 and Equation 15.6 (Sadreay 2013), it is clear that an increase in angle of attack will cause a decrement in the pitching moment coefficient, concluding that Equation 15.7 is satisfied.

$$(x_{cg} - x_{np}) < 0 \tag{15.7}$$

So, in order to have a statically stable configuration, the centre of gravity location must be in front of the neutral point. A small margin between the two points is preferred as the c.g. location might vary during flight as fuel is being expelled, possibly making the UAV unstable. Often, this margin encompasses 5% of the MAC (Sadreay 2013).

The centre of gravity location can be found by analysing the UAV in its total, including fuel and operational items. The location of the neutral point of a flying wing can already be calculated using Equation 15.8 [84].

$$x_{np} = \frac{C_r}{4} \cdot \frac{b(1+\lambda)}{6(1+2\lambda} \cdot tan(\phi_{0.25c}) \quad \text{taper ratio} < 0.375 \tag{15.8}$$

[84] `https://www.mh-aerotools.de/airfoils/flywing1.htm` [cited on: 11-06-2018]

15.1.4. Assessing Dynamic Stability

In general, the aircraft dynamics will be of the form in Equation 15.9. The vector $\boldsymbol{x}$ represents the aircraft state and t the time. The vector mappings f and g represents the system and forcing inputs on the state evolution respectively.

$$\frac{d\boldsymbol{x}}{dt} = f(\boldsymbol{x}, t) + g(t) \tag{15.9}$$

It is more often than not that f and g are highly nonlinear. As solution of Equation 15.9 would then require elaborate stepping schemes, it is chosen to linearise the dynamical system as to be integrable within the design flow. This linearisation is performed about a certain state, implying that its use in state evolution must be limited to short intervals. Additionally, the system is assumed to be autonomous. The resulting dynamical stability equation is shown in Equation 15.10.

$$\frac{d\boldsymbol{x}}{dt} = A\boldsymbol{x} + B\boldsymbol{u} \tag{15.10}$$

with $\boldsymbol{u}$ the forcing vector. By use of Newton's second law and sufficient constitutive relations it is possible to decouple Equation 15.10 in two separate linear equations as shown in Equation 15.11 and Equation 15.12 .

$$\begin{bmatrix} C_{X_u} - 2\mu_c D_c & C_{X_\alpha} & C_{Z_0} & C_{X_q} \\ C_{Z_u} & C_{Z_\alpha} + (C_{Z_{\dot\alpha}} - 2\mu_c)D_c & C_{X_0} & C_{Z_q} + 2\mu_c \\ 0 & 0 & -D_c & 1 \\ C_{m_u} & C_{m_\alpha} + C_{m_{\dot\alpha}} D_c & 0 & C_{m_q} - 2\mu_c {K_Y}^2 D_c \end{bmatrix} \begin{bmatrix} \hat{\mathrm{u}} \\ \alpha \\ \theta \\ \frac{q\bar{c}}{V} \end{bmatrix} = \begin{bmatrix} -C_{X_{\delta_e}} & -C_{X_{\delta_t}} \\ -C_{Z_{\delta_e}} & -C_{Z_{\delta_t}} \\ 0 & 0 \\ -C_{m_{\delta_e}} & -C_{m_{\delta_t}} \end{bmatrix} \begin{bmatrix} \delta_e \\ \delta_t \end{bmatrix} \tag{15.11}$$

$$\begin{bmatrix} C_{Y_\beta} + (C_{Y_{\dot\beta}} - 2\mu_b)D_b & C_L & C_{Y_p} & C_{Y_r} - 4\mu_b \\ 0 & -\frac{1}{2}D_b & 1 & 0 \\ C_{l_\beta} & 0 & C_{l_p} - 4\mu_b K_X^2 D_b & C_{l_r} + 4\mu_b K_{XZ} D_b \\ C_{n_\beta} + C_{n_{\dot\beta}} D_b & 0 & C_{n_p} + 4\mu_b K_{XZ} D_b & C_{n_r} - 4\mu_b K_Z^2 D_b \end{bmatrix} \begin{bmatrix} \beta \\ \phi \\ \frac{pb}{2V} \\ \frac{rb}{2V} \end{bmatrix} = \begin{bmatrix} -C_{Y_{\delta_a}} & -C_{Y_{\delta_r}} \\ 0 & 0 \\ -C_{l_{\delta_a}} & -C_{l_{\delta_r}} \\ -C_{n_{\delta_a}} & -C_{n_{\delta_r}} \end{bmatrix} \begin{bmatrix} \delta_a \\ \delta_r \end{bmatrix} \tag{15.12}$$

For further clarification on the symbols used, one can refer to the Nomenclature. Additionally, the synthesis of Equation 15.11 and Equation 15.12 implies that the asymmetric motion is assumed to be independent of the symmetric motion. Note that Equation 15.10 may be employed to reveal important information regarding the stability of the aircraft. As any solution to this differential equation is a linear combination of the fundamental solution set, one can consider this array in evaluation of stability. These solutions are all defined by some eigenvalue, which determines their time evolution. Such an eigenvalue λ is defined as in Equation 15.13. Consequently, they form the solution to the characteristic polynomial in Equation 15.14.

$$A\boldsymbol{\xi} = \lambda\boldsymbol{\xi} \tag{15.13}$$

$$|A - \lambda I| = 0 \tag{15.14}$$

These eigenvalues can be assessed on stability by requiring $\mathrm{Re}(\lambda) < 0$. This methodology is built into the design software.

15.1.5. Providing Weathercock Stability

The weathercock stability concerns the ability of the aircraft to recover from disturbances in yaw. This directional stability is provided by vertical stabilising surfaces. The winglet in the current design will be designed to act as a vertical stabiliser as this will give the surface for directional stability the most aft position and therefore the highest effectiveness. As no requirements are present for the directional stability, typical values for the measure of directional stability are used to compute the required area of the winglet to provide sufficient directional stability. The measure of directional stability σ_f is defined as follows.

$$\sigma_f = \frac{S_f \, r_f}{S \, \frac{b}{2}} \tag{15.15}$$

Here, S_f is the surface area of the vertical surfaces or winglets in this specific case and r_f is the distance between the neutral points of the wing and fins. The neutral points in this context is assumed to be at the quarter-chord of the wing surface. The measure of directional stability relates the required surface area of the vertical fins to other geometric properties of the wing.

15.2. Control Analysis

Implementation of the control model is necessary to size the control surfaces used by the UAV to manoeuvre during flight. In this chapter the control model is presented. Initially the implementation of the control model is discussed, subsequently the analysis used in the control model is displayed. Finally, the verification and validation of the model is discussed.

15.2.1. Implementation of Control Model

The sizing of the control surfaces of an aircraft is a process where the required dimensions of the control surfaces are determined based on the required manoeuvrability of the aircraft. The effectiveness of the control surfaces is dependent on the geometry of the wing, as well as the characteristics of the airfoil of the wing, which follow from the aerodynamic analysis of the aircraft. The roll performance of the aircraft surfaces depends on the geometry of the control surfaces and the mass properties of the aircraft which result from the weight estimation of the aircraft. The results of the model are the dimensions of the control surfaces as well as the added weight and trim drag produced by the control surfaces to counteract the shift in mass properties due to fuel burn.

15.2.2. Control Model Analysis

The control model concerns the sizing of the control surfaces used on the UAV. These include the elevators, ailerons and rudder. A possible combination of the elevator and aileron control surface, called elevon, is also assessed and a comparison has been made between the use of an elevon and the use of separate ailerons and elevator. The control surfaces will be analysed separately and their combined contribution in terms of weight, drag and complexity will be determined to find the optimal configuration of the control surfaces of the UAV.

15.2.3. Requirements

FAR 23.2135 states that "the airplane must be controllable and manoeuvrable, without requiring exceptional piloting skill, alertness, or strength"[85]. There are no specific roll, pitch or yaw rates mentioned by the FAA. However, the roll and pitch rate are specified in MIL-F-8785C regulations(Sadreay 2013)(Elham 2016). These are U.S. military regulations that are often used in literature for similar applications. The required roll rate of the aircraft is 60 degrees in 1.3 seconds during a constant roll. For the elevator, the required moment that needs to be opposed is the moment created by the weight during every instance of the mission together with the angular acceleration of the pitch during take-off. This is specified for a remote control model to be between 10 and 15 deg/s^2 (Sadreay 2013). For this reason the required angular acceleration is determined to be 12.5 deg/s^2 for MAINTAIN. Next to the take-off pitch it is important that the pitch is regulated for all the positions of the centre of gravity.

15.2.4. Aileron

The aileron is a primary control surface which makes the aircraft roll abound its longitudinal axis. Figure 15.2 shows the schematic flow for the determination of the size of the aileron.

1. **Determine required roll performance:** as mentioned in subsection 15.2.3 the required roll rate is 60 degrees in 1.3 seconds, resulting in a roll rate P of 46 degrees per second, based on MIL-F-8785C.
2. **Determine the roll damping coefficient** C_{l_p} with Equation 15.16 based on the 2D airfoil characteristics.

$$C_{l_p} = -\frac{4(c_{l\alpha} + c_{d_0})}{S_{ref} b^2} \int_0^{b/2} y^2 c(y) dy \tag{15.16}$$

3. **Determine the aileron control derivative** $C_{l_{\delta_a}}$ with Equation 15.17. For this computation, it is assumed that differential ailerons are used to minimise adverse yaw, and the aileron has a maximum deflection of 20 degrees as this is a typical configuration for smaller aircraft. This results in an effective aileron deflection δ_a of 17.5 degrees.

$$C_{l_{\delta_a}} = -\frac{P C_{l_p} b}{\delta_a 2V} \tag{15.17}$$

4. **Determine the aileron span** with Equation 15.18 where b1 and b2 are the start and end position of the aileron. τ is a function of the chord ratio of the wing and the control surface. Since this function is dependent on the chord, the

[85] https://www.ecfr.gov/cgi-bin/text-idx?SID=685dc1ae97ae3f5e5569e47880fab01e&mc=true&node=pt14.1.23#se14.1.23_12135

span and the position of the aileron some variables are set. For multiple combinations of set aileron chords and outboard positions of the aileron the required aileron span is determined.

$$C_{l_{\delta_a}} = \frac{2c_{l\alpha}\tau}{S_{ref}b}\int_{b1}^{b2} c(y)ydy \tag{15.18}$$

5. **List possible ailerons**. Since different chords and different positions of the aileron are used there is not just one possible aileron. A list is generated for the different aileron chords and positions with their corresponding aileron span.

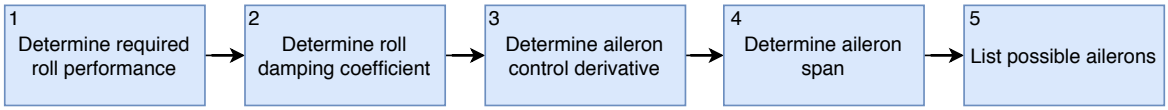

Figure 15.2: Schematic flow of the algorithm for the determination of the aileron.

15.2.5. Elevator

The elevator is a primary control surfaces which makes the aircraft pitch around its lateral axis. The pitch of an aircraft can be altered by changing the moment of the vehicle. In a conventional aircraft this moment is regulated by the elevator on the horizontal tail. Since the flying wing does not have a horizontal tail the pitch needs to be managed differently. By changing the lift distributions on the wing the moment changes as well. With the use of a control surface, such as an elevator, the lift distributions and thereby the moment of the flying wing can be altered. Based on the required moment change the elevator can be sized. Figure 15.3 shows the schematic flow for the determination of the size of the elevator based on a method of (Torenbeek 1982) as explained below.

1. **Determine required moments:** as mentioned in subsection 15.2.3 the required angular pitch acceleration during take-off is 12.5 deg/s^2. The elevator should also be able to regulate the pitch for all the positions of the centre of gravity. Those two requirements are translated in a required moment around the aerodynamic centre.
2. **Determine change in lift** with Equation 15.19. The 2D lift change is dependent on the elevator effectiveness τ, function of ratio of the elevator chord ratio and wing chord, and an maximum elevator deflection of 20 degrees(Sadreay 2013). This equation needs to be filled in for multiple aileron chords.

$$\Delta c_l = \tau\delta_e c_{l_\alpha} \tag{15.19}$$

3. **Determine moment change** the airfoil will produce with Equation 15.20. Where μ and $c_{increase}$ are both dependent on the chord of the elevator and its deflection.

$$\Delta c_m = -\mu\Delta c_l \frac{\bar{c} + c_{\textbf{increase}}}{\bar{c}}\left(\frac{\bar{c} + c_{\text{increase}}}{\bar{c}} - 1\right) \tag{15.20}$$

4. **Determine elevator span** with the required moment change of the wing and Equation 15.21.

$$\Delta C_m = \frac{c\Delta c_m b_{\text{elevator}}}{S_w} \tag{15.21}$$

5. **List all possible elevators** for the different elevator chords used in step 2 and 3.

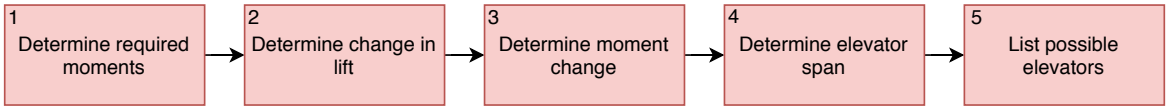

Figure 15.3: Schematic flow of the algorithm for the determination of the elevator.

15.2.6. Elevon

An elevon is a combination of the previously mentioned aileron and elevator and is able to both pitch and roll the vehicle. This option as control surface is similarly assessed and compared with the configuration with a separate aileron and elevator. The dimensions of the elevons have been determined in the following manner as illustrated in Figure 15.4.

1. **Select control surfaces that comply with all requirements.** This will be done by comparing the lists of the aileron and the elevator: they both consist the chord, the position and span of the control surface. For the same control surface chord and position the biggest span will be chosen since this will comply with both the roll and pitch requirements.

2. (a) **Determine drag during cruise** based on a method from (Roskam 2000). The drag is the summation of the profile, induced and interference drag of the elevon. The differences between the drag of the elevons will be caused by the difference in chord and span.

   (b) **Execute weight comparison**. The weight of the control surface will be based on Equation 15.22 which is a Class II weight estimation of (Gundlach 2014) where F_{FCS} is assumed 0.0002.

$$W_{FCS} = F_{FCS} S_{CS} V_{EQ,Max}^2 0.45359237 \tag{15.22}$$

3. **Select best suitable elevon** based on the trim drag and extra weight of each elevon. The elevon model is implemented in the general model and the effect of the control surface on the fuel consumption is evaluated. The elevon configuration that minimises the fuel consumption.

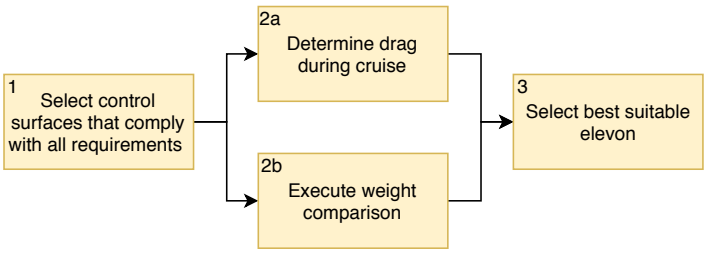

Figure 15.4: Schematic flow of the algorithm for the determination of the elevon.

15.2.7. Rudder

The rudder is a primary control surface which makes an aircraft yaw around its vertical axis. Although a rudder is not necessary for yaw movement it is almost always implemented on a conventional aircraft configuration. A rudder is designed to perform the following functions: cross-wind landing, spin recovery, coordinated turn and adverse yaw(Sadreay 2013). Despite the multiple implementations for the rudder an aircraft is able to fly without a rudder. In fact, during nominal flight conditions a rudder is not used except for the possibility of cross-wind landing and cross-wind take-off. This is because when an aircraft rolls the down going wing experiences an extra force in the positive longitudinal direction due to an increased angle of attack while the up going wing experiences an extra backward pointed force(Mulder et al. 2013). This causes a yawing moment without using a rudder.

From existing flying wings it can be seen that a rudder is not necessary. For example multiple flying wings from Northrop, such as the Northrop B-2 and Northrop YB-35, the Horten Ho 299 and the NASA Prandtl wing have no rudder. But not only manned flying wings exist without a rudder: the Skywalker X8 flying wing is a UAV without a rudder.
Because a rudder is not necessary for yawing, there is proof of concept of flying wings without rudders. A rudder will add extra weight and complexity it is decided that the aircraft will not have a rudder. With the design of the differential ailerons the coordinated turn and adverse yaw requirements are already taken care of. However, without the rudder some constrains will arise on the maximum wind speed during the execution of a cross-wind landing or take-off.

15.3. Results

This section presents the results of the stability and control system design. Firstly, the eigenvalues of the system matrices shown in Equation 15.11 and Equation 15.12 are shown in Figure 15.5. **All eigenmodes but the spiral mode are stable as they are located to the left of the imaginary axis. However, the eigenvalue of the spiral mode is incredibly low and the mode can thus always be corrected by the autopilot.** A quantification of these eigenvalues is given in Table 15.1.

Table 15.1: Numerical eigenvalues of the dynamic modes of the UAV.

Eigenmode	Real part	Imaginary part
Short period	-4.22	± 7.84
Phugoid	$-4.58 \cdot 10^{-3}$	$\pm 2.05 \cdot 10^{-1}$
Aperiodic roll	-7.32	0
Dutch roll	$-2.4 \cdot 10^{-3}$	$\pm 5.04 \cdot 10^{-1}$
Spiral	$4.52 \cdot 10^{-3}$	0

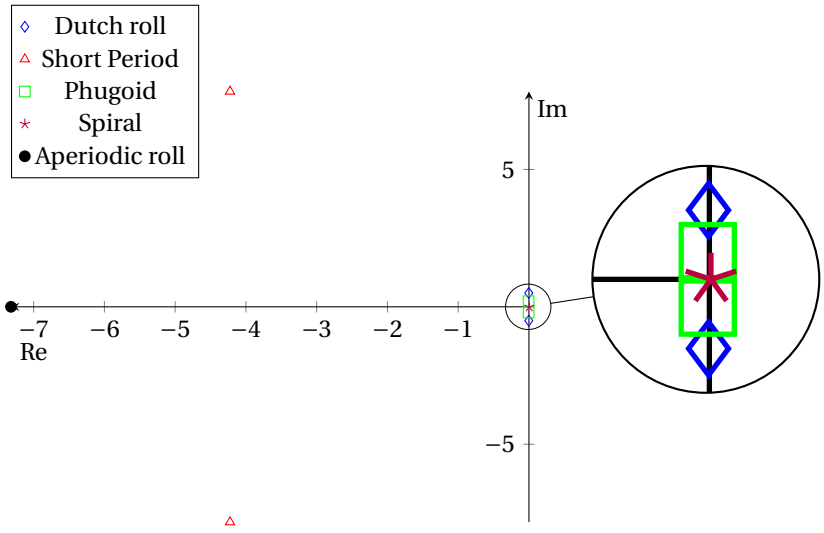

Figure 15.5: The system stability eigenvalues plotted in the complex plane.

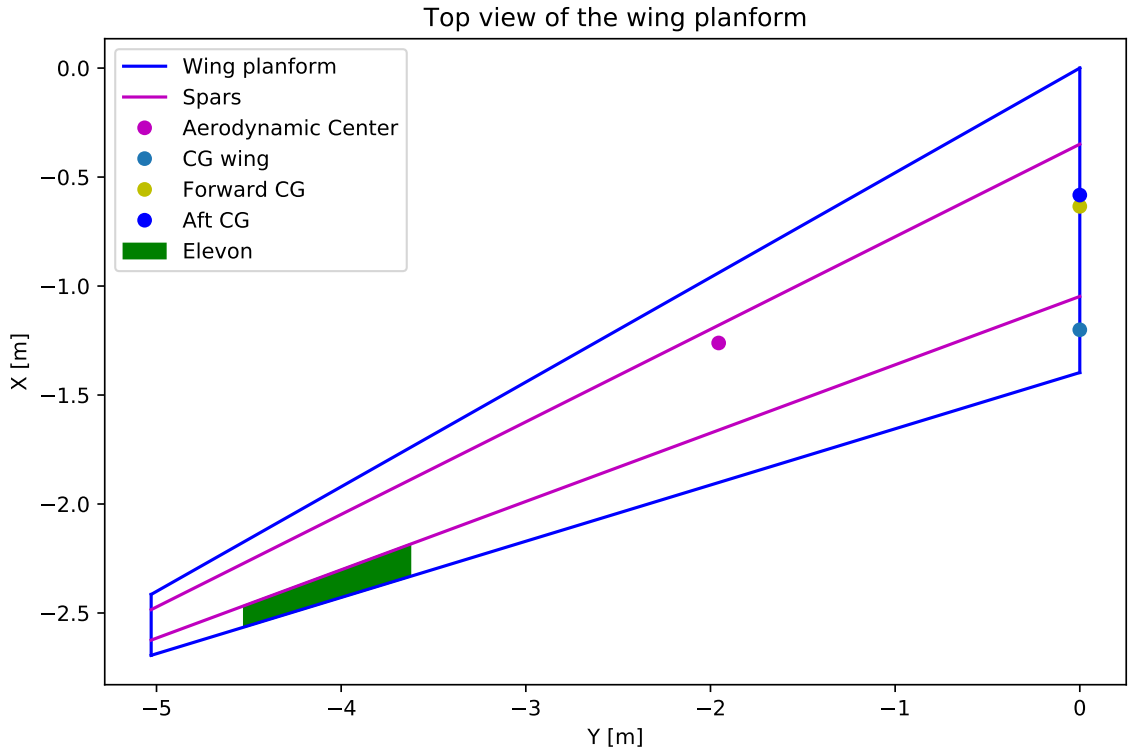

Figure 15.6: Top view of the wing planform showing the placement of the elevon, aerodynamic centre and centre of gravity locations.

The final wing planform with integrated control surfaces, together with the centre of gravity locations, is shown in Figure 15.6. **It is clear that the placement of the fuel, engine and payload has minimised centre of gravity excursion.**

15.4. Verification and Validation

Verification and validation will be done for both the stability and control model. Within the VV for stability, not only the wing itself will be assessed, but also the winglet sizing. The general validation method for both models will consist of comparison with available data of other aircraft.

15.4.1. Stability

Verification of the stability model can be performed by checking how accurate the model is in representing the physical system. The stability model uses the linearised equations of motion to analyse the different eigenmotions. In the linearisation process of these equations, higher order terms are neglected, which leads to a loss in accuracy but decreases the computational effort. However, in the academic community, the linearised equations of motion are considered a valid approximation. Furthermore, the assumption is made that the stability derivatives are constant with varying surface area. This assumption could be made based on the findings of AVL, where the stability derivatives of scaled wings could be obtained.

Validation of the stability model was done by means of comparison with the Cessna Citation of the TU Delft, as the stability derivatives of this aircraft are known, as well as its response to control inputs. Using these stability derivatives as input for the stability model, the modelled response of the Cessna Citation could be obtained. Comparing this response with the known response, it is clear that the model returns correct results and thus can be considered validated.

Winglet

The computation of the size of the winglet is verified by comparing the resulting values with existing aircraft with a similar configuration. It was found that the relative surface area compared to the wing surface area is comparable to the other aircraft that were used for verification. The validation of the model was done by determining the area of the winglets of the Armstrong Whitworth A.W.52 flying wing. This is a flying wing that similarly uses winglets as vertical stabilisers for directional stability. It was found that the deviation between the result from the model and the actual dimensions of the A.W.52 is 3%. The winglet of the A.W.52 can be found to have a span of 3.8 meters, where the model yielded a required span of 3.6 meters. The deviation can be appointed to the measure of directional stability, for which a typical value for flying wing aircraft is chosen. This value can deviate for different aircraft.

15.4.2. Control

The control model was verified by comparing the relative size of the control surface with respect to the wing to other aircraft with a similar configuration. It was found that the possible configurations of the ailerons, elevators and elevons have similar dimensions as corresponding aircraft. The validation of the model was done by sizing the control surfaces of an existing aircraft, the Fokker 27. Using available data of this aircraft, a sizing of the control surfaces of the aircraft was performed using the model to size the ailerons and elevator as described in subsection 15.2.4 and subsection 15.2.5. The results are shown in Table 15.2. **It was found that the control model had a deviation of 5 % for the computation of the aileron span and a deviation of 10 % for the computation of the elevator span.** The model does not account for tail surfaces on the aircraft as the chosen concept has a flying wing configuration. This will cause the roll damping and therefore the required span for the aileron to be underestimated. The deviation of the elevator span can be assigned to the estimation of the inertia of the aircraft. As no information was available on this parameter, a rough estimation of the moments of inertia of the aircraft was made.

Table 15.2: Validation results of the aileron and elevator sizing.

Control surface	Wing span	Validation method	Model results	Deviation	Interpretation of results
Aileron	3.8 m	Used to find aileron span Fokker 27	3.6 m	5 %	Neglecting the tail surface
Elevator	5.2 m	Used to find elevator span of Fokker 27	4.7 m	10 %	Inaccurate estimation of MMOI

16
Electrical Subsystem

In this chapter the electrical subsystem will be designed, which includes the navigation and communication subsystem, as well as the hardware and software the UAV comprises. First of all, the navigation and communication system design is elaborated on in section 16.1 and section 16.2. Secondly the hardware and software diagram are explained in section 16.3 and section 16.4. From these diagrams, the electrical block diagram is composed in section 16.5. Finally, the data handling diagram is portrayed in section 16.6.

16.1. Navigation System Design

Navigation systems are required to record and control the flight path of the aircraft. Combining different means of navigation systems provides an accurate navigation subsystem on which the UAV can rely. A study into the integration of INS, GPS, Magnetometer and Barometer (Sokolevic, Dikic, and Stancic 2013) alleges: "integrated navigation system provides continuous and reliable navigation solutions." Following this study, the UAV will incorporate an Inertial Navigation System (INS), Global Positioning System (GPS) and an altimeter which is a special type of barometer. In addition, a camera will provide a pilot with visual information when flight control is taken over by the ground segment.

16.1.1. INS, GPS and Altimeter

Different solutions exist which combine the INS, GPS and Altimeter into one in order to provide the customer with a complete solution in designing the navigation subsystem. Comparing a total of 201 systems[86] a selection is made of systems combining these three sensors into one integrated solution. **In the end the μINS system of Inertial Sense, a well-known company specifically designing navigation systems for UAVs, was found to be most suitable.** The most important features of the system can be found in Table 16.1, and a visualisation in Figure 16.1[87]. Different output types are possible, of which one is RS-232.

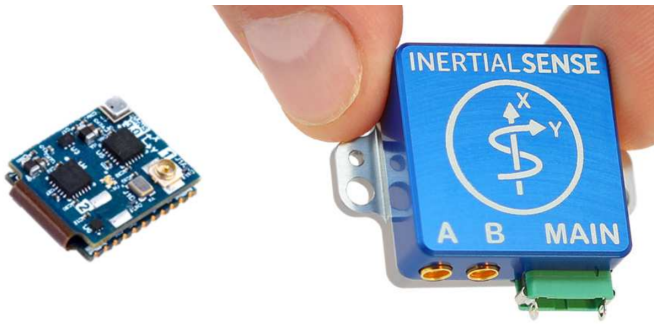

Figure 16.1: Inertial Navigation System.

Table 16.1: Specifications of μIMS.

Performance Accuracy		**Operational limits**		**Electrical**	
Position	2.5 m	Altitude (GPS)	50 km	Power consumption	0.412 W
Velocity	0.05 m/s	Altitude (Altimeter)	10 km	Supply voltage	3.0-3.6 V
Angular Resolution	0.05°	Velocity	500 m/s	Weight	1.3 g
Roll/pitch	0.1°	Temperature	-40 - 85 °C	Cost	695 USD
Static heading	2.0°	Acceleration	10 g	Size	16.5x12.6x4.6 mm

[86] `https://damien.douxchamps.net/research/imu/` [cited on: 12-06-2018]
[87] `https://inertialsense.com/product/ins/` [cited on: 12-06-2018]

16.1.2. Camera

Selecting a camera to allow for pilot visibility and obstacle detection is an important step in designing the electrical system layout. Since the UAV should be able to operate at night, night vision is required too. Hence, the design should include both a camera for the visual spectrum and an infrared camera, which both will be able to visualise the UAVs surroundings up to 500 m. First, two solutions are compared being the Sony FCB-EV7500 and Hitachi DI-SC120R, of which the most important specifications are listed in Table 16.2[88] [89]. These cameras are both used in UAV applications in which a pilot needs visual information during flight. Both cameras are really comparable, except for the power used and the maximum image quality. The image quality is not of big importance since the communication system will not be able to provide a high definition livestream, but the power used is an important figure. **Due to this slight difference and the even better performance of the Sony, it is the chosen camera.**

Table 16.2: Camera comparison.

	Sony FCB-EV7500	**Hitachi DI-SC120R**
Zoom	30x	30x
Size	50x89x60 mm	50x89x60
Weight	260g	260g
Operating temperature	-5 - 60°C	-10 - 60°C
Voltage	6-12 V DC	9-12 V DC
Price	729.95 USD	750 USD
Power	3 W	5.9 W
Pixels	1920x1080	1280x720

During night, visual information is provided to the pilot using an infrared camera. A common solution is the Flir Quark 2, which will be the camera used. The most important features of this camera are listed in Table 16.3.

Table 16.3: Specifications and operational limits of Flir Quark 2.

Specification	**Value**	**Specification**	**Value**
Size (without lens)	22x22x12 mm	Voltage	3.3 V DC
Weight	23 g	Price	6000
Pixels	640x512	Power	1.2 W
Spectral band	7.5-13.5 μm	Maximum altitude	40,000
Operating temperature	-40 - 80°C		

16.2. Communication System Design

Since the UAV has a range of no less than 1000 km, the communication system chosen should cover at least 1000 km. In addition, data will be send back to the ground station continuously, providing vital information of the observed pipelines immediately, accompanied by location data and the UAV system status. Currently, Long Term Evolution (LTE) telecommunication is a promising development and communicating using this system is a future possibility. LTE has global coverage and is a standard for fast wireless communication for mobile devices. It could for instance be used in remote regions where even GPS is not properly working (Kassas et al. 2017). **To reduce technical risk, a more mature design is chosen as the communication system to be used, which is the Aviator UAV 200 from Inmarsat, as visualised in Figure 16.2.** This system provides the UAV with Satcom connectivity, which means that nearly global coverage is assured[90]. The most important features of the system can be found in Table 16.4[91] [92]. The approximate cost of this Satcom technology is 7.5 USD/km for continuously streaming 128 kbps at a flight speed of 80 km/h and using a software to reduce data quality whenever possible would even bring down this number to 1.7 USD/km (Skinnemoen 2014). Since there is no need for continuous streaming as the vehicle will in principle operate autonomously, the cost seem reasonable. As seen in Table 16.4, there are some requirements on the navigation data input. All are met by the μINS system chosen in section 16.1.

[88] `http://www.ascentvision.com/assets/disc120r_daylight_sensor_datasheet.pdf` [cited on: 13-06-2018]

[89] `http://www.aegis-elec.com/media/wysiwyg/pdf/FCB-EV7500.pdf` [cited on: 13-06-2018]

[90] `http://www.satcomglobal.com/` [cited on: 23-06-2018]

[91] `https://www.cobham.com/communications-and-connectivity/satcom/cockpit-and-cabin-connectivity/special-purpose-aircraft-connectivity/aviator-uav-200/aviator-uav-200-brochure/docview/` [cited on: 14-06-2018]

[92] `https://www.inmarsat.com/wp-content/uploads/2016/09/Inmarsat_Global_Government_SB-UAV-_June_2017_EN_lowres.pdf` [cited on: 14-06-2018]

Figure 16.2: Aviator UAV 200 communication system.

Table 16.4: Specifications of Inmarsat Aviator UAV 200.

Specifications		**Requirements on navigation data**	
Weight	1.45 kg	GPS position accuracy	50 m
Size	240x160x60 mm	Velocity data accuracy	1 m/s
Datarate	200 kbps	Attitude accuracy	0.25°
Power	28 W	Heading	1°
Voltage	14-28 V DC	Navigation data in	RS-232 or Ethernet

Whenever connection is lost, the connection will be tried to reestablish continuously whilst the UAV follows its initial flight path. Since a loss of connection does not mean the radio system is malfunctioning, an automatic message will be sent to the ATC stating that the connection is lost and the UAV will follow its initial flight path. When the connection is lost for more than one minute, the UAV will automatically land at a nearby airport. The ground segment is of course aware of this and will arrange necessary clearance with the ATC.

16.2.1. Communication with ATC

During flight, the UAS should communicate with ATC in order to fly in the National Airspace System (NAS). Generally, two methods exist to do so: Visual Flight Rules (VFR) and Instrument Flight Rules (IFR). With VFR, aircraft have to avoid conflicts on their own but still have to be in contact with ATC when taking-off and landing. In addition, a clear sky is required in order to actually see other aircraft. Therefore, IFR would be more suitable since the aircraft can fly in all weather conditions and the aircraft should be able to fly autonomously, hence incorporating a pilot to fly VFR would violate this requirement. IFR requires the pilot to hand in a flight plan beforehand, which needs to be confirmed by ATC. Any changes made to this plan during flight need to be communicated to ATC. As of 2020, all aircraft will be equiped with ADS-B to broadcast the aircraft's location to ATC and other aircraft. This technology could be used in the future to make requests to ATC when flight plan deviations are required. In UAVs, it would be most convenient if the aircraft is able to make a request autonomously, e.g. using a synthesised voice. Doing so does not yet exist, but "is a minor technological issue that would need to be resolved"[93]. UAV regulations are constantly changing, yet at later design stages communication with ATC should be reconsidered. **For now, IFR is the chosen means of communication and the exact role of the pilot should still be investigated.**

16.3. Hardware Diagram

The hardware the UAV consists of is actually every single component of the UAV. However, the hardware discussed in this section will only be the components that are directly affected by the software involved, which is discussed in the next section. Figure 16.3 visualises the hardware of the UAV. The inputs to the Central Proccessing Unit (CPU) is the data from the payload, sensors and electric power. In addition, data will be send by the ground segment via the LTE communication module as discussed in section 16.2. The CPU will output commands to the elevons, which are the only aerodynamic control surfaces on the UAV, the propulsion system, the landing gear and the fuel system.

[93] `https://www.mercatus.org/system/files/mercatus-holcombe-integrating-drones-v1.pdf` [cited on: 15-06-2018]

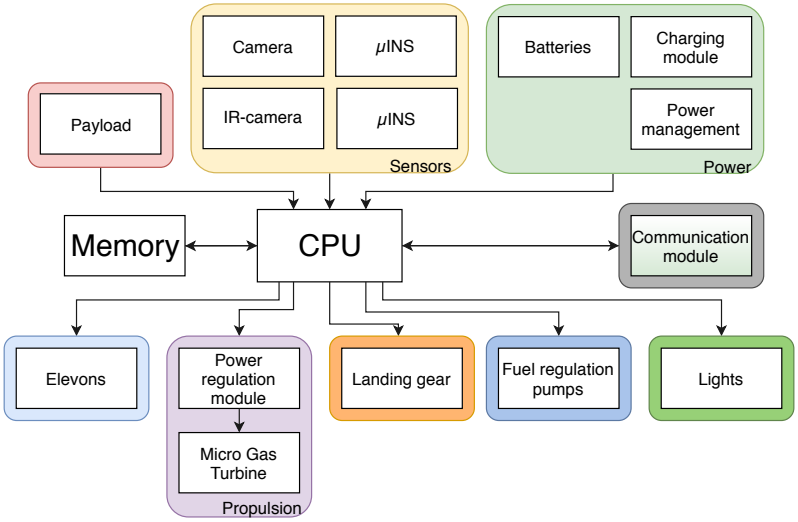

Figure 16.3: Hardware diagram of the UAV.

16.4. Software Diagram

The software running on and affecting the hardware just presented is visualised in Figure 16.4. Note that this software diagram is only at a very high level, showing the different functions the software performs and the relation between the different code blocks. It does not show the precise functioning of the software running on the UAV.

As can be seen in the diagram, the UAV will fly autonomously by comparing its position to the flight plan and adjusting its throttle and control surfaces accordingly. Doing so continuously will ensure that the aircraft is within 10 m of its planned flight path. One function requires some elaboration, which is the 'monitor system performance' function. This function includes all functions listed in chapter 7, hence checking the various subsystems. The results of this will be fed into the flight path planning module on the one hand, and be communicated to the ground on the other.

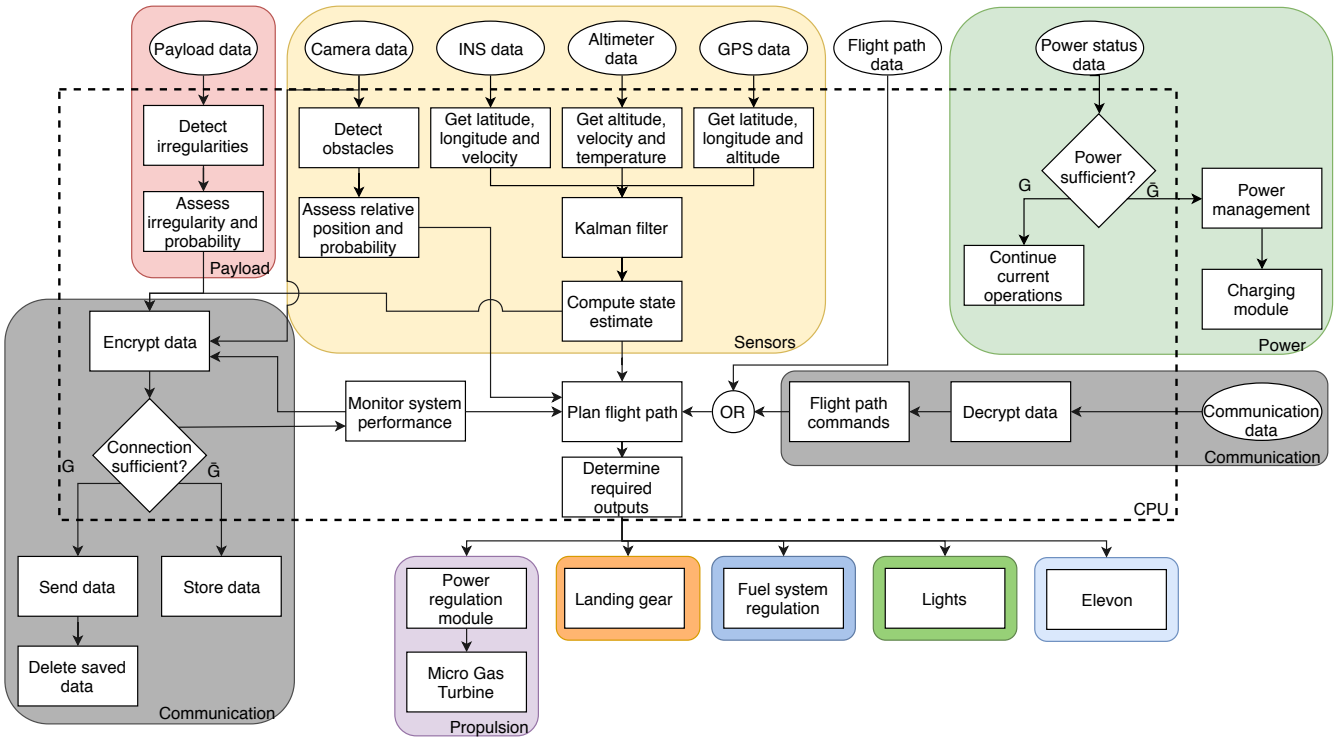

Figure 16.4: Software diagram of the UAV. Note that input data are represented by oval blocks, and that the colouring scheme is similar to the hardware diagram (Figure 16.3).

16.5. Electrical Block Diagram

Now that the software and hardware of the system are designed, the electrical block diagram can be constructed, visualising the electric interaction in between the various components of the system. Figure 16.5 shows the electrical block

diagram for the UAV, including the different types of wire between the essential bs and the sensors, which are using a type of American Wire Gauge (AWG) depending on length the wire covers and the current flowing through it[94]. The DC input at the left hand of the figure represents the generator of the engine. Typically the generator of a turboprop engine delivers 28 V DC voltage[95]. In order to make sure that the DC current from the generator is stable, a voltage regulator is set at 28 V. Following, the current is measured before entering into the generator bus. This bus outputs to the main bus, which in turn powers all non-essential components, and the battery charging bus which powers all essential systems. Since flight control should be taken over by the pilot whenever it is required, both the camera and INS are regarded essential components. The landing gear is assumed to use the full possible 28 V and the lights will use 28 V too [96]. In principle, the essential components powered by the essential bus are the safe mode of the vehicle, which can be powered by purely the batteries if necessary. Two batteries are included, complying with requirements posed on the power subsystem. The different busses involve necessary voltage transformers for the various required outputs, and have the possibility to deliver 28 V DC complying with requirements posed on the electrical system. The different switches are used to possibly isolate part of the system (Administration 2016). Regarding the payload, the exact power consumption and required voltage is still unknown, since the payload is not completely developed yet chapter 10. However, a comparison can be made with the Riegl VQ-780i which weights only 20 kg and uses 150 W at a voltage of 18-32 V DC[97]. Since the payload will weigh approximately 70 kg, it is assumed to consume at least this amount of power. Hence, the generator is designed to deliver at least 150 W of power, as is required. Finally, it should be noted that a Ground Power Unit (G.P.U.) will be used to start the turboprop engine.

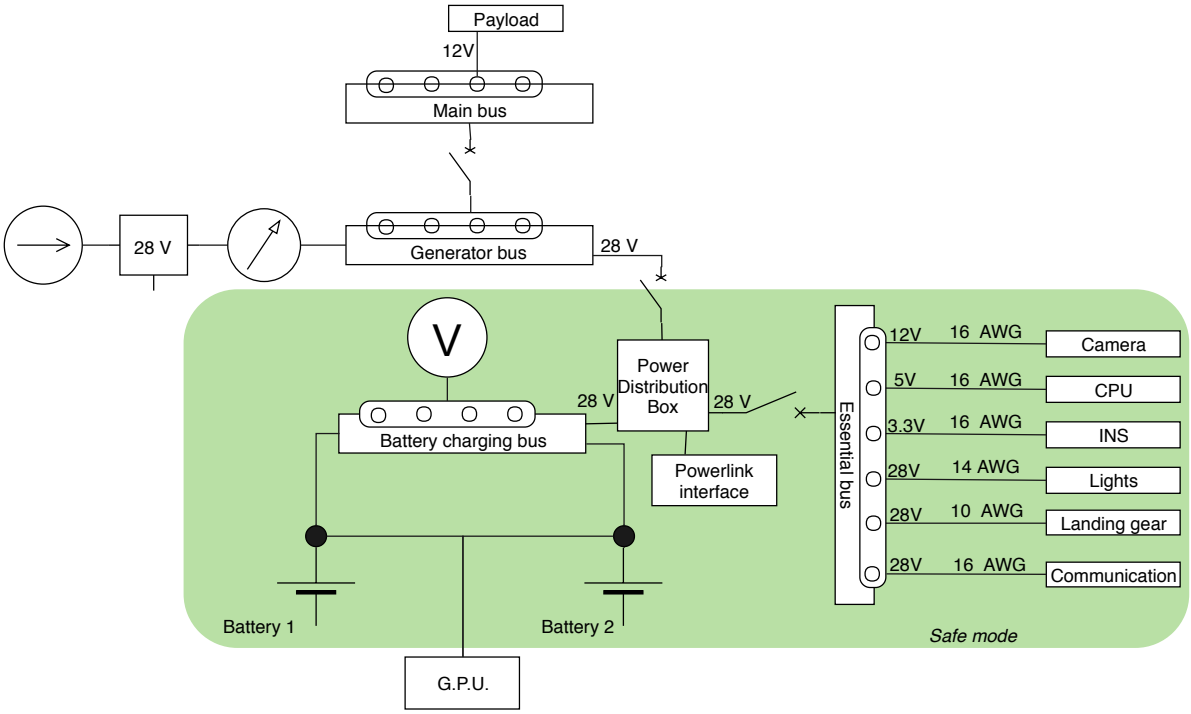

Figure 16.5: Electrical diagram of the UAV.

16.6. Data Handling Block Diagram

Finally, the data handling throughout the UAV subsystems should be investigated. The resulting diagram is shown in Figure 16.6. Note that a lot of data links are not quantified due to the fact that the the characteristics of various data flows are not yet fully known in this design stage.

At the heart of the diagram, a Central Processing Unit (CPU) is connecting all other components. The exact required specifications of the CPU are not yet known, but the main algorithm that runs of the CPU will be the detection of flaws in the images of the pipelines gathered by the payload. **Since this algorithm will probably be comparable to a facial recognition algorithm, (Hulens, Verbeke, and Goedemé 2015) finds the most optimal CPU in a UAV for this purpose to be the Odroid XU4, which is currently replaced by the XU4.** This CPU has 8 cores, with 1.4-2.0 GHz. The CPU connects various components; first of all, the memory bus which combines both Random-Access Memory (RAM) and Solid State

[94] https://www.bluesea.com/support/articles/Circuit_Protection/1437/Part_1%3A_Choosing_the_Correct_Wire_Size_for_a_DC_Circuit [cited on: 02-07-2018]

[95] http://www.aerospaceweb.org/question/electronics/q0219.shtml [cited on: 15-06-2018]

[96] http://microuav.com/UAVLighting [cited on: 15-06-2018]

[97] http://riegl.com/uploads/tx_pxpriegldownloads/RIEGL_VQ-780i_DataSheet_2018-04-12_Preliminary.pdf [cited on: 22-06-2018]

Memory (SSM) for short- and long-term storing of data. The RAM is assumed to have a size of 2 gigabytes, which is used when processing the payload data and assessing the critical points along the pipeline. Note that this RAM is build-in in the chosen processor. The SSM is of size 64 gigabytes and used when the communication system is not working and data needs to be stored. Since only data on the type of critical points and their respective locations will be stored, this size is sufficient. There are various storage possibilities using the Odroid XU4 processor, such as a micro-SD card of up to 64 gigabytes or an embedded Multi-Media Card (eMMC) flash storage of up to 128 gigabytes. The communication system is discussed in section 16.2.A watchdog timer will be used to detect malfunctions in the CPU and to try to recover from them. Such a device is common to include in spacecraft and UAVs; vehicles without continuous human input and control.The sensor and payload signals will be communicated to the CPU via Low-Voltage Differential Signalling (LVDS), which is a fast means of data communication within electrical systems. The payload and visual sensors will receive commands when required, like changing a camera's orientation or zoom setting. The payload data rate currently is set to 'mbps' which means that the order of magnitude is known but the exact figure is not, since the payload is not fully developed yet as discussed in chapter 10.Finally, the different subsystems will send data to the CPU, which will mainly consist of an update on the subsystems' functioning. In return, the CPU will send various commands to the respective systems.

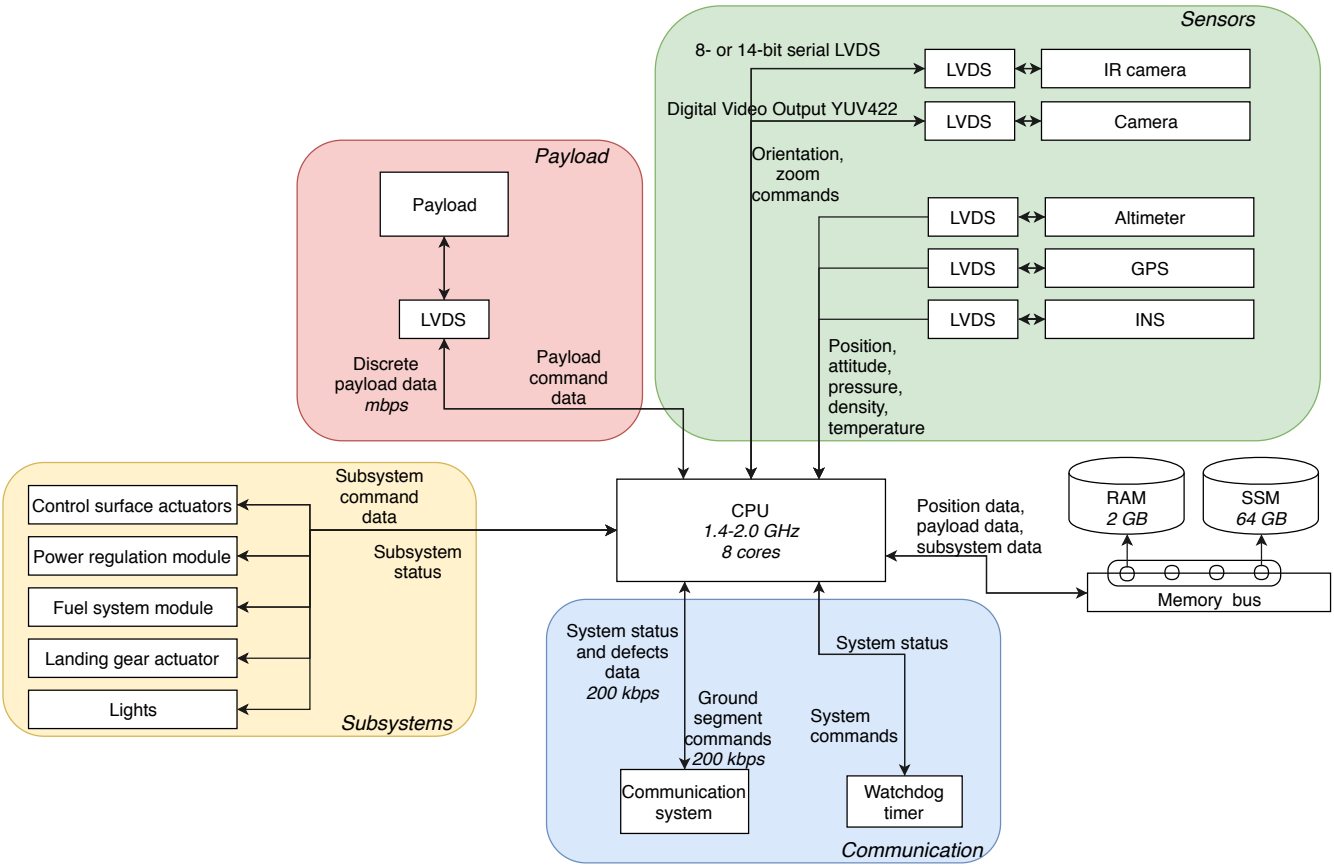

Figure 16.6: Data handling block diagram.

17
Design Optimisation and Final Results

Now that all the analysis and sizing models are explained, the connection of them remains. It is desired to make every individual model drive the design to a reasonable extend, in order to finally arrive at optimum. This chapter presents the method used to achieve compliance between the previously presented disciplinary analyses and the manner in which the complete design was optimised. The manner of optimisiation, including object oriented design with multiple disciplines to account for, is introduced in section 17.1 and section 17.2. The results obtained from the optimisation are stressed in section 17.3, which is followed by a technical sensitivity analysis in section 17.4.

17.1. Interface Management with Object Oriented Design

Disciplinary contradictions are inherent to the design of aircraft. The most simple yet crucial example is the design of an aircraft's wing. Most involved in this design are the aerodynamic and structural disciplines, which desire completely different aspects of the design. The aerodynamic design group aims at synthesising a thin and slender wing, whereas the structural designers prefer a short and thick wing. As such, it is of paramount importance to recognise such critical design interfaces early on in the design process (B. van Beurden et al. 2018a) and adjust the process accordingly.

In order to mitigate the risks associated with incomplete communication of information between disciplines, a new design paradigm was chosen: Object Oriented Design (OOD). This can be viewed as an engineering extension to the principle of Object Oriented Programming (OOP). In fact, these objects were all implemented as classes within the Python programming language, allowing each of the disciplines to see what information was accessible to them. By defining the design actions of a discipline as transformations of these objects, the coupling of these analyses was simplified. The OOD paradigm allowed quick and detailed assessment of conceptual designs (B. van Beurden et al. 2018a).

17.2. Implementation of Multi-Disciplinary Design Optimisation

This section elaborates upon the chosen design strategy and the software developed to finalize the MAINTAIN UAV.

17.2.1. Background and Challenges

The sequential aircraft design process presented in (Roskam 2000) has been, with the increase of available computing power, partially replaced with that of Multi-Disciplinary Design Optimisation (MDO). This approach to the design of complex engineering systems recognises the innate coupled nature of such systems and that sequential design lacks both in computational efficiency and final design performance. Disciplinary analyses are coupled in a computational graph in order to optimise some user-defined objective function. The main challenges in the creation of a proper MDO routine are:

1. Placement and interrelation of disciplines to achieve inter-disciplinary compliance of design variables and performance.
2. The computation of the objective's gradient in order to drive the objective function to the desired direction while satisfying the user defined constraints.

The first challenge is one that can be solved by having some previous design experience and overview of the myriad of the design variables. However, the second has been subject to an extensive amount of research. When the disciplinary analyses constitute the solution of some set of differential equations with a numerical method, the straightforward method of computing the gradient becomes too expensive.

17.2.2. Aerostructural Optimisation Using the Adjoint Method

Consequently, the relevant disciplinary analyses are coupled to form a separate entity within the computational graph. The gradient computation for this entity is then carried out using the adjoint method. The disciplines in this case are the aerodynamic and structural analysis of the wing, forming an aerostructural optimisation problem. This extensively studied problem has its main difficulties in its broad constraint definition (structural failure shall not occur throughout the entire wing structure) and the complexity of the governing partial differential equations. The objective for the aerostruc-

tural problem is defined to be of the form in Equation 17.1 with gradient Equation 17.2. Note that any derivative of a function f with respect to the vector of design variables is displayed as df for brevity.

$$J = \alpha C_D + \beta W_{\text{wing}} \tag{17.1}$$

$$dJ = \alpha dC_D + \beta dW_{\text{wing}} \tag{17.2}$$

The computation of dW_{wing} is simple, as it purely relies on the problem setup and not on the solution of the PDEs. The derivative dC_D is what requires the adjoint formulation.

The set of structural failure constraints may be posed as in Equation 17.3 with m the point of evaluation of the Von Mises stress. Computation of these constraints is greatly simplified by lumping the set into a single Kreisselmeier-Steinhauser (KS) function as in Equation 17.4 which has the property that for $\rho > 0$ it provides an upper bound to the constraints g_m and in the limit of $\rho \to \infty$ it approaches the maximum constraint value. This allows it to be used as a constraint aggregation method and simplifies the adjoint method.

$$g_m = \frac{\sigma_m}{\sigma_y} - 1 \leq 0 \tag{17.3}$$

$$\text{KS} = -\frac{1}{\rho} \ln \left[\sum_m e^{-\rho g_m} \right] \tag{17.4}$$

Let us now derive the sensitivity computation. The objective J may be written as a function of design variables $\boldsymbol{x}$ and state variables $\boldsymbol{y}$ as in Equation 17.5. The design variables and state variables are coupled in the solution of the governing PDEs as shown in Equation 17.6.

$$J = J(\boldsymbol{x}, \boldsymbol{y}) \tag{17.5}$$

$$\mathscr{R}(\boldsymbol{x}, \boldsymbol{y}(\boldsymbol{x})) = 0 \tag{17.6}$$

The gradient may be written as in Equation 17.7. The governing equations are also subject to a derivative constraint in that it must be zero as in Equation 17.8. This is because any small change in the underlying problem variables is still required to satisfy the governing equations.

$$dJ = \frac{\partial J}{\partial \boldsymbol{x}} + \frac{\partial J}{\partial \boldsymbol{y}} d\boldsymbol{y} \tag{17.7}$$

$$d\mathscr{R} = \frac{\partial \mathscr{R}}{\partial \boldsymbol{x}} + \frac{\partial \mathscr{R}}{\partial \boldsymbol{y}} d\boldsymbol{y} = 0 \tag{17.8}$$

Equation 17.6 can be rewritten to Equation 17.9 to yield a new form of the objective gradient, shown in Equation 17.10 which will be shown to be computationally efficient.

$$\frac{\partial \mathscr{R}}{\partial \boldsymbol{y}} d\boldsymbol{y} = -\frac{\partial \mathscr{R}}{\partial \boldsymbol{x}} \tag{17.9}$$

$$dJ = \frac{\partial J}{\partial \boldsymbol{x}} - \underbrace{\frac{\partial J}{\partial \boldsymbol{y}} \left[\frac{\partial \mathscr{R}}{\partial \boldsymbol{y}} \right]^{-1}}_{-\boldsymbol{\Psi}} \frac{\partial \mathscr{R}}{\partial \boldsymbol{x}} \tag{17.10}$$

The vector $\boldsymbol{\Psi}$ is the adjoint vector. Note that one may compute this by solving the adjoint system defined in Equation 17.11.

$$\frac{\partial \mathscr{R}}{\partial \boldsymbol{y}} \boldsymbol{\Psi} = -\frac{\partial J}{\partial \boldsymbol{y}} \tag{17.11}$$

As one now does not need to compute $d\boldsymbol{y}$ but only solve the system Equation 17.11. **Thus, the cost of the adjoint method greatly outperforms the direct method for when the number of design variables is much larger than one, which is the case for an aerostructural design problem.**

The implementation of the aerostructural optimisation is shown in Figure 17.1. Herein, A and S represent the governing equations of the aerodynamic and structural analysis respectively. The vector $\boldsymbol{w}$ represents the aerodynamic state variables and $\boldsymbol{u}$ the structural state variables.

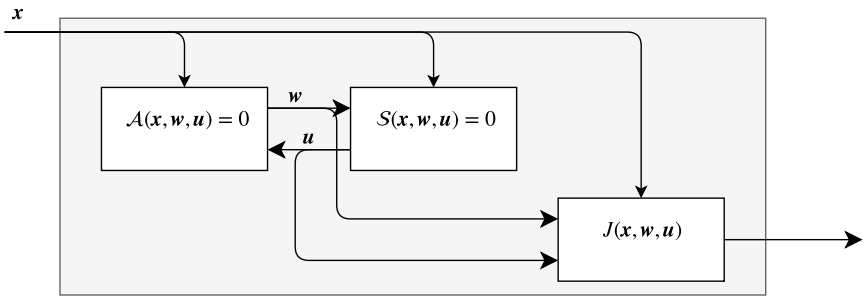

Figure 17.1: Representation of the aerostructural problem.

The vortex-lattice method described in chapter 13 is used for the aerodynamic analysis of the coupling. The structural model described in chapter 14 was found to be overly complex and unsuited for proper optimisation when integrated within the optimisation work-flow as the resulting derivatives were unsmooth. As such, a different model was adopted for the aerostructural analysis. A Finite Element Analysis (FEA) was developed which is known to exhibit smooth first order derivatives. The wing structure is represented as a tubular spar, having bending and torsional resistance. This geometry is visualised in Figure 17.2, having its wall thickness and radius as design variables. The spar is discretised into spatial beam elements with each constituting node having 6 degrees of freedom. As the total number of degrees of freedom is 12, the stiffness matrix of an element is given by Equation 17.12.

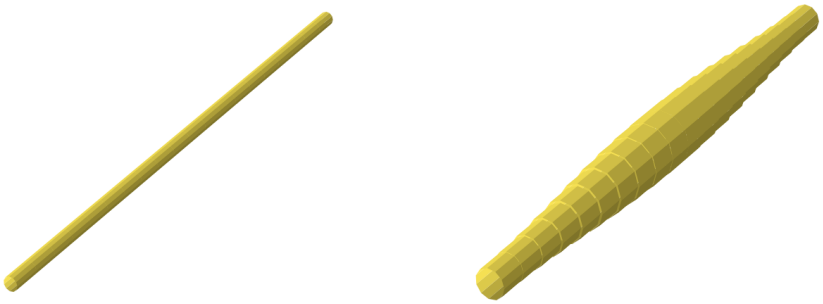

Figure 17.2: Illustration of the tubular spar used within the FEA part of the aerostructural optimisation routine.

$$
[k]_e = \begin{bmatrix}
k_1 & 0 & 0 & 0 & 0 & 0 & -k_1 & 0 & 0 & 0 & 0 & 0 \\
0 & 12k_2^z & 0 & 0 & 0 & 6k_2^z l & 0 & -12k_2^z & 0 & 0 & 0 & 6k_2^z l \\
0 & 0 & 12k_2^y & 0 & -6k_2^y & 0 & 0 & 0 & -12k_2^y & 0 & -6k_2^y l & 0 \\
0 & 0 & 0 & k_3 & 0 & 0 & 0 & 0 & 0 & -k_3 & 0 & 0 \\
0 & 0 & -6k_2^y l & 0 & 4k_2^y l^2 & 0 & 0 & 0 & 6k_2^y l & 0 & 2k_2^y l^2 & 0 \\
0 & 6k_2^z l & 0 & 0 & 0 & 4k_2^z l^2 & 0 & -6k_2^z l & 0 & 0 & 0 & 2k_2^z l^2 \\
-k_1 & 0 & 0 & 0 & 0 & 0 & k_1 & 0 & 0 & 0 & 0 & 0 \\
0 & -12k_2^z & 0 & 0 & 0 & -6k_2^z l & 0 & 12k_2^z & 0 & 0 & 0 & -6k_2^z l \\
0 & 0 & -12k_2^y & 0 & 6k_2^y & 0 & 0 & 0 & 12k_2^y & 0 & 6k_2^y l & 0 \\
0 & 0 & 0 & -k_3 & 0 & 0 & 0 & 0 & 0 & k_3 & 0 & 0 \\
0 & 0 & -6k_2^y l & 0 & 2k_2^y l^2 & 0 & 0 & 0 & 6k_2^y l & 0 & 4k_2^y l^2 & 0 \\
0 & 6k_2^z l & 0 & 0 & 0 & 2k_2^z l^2 & 0 & -6k_2^z l & 0 & 0 & 0 & 4k_2^z l^2
\end{bmatrix} \tag{17.12}
$$

The relevant stifnesses are

$$
k_1 = \frac{EA}{L}, \qquad k_2^z = \frac{EI_z}{l^3}, \qquad k_2^y = \frac{EI_y}{l^3}, \qquad k_3 = \frac{GJ}{l} \tag{17.13}
$$

where J in this case is the torsional rigidity of the element. The beam elements are connected end-to-end and hence the resulting global stiffness matrix K will exhibit a banded structure. After assembly, the linear system

$$
K\boldsymbol{u} = \boldsymbol{f} \tag{17.14}
$$

is solved where $\boldsymbol{f}$ are the forces and moments. The resulting stiffness functions of the optimisation are translated to more detailed structural components with the method presented in chapter 14.

17.2.3. Overall Design Procedure

It was concluded, based on the complexity of the remaining disciplinary analyses, that the adjoint coupling method was only required for the aerostructural section of the design process. Consequently, the process shown in the Extended Design Structure Matrix in Figure 17.3 was devised and used to find the optimum UAV design.

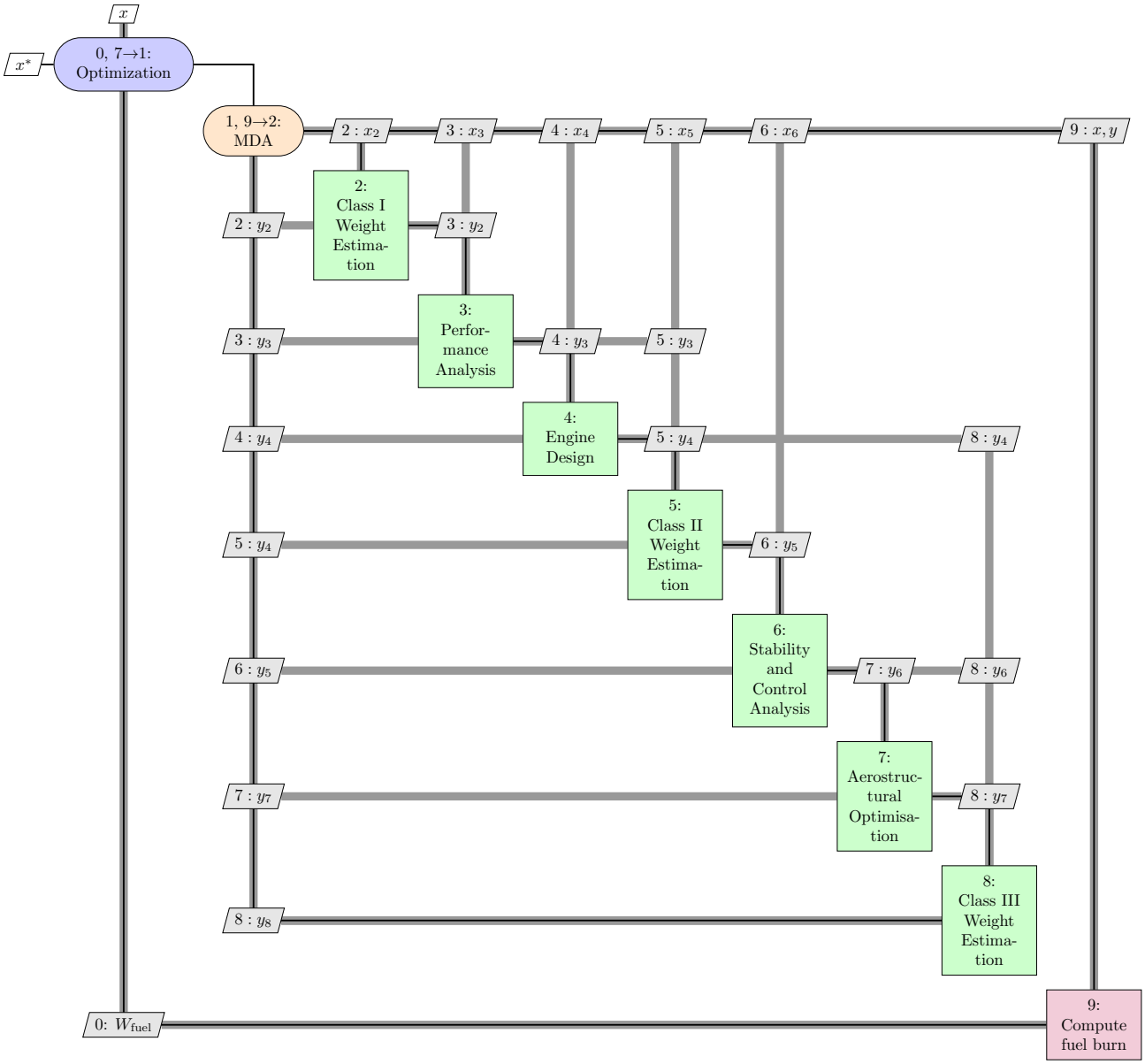

Figure 17.3: Extended Design Structure Matrix for the design software.

17.2.4. Formal Optimisation Problem

To formalise the previously discussed measures taken for optimisation, the official problem statement is shown below

$$\min_{\boldsymbol{x}} \quad W_{\text{fuel}} \qquad \text{s.t.} \quad g_i(\boldsymbol{x}, \boldsymbol{y}) \quad \forall \quad i \tag{17.15}$$

The implicitly imposed constraints are listed in Table 17.1. Other constraints, such as the landing gear structural integrity one, have been imposed explicitly within the design routines. The implicit constraints are handled by the optimiser. The top level design vector $\boldsymbol{x}_{\text{top level}}$ is defined in Equation 17.16. Note that the design variables presented in chapter 12 are also part of the optimisation but not repeated here for reasons of brevity. The same holds for the constraints.

$$\boldsymbol{x}_{\text{top level}} = [\Lambda_{0.25c_{\text{wing}}}, \lambda_{\text{wing}}, \text{AR}_{\text{wing}}, \Gamma_{\text{wing}}, \Lambda_{0.25c_{\text{winglet}}}, \lambda_{\text{winglet}}, \text{AR}_{\text{winglet}}, \Gamma_{\text{winglet}}]^T \tag{17.16}$$

The chosen optimisation algorithm is SLSQP for its ability to handle design variable bounds and efficiently impose constraints (Sun and Yuan 2006). The MDO structure of the design software is achieved through the open-source OPENMDAO package (Heath and Gray 2012).

Table 17.1: Top level constraints for the MDO problem.

Mathematical formulation	Rationale
$0.5 - \text{SM} \leq 0$	Static margin larger than half the mean aerodynamic chord
Stability	
$-\text{Re}(\lambda_{\text{Dutch roll}}) < 0$	Stable Dutch Roll
$-\text{Re}(\lambda_{\text{Short period}}) < 0$	Stable Short period
$-\text{Re}(\lambda_{\text{Phugoid}}) < 0$	Stable Phugoid
$C_{m_\alpha} < 0$	Longitudinal static stability
$C_{n_\beta} > 0$	Directional static stability
$C_{l_\beta} > 0$	Lateral static stability
$KS_{\text{wing}} \leq 0$	Wing structural failure constraint
$KS_{\text{turbine}} \leq 0$	Turbine structural failure constraint
$KS_{\text{compressor}} \leq 0$	Compressor structural failure constraint
$KS_{\text{propeller}} \leq 0$	Propeller structural failure constraint

17.3. Final Design Results

This section presents the resulting design parameters and variables after the optimisation was completed. The effects of the optimisation can be visualised through Figure 17.4 where the wing planform and spar are shown at iteration 0 and iteration 114, which was the final iteration. Clearly, the wing is pushed towards a swept-configuration in order to satisfy stability constraints. Additionally, its aspect ratio is enlarged to yield higher aerodynamic efficiency's.

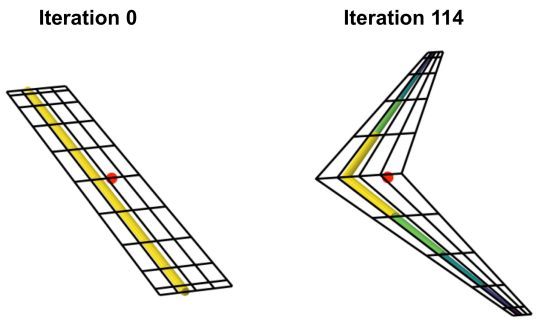

Figure 17.4: Wing planforms at the first and final iteration of the optimisation scheme. Darker colors of the spar indicate smaller thicknesses.

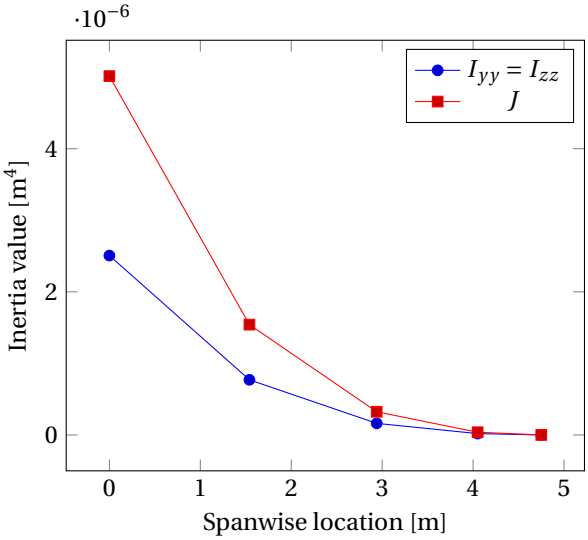

Figure 17.5: Structural property distributions along the semi-span. Note that the curves for I_{zz} and I_{yy} are identical as the modelled spar is symmetric.

The final design values can be found in Table 17.2. For more elaborate specifications of disciplinary results one can refer back to the relevant discipline's chapter. Additionally, as the aero-structural optimisation has been discussed only in this chapter, the results for the cross-sectional properties are presented here in Figure 17.5.

Table 17.2: Final design parameters.

Symbol	Name	Value
b	Wing span	10.6 m
S	Wing area	9.4 m^2
AR_{wing}	Wing Aspect Ratio	12
λ_{wing}	Wing Taper Ratio	0.2
$c_{r_{wing}}$	Wing root chord	1.5 m
$c_{t_{wing}}$	Wing tip chord	0.3 m
$\Lambda_{0.25c_{wing}}$	Quarter chord sweep	25 deg
$b_{winglet}$	Winglet span	1.0 m
$\lambda_{winglet}$	Winglet taper ratio	0.5
$c_{t_{winglet}}$	Winglet tip chord	0.15 m
$\Lambda_{0.25c_{winglet}}$	Winglet quarter chord sweep	10 deg
MTOW	Maximum take-off weight	160.4 kg
$W_{payload}$	Payload weight	68 kg
W_{fuel}	Fuel weight	19.5 kg
OEW	Empty weight	72.9 kg
P_{max}	Maximum power	3.75 kW
$x_{a.c.}$	x coordinate of wing aerodynamic centre	1.04 m
$x_{c.g_{aft}}$	Most aft centre of gravity	0.58 m
$x_{c.g._{front}}$	Most forward centre of gravity	0.56 m
$y_{start_{elevon}}$	Spanwise start location of elevon	3.77 m
$y_{end_{elevon}}$	Spanwise end location of elevon	4.77 m
$\left(\frac{x}{c}\right)_1$	Location front spar	0.2
$\left(\frac{x}{c}\right)_2$	Location aft spar	0.75
Δy_{ribs}	Rib spacing	0.54 m
SFC	Specific Fuel consumption	290 g/kWh

A three-view drawing of the complete final design of the UAV is given in Figure 17.6. Note that the fuel tank will be located aft of the payload and in front of the engine in order to minimise centre of gravity excursion.

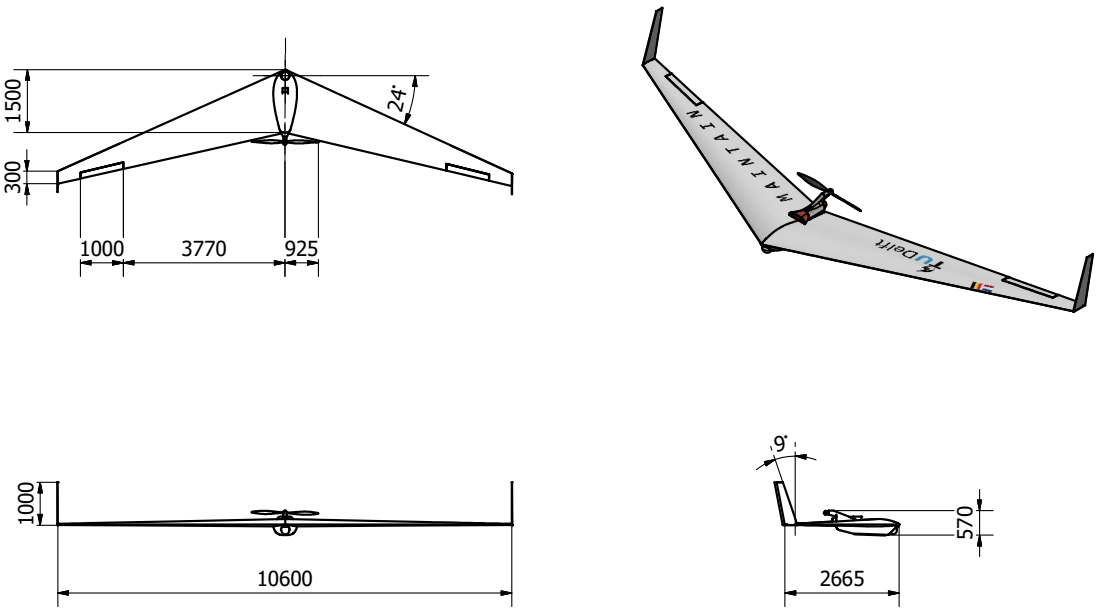

Figure 17.6: Three view drawing of the final design of the MAINTAIN UAV. Dimensions are in millimeters.

17.4. Sensitivity Analysis and Uncertainty Propagation

In order to assess the uncertainty in design variables, arising either from the immaturity of certain technologies or inaccuracy in prediction models, a sensitivity analysis on the final analysis is performed.

A sensitivity analysis can be viewed as numerical computation of the gradient of some objective function f with respect to the set of design variables $\{x_i\}$ (Sobieszczanski-Sobieski, Morris, and M. J. L. v. Tooren 2015). One finds such a partial

as:

$$\frac{\partial f}{\partial x_i} \approx \frac{f(x_i + \Delta x) - f(x_i)}{\Delta x} \tag{17.17}$$

Where $\{x_j\}_{j \neq i}$ remain constant. This approach neglects the absolute value differences of design parameters (e.g. propeller efficiency versus wing span) and thus the partial is normalised to yield sensitivity S_i:

$$S_i = \frac{f(x_i + \Delta x) - f(x_i)}{f(x_i)} \frac{\Delta x}{x_i}. \tag{17.18}$$

This sensitivity analysis can be performed for any desired design characteristic. However, for reasons of brevity and computational complexity it was chosen to focus on the fuel burn and maximum take-off weight (MTOW). These two parameters are the largest contributors to design cost, and albeit related, offer different views of the sustainability and efficiency of the design. The chosen design parameters for assessing the effect of their uncertainty are elaborated upon in Table 17.3. Note that most of these are not the design variables, as a sensitivity analysis on those would, in the case of a true optimum, reveal a trivial result.

Table 17.3: Parameters included in the sensitivity analysis including rationales.

Name	**Symbol**	**Reason for inclusion**
Payload weight	W_{payload}	Payload is still in development
Propeller efficiency	η_{prop}	Propeller validation is difficult and requires experiment
Compressor efficiency	η_c	Accurate validation requires experiment
Turbine efficiency	η_t	Accurate validation requires experiment
Compressor pressure ratio	π_c	Greatly depends on material used which requires more analysis
Turbine inlet temperature	TIT	Accurate validation requires experiment
Yield stress Carbon Fibre spars	$(\sigma_{\text{yield}})_{CFRP}$	Material imperfection cannot be avoided
Yield stress GLARE skin	$(\sigma_{\text{yield}})_{GLARE}$	Material imperfection cannot be avoided
Yield stress aluminum stringers	$(\sigma_{\text{yield}})_{\text{aluminum}}$	Material imperfection cannot be avoided

Results for the MTOW are shown in Figure 17.7. Clearly, the payload is the greatest driver of the maximum take-off weight. Results for the fuel burn are shown in Figure 17.8. Evident is how the fuel burn is most sensitive with respect to to the payload weight and propeller and compressor efficiency's. Note that in both diagrams, the effects of $(\sigma_{\text{yield}})_{\text{aluminum}}$ are not shown as its effects are negligible compared to the other analysed parameters.

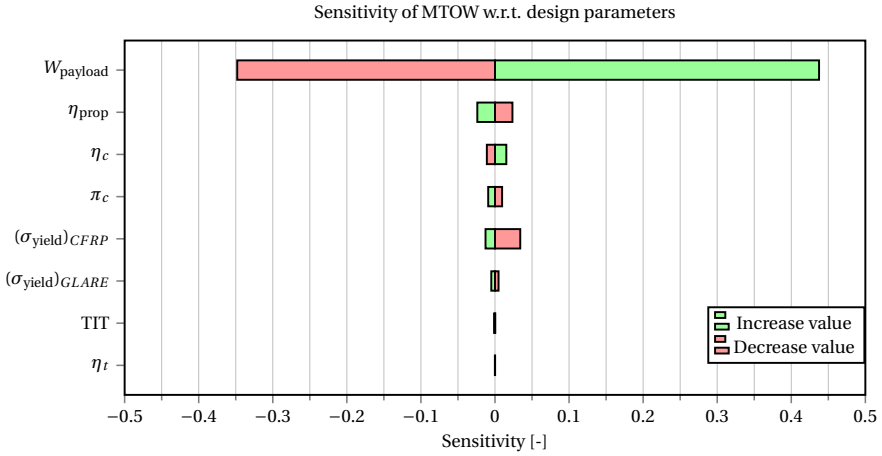

Figure 17.7: Tornado diagram illustrating the sensitivity of the maximum take-off weight of the design to underlying variables.

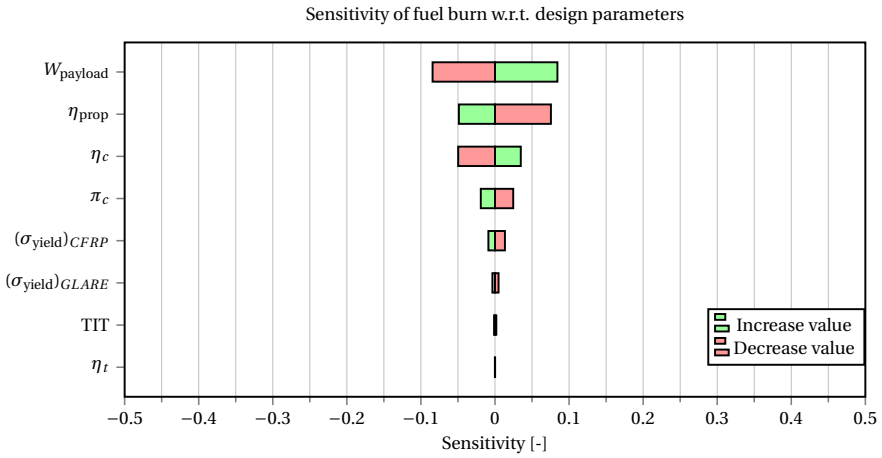

Figure 17.8: Tornado diagram illustrating the sensitivity of the fuel burn of the design to underlying variables.

Using the results of this sensitivity analysis, it is possible to assign confidence intervals to design characteristics. Firstly, all uncertain design variables are assumed to be random variables of the Gaussian kind. Their mean values are the ones specified within the design, and their standard deviations have been obtained from literature (Opgenoord and Willcox 2016). These values are given in Table 17.4. Uncertainty propagation is performed by using the sensitivities, and therefore the design characteristics F become random variables as well as with realisation in Equation 17.19.

Table 17.4: Parameters studied in the uncertainty propagation and their mean values and standard deviations.

Design Parameter	**Mean value μ**	**Standard deviation σ**
$W_{payload}$	68 kg	5 kg
η_{prop}	0.93	0.05
η_c	0.82	0.05
η_t	0.85	0.05
π_c	6	0.50
TIT	1210 K	20 K
$(\sigma_{yield})_{CFRP}$	1600 MPa	100 MPa
$(\sigma_{yield})_{GLARE}$	620 MPa	20 MPa
$(\sigma_{yield})_{aluminum}$	503 MPa	10 MPa

$$F(\boldsymbol{Y}) = \bar{F} + \boldsymbol{s}^T \boldsymbol{y} \tag{17.19}$$

In Equation 17.19 $\bar{F}$ is the mean value of the characteristic, $\boldsymbol{s}$ the vector of sensitivities and $\boldsymbol{y}$ a vector containing realisations of the random variables. Note that $\boldsymbol{s}$ is a function of $\boldsymbol{y}$ in that it checks for an increase or decrease of the design parameter to assign the correct sensitivity value.

Results of the uncertainty propagation are shown in Figure 17.9 for the fuel burn and MTOW. These results were achieved by a Monte-Carlo simulation on the uncertainty space of $\boldsymbol{Y}$ using 100,000 samples. Such a simulation samples the underlying random variables to find a realisation of the governing objective random variable. By using a sufficient number of samples, the probability distribution of the governing objective random variable can be reconstructed. Using these results, the following 95% confidence intervals are constructed.

$$158.95 \leq MTOW \leq 171.6 \qquad 17.34 \leq W_{\text{fuel}} \leq 28.0$$

From these confidence intervals it is concluded that the uncertainty in the underlying design parameters does not affect the feasibility of MAINTAIN.

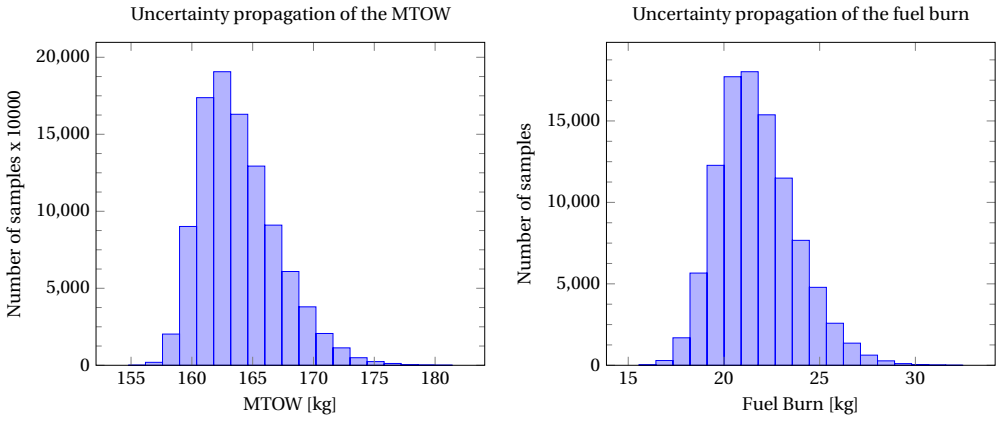

Figure 17.9: Results of the uncertainty propagation analysis using a Monte-Carlo analysis with 100,000 samples for the MTOW and fuel burn.

18
Cost Analysis

An initial selling price of the MAINTAIN system was the result of the market analysis. However, when determining the profitability of a product, the projected revenue needs to be compared to the estimated cost. This chapter will therefore elaborate on the cost estimation of the development, production and operational processes of MAINTAIN. First, a Cost Break-down Structure (CBS) is presented. Followed by an introduction on possible business strategies in section 18.2. In section 18.3 a cost estimation method is used to obtain monetary values for the development, production and unit cost. Next the operational cost are evaluated in section 18.4. Subsequently, in section 18.5 and section 18.6, an analysis is performed to determine the moment of the break even point, the Return on Investment (RoI) and the operational profit which are important to convince potential investors that their investment is profitable. Finally the obtained cost analysis will be compared with the market analysis in section 3.1.

18.1. Cost Break-Down Structure

The CBS, shown in Figure 18.1, contains all the elements of post-DSE activities necessary to complete the development and production of the MAINTAIN system. The three main divisions which the costs are allocated to are the design, the actual production and the overhead costs which consist of administrative, sales and legal costs.

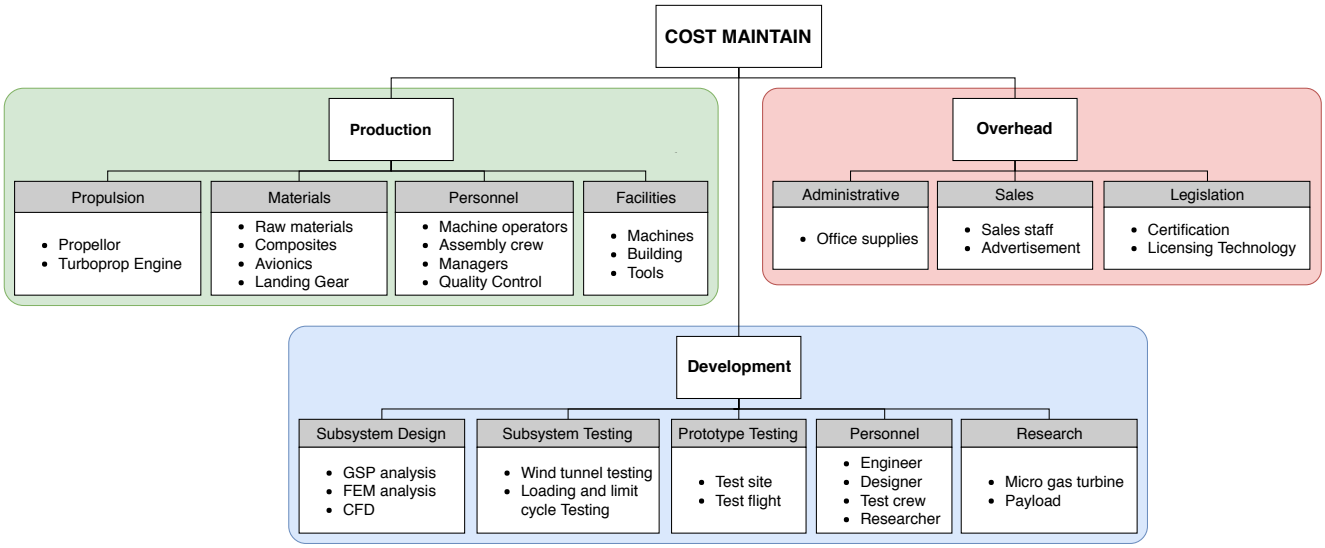

Figure 18.1: Cost break-down structure of MAINTAIN focussing on the design, development and production of the system in the post-DSE phase.

18.2. Business Strategies

There are many possibilities for offering gas pipeline monitoring services. Since not every customer expects the exact same service from MAINTAIN, the service will be adjusted to the customers needs. However, an extensive business strategy description is not in the scope if the DSE. Therefore, only the basis of two possible services will be set. The two options MAINTAIN is going to offer to costumers are:

1. The customer can buy a MAINTAIN system with maintenance service and provided ground crew;
2. The customer can hire the total service of monitoring gas pipelines.

For the first option the customer can buy the UAV system, including a ground segment, for 2 million USD as explained in subsection 3.4.2. In this option maintenance service will be included for 129,630 USD per year and for 148,425 USD per year ground crew will operate the system. This price is based on a 30% profit margin over the cost for MAINTAIN for offering maintenance and ground crew service. It is assumed that in the first 5 years from market entry 30 UAVs will be

sold. Table 18.1 shows the expected annual sale. In chapter 18 a cost analysis will be made based on this option and the mentioned expected annual sales.

Table 18.1: Expected annual sales of MAINTAIN system for first 5 years from market entry.

Year	Number of UAVs sold
1	3
2	4
3	5
4	8
5	10

To offer the customer more flexibility option two is added. For the second option the customer pays for a total service: not buying the UAV but paying per km. MAINTAIN will make sure the right pipelines will be monitored and the customer will receive the desired data. With this option the customer does not have to invest 2 million USD all in once. Comparing both the services: the price per km for the second option will be rated higher than for the first option but the entry fees are lower. Therefore, if a customer wants to cover a large area of pipelines annually it will be more beneficial to go for option one. But in case a customer only wants to monitor once or just a small part it is not worth it to buy a whole UAV. For every strategy a different cost analysis can be made. Since the analysis of different business strategies is outside the scope of this design stage only one strategy will be evaluated in the cost analysis. The first strategy will be evaluated: selling a MAINTAIN system combined with maintenance and ground crew service.

18.3. Development, Production and Unit Cost

The CBS is taken as the basis of the cost estimation. The development and procurement costs of aircraft (DAPCA) method is used to make a cost analysis for MAINTAIN. The DAPCA method is a method from the RAND corporation and is used to estimate cost of new (military) aircraft. The DAPCA model used, the Eastlake Model, is a cost estimation method for General Aviation Aircraft from (Gudmundsson 2013). The choice for this method is verified, since the aircraft to which this method applies, all have to comply with FAR part 23 regulations which also holds for MAINTAIN. For the sake of completeness, some adjustments on the method are applied: extra cost are granted for software engineering, the ground control segment, the certification flight test and the R&D and production cost of the MGT. First the development and production cost of one UAV are estimated and then the total unit cost will be computed. To compute the total unit cost, an estimation of the sales and marketing budget and transportation fees is also performed. All the calculated costs are corrected for inflation using the Consumer Price Index (CPI), also known as the cost of living index.

18.3.1. Development and Production Cost

The process starts with an estimation of the required number of engineering man-hours H_{ENG}, tooling man-hours H_{TOOL} and manufacturing labour man-hours H_{MFG}. They are computed with Equation 18.1, Equation 18.2 and Equation 18.3 respectively. Since the DAPCA method is based on GA there is no time included for writing special software to make the vehicle unmanned such as the autopilot, landing and take-off and anti-collision software. It is assumed that one month, 180 hours, is needed for this software design.

$$H_{ENG} = 0.0396 \cdot W_{\text{airframe}}^{0.791} \cdot V_H^{1.526} \cdot N_{a/c}^{0.183} \cdot F_{CERT} \cdot F_{CF} \cdot F_{COMP} \cdot F_{PRESS} + H_{ENG_{\text{software}}} \tag{18.1}$$

$$H_{TOOL} = 1.0032 \cdot W_{\text{airframe}}^{0.764} \cdot V_H^{0.899} \cdot N_{a/c}^{0.178} \cdot Q_m^{0.066} \cdot F_{TAPER} \cdot F_{CF} \cdot F_{COMP} \cdot F_{PRESS} \tag{18.2}$$

$$H_{MFG} = 9.6613 \cdot W_{\text{airframe}}^{0.74} \cdot V_H^{0.543} \cdot N_{a/c}^{0.524} \cdot F_{CERT} \cdot F_{CF} \cdot F_{COMP} \tag{18.3}$$

Subsequently, combining the required man-hours with the labour rate results in costs for engineering C_{ENG}, manufacturing C_{MFG} and tooling C_{TOOL}. This is visualised by Equation 18.4, Equation 18.5 and Equation 18.6. The assumed labour rate for an engineer is 174 USD per hour, according with the labour rate set by the Delft University of Technology (Hamann and M. v. Tooren 2006). The labour rates for tooling and manufacturing can be found in Table 18.2 and Table 18.3 respectively.

$$C_{ENG} = 2.0969 \cdot H_{ENG} \cdot RA_{ENG} \cdot CPI_{2012} \tag{18.4}$$

$$C_{MFG} = 2.0969 \cdot H_{MFG} \cdot RA_{MFG} \cdot CPI_{2012} \tag{18.5}$$

$$C_{TOOL} = 2.0969 \cdot H_{TOOL} \cdot RA_{TOOL} \cdot CPI_{2012} \tag{18.6}$$

As can be seen from Equation 18.9, in order to calculate the certification costs C_{CERT} the cost of development support C_{DEV} and the cost of flight test operations C_{FT} first need to be computed. The cost of development support include for

example the overhead cost, logistics and facility maintenance personnel. It is computed according to Equation 18.7. C_{FT} concerns costs associated with the development and certification flight-test program and the computation is shown by Equation 18.8. F_{CERT} is the certification factor. For the cost flight operation cost Light Sport Aircraft (LSA) F_{CERT} is 10 while for 14 CFR part 23 aircraft this factor is 3. Since a lot of exceptions on FAR part 23 need be requested a certification factor of 3 instead of 1 is assumed.

$$C_{DEV} = 0.06458 \cdot W_{\text{airframe}}^{0.873} \cdot V_H^{1.89} \cdot N_P^{0.346} \cdot CPI_{2012} \cdot F_{CERT} \cdot F_{CF} \cdot F_{COMP} \cdot F_{PRESS} \tag{18.7}$$

$$C_{FT} = 0.009646 \cdot W_{\text{airframe}}^{1.16} \cdot V_H^{1.3718} \cdot N_P^{1.281} \cdot CPI_{2012} \cdot F_{CERT} \tag{18.8}$$

$$C_{CERT} = C_{ENG} + C_{DEV} + C_{FT} + C_{TOOL} + C_{R\&D_{MGT}} \tag{18.9}$$

In Table 18.2 the all the components of the certification cost are shown according with Equation 18.1 until Equation 18.9. Extra R&D cost for the MGT are added due to the high extra cost of developing a new technique. The cost are assumed to be 10 million USD based on information from Dr.ir. W.P.J. Visser [98]. The cost per unit arises from dividing the accumulatedx cost by the number of units produced in 5 years. Based on the expected sales, the assumption is made that 30 units will be produced in 5 years. This leads to an **estimated certification cost of 412,395 USD per UAV.** Since MAINTAIN will have a weight of 160.4 kg this means the **development cost are 2571 USD per kg** (2206 euro per kg).

Table 18.2: Certification cost of MAINTAIN.

Class	Man Hours [-]	Rate [USD/hr]	Total Cost [USD]	Cost per Unit [USD]	
Engineering	4,025	174.27	1,470,920	49,031	
Development Support			31,083	1,036	
Flight Test Operations			17,100	570	
Tooling	6,006	67.71	852,736	28,425	
Research and Development MGT			10,000,000	333,333	+
Certification Cost			**12,371,839**	**412,395**	

To ensure the quality of every produced UAV, a quality control system has to be established. The cost of the technicians and equipment necessary to perform this task can be found using Equation 18.10. Furthermore, the cost of the raw materials (e.g. aluminium sheets and composites) are estimated with Equation 18.11.

$$C_{QC} = 0.13 \cdot C_{MFG} \cdot F_{CERT} \cdot F_{COMP} \tag{18.10}$$

$$C_{MAT} = 24.896 \cdot W_{\text{airframe}}^{0.689} \cdot V_H^{0.624} \cdot N_{a/c}^{0.792} \cdot CPI_{2012} \cdot F_{CERT} \cdot F_{CF} \cdot F_{COMP} \tag{18.11}$$

Subsequently, the cost of the propulsion subsystem is estimated. The engine type of MAINTAIN is a turboprop and for the cost estimation the cost of the engine and the propeller are separated. The cost of the turboprop engine C_{PP} follows the relation of Equation 18.12. This equation would estimate the price of the turboprop as 2,105 USD which seems really off. In (Head and W. J. Visser 2012) it is stated that costs for a turbo generator can only be scaled to power rating to a limited extent. Since the cost for certain parts of the turbine remain the same independent of the size. To be more precise: according to (Head and W. J. Visser 2012) the manufacturing cost of a 20 kW and a 200 kW engine is essentially the same. Based on personal communication with Dr.ir. W.P.J. Visser [98] the Rolls-Royce M250 turboshaft is chosen as reference engine. The selling price ranges between 265,600 USD and 323,400 USD [99]. It is assumed that 50% of the selling price is the production cost. Therefore, the assumption is made that the engine of MAINTAIN will cost 147,500 USD. The propeller has a variable pitch and therefore follows from Equation 18.13.

$$C_{PP} = 377.4 \cdot N_{PP} \cdot P_{SHP} \cdot CPI_{2012} \tag{18.12}$$

$$C_{\text{CSTPROP}} = 209.69 \cdot N_{PP} \cdot CPI_{2012} \cdot D_P^2 \left(\frac{P_{SHP}}{D_P}\right)^{0.12} \tag{18.13}$$

Next to a UAV, the MAINTAIN system also contains a ground segment. The ground segment accommodates data transfer, control and support of the UAV and payload. The Cost Estimation Relation (CER) for the ground segment is from (Cherwonik 2003) and displayed by Equation 18.14. For the cost analysis it is assumed that every UAV has its own ground segment.

$$C_{GS} = 433.4 \cdot R_{GS}^{0.507} \cdot e^{0.398} \cdot CPI_{2003} \tag{18.14}$$

[98] E-mail contact with Dr. Visser about R&D and production cost of MGT

[99] `http://www.fi-powerweb.com/Engine/Rolls-Royce-M250.html` [cited on: 22-06-18]

The products liability cost should also be included in the total development and production cost. The liability is assumed to be 15% of the total cost to produce (Gudmundsson 2013). Summing up all the development and production cost leads to a **total development and production cost of 863,882 USD per UAV** as shown in Table 18.3.

Table 18.3: Development and production cost of MAINTAIN system.

Class	Man Hours [-]	Rate [USD/hr]	Total Cost [USD]	Cost per Unit [USD]	
Certification Cost			12,371,839	412,395	
Manufacturing Labour	25,844	58.83	3,188,171	106,272	
Quality Control			600,970	20,032	
Materials/Equipment			162,987	5,433	
Engine				147,500	
Propeller				8,383	
Avionics				14,887	
Ground Segment				36,299	+
Total Cost to Produce				**751,202**	
Manufacturer's Liability Insurance				112,680	+
Total Cost				**863,882**	

18.3.2. Unit Cost

To complete the computation of the unit cost, information about the costs of the sales, marketing and delivery process are required. In order to facilitate the sales process, resources are allocated to the marketing and sales department. It was found that Airbus takes 6% of the total revenue and assigns it to the marketing department (Airbus 2010). Since MAINTAIN has no market share yet and is in its starting phase it is decided to double the marketing budget, so 12% of the total revenue. The sales department consists of two full time salesmen with a salary of 35,000 USD per year (Avjobs 2018). The cost for delivery is estimated to be around 4000 USD based on 400 kg freight weight over a distance of 2000 km, since this is the maximum distance from the middle of the US, using FedEx (FedEx 2018).

From Table 18.1, it can be seen that the total expected sales in the first five year equal 30 units. The accumulated sales and marketing costs of the first five years are evenly distributed over the 30 UAVs. The total unit cost of MAINTAIN can now be computed and can be found in Table 18.4 which also shows its components. The table shows that the total cost of one UAV system is 1,487,549 USD. Since this estimation is based on statistical data an uncertainty margin of 50% is applied(NASA Exploration System Directorale 2008)(Verhagen n.d.). This gives an **estimated cost of 1,487,549 $\pm$ 743,775 USD for one UAV system.**

Table 18.4: MAINTAIN system unit cost break-down.

Class	Cost per Unit [USD]	
Marketing	8000	
Sales	11667	
Payload	600,000	
Transportation	4,000	
Development and Production	863,882	+
Total Cost	**1,487,549**	

18.4. Operational Cost

To provide the customer with more inside into the costs associated with normal operation of MAINTAIN, an operational cost analysis is performed. Similar to the development and production cost estimation, a method from (Gudmundsson 2013) is used as a basis. Again some alterations are made to adapt the method for the MAINTAIN system: a safety factor on the insurance cost, including cost for a ground control crew and including landing and take-off fees. First, the annual operational cost are computed and dividing this number with the annual flight hours results in the operational cost per flight hour. It is assumed that the UAV will fly 20 hours per day for 200 days a year. Figure 18.2 displays a breakdown of the operational cost.

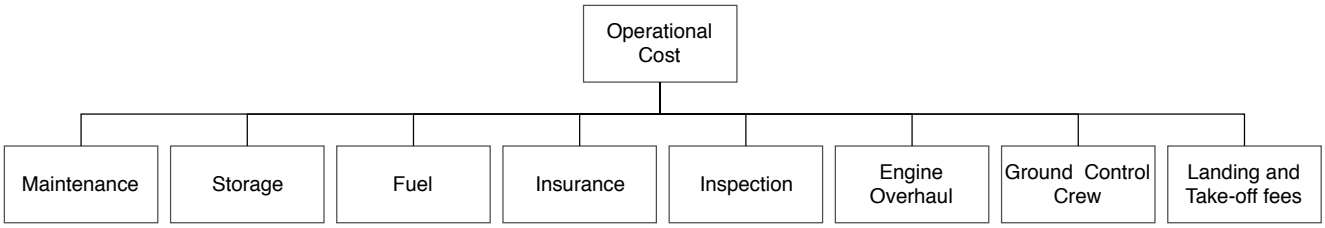

Figure 18.2: Operational cost breakdown MAINTAIN system.

The first part that is assessed are the cost of maintenance of the UAV, C_{AP}. This is done by Equation 18.15 in which the ratio of maintenance man-hours to flight hours F_{MF} is 0.37. The storage cost can be found with Equation 18.16 in which the monthly rent RA_{AP} is converted to an annual cost. RA_{STOR} is assumed to be 250 USD per month (Gudmundsson 2013). The fuel cost per year are calculated with Equation 18.17 with an fuel price of 0.94 USD per litre.

$$C_{AP} = F_{MF} \cdot RA_{AP} \cdot Q_{FLGT} \tag{18.15}$$

$$C_{STOR} = 12 \cdot RA_{STOR} \cdot CPI_{2012} \tag{18.16}$$

$$C_{FUEL} = FF_{\text{CRUISE}} \cdot RA_{\text{FUEL}} \cdot Q_{FLGT} \tag{18.17}$$

The insurance cost C_{INS} are determined by factors such as pilot experience and price and type of aircraft. The cost can therefore vary significantly. Equation 18.18 shows a general estimate, but since MAINTAIN has an unconventional, new design and mainly operates autonomously, a safety factor of 2 is applied to this initial estimate. The inspection cost C_{INSP} are found with Equation 18.19.

$$C_{INS} = 2 \cdot (500 + 0.015 C_{AC}) \tag{18.18}$$

$$C_{INSP} = 500 \cdot CPI_{2012} \tag{18.19}$$

The overhaul cost of the engine C_{OVER} is determined by Equation 18.20. It is assumed that the time between overhaul (TBO) and overhaul cost of the MAINTAIN engine are similar to Lycoming and Continental engines (Gudmundsson 2013). Finally, the cost per flight hour C_{HR} is found with Equation 18.21.

$$C_{OVER} = 5 \cdot Q_{FLGT} \tag{18.20}$$

$$C_{HR} = \frac{C_{YEAR}}{Q_{FLGT}} \tag{18.21}$$

The operational cost are collected in Table 18.5. Note that depreciation is not taken into account in the operational cost. The total operational cost per flight hour is 105.63 USD and assuming an average speed of 96 km/h, the chosen cruise speed for the final design, the operational cost per km is 1.10 USD. Since the operational cost are also based on statistical data, an uncertainty margin of 50% is again applied. This leads to a **operational cost per km of 1.10 ± 0.55 USD**. When the depreciation is taken into account, with the assumption MAINTAIN will operate 10 years, the cost per flight hour is 155.63 USD and **the cost per km is 1.62 ± 0.81 USD**. Even if the operational cost will be doubled to be profitable, MAINTAIN is competitive within the current market comparing it with the price of 83.33 USD per km for helicopter monitoring from chapter 3.

Table 18.5: Operational cost MAINTAIN system given in annual cost and cost per flight hour.

Class	**Annual Cost [USD]**	**Cost per flight hour [USD/hr]**
Maintenance	99,160	24.79
Storage	3,330	0.83
Fuel	4,941	1.24
Insurance	61,000	15.25
Inspection	555	0.14
Engine overhaul	22,200	5.55
Ground Control Crew	228,346	57.09
Landing and Take-off fees	3,000	0.75 +
Total Cost	**422,532**	**105.63**

18.5. Break-Even Point

The break-even point is reached when the cost equals the revenue. In a break-even analysis the number of products that needs to be sold to hit the break-even point is determined with Equation 18.22. The total fixed cost equals C_{CERT} and the unit variable cost is the sum of manufacturing labour, quality control, materials/equipment, landing gear, engines, propellers, avionics, ground segment, marketing, sales, liability and payload per unit. In this break-even analysis the

maintenance and ground crew service is not taken into account. **To reach the break even point, 18 UAVs should be sold** as can be seen in Figure 18.3. This will be after 4 years with the current projected sales.

$$N_{BE} = \frac{\text{total fixed cost}}{\text{unit sales price} - \text{unit variable cost}} \tag{18.22}$$

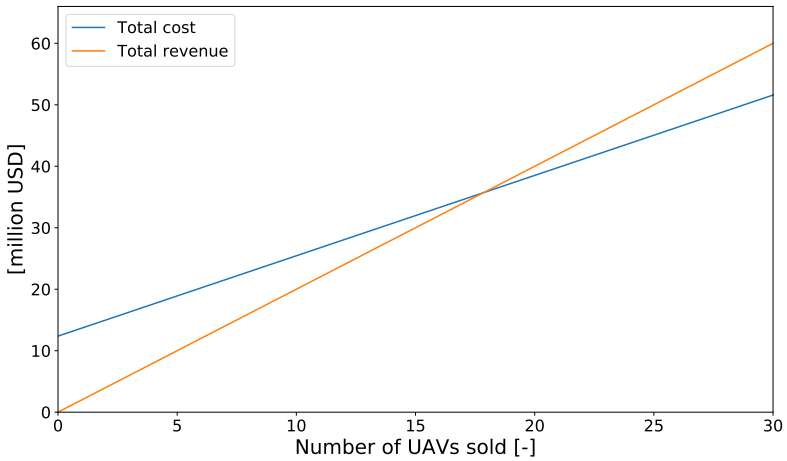

Figure 18.3: Revenue and cost per sold MAINTAIN showing the break even point.

18.6. Operational Profit and Return on Investment

The operational profit is the balance between the revenue and the cost as can be seen in Equation 18.23. The Return on Investment (RoI) is the operational profit divided by the cost per year shown in Equation 18.24. For both the operational profit as the RoI, the earlier mentioned business plan is assumed: a customer buys a UAV together with maintenance and ground crew service. MAINTAIN will have a 30% profit margin over the service. It is presumed that the costumer wants at least 5 years of maintenance and ground crew. This means only service profit will be made on the sold UAVs: in the first year service profit will be made over 3 UAVs while in the second year the profit will be made over 7 UAVs. This leads to the annual operational profit shown in Figure 18.4 and the annual RoI of Figure 18.5. The operational profit shows that **after three years, MAINTAIN will become profitable**. It should be noted that year 1 in both graph means the first year MAINTAIN will be on the market. Since the remaining time necessary for development is unknown, it is uncertain when "year 1" of both graphs will be reached.

$$\text{Operational Profit} = \text{unit sales price} \cdot \text{N} - \text{total fixed cost} - \text{unit variable cost} \cdot \text{N} \tag{18.23}$$

$$\text{RoI} = \frac{\text{unit sales price} \cdot \text{N} - \text{total fixed cost} - \text{unit variable cost} \cdot \text{N}}{\text{total fixed cost} + \text{unit variable cost} \cdot \text{N}} \tag{18.24}$$

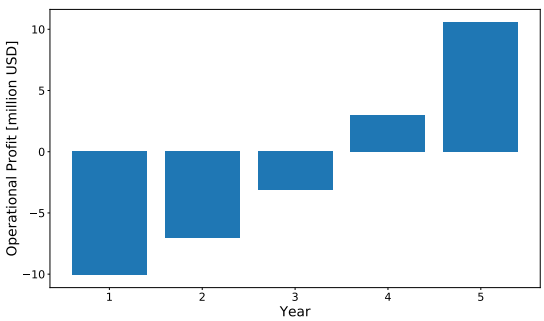

Figure 18.4: Annual operational profit for first 5 years after market entry.

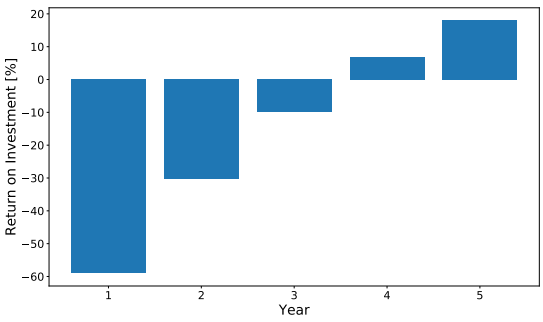

Figure 18.5: Annual return on investment for first 5 years after market entry.

19
Resource Allocation and Budget Breakdown

A resource allocation analysis is performed to estimate the value of different technical resource parameters. Once these parameters are estimated, a certain margin or contingency is added to allow for some uncertainty in the design phase. During the design process, the goal is to stay within the allocated budget to prevent the diverging of costs. Technical resources can be identified as cost driving parameters such as mass and power. First, the resource parameters at every design phase are analysed in section 19.1. Following this analysis, the budgets for these parameters are determined in section 19.2.

19.1. Resource Parameters

In this section, the resource parameters will be analysed throughout the design process. The three main phases are the Baseline, the Midterm and lastly the Final stage. The relevant technical parameters which will be analysed are:

- OEW
- Propulsive power
- MTOW
- Fuel burn

These resource parameters are chosen to be analysed as they are driving parameters for the unit price of the UAV; therefore, the cost is also analysed in the following subsections. Also, they were determined during each design phase. Not all technical resource parameters are estimated during every phase, which makes it impossible to construct the budget margin graphs for those throughout the different design phases.

19.1.1. Baseline

As Raymer states in his 'Aircraft Design' book: in order to generate a preliminary budget, a statistical approach is generally considered the most powerful tool in the early design stage (Raymer 2012). Therefore, a regression analysis was considered for the Baseline Report (B. van Beurden et al. 2018b). This regression is based upon the range and endurance requirements; respectively MTN.SYS.UAV-10 and MTN.SYS.UAV-8. These requirements state that the UAV system should have a range of at least 1000 km and an endurance of up to 20 hours, both values can be seen as the absolute minimum.

Using these as input and an initial payload estimate of 50 kg as inputs for the regression analysis functions, the following output values could be obtained, with belonging quality indicators:

Table 19.1: Summary of regression output.

Parameter	**Output**	**Linked Parameters**	**R^2**
OEW [kg]	245.75	Endurance, Range	0.995
Power [kW]	42.58	OEW	0.938
Cost [million USD]	2	Payload, Power	0.83
MTOW [kg]	460.15	OEW	0.995
Fuel Burn [kg]	109.21	MTOW	0.995

19.1.2. Midterm

After the trade-off between the five selected concepts from the Baseline (B. van Beurden et al. 2018b), a final concept was chosen in chapter 12 of the Midterm report (B. van Beurden et al. 2018a). The relevant design parameters of the final concept are shown in Table 19.2.

As can be seen in Table 19.1, the parameters are a lot smaller smaller than there were in subsection 19.1.1. The reason for this is that the Baseline results were purely based on statistics while at this stage, no statistical data was used anymore. The difference between the statistics and the actual design has turned out to be quite large. More on that in subsection 19.2.2.

Table 19.2: Summary of the design parameters of the final concept.

Parameter	Result
OEW [kg]	81
Power [kW]	10
Cost [million USD]	2
MTOW [kg]	191
Fuel Burn [kg]	60

Table 19.3: Summary of the design parameters of the optimised final concept.

Parameter	Result
OEW [kg]	72.9
Power [kW]	3.75
Cost [million USD]	2
MTOW [kg]	160.4
Fuel Burn [kg]	19.5

19.1.3. Final Optimised Design

Lastly, in this report the final design was optimised. The relevant design parameters as determined earlier of the optimised concept are shown in Table 19.3.

19.2. Budget

For most products in development, estimations of resource budgets are made. However, these resource budgets are not perfectly accurate. In addition, estimates of resource budgets will increase in accuracy when more decisions in the development process are made and more parameters of the end product are known. To ensure that uncertainties in estimates made in an early stage of the design process do not lead to an over-designed end product, margins of error are added to the estimates.

19.2.1. Contingency Management

The margin between an initial estimate and the estimated end value is called a contingency. These contingencies reduce with increasing time of the development. This will ensure that the estimated specifications of the end product will be consistent throughout the various stages of the design process and will ensure that uncertainties will not affect the characteristics of the final product. Implementing careful contingency management would mean that the new set budget estimate remains within the margin of the previous estimates. This ensures that the cost driving parameters do not divert the cost significantly.

In the resource budget contingencies will be implemented to ensure a realistic estimation of the end product. Typical values used in the aerospace industry will be used to determine the magnitude of the contingencies and define the various stages where the different contingencies will be applied. The overview of the propagation of the contingencies is shown in Table 19.4 (NASA Exploration System Directorale 2008)(Verhagen n.d.).

Table 19.4: Contingency values at various stages of the design process.

Design stage	Contingency [%]
Statistical regression	50
Preliminary design	20
Determining layout	15
Prerelease drawing	10
Released drawing	5
Specification	3
Actual measurement flight hardware	0

19.2.2. Budget Breakdown

The budget is a design margin. From Table 19.4, it is clear that different contingencies should be used during the different design stages. This means that on the outcome of the Baseline, a contingency of 50% will be applied as this outcome was purely based on statistics. Next, for results of the Midterm (preliminary design phase) a contingency of 20% was used. Lastly, there is a contingency of 10% applied on the results of this report as there are prereleased drawings made of the final design. Having the contingency intervals, graphs which visualise the estimates of the different technical resource parameters can be constructed. These intervals will give a clear overview of how the parameters changed throughout the design phases.

In the following two figures, one can see the budget margins of the OEW and of the MTOW:

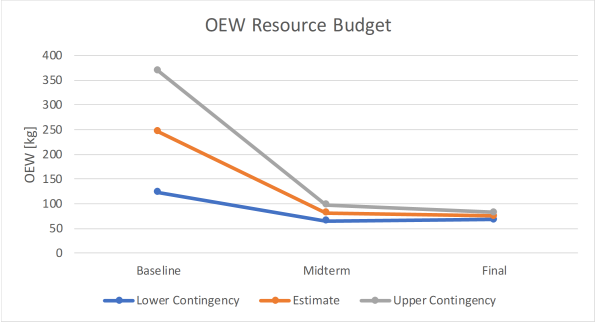

Figure 19.1: OEW budget margin during the design phases.

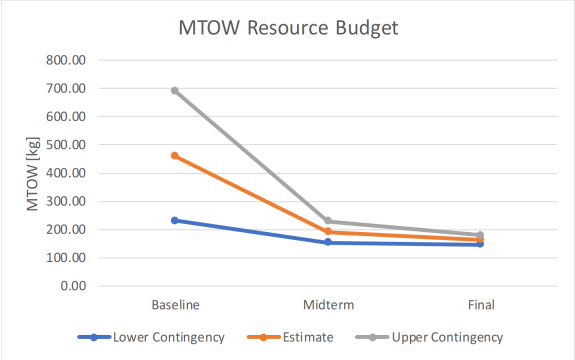

Figure 19.2: MTOW budget margin during the design phases.

In Figure 19.3 and Figure 19.4, the budget margins of the power and of the furn burn resource parameters are visualised:

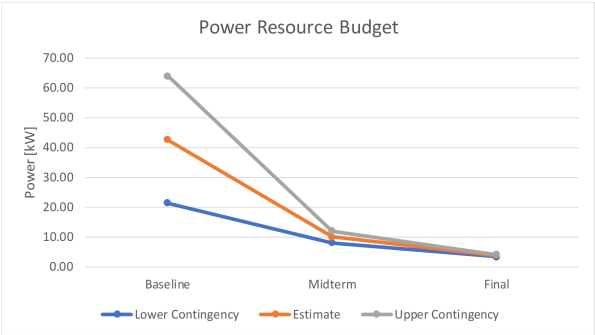

Figure 19.3: Power budget margin during the design phases.

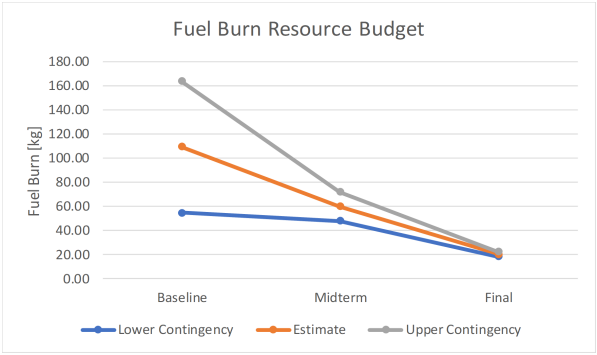

Figure 19.4: Fuel Burn budget margin during the design phases.

In the introduction of this chapter, it was mentioned that the goal is to stay within the allocated budget throughout the whole design process to prevent the diverging of costs. From the above four graphs, it is clear that this purpose has not been accomplished between the Baseline and the other phases. There are several reasons for this. First of all, although there has been used a big contingency interval for the statistical regression, it turned out that the statistical study was not applicable on this mission. The reason for this is the selection of UAVs which are used to conduct the regression upon. To do a statistical study, data from previous aircraft is required. It turned out that hardly any UAVs were built for this purpose and with this mission profile. Therefore at that stage, data was chosen from military drones as these drones matched the mission profile of MAINTAIN best in terms of range and endurance. This was clearly an assumption which was not valid to obtain first estimates for MAINTAIN. However, due to a lack of alternative UAV data, it was decided to use this regression at that stage anyway.

Secondly, MAINTAIN makes use of a micro gas turbine engine. It is the first time that such an engine is being used on a UAV. It is well known that the engine type has a lot of influence on a drone's design, so consequently its technical parameters. That is also a reason why the goal of staying within the original margins has not been accomplished. However, it is important to mention that not staying within the original contingency interval does not imply that the final optimised concept is bad by definition. For MAINTAIN this is actually a good thing. Have a look at Figure 19.5:

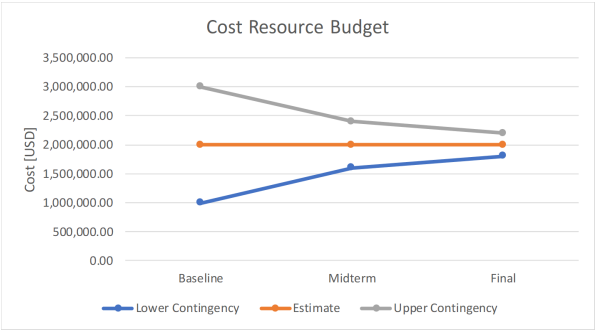

Figure 19.5: Cost budget margin during the design phases.

As one can find on the above picture, the cost expectation did not change through the different design phases; in which this cost is the selling price of the UAV. This means that the first estimate which has been made in the Baseline based on the market study, was a good estimate. So the fact that the OEW, MTOW, Power and Fuel Burn turned out to be lower than expected is actually beneficial for the design.

20
RAMS Characteristics

Reliability, Maintenance, Availability and Safety characteristics must be incorporated in the design process because nearly all components of MAINTAIN influence these characteristics. MAINTAIN's degree of safety shall be crucial for the success of the project as safety regulations on unmanned vehicles are very strict. Therefore, the reliability characteristics are assessed in section 20.1. Next, in section 20.2, using the reliability analysis, the maintenance characteristics are discussed. Flowing down from the reliability and maintainability assessments, the availability of MAINTAIN is determined in section 20.3. Finally, the safety characteristics are presented in section 20.4.

20.1. Reliability

In order to assess the reliability of MAINTAIN a Fault Tree Analysis (FTA) is performed. The FTA visualises the failure modes of MAINTAIN. From these failure modes, the critical ones are identified so measures can be taken to prevent these hazardous events from happening. The failure of MAINTAIN is divided into three sub-categories(Petritoli, Leccese, and Ciani 2017) which are:

- Critical failure: A failure mode that causes the UAV to crash and possibly cause injury or casualties on the ground.
- Severe failure: A failure mode that causes severe, probably irreparable, damage to the drone.
- Moderate failure: A failure mode that causes malfunctioning of the drone, may cause a "mission abort" but not cause it to be severely damaged.

Based on the failure types, the FTA is divided into three different fault trees. The first fault tree, presented in Figure 20.1, shows the analysis of all failure modes that will cause catastrophic failures. As can be seen in Figure 20.1, there are two critical failure modes, namely fly-by-wire failure and failure due to a loss of structural integrity. To maximise the reliability of the identified critical failure modes, these shall be checked and tested thoroughly during maintenance procedures and pre-flight inspections which shall further be elaborated on in section 20.2. Furthermore sensors will be installed on the structure of the UAV to monitor its state. To minimise loss of structural integrity from occurring, the UAV is over-designed by implementing a safety factor of 1.5 on top of the maximum loading factor. Next to that, there are some redundant failure modes implemented to increase the reliability of MAINTAIN. It is decided to use two batteries for the power-unit to make the power unit redundant as it is of primary importance for the UAV. Also, there are three independent hydraulic systems for the control surfaces. Each control surface has three actuators that can control the control surface independently. Lastly, the fly-by-wire is made internally redundant by installing multiple flight control computers and sensors within the system.

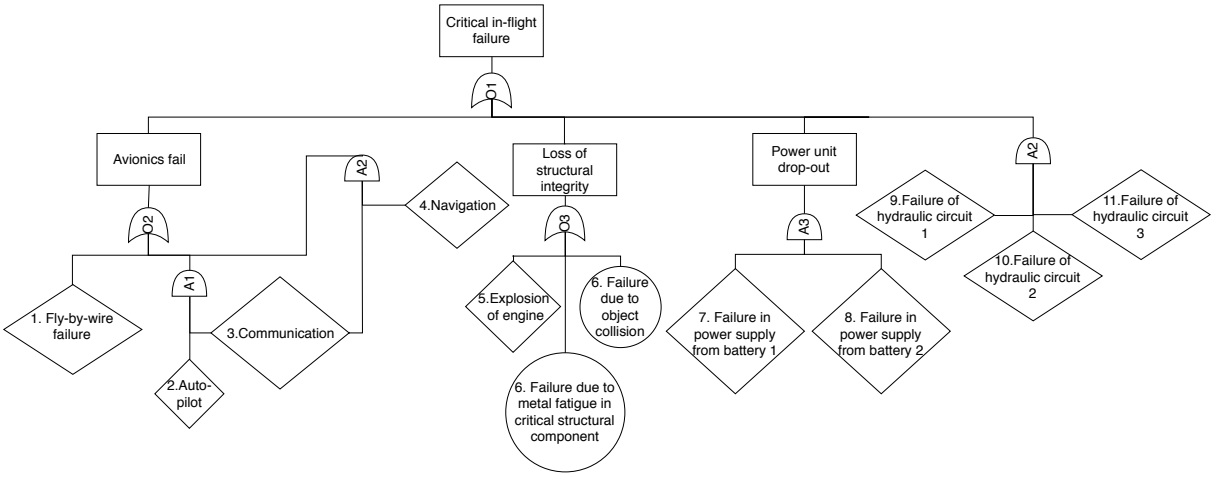

Figure 20.1: Critical in-flight fault tree.

The second fault tree, presented in Figure 20.2 analyses the failure modes that cause severe failure of the UAV. As can be seen, there is only one "AND" tree. Therefore the critical failure modes shall be checked frequently. The landing gear is made redundant by adding an emergency extension extraction system, consisting of a redundant hydraulic system and an unlatching device in case also the redundant hydraulic system fails[100].

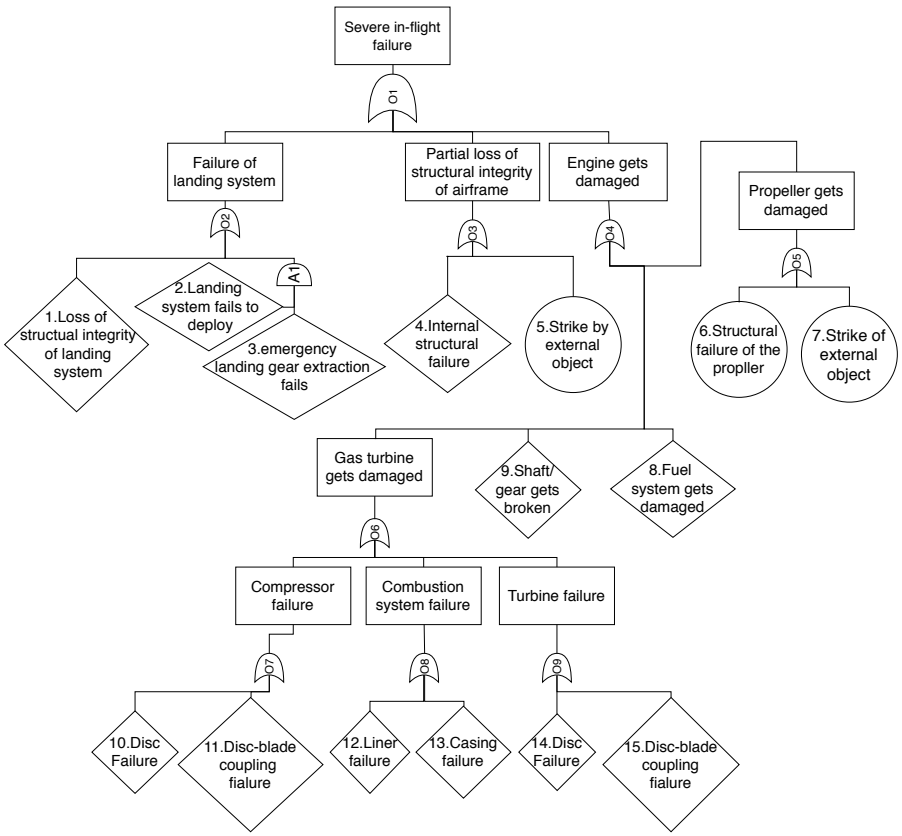

Figure 20.2: Severe in-flight fault tree.

Finally, the fault tree presented in Figure 20.3 shows the failure modes that cause moderator failure of the system. A moderate failure implies that if one of the failure modes occurs, the mission is aborted. A failure mode is identified as moderate whenever it causes a system to become non-redundant or causes the UAV to be incapable of performing its mission. Furthermore it is noted that a communication failure is defined in section 16.2. A failure which results in a drop-out of the engine is a moderate failure as MAINTAIN is designed to be capable of gliding towards a suited area to land, due to which the drone shall not be damaged. Next to this, to make the fuel system redundant, two pumps are implemented.

[100] `http://okigihan.blogspot.com/p/landing-gear-emergency-extension-systems.html` [cited on: 21-06-2018]

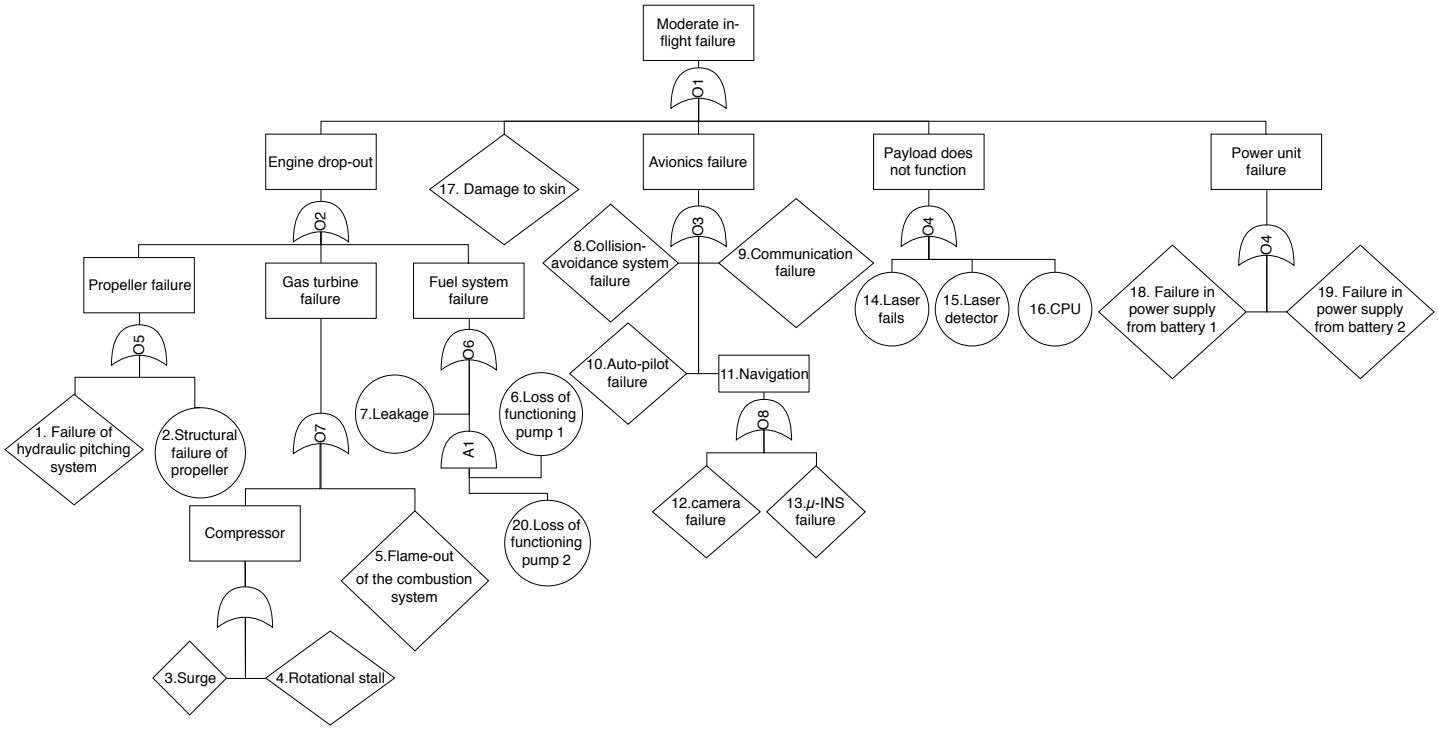

Figure 20.3: Moderate in-flight fault tree.

Using these fault trees, the reliability of subsystems can be evaluated in the future to compose the overall reliability of MAINTAIN. However, at this design phase, the reliability of the several components cannot be evaluated yet. Therefore, to quantify the reliability of the UAV, a statistical regression using comparable drones is done.

To assess the reliability of MAINTAIN, a literature study is performed on the reliability of existing UAVs. Based on the failure rate of existing UAV, an estimate of the failure rate of MAINTAIN can be determined. Table Table 20.1 gives an overview of the average failure rates of several existing UAV. A correlation is found between the reliability and the size of a UAV (Yu 2008). Based on the data a regression is made between the failure rate and the wing span of the UAV. A negative monomial regression function or exponential function is considered for the regression since the regression line is never to reach the value of zero. A negative monomial is chosen because this resulted in the lowest coefficient of determination. However due the limited amount of failure rate data of UAVs, the regression line is subject to outliers. Based on the regression the failure rate per hour of MAINTAIN is estimated to be $1.9 \cdot 10^{-3}$ failures per flight hour. Considering an operability of 200 days, this comes down to 8 failures per year. Therefore **the reliability of MAINTAIN is estimated to be 0.998 per flight hour**.

Table 20.1: Failure rates of existing UAV.

UAV	Failure Rate [failures/operational hour]
UAV ANTEX X02 EXPANDED	$4.99 \cdot 10^{-3}$ (Gonçalves, Sobral, and Ferreira 2016)
Predator	$2.1 \cdot 10^{-4}$ (Petritoli, Leccese, and Ciani 2017)
Global Hawk	$1.34 \cdot 10^{-3}$ (Petritoli, Leccese, and Ciani 2017)
Pioneer	$1.2 \cdot 10^{-2}$ (Petritoli, Leccese, and Ciani 2017)
Hunter	$2.3 \cdot 10^{-3}$ (Yu 2008)

Future Recommendations
As reliability is highly coupled with safety, it is important to get an accurate estimate of MAINTAIN's reliability. The current design phase is however not detailed enough to establish a probability of the failure modes in the fault trees to occur. From these probabilities a more precise failure rate can be established. Next to that, a detailed FTA must be made of pre-flight failure as well.

20.2. Maintenance

In order to guarantee a safe operation of the UAV with a minimised risk for failures, it is of utter importance to conduct maintenance activities regularly. Even more, due to the fact that this aircraft is unmanned, specific maintenance services are necessary compared to regular aviation because of the relative lack of knowledge of component behaviour of UAVs

[101]. Also, there is no crew in the aircraft who might feel or hear non-vital defects. To help with this, the MAINTAIN UAV will be equipped with sensors throughout the aircraft to detect eventual problems if there are. Furthermore, the maintenance specific tasks flow down from the fault trees which were constructed in section 20.1 to increase the reliability of the UAV. In following flowchart[102], the maintenance planning is illustrated:

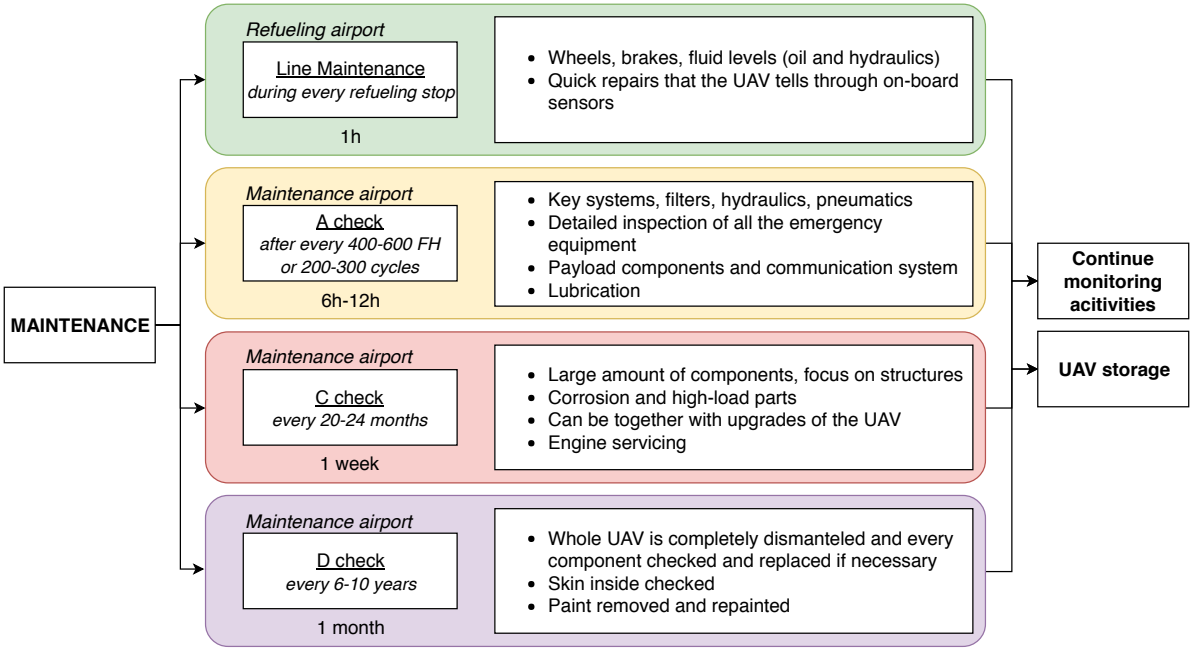

Figure 20.4: Maintenance planning.

As one can see, there are different maintenance activities at different moments. It depends on the amount of flying hours, the take-off/landing cycles and the operational time. Most of the maintenance is performed at maintenance airports, as described in the Operation and Logistics chapter 5. However, one can see that the Line Maintenance is done during every refueling stop. These are some general small general tasks which should be done by the ground crew as the control group (which is not at that specific refueling airport) is not able to do these checks. The ground crew will be trained to make sure that they conduct the line maintenance as required. The A check, C check and D check are carried out at the maintenance airports. For these activities, a specialised support crew is necessary. These checks happen after a certain amount of flying hours (FH in short), take-off and landing cycles or a certain amount of operational time. After the maintenance services, the UAV will either continue its monitoring activities or it will be stored when the craft is not necessary at that time. For modern aircraft, the B check is absorbed by several A checks or they are pushed to the next C check to be more time efficient and operational[103].

Next, an example of the downtime of a MAINTAIN UAV will be calculated. This is of course dependent on the flight planning of the UAV throughout its mission lifetime and should be iterated after every mission to make sure that no maintenance service is overseen. To optimise this, a well thought out maintenance schedule should be set up. So the downtime is the amount of time which the UAV will thus be grounded for maintenance. With that, the availability can be determined. This will done in a cycle of one year. With following assumptions:

- The UAV shall fly at least 200 days a year (requirements).
- There will be 1 flight of 20h per operation day.
- After every flight, line maintenance of 1h will be conducted.
- After 400 flying hours (so after 20 flights), an A check of 12h will be performed.
- Every two years, a C check of one week week be carried out.
- Every 6 years, a D check of one month (31 days) will be done.
- A maintenance working day consist of 8h.

The total maintenance time per year can be calculated as follows:

[101] https://humansystems.arc.nasa.gov/publications/UAV_interimreport_Hobbs_Herwitz.pdf [cited on: 20-06-18]
[102] https://www.lufthansa-technik.com/aircraft-maintenance [cited on: 21-06-2018]
[103] https://www.qantasnewsroom.com.au/roo-tales/the-a-c-and-d-of-aircraft-maintenance/ [cited on: 21-06-2018]

$$\text{Total Line Maintenance time} = 200 \cdot 1h = 200h \tag{20.1}$$

$$\text{Total A check time} = \frac{200}{20} \cdot 12h = 120h \tag{20.2}$$

$$\text{Total C check time} = \frac{1}{2} \cdot 7 \cdot 24h = 84h \tag{20.3}$$

$$\text{Total D check time} = \frac{1}{6} \cdot 31 \cdot 24h = 124h \tag{20.4}$$

Keep in mind that to calculate the C and D check time per year is the total time it takes per check divided by the frequency per year it should be conducted. In other words, the UAV needs $\frac{1}{2}$ of C checks a year and $\frac{1}{6}$ of D checks. So summing the above outcomes gives a total of 528h maintenance a year. **This means that if the UAV flies 200 days per year, it will be in total $\frac{528h}{8h/\textbf{day}} = 66$ days under maintenance**. This again implies that the UAV can be operable more than 200 days a year, on the condition that there were no further failures or complications. One can calculate the total amount of maintenance days per year in function of the operational days using following formula:

$$\text{Maintenance Days} = \left(\text{Ops}_{\text{days}} \cdot 1 + \frac{\text{Ops}_{\text{days}}}{20} \cdot 12 + \frac{1}{2} \cdot 7 \cdot 24 + \frac{1}{6} \cdot 31 \cdot 24\right) \cdot \frac{1}{8} \cdot 1.5 \tag{20.5}$$

In which the sum of the maintenance days and the Ops_{days} cannot be larger than the amount of days in that year. The $\frac{1}{8}$ comes from the fact that there are 8 working hours a day as stated in the assumptions and a safety factor of 1.5 has been used in order to account for delays and extra complications.

20.3. Availability

Availability is the degree that a system will be available for use. The availability flows down from reliability and maintainability. Availability is usually split up in three types, namely the inherent, achieved and operational availability(Hamann and M. v. Tooren 2006). The inherent availability excludes maintenance actions and logistic or administrative delays. The achieved availability also includes scheduled maintenance. Lastly, the operational availability also includes logistic an administrative delays.

The current design phase is however not detailed enough to evaluate the logistic and administrative delays. Therefore a first estimation for the achieved availability is made by combining the reliability with the availability derived from the standard scheduled maintenance. Following requirement MTN.SYS.UAV-11, which states that the UAV shall be operable for at least 200 days a year, the UAV shall be under maintenance for 66 days. The UAV has a availability incorporating the scheduled maintenance of $\frac{299}{365}$. Using Equation 20.7, in which R_{year} is the yearly reliability which can be calculated using Equation 20.6, the estimated achieved availability can be determined. **This results in an estimated achieved availability of 0.80 on a yearly basis**.

$$R_{\text{year}} = \frac{365 - (\text{failure rate}) \cdot (\text{flight hours per year})}{365} \tag{20.6}$$

$$A_{\text{year}} = A_{\text{maintenance}} \cdot R_{\text{year}} \tag{20.7}$$

Based on the achieved availability, the drone shall be available for 292 days per year. Although the operational availability shall be lower, **it can be concluded that the drone will be operable for at least 200 days a year**.

Looking at the lifetime of MAINTAIN, metal fatigue is the primary determinant. The lifetime of general aviation is usually expressed in the amount of pressurisation cycles an aircraft can sustain[104]. However, as MAINTAIN is a UAV, it will not be subject to pressurisation cycles and therefore won't be stressed as severely as general aviation. The MQ-1/RQ-1 Predator for example, which was the first UAV capable of carrying weapons, was retired in March 2018 after a lifetime of 21 years. Next to the fact that UAVs are not pressurised, MAINTAIN uses advanced composite materials just as the Predator which have good fatigue properties. Furthermore, rivets shall be replaced every 6-10 years during D-check maintenance if necessary, based on the degree of material degradation, to prevent the adhesives from failing a priori to the structure. Next to structural lifetime, the UAV shall be kept up to date by implementing new technologies during C-checks of the maintenance. Also, a new payload could be implemented in case a more innovative method to detect gas leakages/corrosion enters the market to keep MAINTAIN competitive. The requirements state that MAINTAIN shall have a minimum lifetime of 10 years, or 3650 cycle loads. Concluding from this analysis, this requirement shall be met if the correct measures are taken in further design stages to ensure structural integrity and competitiveness on the market.

[104] `https://www.airspacemag.com/need-to-know/what-determines-an-airplanes-lifespan-29533465/` [cited on 22-06-2018]

20.4. Safety

In order to determine the safety of MAINTAIN an operating hazard analysis is performed. First the probability of an on ground fatality caused by MAINTAIN is determined. Second, other hazards associated with MAINTAIN are discussed.

Based on the failure rate of MAINTAIN, an assessment of the number of accidents resulting in a fatality is performed. The worst case scenario is examined, which means all failures are assumed to be catastrophic. First, the mishap rate (MR) of the system per flight hour is determined by Equation 20.8. This describes the probability of the UAV to crash per flight hour. Other causes than failure of the UAV itself and a midair collision are not taken into account in the calculation of the MR. The amount of midair collisions causing debris (MC_{debris}) is assumed to be based on the amount of fatal accidents on the ground in general aviation. From data it is determined that $\frac{1}{5}$ of the on ground accidents are caused by falling debris. Combing the MR with the population density and lethal area of MAINTAIN, the Safety Objective (SO) is determined. The SO represents the expected amount of fatalities per flight hour and is calculated by Equation 20.9. Table 20.2 and Table 20.3 show an overview of the calculation to determine the Safety Objective (Clothier and Walker 2006).

$$MR = FR + MC_{\text{debris}} \tag{20.8}$$

$$SO = MR \cdot \rho \cdot A_L \tag{20.9}$$

Table 20.2: Input of the calculation of the SO.

Parameter	Unit	Value
FR	[failures/h]	$1.9 \cdot 10^{-3}$
MC_{debris}	[midair collision causing debris/h]	$3 \cdot 10^{-8}$ (Clothier and Walker 2006)
$\rho_{\text{population}}$	[people/m^2]	$1.971 \cdot 10^{-5}$ [105]
A_L	[m^2]	88.25

Table 20.3: Output of the SO Calculation.

Parameter	Unit	Value
SO	[ground fatalities/h]	$3.3 \cdot 10^{-6}$

The SO of MAINTAIN is $\frac{1}{76}$ on a yearly basis. Now the SO of MAINTAIN is compared to the amount of fatalities caused by general aviation. On average general aviation causes $1.09 \cdot 10^{-5}$ fatal accidents per operational hour, which corresponds to a probability of $\frac{1}{23}$ on a yearly basis. Comparing this with the SO of MAINTAIN presented in Table 20.3, it is clear that by using MAINTAIN the amount accidents causing fatalities per operating hour is strongly reduced. To be exact, **a reduction in fatal accidents of 70 % compared to general aviation is achieved**.

[105] (`https://www.indexmundi.com/facts/north-america/population-density` [cited on: 20-06-2018]

21 Sustainability

With the increasing discussion on aircraft sustainability and the sustainable nature of a maintenance service, this aspect is appointed priority within the maintain system. Following on the sustainability approach presented in the midterm report (B. van Beurden et al. 2018a), an overview of the status of sustainability within the project is given. This is documented after the final selection of the design, because it includes an extensive assessment of the sustainability. However, the topic has been a pillar throughout MAINTAIN's entire design process. First, a description of the sustainability approach is given in section 21.1. Next, in section 21.2, the sustainability of the final design is assessed based on different sustainability indicators. To conclude, a comparison is made between the environmental footprint of a gas pipeline inspection mission performed by MAINTAIN versus the current services in section 21.3.

21.1. Sustainability Approach

Over the course of the project, sustainability has been assessed and implemented extensively. A flowchart containing the complete sustainability approach of MAINTAIN is presented in Figure 21.1. Indicated in the green box, one can find the final steps to be taken in the analysis. Before the generation of a concept, the sustainability requirements were set up in step 7 in order to drive the design to a certain extent. The evaluation of the requirements and the research on the possibilities to make the system more sustainable, step 8 and 9 respectively, are performed in this chapter as well.

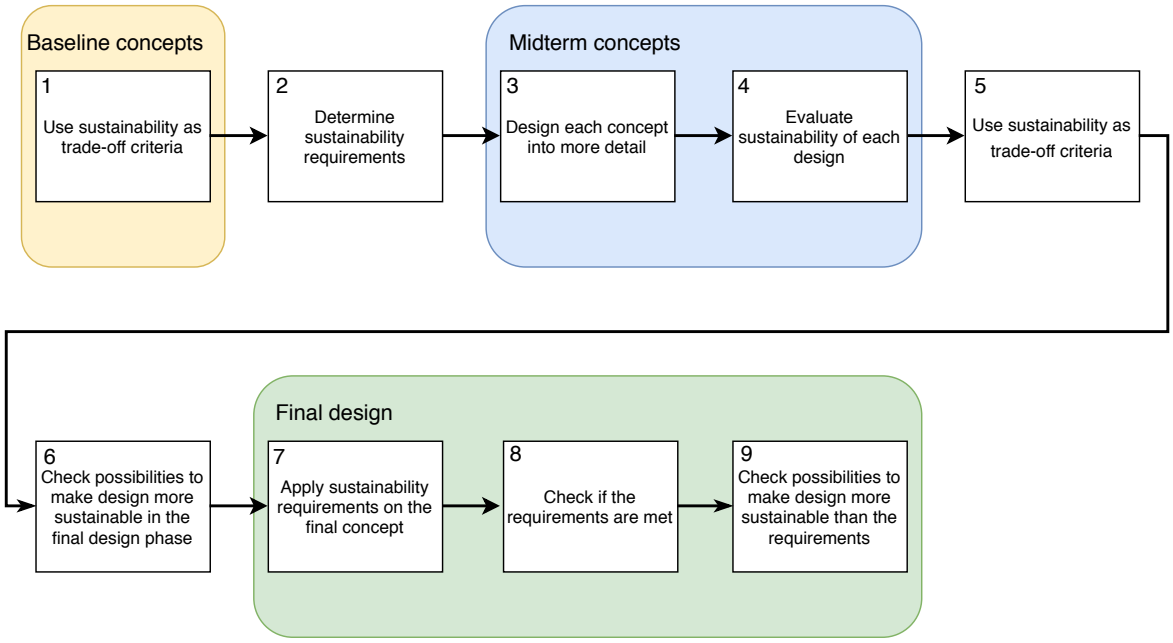

Figure 21.1: Sustainability approach flow diagram.

21.2. Sustainability Assessment

To assess the sustainability of the final design, the design is evaluated on the five different sustainability indicators. As described in the midterm report (B. van Beurden et al. 2018a), these five sustainability indicators are: noise, safety, recyclability, emission and contamination. First, the requirements and goals with respect to these sustainability indicators are stated. Thereafter, an assessment of each sustainability indicator is performed, followed by a check if the goals and requirements are met.

21.2.1. Requirements and Goals

Table 21.1 gives the requirements and goals with respect to sustainability. The origin described in the table explains on what a particular requirement or goal is based.

Table 21.1: Overview of goals and requirements categorised per sustainability indicator.

Sustainability indicator	**Requirements & Goals**	**Identifier**	**Orgin**
Noise	• The Propulsion Subsystem shall emit less noise than 87 dB.	MTN.SUB.PRO-6	• Based on noise exerted by a manned inspection mission.
Safety	• The probability of loss of a critical function shall be lower than $1.0 \cdot 10^{-7}$ per flight hour.	Goal-01	• Based on FAR 23 regulations and the Advisory Circular(AC) (King, Bertapelle, and C 2005).
	• The number of accidents resulting in a fatality shall be lower than $1.09 \cdot 10^{-5}$ per flight hour.	Goal-02	• Based on fatalities caused by general aviation (King, Bertapelle, and C 2005).
Recyclability	• The UAV its components shall be recyclable.	MTN.SYS.UAV-34	-
Emission	• The Propulsion Subsystem shall have a maximum equivalent CO_2 emission of 63 g/MJ.	MTN.SUB.PRO-5	• Based on emission exerted by non-bio fuels.
	• The UAV shall have a lower CO_2 emission than current alternatives.	MTN.SYS.UAV-35	-
	• MAINTAIN shall use less than 491.72 kg of fuel per inspection mission (1030 km)[106].	Goal-03	• Based on fuel burn during manned inspection mission.
Contamination	• Residues of the recycling processes shall be disposed according to the regulations stated in Resource Conservation and Recovery Act (RCRA).	Goal-04	• Based on Code of Federal Regulation(CFR).
	• Toxic and non-toxic waste produced during manufacturing shall be be disposed according to the regulations stated in Resource Conservation and Recovery Act (RCRA).	Goal-05	• Based on Code of Federal Regulation(CFR).
	• Waste produced during manufacturing shall be minimised.	Goal-06	-

21.2.2. Noise

Aircraft noise prediction models can be classified into two broad categories: theoretical and best-practice methods. Noise is fundamentally a result of the unsteadiness of the pressure field over the aircraft body. As pressure fields are already difficult to obtain and require a numerical solution of the Navier-Stokes equations, accurate and efficient theoretical prediction of aircraft noise is a problem that is yet to be solved. For these reasons, a best-practice model is implemented for noise assessment. Such models are a combination of lower-order approximations to the underlying physical process and statistical regressions. The propeller is assumed to be the main noise contributor and is therefore the only component assessed.

[106] `http://www.deltahelicopters.com/bell206b.html` [cited on: 14-06-2018]

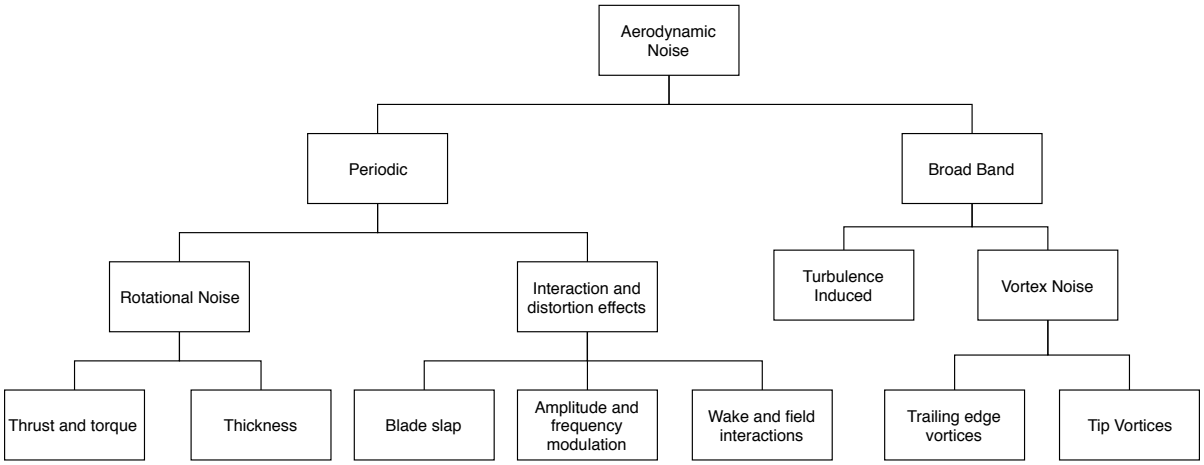

Figure 21.2: Aerodynamic noise decomposition adapted from (Marte and Kurtz 1970).

An extensive decomposition of aerodynamic noise has been presented in (Marte and Kurtz 1970) and is illustrated in Figure 21.2. Rotational noise and vortex noise have been found to be the major contributors to overall aerodynamic noise. The first is caused by the pressure distributions over the propeller blades which are steady in a frame rotating with the blade, but unsteady in the inertial frame. Vortex noise is caused by the shedding of vortices by the blades.

The noise measure to be assessed is the sound pressure level (SPL) which is a log-scale formulation of the root mean square (RMS) of the pressure field. This measure is defined as:

$$\text{SPL} = 20 \cdot \log\left(\frac{p_{RMS}}{p_{\text{ref}}}\right) \tag{21.1}$$

Where $p_{\text{ref}} = 2 \cdot 10^{-5}$ Pa as it approximately represents the human hearing threshold at 1000 Hz.
The rotational noise can be obtained by a Fourier transform of the pressure distribution. This is shown in Equation 21.2 (Marte and Kurtz 1970). In this equation, p_m is the RMS sound pressure level, m the order of the harmonic, M_t the tip Mach number and J_{mB} the Bessel function. All other symbols have been defined in chapter 2.

$$p_{RMS_m} = \frac{169.3mBRM_t}{SA}\left[\frac{0.76P_h}{M_t^2} - T\cos(\theta)\right] J_{mB}(0.8M_t mB\sin(\theta) \tag{21.2}$$

These harmonics are frequency multiples of the blade passage frequency which is found as:

$$f_{\text{blade passage}} = 2\pi\Omega B \tag{21.3}$$

The vortex noise is obtained through:

$$\text{SPL} = 10\log\frac{kA_b(V_{0.7})^6}{10^{-16}} \tag{21.4}$$

Where $k = 3.8 \cdot 10^{-27}$ is a constant of proportionality from (Marte and Kurtz 1970). The blade area A_b and air speed at 70 % $V_{0.7}$ are also required. Attenuation of the noise is done by the inverse square law.

The results of the rotational noise for the designed propeller are shown in Figure 21.3 for a distance between propeller and observer of 300 meters and at an index angle of 120 degrees as this yields the maximum perceived noise.

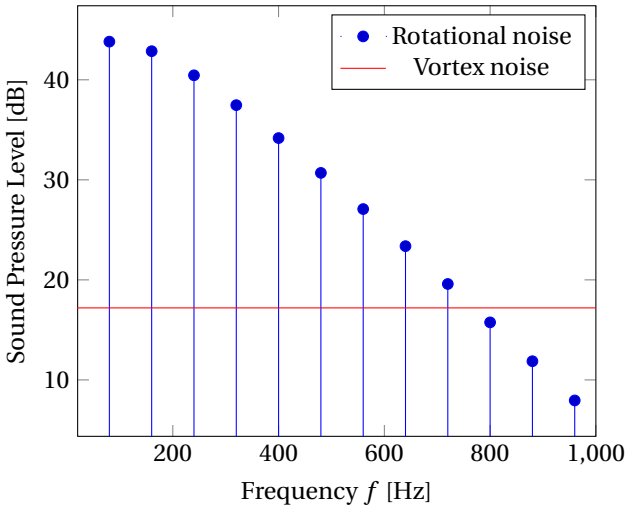

Figure 21.3: Results for the rotational and vortex noise of the propeller.

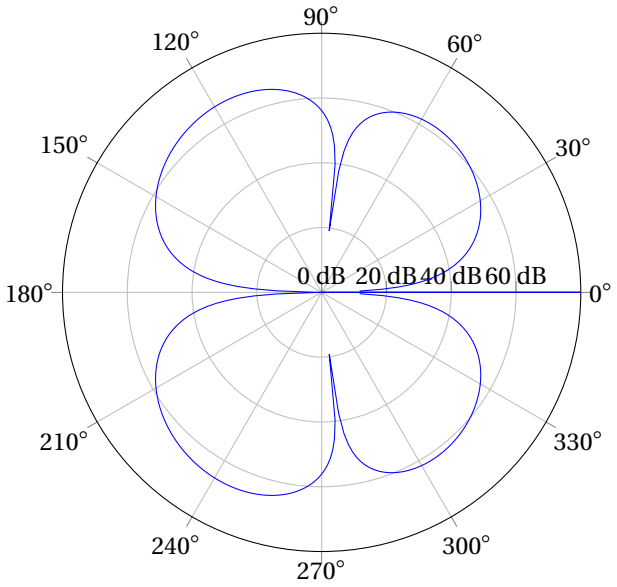

Figure 21.4: Polar plot of the sound pressure level at a distance of 300 meters indicating the noise level relation to directivity.

Based on Figure 21.3, Figure 21.4 and using the square root of the sum of squares of the SPL levels within the human audible frequency range, the final noise level at a distance of 300 meters is found to be:

$$\text{SPL} = 65.2 \text{ dB}. \tag{21.5}$$

Requirements

The requirement with respect to noise is to produce less than 87 dB, which is based on the noise emission of a manned gas pipeline inspection mission performed by a helicopter. As stated above **the noise emission of MAINTAIN is 65.2 dB**. Therefore the requirement is achieved.

21.2.3. Safety

The safety of MAINTAIN is assessed in section 20.4. Therefore this section is only focused on whether the goals with respect to safety are achieved.

Goals

The first goal concerning safety (Goal-01) directly specifies a minimal failure rate for MAINTAIN. This failure rate includes critical, severe and moderate failure modes as specified in section 20.1. This value is based on the FAR 23 regulations, which are specified for small general aviation aircraft up to a gross weight of 6,000 pounds. The posed failure rate of FAR 23 is $1.0 \cdot 10^{-7}$ per flight hour, which corresponds to a failure rate of $\frac{1}{2500}$ on a yearly basis, when having the same amount of operational hours as MAINTAIN. This value is obtained using the interpretation of the Advisory Circulars (AC), which uses a safety assessment process where qualitative scores are quantified. The failure rate of MAINTAIN, determined in section 20.4 is $1.9 \cdot 10^{-3}$ per flight hour, which corresponds to a failure rate of 7.6 on a yearly basis. It is evident that the goal with respect to the failure rate is not achieved. However, it should be noted that the FAR 23 is established for general aviation and regulations specifically for UAVs the size of MAINTAIN are not in place. Special classes of aircraft can however be certified by establishing new criteria with equivalent level of safety (King, Bertapelle, and C 2005). This brings up the Goal-02 with respect to safety, which posed MAINTAIN to cause less fatalities than general aviation. The amount of fatalities of MAINTAIN is expected to be $3.3 \cdot 10^{-6}$ per flight hour, while general aviation has an fatality expectancy of $1.09 \cdot 10^{-5}$ per flight hour. **Translating this to a yearly basis, the probability of MAINTAIN causing a fatality is $\frac{1}{76}$. General aviation aircraft with the same amount of hours have a chance of $\frac{1}{23}$ to cause a fatality. Therewith, the Goal-02 with respect is safety is met.** Due to the fact that MAINTAIN causes less fatalities then general aviation, MAINTAIN is found to have an equivalent level of safety. Therefore it is expected that MAINTAIN will get approved for certification with the current failure rate level.

21.2.4. Recyclability

To assess the recyclability of MAINTAIN at end of life, a schematic overview of the materials and components is given in Figure 21.5. The extent to which recyclability is possible, together with the accompanying recyclability methods and routes are discussed per material and component. Finally a comparison is made between the recyclability of MAINTAIN and a manned mission.

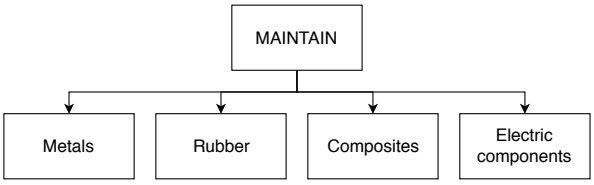

Figure 21.5: Recycling process of electrical components.

Metals
Metals are very suitable for recycling. Most metals can be recycled over and over again without degradation of its properties[107]. Once metels are sorted by the type of metal the recycling process is started. First the metals are shredded to increase the surface area which will reduce the energy required for the next step: melting of the metal. However the melting process consumes less energy than production of the metal from raw materials, which makes the recycling process viable[107]. Next the metal is purified, a common methods for this is electrolysis. Finally, the metal is solidified and can be used for the produced of a new product. The metals which are included in MAINTAIN are aluminium and steel. Once these types of metals are properly sorted the recycling rate can reach up to 100 %[108] [109].

Rubber
Several components in the UAV are produced using rubber. One important part are the tires of the landing gear. As these have to replaced on a regular basis, the recycling of the rubber within MAINTAIN is important for the overal recyclability. Rubber is related to thermo-plastic-electic materials and transformed into a thermoset during the manufacturing of rubber products (Yehia 2007). This causes the recycling process to be more difficult than those of thermoplastics, which can be molten easily. However, recently effective rubber recycling methods are established[110]. The main recycling route of rubber in the USA is by conversion into energy. This type of recycling is classified as quaternary recycling, which is not the most desirable type of recycling (Hopewell, Dvorak, and Kosior 2009). Preferably the rubber is recycled into higher value products (Singh et al. 2016). Luckily, the trend for recycling rubber is slowly shifting from rubber-derived fuel to ground rubber. Most common applications for ground rubber are moulded or extruded rubber products (35%) sports surfaces (25%) and asphalt (15%)[110].

Composites
Composites exist of matrices and reinforcement materials; these two materials are blended into each other. This poses the first challenge in recycling composite, since separation of the materials is difficult. The second reason why composites pose challenges with recycling is introduced by the fact that matrix materials are often thermosets, which can not easily be molten or deformed into a different shape. In general, all composites can be recycled using mechanical processing, which means the material is shredded into small pieces (Reynolds and Pharaoh 2010). However the recycled material is only suitable for low-value applications (Pimenta and Pinho 2011). In MAINTAIN two types of composites are present: CFRP and GLARE. CFRP has relatively good recycling possibilities compared to other composites. The main recycling process, which is currently commercially established, is pyrolysis. However, in the USA only one company performing pyrolysis of CFRP commercially is known (Oliveux, Dandy, and Leeke 2015). The pyrolysis process has the potential to both recover the resin and the fibre, while still retaining quite high mechanical properties (Reynolds and Pharaoh 2010). A drawback is that environmentally hazardous gasses are produced during this recycling process. For GLARE on the other hand, no commercially available recycling method is in place yet (Zhu 2012). Due to these complications, the use of composites does negatively effect the recyclability of MAINTAIN compared to for example the use of aluminium.

Electric Equipment

The electrical components inside MAINTAIN are mainly represented by the board computer containing microprocessors, wires, sensors and the electronics of the payload. Wires consist of a conducting metal and thermoplastic sheath. The recyclability of these materials can be found in 'metals' and 'composites'. First of all, all electrical components that are not obsolete or broken at the end of life of MAINTAIN can be reused in new applications as a whole.
If an electronic equipment is discarded, the electrical equipment is classified as Waste Electrical and Electronic Equipment (WEEE) and a recycling process is stated (Debnatha, Roychowdhury, and Kunduc 2016). An overview of the different materials of WEEE is presented in Table 21.2. Most electrical components are connected to a Printed Circuit Board (PCB), therefore a flowchart to visualise the recycling process of PCBs is presented in Figure 21.6. Once the electrical equipment

[107] https://www.thebalancesmb.com/an-introduction-to-metal-recycling-4057469 [cited on: 20-06-2018]
[108] https://www.tatasteeleurope.com/en/sustainability/steel%E2%80%93for%E2%80%93a%E2%80%93sustainable%E2%80%93future/the-life-cycle-of-steel/recyclable-or-recycled [cited on: 20-06-2018]
[109] http://www.aluminum.org/sustainability/aluminum-recycling [cited on: 20-06-2018]
[110] http://www.reliance-foundry.com/blog/rubber-recycling#gref [cited on: 20-06-2018]

us specified as WEEE in step one, the detaching of electronical components from the PCB is started in step 2. Next, in step 3, all individual components are tested on several criteria, which are related to the specific type of electrical component (for example, resistors, processors or controllers). If the EC passes all criteria, it is reused in new electronic equipment (step 7). If one of the criteria is not met, the electrical equipment is decomposed and the remaining material are either recycled using common recycling routes or classified as waste (step 5 and 6). An overview of the different materials in electrical components is presented in Table 21.2. Further elaboration of the methods used in this process can be found in (Debnatha, Roychowdhury, and Kunduc 2016).

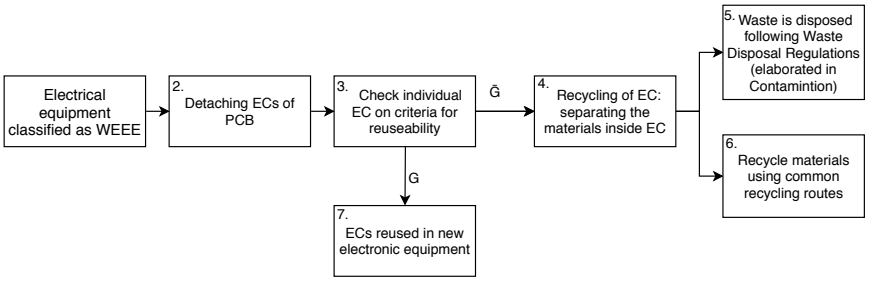

Figure 21.6: Recycling process of electrical components.

Table 21.2: Composition of WEEE.

Material	% in WEEE
Iron & Steel	50
Plastics	21
Non-ferrous Metals	13
Other (rubber, concrete, ceramics)	16

Requirements

The requirement with respect to recyclability is: The UAV its components shall be recyclable (MTN.SYS.UAV-34). **In the recyclability analyses above, it was found that it is possible to recycle all components of the UAV.** However, some residues of the recycling process will still end up as waste, due to for example the difficulties with decomposing adhesive bonds, and not all materials can be recycled into high value products. Besides, not all recycling techniques discussed above are widely available in the USA. This will probably cause some operational problems in recycling all components of MAINTAIN in practice.

21.2.5. Emission

In this section, the emission of MAINTAIN will be compared to the emission of an equivalent manned mission. The manned mission chosen in this comparison will be a mission flown by Lasen with a Bell 206B helicopter. Comparing the total fuel burn for the sample mission as shown in section 11.1 and the specific fuel consumption of both propulsive systems, part of the emission analysis is performed. Secondly, the emission is decomposed in various components to assess the emission per kilogram of fuel for both systems. Finally, the total emission for both missions will be compared.

Fuel Burn and Specific Fuel Consumption

Comparing the fuel burn and specific fuel consumption of the Bell 206B and MAINTAIN for the sample mission of section 11.1, the main differences between both systems will be covered. First of all, the Bell 206B uses an Allison 250-C30P turboshaft engine featuring a power of 190 kW and a specific fuel consumption of 0.468 kg/kWh. During the sample mission described, the Bell 206B will burn 491.72 kilograms of fuel. A comparison between this manned mission and MAINTAIN is provided in Table 21.3.

Table 21.3: Fuel burn comparison between Bell 206B and MAINTAIN.

	Bell 206B	MAINTAIN	Difference [%]
Fuel burn [kg]	491.72	19.5	-96.03
Specific fuel consumption [kg/kWh]	0.468	0.29	-38.03

As can be clearly seen from the table, the fuel burn differs a lot between both systems. Not only does the Bell 206B need more fuel to produce the same amount of energy, it also needs significantly more power and hence fuel to complete the sample mission. Even installation of a more efficient engine on this helicopter would still mean it burns more fuel due to its large required power which follows from its larger weight.

Fuel Specific Emissions

The fuel specific emissions are determined and presented in table Table 21.4. The relatively high uncertainty is the result of the deviations in emission with varying operational conditions. For example, uncertainty in the NO_x emission is the result of the fact that the amount NO_x emissions is a trade off between engine efficiency, other emissions like small

particles and NO_x emissions themself[111] (Coperation 2016). It should be noted that the CO_2 emission is defined as the amount of non-renewable carbons which are added to the atmosphere. Therefore, the high reduction of CO_2 emission is the result of the use of renewable hydrocarbons.

Table 21.4: Emission comparison between diesel and HVO.

Emission	Diesel [g/kg]	HVO [g/kg]	Difference [%]
CO_2	3142.89[112]	628.57 (±10%)[113] [114]	-80
CO	42.60 (Jun, Gillenwater, and Barbour n.d.)	25.74(±62%)	-40
NO_x	63.90 (Jun, Gillenwater, and Barbour n.d.)	59.07 (±4%)	-8

Total Emission per System
Comparing the total emissions of both systems in terms of listed components, Table 21.5 results.

Table 21.5: Total emissions comparison between Bell 206B and MAINTAIN.

Emission	Bell 206B	MAINTAIN	Difference [%]
$CO_2[kg]$	1545.4	12.2	-99.2
CO [kg]	20.9	0.5	-97.6
NO_x [kg]	31.4	1.2	-96.1
Total CO_2 equivalent [kg]	12165 [115]	359 [115]	-0.97

Only primary effects on global warming are included in the calculation to determine the amount of total CO_2 equivalent emission, which is a measure for the global warming caused by MAINTAIN. Due to due limited data availability, not all Green House Gas (GHG) emission are assessed. Only primary effects on global warming are included in the calculation to determine the amount of total CO_2 equivalent emissions, which is a measure for the global warming caused by MAINTAIN. CO production does not effect the total CO_2 equivalent of both missions, because it only secondary effects global warming. Therefore, the CO_2 equivalent emissions are in this case based on the CO_2 and NO_x emissions. However, when considering the secondary effects of CO, it turns out to be contributing more to global warming then suggested by the low Global Warming Potential (GWP). This effects is the result of the fact that CO reacts with hydroxyl radicals in the atmosphere, which helps to reduce the lifetime of strong-greenhouse gasses[116].

Goals and Requirements
From the emission assessment it is concluded that Goal-03 and requirement MTN.SYS.UAV-35 with respect to emission are achieved. **From Table 21.5 it is concluded that MAINTAIN reduces both CO_2 emission and fuel burn when used for a gas pipelines inspection mission instead of a manned mission**. Requirement MTN.SUB.PRO-5 needs a small elaboration. The MTN.SUB.PRO-5 requirement is: The Propulsion Subsystem shall have a maximum equivalent CO_2 emission of 63 g/MJ. This can be extracted easily from Table 21.4 combined with the LHV of HVO. **The equivalent CO_2 emission is of HVO is 15.6 g/MJ, which means all requirements and goals are achieved.**

21.2.6. Contamination

Contamination is usually defined as "the result of industrial activity that has resulted in spillage, leaks or deposists from air emissions and wastes" (RICS 2010). When studying sustainability, contamination must therefore be kept to a minimum. Investigating sustainability in the complete system of MAINTAIN, the UAS system can be subdivided into the UAV and the ground segment. A further decomposition is visualised in Figure 21.7. Note that emission and recyables are discussed in previous sections and will not be included in the study into contamination. The discussion of contamination will be conducted in a quantitative way, since the exact figures can only be performed in an even more detailed design stage.

[111] `http://clean-carbonenergy.com/nox-emissions.html` [cited on: 21-06-2018]
[113] Based on calculations made on the molucular combustion reaction
[114] `https://www.honeywell.com/newsroom/pressreleases/2017/03/diamond-green-diesel-to-expand-renewable-fuel-capacity-\using-ecofining-technology-from-honeywell-uop` [cited on: 21-06-2018]
[115] Based on GWP_{20}
[116] `http://www.ghgonline.org/otherco.htm` [cited on: 21-06-2018]

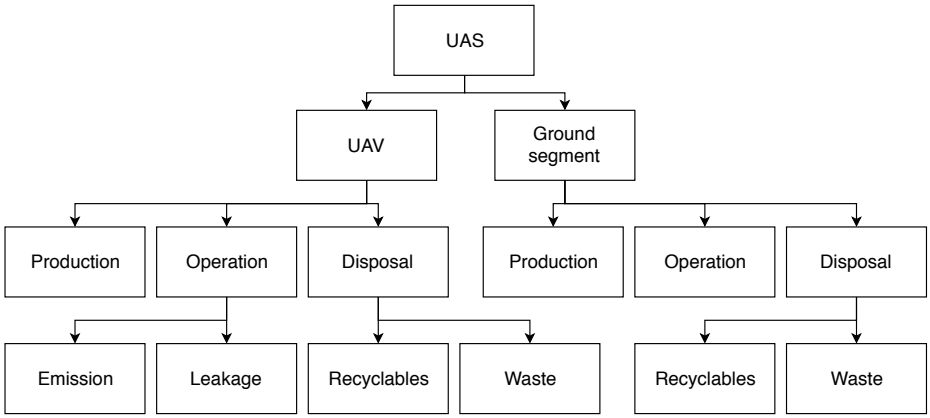

Figure 21.7: Breakdown of MAINTAIN system when investigating contamination.

UAV Production

During the production of the UAV, several materials, processes and assembly means are used. In general, manned missions will consist of more parts, involve more methods and use more material. As stated in chapter 22, the UAV will consist of Glare, Aluminium, CFRP and Steel. Comparing these materials to a manned mission, it should be noted that overall less material is used due to the relatively low weight and small size of the vehicle. Besides, during the production of MAINTAIN the principle of Lean Manufacturing should be implemented. This means that during the manufacturing of MAINTAIN constant attention is payed to the reduction of waste and the use of other resources without adding value. Comparing the specific materials used, Glare and CFRP are composites which require extensive production methods and will probably involve more contamination than steel and aluminium. Compared to manned missions using mainly aluminium, the UAV will score worse. However, also manned missions are converting to the use of composites in the construction of several components and like said, less material will be used.

Comparing the manufacturing processes for all materials, the same can be said. Manufacturing of composite parts might involve more contamination, but less will be needed due to the vehicle size. Regarding the assembly methods used during the production of the UAV, rivet and adhesive bonding will be used whilst manned missions will probably also include other manufacturing methods, such as bolting. These techniques often involve less contamination due to the fact that components are better recyclable compared to adhesively bonded parts, which is elaborated on when studying disposal of the UAV.

UAV Operation

During the operation of the UAV it will have various emissions as discussed in subsection 21.2.5. Next to these emissions, leakages will occur, which is an important factor in the study of contamination. Even the smallest amount of leakage during the operation phase will have a large impact on the sustainability of a mission, since in general the operational phase will have a long duration. Comparing the leakage of the UAV with a manned mission, less leakage will be present due to the relatively small size of the vehicle meaning it has a lower fuel burn and smaller components suffering from leakage. In addition, it has only a limited amount of subsystems. For example, the UAV will only have two elevons, compared to manned missions which often have two ailerons, an elevator and a rudder in the case of an aircraft, whilst in the case of a helicopter hydraulic actuators are used to overcome high control forces[117]. All of these control surfaces have to be driven using a hydraulic system involving pipelines, regulators and other components where leakage can occur.

UAV Disposal

After the operational phase of the UAV, disposal of the vehicle takes place. Studying contamination, only waste that remains after recycling will be considered; recycling is elaborated upon in subsection 21.2.4. Waste should be minimised at all times and should be recycled according to RCRA regulations. One example of waste that remains after recycling is waste following from Waste Electrical and Electronic Equipment (WEEE), which remains after recycling most components as explained in Figure 21.6. In general, waste remaining after recycling will be less than for a manned mission, since less there is in general less material used and hence a smaller amount of waste will remain. However, especially regarding composites a lot has to be improved in the industry and when the system is to be disposed care should be taken when choosing the waste company. Currently, only 2% of the composites-related companies are active recyclers, whilst more than 80% of aluminium is successfully recycled[118].

[117] `http://www.danubewings.com/helicopter-hydraulics/` [cited on: 22-06-2018]

[118] `https://www.compositesworld.com/blog/post/composites-recycling-is-gaining-traction` [cited on: 20-06-2018]

Ground Segment
MAINTAIN requires specific ground segments, including hardware, software, personnel, bio-fuel tanks and a GPU. Part of these are also required by manned missions: a GPU, fuel tanks and personnel. However, MAINTAIN requires specific hardware and software which have to be produced. Contamination during production of these components therefore adds negatively to the overall sustainability of the system. Especially the design of the hardware will involve some waste, which should be minimised where possible. During the operational and disposal phases of the system, the same reasoning as for the UAV holds.

Goals
Reflecting on set goals regarding contamination which can be found in subsection 21.2.1, it is stressed that these goals should be strived for during the whole lifecycle of the system. **Waste which remains during disposal of the vehicle and ground segment should be recycled according to RCRA regulations. In addition, waste produced during manufacturing should be minimised at all times. When waste is produced during manufacturing, these should be recycled according to RCRA regulations too.** Selection of both waste companies and manufacturers should be considered carefully, to make sure set goals are met.

21.3. Comparison of Environmental Footprint

This summarising section provides what impact the implementation of MAINTAIN has on the sustainability of the service. The environmental footprint of an activity represents the effect that a specific activity has on the environment. Examples are the amount of natural resources they use and the amount of harmful gasses that they produce[119]. In order to compare the difference in environmental footprints of a manned inspection mission versus a MAINTAIN inspection mission, several effects are examined. The mission examined is the sample missions presented in section 11.1. First the fuel burn is examined, this represents the amount of natural resources that are used. Second the CO_2 emission is evaluated. Next, the noise produced by both missions is included because this might effect the wildlife in the operational environment of the mission (Radle 2007). Finally, the CO_2 equivalent emission is evaluated and represents the amount of harmful gasses that are released into the atmosphere. Table 21.6 presents the complete comparison. A large decrease in environmental footprint can be seen when performing an inspection mission using MAINTAIN compared to a manned helicopter mission. **All environmental parameters which determine the environmental footprint, except for noise, are decreased over 90%.** Noise is evaluated in dB, which is a logarithmic scale. Therefore, the reduction of noise is less than the actual reduction of the energy of the noise emitted by MAINTAIN.

Table 21.6: Comparison between footprint of inspection mission performed by MAINTAIN versus manned helicopter mission.

	Fuel Burn [kg]	CO_2 **emission [kg]**	**Noise [dB]**	CO_2 **equivalent emission [kg]**[120]
Manned helicopter inspection mission	491.72[106]	1545.4[121]	87[122]	12165
MAINTAIN inspection mission	19.5	12.2	65.2	359
Decrease of environmental footprint	-96 %	-99 %	-21.8 dB	-97 %

[119] `https://dictionary.cambridge.org/dictionary/english/environmental-footprint` [cited on: 15-06-2018]
[120] Includes CO_2 and NO_x
[121] Based on calculations on the molecular combustion reaction of Diesel
[122] `http://hearinghealthmatters.org/lawandhearing/2011/helicopter-noise/` [cited on: 15-06-2018]

22
Production Plan

Once the design of the UAV is completed, the production of the aircraft is to be performed. Planning the production leads to an optimal utilisation of the available resources during the manufacturing, assembly and integration of the aircraft and its components. This chapter presents the production plan of the MAINTAIN UAV and gives an outline of the activities required to construct the aircraft. In this chapter manufacturing, bonding and the assembly of the aircraft are discussed in section 22.1-section 22.3, respectively. Subsequently, in section 22.4, the integration of the production process is presented.

22.1. Manufacturing

In this section, the manufacturing processes which are necessary to produce the UAV elements will be determined and discussed. First of all, these are the parts which have to be manufactured and their material as determined in chapter 14:

Table 22.1: Overview of the structural components and their material.

Elements	Material
Skin	GLARE
Stringers	Aluminium 7075-T6
Spars	CFRP
Ribs	CFRP
Landing Gear	Steel Alloy 4340

22.1.1. Manufacturing of the Skin

The first element, the skin, is a thin-walled lightweight structure which determines the outer shape of the wing. The chosen material is GLARE, a Fibre Metal Laminate or FML in short. GLARE, which stand for glass reinforced aluminium, is a multilayer laminate material composed of aluminium, glass fibres and an epoxy matrix. To manufacture GLARE, composite techniques are used, which makes use of prepregs. Prepregs are made up of the glass fibres along the required direction laid up in the epoxy matrix. **To compose the final GLARE material, a lay-up of both the metal and the prepreg layers is done**, as visualised in Figure 22.1 (Elton 2010). That way, the skin can be made in one process cycle. As the skin is single curved, roll bending can be used to deform it into the right shape. The roll bending technique is illustrated in Figure 22.2. The spring back depends on the fibre direction. If the fibres are along the longitudinal direction of the roll bending, there is minor spring back to be expected. However, if they are in the circumferential direction, roll bending might be a problem which should be accounted for using safety factors (Sinke. 2003).

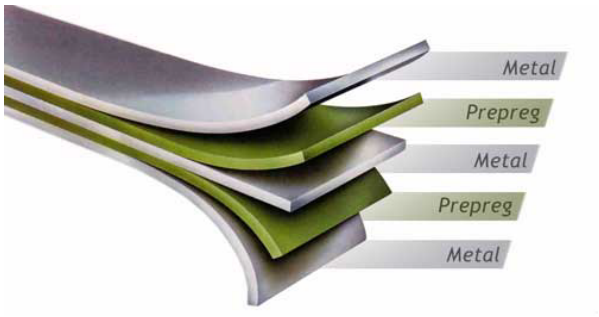

Figure 22.1: Illustration of GLARE lay-up.

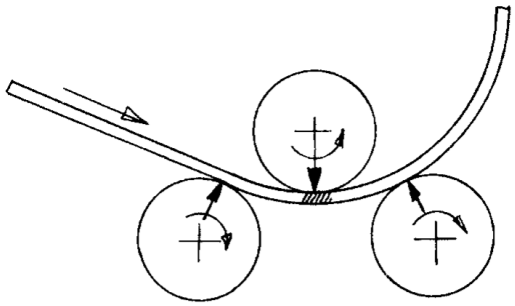

Figure 22.2: Illustration of the roll bending technique.

22.1.2. Manufacturing of the Stringers

Next, there are the stringers. The stringers are chosen to be of Aluminium. Therefore, conventional manufacturing techniques will be the best option as these are relatively cheap, proven and widely applied in these kind of structures

nowadays. In Figure 22.3, one can see the stringer type which will be used in the MAINTAIN UAV. **The best technique to manufacture this stringer will be extrusion.** Extrusion forces a billet metal through a die with a certain shape which extrudes the desired product. It plastically deforms the Aluminium by performing work on the material. The technique is visualised in Figure 22.4[123].

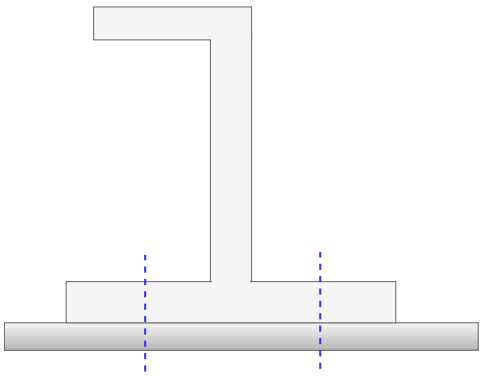

Figure 22.3: The stringer type used for the MAINTAIN UAV.

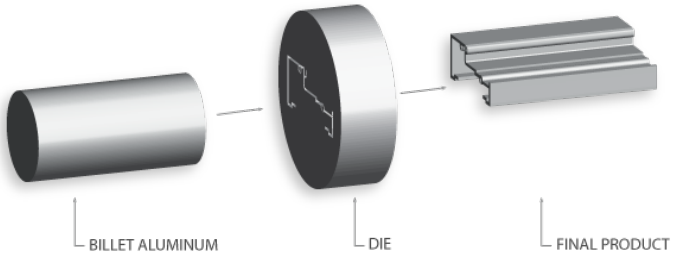

Figure 22.4: Illustration of the metal extrusion technique.

22.1.3. Manufacturing of the Spars and the Ribs

Thirdly, there are the spars and the ribs which are both of CFRP; which stands for Carbon Fibre Reinforced Polymers. This is also a composite material, meaning that composite manufacturing techniques will have to be used. However, the two elements will make use of a different technique. The spars are vital to the wing strength as they take up a lot of loads. Failure of the spars will fail the whole UAV, therefore it should be guaranteed that the spars are of high quality. This means that a manufacturing technique should be used which assures great material properties and eliminates production impurities. **Therefore, an autoclave would be a good solution** (Sinke n.d.[a]). Although quite a large autoclave will be necessary (it should be at least half the length of the span), it is the best alternative to ensure the highest possible material quality. During the autoclaving process, prepregs are used which merge into a composite material after the lay-up and the resin matrix are cured. The curing is performed under increased pressure and temperature conditions. The pressure enhances the bonding strength of the material and minimises the risk for undesired voids. The drawback of this technique is that it is rather expensive for this size and that is will be quite labour intensive. However, the benefits will outweigh the disadvantages. An autoclave is visualised in Figure 22.5[124]:

Figure 22.5: Illustration of an autoclave.

Due to the rib structure, which consist of rather sharp corners and edges, using an autoclave is not the best option (Sinke n.d.[a]). Also, more ribs are needed than spars which means that a less labor intensive techniques could be more cost effective. **Therefore, Resin Transfer Moulding (RTM) is a better alternative** (Sinke n.d.[a]). RTM is a closed-mould, low pressure process which allows for more complex high-performance structures. The process is visualised in Figure 22.6[125]. First, a lay-up of fibres is pre-shaped after which the dry reinforcement is placed into the mould. The mould is then closed and the epoxy resin is injected. After that, the material is being cured. During the RTM process, one should be careful that no voids are introduced in the material as this lowers its quality significantly.

[123] http://www.non-ferrous.com/website/aluminum-information/ [cited on: 18/06/2018]
[124] https://www.italmatic.net/slider/industry-slider/autoclave-for-boatyards-and-shipyards-for-composite-materials/ [cited on: 18/06/2018]
[125] https://www.slideshare.net/HinaIbrahim1/resin-transfer-molding [cited on: 18/06/2018]

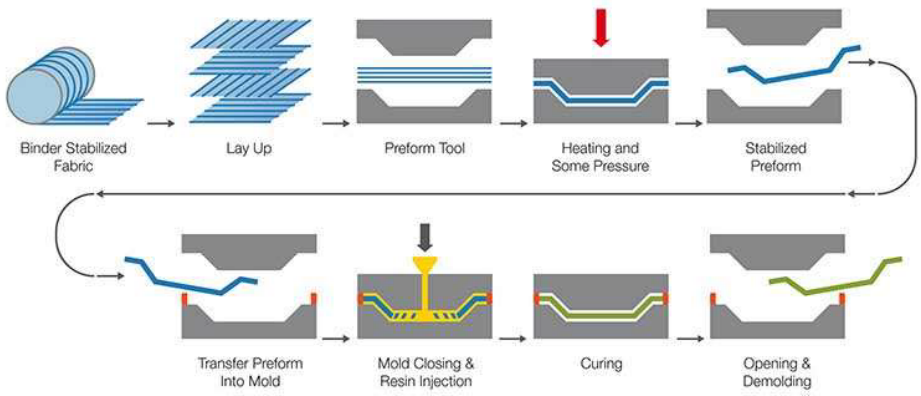

Figure 22.6: Illustration of the resin transfer moulding technique.

22.1.4. Manufacturing of the Landing Gear Strut

Lastly, there is the landing gear structure which is made of steel alloy 4340 due to the high loads it should withstand. Although it is a metal, landing gear struts are not that straightforward to manufacture. That is because that struts are hollow on the inside, meaning that quite some techniques already fall out. Also, steel is used. Steel is known for its high yielding strength capabilities; this alloy has a tensile yielding strength of 472.3MPa. This makes conventional forming techniques more difficult as the manufacturing tools should be able to overcome this high strength. The mostly used and best feasible manufacturing technique for this kind of structure is extrusion. However, the conventional forming method should be adapted for these struts as there they should be hollow. In order to make a hollow shape, there are two options. Either the billet already contains a hole or it is moulded and welded afterwards. For this case, it is better to make the hollow shape beforehand with the use of a mandrel as illustrated in Figure 22.7:

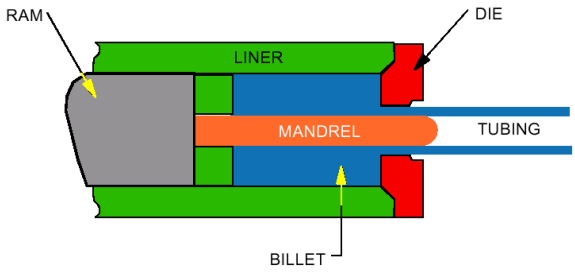

Figure 22.7: Illustration of the mandrel in the extrusion technique.

This mandrel will make the billet material hollow before it is forced through the die. This is the best way to minimise manufacturing impurities and stress concentrations which should be avoided for landing gear struts at any time.

22.2. Bonding

Now that the materials and their manufacturing techniques are described, it is time to discuss the bonding of the different components in this section. Different components and materials mean different required bonding techniques as these techniques are very structure and material specific. First of all, the stringers should be attached to the skin. The skin is made of GLARE and the stringers are made of Aluminium. A long well-proven and widely used option is to rivet the two materials, as shown in Figure 22.8[126]. In this method, a rivet (Figure 22.9[127]) keeps two different components together by means of mechanical forces. Rivets are very cost effective and it can be removed if necessary; however, this has its limitations as it should be drilled out to be removed. The only thing which should not be forgotten is that GLARE is not of only Aluminium. This will also introduce extra difficulties as it is also composed of glass fibres. The difficulties which will be encountered can be delamination of the composite and it resistance to fatigue will decrease (C. D. Rans et al. 2005). These are factors which should be kept in mind during the design and manufacturing process.

[126] http://www.mech4study.com/2016/02/types-of-rivets-joints.html [cited on: 18/06/2018]
[127] http://www.fastenersplusintl.com/products/rivets/ [cited on: 18/06/2018]

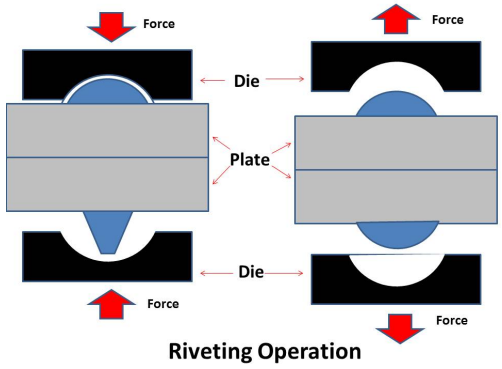

Figure 22.8: Illustration of the rivet bonding technique.

Figure 22.9: Illustration of rivets.

Next, there is the bonding of the spars and the ribs to the skin. This will be more complicated as it won't be possible to bond the components mechanically. That is because it is quite inconvenient to make holes in Carbon Fibre Reinforced Polymers. Therefore, another alternative is required. The best option is to make use of adhesive bonding. These techniques will assure that neither the CFRP nor the GLARE will be affected because of mechanical holes in the structure. The principle of adhesive bonding is visualised in Figure 22.10 (Sinke n.d.[b]):

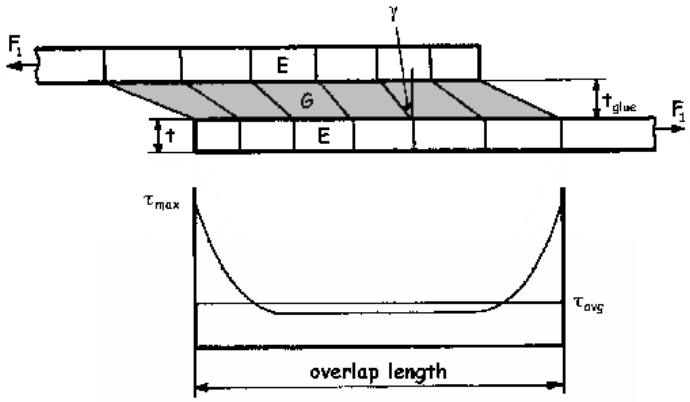

Figure 22.10: Illustration of the adhesive bonding technique.

From Figure 22.10, one see can two components (in white) which are adhesively bonded together with a glue (in grey). They are loaded under a force F_1. The important parameters which should be considered of the bonding material is its shear modulus G and the maximum shear stress τ_{max} it can withstand without plastically deforming. From the picture, it is clear that the maximum shear stress occurs at the edges of the bond, which is consequently the design point for the joint. Making the joining length longer has thus no big influence on the overall strength.

22.3. Assembly

The assembly aspect of the production describes the combination of single parts into larger parts or sub-assemblies and subsequently joining these sub-assemblies until the final product is finished. Divisions are used in the assembly process to provide structure to the process. The layout of divisions can be optimised by considering the following criteria (Sinke n.d.[c]):

- **Efficiency:** if work is divided unevenly between multiple divisions, waiting times for different parts of the assembly will increase.
- **Cost:** expensive parts shall be added to the assembly as late as possible as this will minimise the investment cost. Subdividing complex divisions in subdivision will result in shorter times expensive parts are used in the assembly process.
- **Accessibility:** if accessibility at all stages of the assembly can be improved, production time will decrease. By implementing an order of assembly which takes into account the locations of the parts to be assembled, better accessibility can be achieved.
- **Structure:** crossing components such as stringers and ribs need to be connected properly. The order and divisions of assembly shall be constructed such that these components can be implemented in the correct manner.

When constructing the assembly process, the above mentioned criteria are used to determine to optimal configuration. A schematic overview of the assembly process can be found in the production Figure 22.11. In the flowchart the different division of the assembly in a wing group and a body group can be distinguished. It should be noted the wing assembly shall take place in twofold in order to simultaneously supply the final assembly process with two wings and a body.

The body assembly starts with the installation of the powerplant. This is a delicate process and takes place in the early stages of the assembly in order to minimise risk of damaging other parts and provide maximum accessibility. Subsequently, the landing gear and electronics are added to the body as it requires a high level of accessibility. The body assembly is completed after the installation of the landing gear doors and skin panels. The wing installation starts with the assembly of the wing box. Subsequently, the assembly of the elevon and winglets is started. The parts together with the actuator are used to complete the assembly of the wing. The wings and body are passed on to the final assembly process where the hydraulic system and the electronic wiring are installed. These systems require connection between parts of different assembly divisions and are therefore installed in the final assembly process. Finally, the payload is installed to minimise waiting cost.

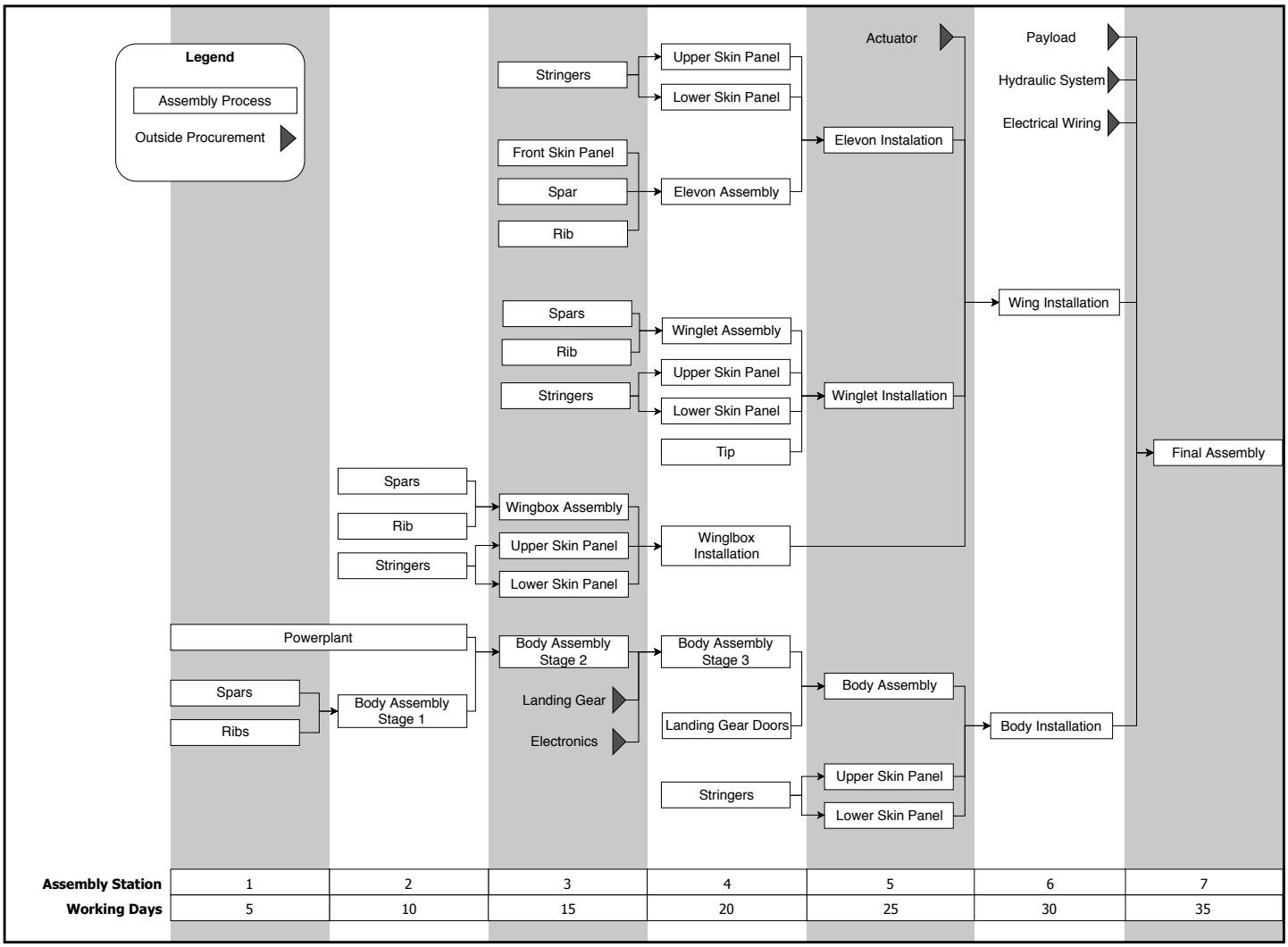

Figure 22.11: Assembly sequence chart.

22.4. Integration

The manufacturing processes and assembly of the aircraft as described above present what techniques will be used to transform the raw materials used for constructing the aircraft into the assembled aircraft. This section present how these processes will be organised.

Since the number of aircraft to be produced is limited and the size of the aircraft is relatively small, the manufacturing and assembly of the aircraft shall take place in a single factory with a line production if possible. This reduces transport cost and waiting time and also generates routine for the production crew (Sinke n.d.[d]). Furthermore, this process allows for a clear overview of the production process (Sinke n.d.[d]). Any delays in the production process can be spotted as different production stages will start at the same time.

However, not all parts used for the production of the aircraft are suited for line production. For example, these products may have a manufacturing time that is not corresponding to the time assigned to each working station such that the advantages of the line production in a single factory will be outweighed by the added cost of production. For this reason, a division is made between parts that will be produced in line production, batch production and parts that will be supplied by external companies. Table 22.2 illustrates a division of the parts and their production processes.

Table 22.2: Production processes selected for different parts.

Part	**Production process**
Actuator	External supply
Electronic wiring	External supply
Electronics	External supply
Hydraulic system	External supply
Landing Gear	External supply
Ribs	Batch production
Skin panels	Line production
Spars	External supply
Stringers	Batch production

The following reasons determined the production processes selected for different parts.

- **Actuator:** The actuator is a small piece compared to the other parts of the assembly of the aircraft, but is generally more complex. For this reason the production of actuators requires lots of experience. Furthermore, the production time matches the station time due to the dimensions of the actuator compared to other parts of the assembly, which would increase waiting time of expensive parts. For this reason, it is chosen to outsource the production of the actuators to an external company.
- **Electronic wiring:** The wiring of the aircraft is very delicate and requires special machinery to optimise the production. Therefore, it is chosen to produce the electronic wiring at a specialised company.
- **Electronics:** The electronics such as the navigation system are very complex systems that also require lots of experience and specialised equipment to produce. The high level of complexity of the electronics cause the production time to be higher than for other parts of the assembly of the aircraft. For these reasons, the electronics will be bought from external companies.
- **Hydraulic system:** For the hydraulic system similar reasoning applies as that of the electronic wiring. Since the hydraulic system is very delicate is is chosen to have a specialised company produce the parts.
- **Landing Gear:** The landing gear once again is a part where the production process does not match that of the assembly station. Furthermore is it very common in the aerospace industry that the landing gears are supplied by external companies, resulting in specialised companies that are able to produce these landing gears very efficiently.
- **Ribs:** The ribs will be manufactured by resin transfer moulding, which is performed in a batch process as this is a closed mould process. A closed mould process does not allow for line production.
- **Skin panels:** The skin panels will be assembled from different parts, which allows for line production. In this case, line production is chosen due to the advantages mentioned in the beginning of the section.
- **Spars:** The spars will be manufactured using an autoclave. The autoclave process is performed using very expensive equipment that shall only be available at a specialised company. These companies can supply parts made with an autoclave production process. Therefore, the spars will be supplied by an external company.
- **Stringers:** Stringers are produced using extrusion. The extrusion process uses a billet of material to produce multiple stringers at once and is therefore a batch process.

23
Requirements Compliance Matrix and Feasibility Analysis

Over the course of the project, a range of requirements have been set. In this chapter, it is evaluated whether the requirements are met. In section 23.1, all subsystem and system requirements are stated, accompanied by either a tick or a cross. Next to this tick or cross, there is space reserved for a small elaboration. In section 23.2, it is discussed whether the concept proves to be feasible. Here, all rationale is provided why certain requirements are not met. Moreover, actions can be discussed that make the design meet the requirements and with that, increase the feasibility.

23.1. Requirements Compliance Matrix

For the mission, three systems are distinguished: the UAV system, the Ground Control System and the Ground Operations System. All systems are broken down in a specific set of requirements. Consequently, an evaluation of the system requirements is made. At this stage the design is evaluated regarding its compliance with the requirements. If a requirement is not ticked, the actual value is provided and further explanation can be found in the feasibility analysis. Furthermore, it is stressed how and where the data in the table is verified.

Table 23.1: Compliance matrix of subsystem requirements

Subsystem	Identifier	Requirement	Compliance	Verification [128]
		UAV SYSTEM		
Propulsion	*PRO*			
	MTN.SUB.PRO-1	The Propulsion Subsystem shall give the UAV a velocity of at least 50 km/h for 20 hours.	✓	section 12.7
	MTN.SUB.PRO-2	The Propulsion Subsystem shall provide power for the subsystems for at least 20 operating hours.	✓	section 12.7
	MTN.SUB.PRO-3	The Propulsion Subsystem shall operate at an altitude up to 3100 m above sea-level.	✓	section 12.7
	MTN.SUB.PRO-4	The Propulsion Subsystem shall operate on a biofuel.	✓	section 12.1
	MTN.SUB.PRO-5	The Propulsion Subsystem shall have a maximum equivalent CO2 emission of 63 g/MJ.	✓	subsection 21.2.5
	MTN.SUB.PRO-6	The Propulsion Subsystem shall emit less noise than 87 dB.	✓	subsection 21.2.2
Structure	*STRUC*			
	MTN.SUB.STRUC-1	The Structures Subsystem shall be able to withstand a limit load of 3g without plastic deformations.	✓	section 11.5
	MTN.SUB.STRUC-2	The Structures Subsystem shall utilise a safety factor of 1.5.	✓	section 11.5
	MTN.SUB.STRUC-3	The Structures Subsystem shall be able to cope with 3650 loading cycles [129].	✓	section 20.3
	MTN.SUB.STRUC-4	The Structures Subsystem shall be a framework on which other subsystems can be attached.	✓	chapter 14
Telecommunication	*COMM*			
	MTN.SUB.COMM-1	The Telecommunications Subsystem shall use a data link with a data rate of at least 1 Mb/s for the payload data on the L,S,C,X,Ku,K or Ka bandwidth.	X (200 kb/s)	section 16.2
	MTN.SUB.COMM-2	The Telecommunications Subsystem shall use a data link with a data rate smaller than 30 Kb/s for flight control on the HF or VHF/UHF bandwidth.	X (200 kb/s)	section 16.2
	MTN.SUB.COMM-3	The Telecommunications Subsystem shall have separate communication channels for payload data and Attitude Determination and Control.	X (one channel)	section 16.2
	MTN.SUB.COMM-4	The Telecommunications Subsystem shall function until the distance between the ground control unit and UAV is at least 5000 km.	✓	section 16.2
Power	*PW*			
	MTN.SUB.PW-1	The Power Subsystem shall have a safe mode.	✓	section 16.5
	MTN.SUB.PW-2	The Power Subsystem shall not have single point failure.	✓	section 16.5
	MTN.SUB.PW-3	The Power Subsystem shall have at least two rechargeable batteries.	✓	section 16.5

[128] *T: Test; D: Demonstration; A: Analysis; I: Inspection*

[129] 1 loading cycle is the equivalent of flying 1 mission profile

	MTN.SUB.PW-4	The Power Subsystem shall extract power from the propulsion subsystem.	✓	section 16.5
	MTN.SUB.PW-5	The Power Subsystem shall be able to provide 24 V (DC).	✓	section 16.5
	MTN.SUB.PW-6	The Power Subsystem shall provide at least 150 W.	✓	section 16.5
Monitoring	*MON*			
	MTN.SUB.MON-1	The Monitoring Subsystem shall have an IR camera.	✓	section 10.4
	MTN.SUB.MON-2	The Monitoring Subsystem shall have a mass that does not exceed 50 kg.	X (68 kg)	section 10.4
	MTN.SUB.MON-3	The Monitoring Subsystem shall have the correct data quality at cruise altitude required for the inspection of pipelines.	✓	section 10.4
	MTN.SUB.MON-4	The Monitoring Subsystem shall be able to monitor in light rain and light fog.	✓	section 10.4
	MTN.SUB.MON-5	The Monitoring Subsystem shall append a position coordinate to each image frame.	✓	section 16.4
Attitude Determination and Control	*ADC*			
	MTN.SUB.ADC-1	The AD&C Subsystem shall measure the roll, pitch and yaw angle with an accuracy better than 0.5 degrees.	✓	section 16.1
	MTN.SUB.ADC-2	The AD&C Subsystem shall measure the roll, pitch and yaw rate with an accuracy better than 0.5 degrees/s.	✓	section 16.1
	MTN.SUB.ADC-3	The AD&C Subsystem shall not have single point failure.	✓	section 16.1
	MTN.SUB.ADC-4	The AD&C Subsystem shall control roll, pitch, and yaw angle.	✓	section 16.4
	MTN.SUB.ADC-5	The AD&C Subsystem shall control roll, pitch, and yaw rate.	✓	section 16.4
	MTN.SUB.ADC-6	The AD&C Subsystem shall be able to operate autonomously during its entire mission.	✓	section 16.4
Navigation	*NAV*			
	MTN.SUB.NAV-1	The Navigation Subsystem shall determine the horizontal position with an accuracy better than 2 m, 95% of the time.	X (2.5 m)	section 16.1
	MTN.SUB.NAV-2	The Navigation Subsystem shall control the position with an accuracy better than 10 m.	✓	section 16.1
	MTN.SUB.NAV-3	The Navigation Subsystem shall control the throttle setting.	✓	section 16.4
	MTN.SUB.NAV-4	The Navigation Subsystem shall detect other flying objects within a 500 m radius.	✓	subsection 16.1.2
	MTN.SUB.NAV-5	The Navigation Subsystem shall utilise the control surfaces.	✓	section 16.1
		GROUND CONTROL SYSTEM		
Control	*CTRL*			
	MTN.SUB.CTRL-1	The Control Subsystem shall always have 1 pilot on standby.	✓	section 6.1
	MTN.SUB.CTRL-2	The Control Subsystem shall always have 1 person monitoring the UAV flight.	✓	section 6.1
	MTN.SUB.CTRL-3	The Control Subsystem shall always have at least 2 control units ready.	✓	section 6.1
	MTN.SUB.CTRL-4	The Control Subsystem shall overrule the autonomous flight option if needed.	✓	section 6.1
	MTN.SUB.CTRL-5	The Control Subsystem shall compute the initial flight plan.	✓	section 6.1
	MTN.SUB.CTRL-6	The Control Subsystem shall adapt initial flight plan if needed.	✓	section 6.1
Telecommunication	*COMM*			
	MTN.SUB.COMM-1	The Telecommunications Subsystem shall use a downlink data link with a data rate of at least 1 Mb/s for the payload data on the L,S,C,X,Ku,K or Ka bandwidth.	X (200 kb/s)	section 16.2
	MTN.SUB.COMM-2	The Telecommunications Subsystem shall use a data link with a data rate smaller than 30 Kb/s for flight control on the HF or VHF/UHF bandwidth.	X (200 kb/s)	section 16.2
	MTN.SUB.COMM-3	The Telecommunications Subsystem shall have separate datalink channels for payload data and AD&C.	X (one channel)	section 16.2
	MTN.SUB.COMM-4	The Telecommunications Subsystem shall properly function when the distance between the ground control unit and the UAV is 5000 km or more.	✓	section 6.1
Ground Computer	*COMP*			
	MTN.SUB.COMP-1	The Ground Computer process payload data within 10 minutes after reception.	✓	section 6.1
	MTN.SUB.COMP-2	The Ground Computer Subsystem shall analyse flight data.	✓	section 6.1
	MTN.SUB.COMP-3	The Ground Computer Subsystem shall optimise flight route with respect to current weather conditions.	✓	section 6.1
	MTN.SUB.COMP-4	The Ground Computer Subsystem shall optimise flight route with respect to restricted airspace.	✓	section 6.1
	MTN.SUB.COMP-5	The Ground Computer Subsystem shall have memory storage for one week of monitoring.	✓	section 6.1
		GROUND OPERATIONS SYSTEM		
Operations	*OPS*			
	MTN.SUB.OPS-1	A fuel system shall have the green diesel (HVO) bio fuel.	✓	section 6.2
	MTN.SUB.OPS-2	The fuel tank in the fuel system shall have at least 300 liters of bio fuel.	✓	section 6.2
	MTN.SUB.OPS-3	Maintenance of the UAV shall be performed after 400 flight-hour.	✓	section 6.2
	MTN.SUB.OPS-4	Inspection of the UAV shall be performed prior to each flight.	✓	section 6.2
	MTN.SUB.OPS-5	The minimum runway length shall be 420 m.	✓	section 6.2
	MTN.SUB.OPS-6	A carrier shall be available to transport the UAV.	✓	section 6.2
Storage	*STG*			

	MTN.SUB.STG-1	The storage space shall provide a floor area large enough for the UAVs dimensions.	✓	section 6.2
	MTN.SUB.STG-2	The storage space shall keep the UAV in a dry condition.	✓	section 6.2
	MTN.SUB.STG-3	The storage space shall be located within a 5 km radius from landing and take-off site.	✓	section 5.3
		SYSTEM REQUIREMENTS		
Ground Control	*GC*			
	MTN.SYS.GC-1	The Ground Control System shall be able to remotely operate the UAV at any hour of the day.	✓	section 6.1
	MTN.SYS.GC-2	The Ground Control System shall be able to communicate with the air-traffic control.	✓	section 6.1
	MTN.SYS.GC-3	The Ground Control System shall be able to communicate with the UAV.	✓	section 6.1
	MTN.SYS.GC-4	The Ground Control System shall be able to save data from the UAV.	✓	section 6.1
	MTN.SYS.GC-5	The Ground Control System shall be able to process data from the UAV.	✓	section 6.1
	MTN.SYS.GC-6	The Ground Control System shall be able to communicate processed data to customer.	✓	section 6.1
UAV	*UAV*			
	MTN.SYS.UAV-1	The UAV shall have a maximum unit cost of 2.3 million USD.	✓	subsection 18.3.2
	MTN.SYS.UAV-2	The UAV shall be able to detect gas leakages in a gas pipeline.	✓	section 10.4
	MTN.SYS.UAV-3	The UAV shall be able to detect corrosion of a gas pipeline.	X	Table 10.2
	MTN.SYS.UAV-4	The UAV shall be able to detect rust on a gas pipeline.	X	Table 10.2
	MTN.SYS.UAV-5	The UAV shall be able to monitor at every hour of the day.	✓	Table 10.2
	MTN.SYS.UAV-6	The UAV shall autonomously follow the pipeline network it is assigned to.	✓	section 16.4
	MTN.SYS.UAV-7	The UAV shall have a payload of maximum 50 kg.	X (68 kg)	chapter 10
	MTN.SYS.UAV-8	The UAV shall have an endurance up to 20 hours.	✓	section 11.1
	MTN.SYS.UAV-9	The UAV shall have a cruise altitude of at least 300 m.	✓	section 11.1
	MTN.SYS.UAV-10	The UAV shall have a minimum range of 1000 km.	✓	section 11.1
	MTN.SYS.UAV-11	The UAV shall be operable for at least 200 days a year.	✓	section 20.3
	MTN.SYS.UAV-12	The UAV shall have a micro gas turbine engine.	✓	section 12.2
	MTN.SYS.UAV-13	The UAV shall be able to operate in the North-American environment.	✓	section 10.4
	MTN.SYS.UAV-14	The UAV shall land on hard surface areas.	✓	section 14.3
	MTN.SYS.UAV-15	The UAV shall be able to sent its recorded data to a ground station.	✓	section 16.2
	MTN.SYS.UAV-16	The UAV shall be controllable.	✓	section 15.2
	MTN.SYS.UAV-17	The UAV shall be stable.	✓	chapter 13
	MTN.SYS.UAV-18	The UAV shall have a recovery system such that it can land undamaged and without the risk of injuries on ground in case of engine failure.	✓	section 14.3
	MTN.SYS.UAV-19	The UAV shall be detectable by other vehicles.	✓	subsection 16.2.1
	MTN.SYS.UAV-20	The UAV operators shall obey the orders of air traffic control.	✓	subsection 16.2.1
	MTN.SYS.UAV-21	The UAV shall not collide with other air traffic vehicles.	✓	subsection 16.2.1
	MTN.SYS.UAV-22	The UAV shall be able to determine its position at any time.	✓	section 16.1
	MTN.SYS.UAV-23	The UAV shall be able to determine its velocity at any time.	✓	section 16.1
	MTN.SYS.UAV-24	The UAV shall be able to determine its attitude at any time.	✓	section 16.1
	MTN.SYS.UAV-25	The UAV shall be able to endure all loads it encounters during normal operation.	✓	chapter 14
	MTN.SYS.UAV-26	The UAV shall comply with the regulations that exist in the country of operation.	✓	section 5.2
	MTN.SYS.UAV-27	The UAV shall be safe to operate without putting its operators in danger.	✓	chapter 6
	MTN.SYS.UAV-28	The UAV shall avoid obstacles.	✓	section 16.4
	MTN.SYS.UAV-29	The UAV shall have minimal damage after a bird strike.	X	section 23.2
	MTN.SYS.UAV-30	The UAV shall run on a bio-fuel.	✓	section 12.1
	MTN.SYS.UAV-31	The UAV shall have lower fuel consumption than existing solutions.	✓	subsection 21.2.5
	MTN.SYS.UAV-32	The UAV shall have lower noise emissions than current alternatives.	✓	subsection 21.2.2
	MTN.SYS.UAV-33	The UAV shall have lower vibrations than current alternatives.	✓	section 12.5
	MTN.SYS.UAV-34	The UAV its components shall be recyclable.	✓	subsection 21.2.4
	MTN.SYS.UAV-35	The UAV shall have a lower carbon dioxide emission than current alternatives.	✓	subsection 21.2.5
	MTN.SYS.UAV-36	The UAV its lifetime shall be at least 10 years.	✓	section 20.3
	MTN.SYS.UAV-37	The UAV shall have a development cost less than 3000 euro/kg.	✓	subsection 18.3.1
Ground Operations	*GO*			
	MTN.SYS.GO.1	The Ground Operations System shall provide sufficient take-off facilities for the UAV.	✓	section 6.2
	MTN.SYS.GO.2	The Ground Operations System shall provide the bio-fuel needed for the UAVs mission profile.	✓	section 6.2
	MTN.SYS.GO.3	The Ground Operations System shall provide sufficient landing facilities for the UAV.	✓	section 6.2
	MTN.SYS.GO.4	The Ground Operations System shall provide required maintenance for the UAV.	✓	section 6.2
	MTN.SYS.GO.5	The Ground Operations System shall provide storage space for the UAV.	✓	section 6.2
	MTN.SYS.GO.6	The Ground Operations System shall be able to recover the UAV in case of emergency landing.	✓	section 6.2

23.2. Feasibility Analysis

In this section, the feasibility of some requirements is discussed in more detail.

MTN.SUB.MON-2

Initially, the requirement was that the monitoring subsystem should not exceed 50 kg. Throughout the entire design phase, the design team focused on keeping the weight below the set maximum. When the system capabilities were compared with the mission need statement, it was decided that this requirement cannot be met, while providing a more sustainable, less costly alternative to the current solutions. For this reason, the monitoring subsystem mass has increased from 50 kg to 68 kg.

MTN.SUB.COMM-1, MTN.SUB.COMM-2 and MTN.SUB.COMM-3

Regarding MTN.SUB.COMM-1 till MTN.SUB.COMM-3, for both the ground segment and the UAV, the requirement was that two separate channels were to be incorporated, with a data rate of less than 30 Kb/s for flight control and of at least

1 Mb/s for the payload data. Since a system making use of satellites had to be used to comply with MTN.SUB.COMM-4, the high data rate of 1 Mb/s was not met. In addition, it was found to be unnecessary since processing the payload data is being done on board of the UAV and the resulting data rate will be relatively low. The use of separate channels is not included either, since all data can be combined in one data rate and only one communication system is going to be used.

MTN.SYS.UAV-29
The analysis of bird impact on the UAV design is taken into consideration continuously during design of the propulsive system, but cannot be validated yet since the exact engine configuration is not yet decided upon. In later design phases, this requirement should be revisited and validated.

24
Post DSE Gantt Chart

MAINTAIN has the possibility to continue along two different tracks, more specifically, an academic or commercial track. Research will be the main purpose when an academic track would be followed. When a commercial track would be chosen, the following Gantt chart provides more insight in the steps to be taken.

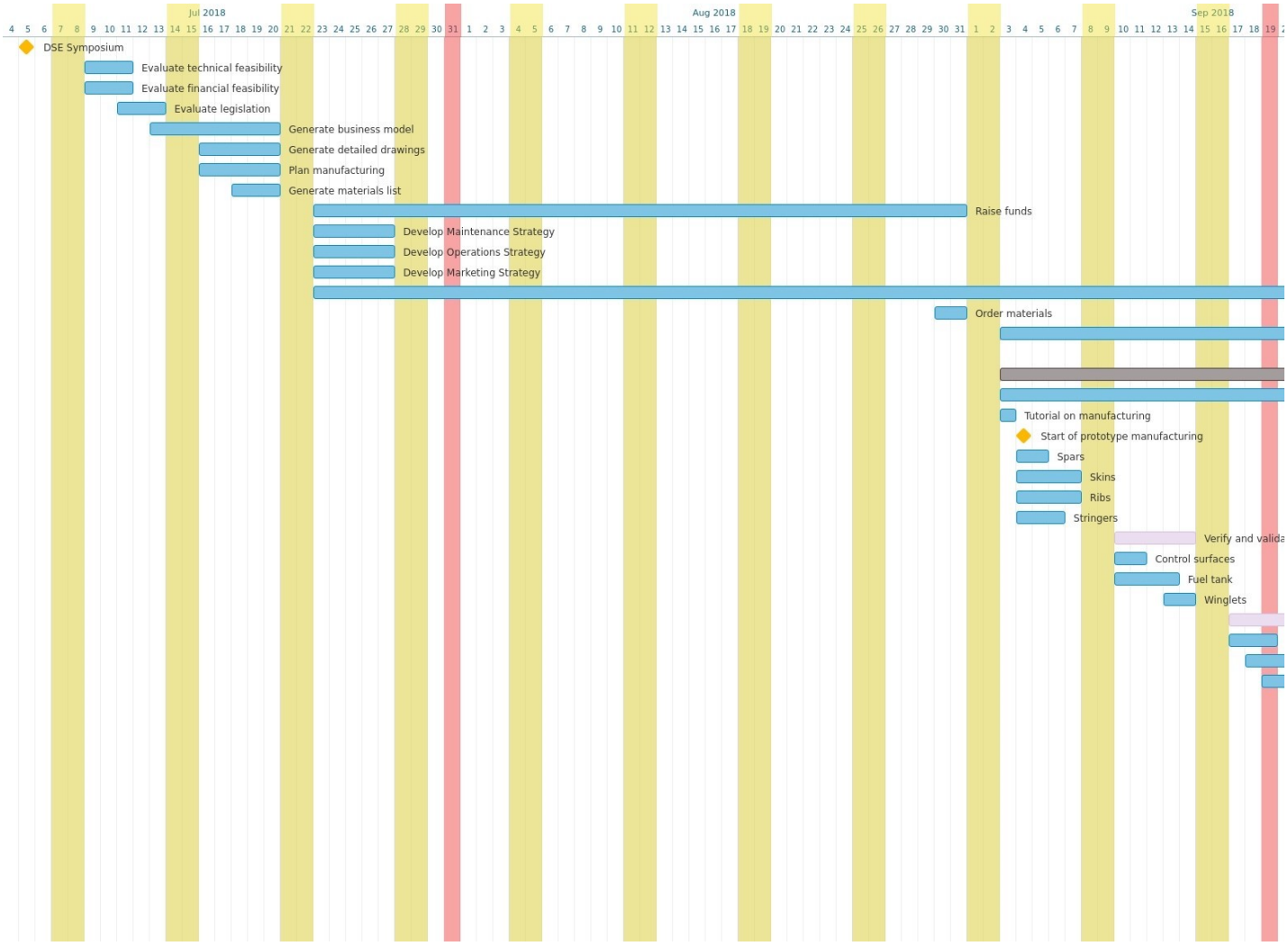

Figure 24.1: Phase 1 post DSE Gantt chart.

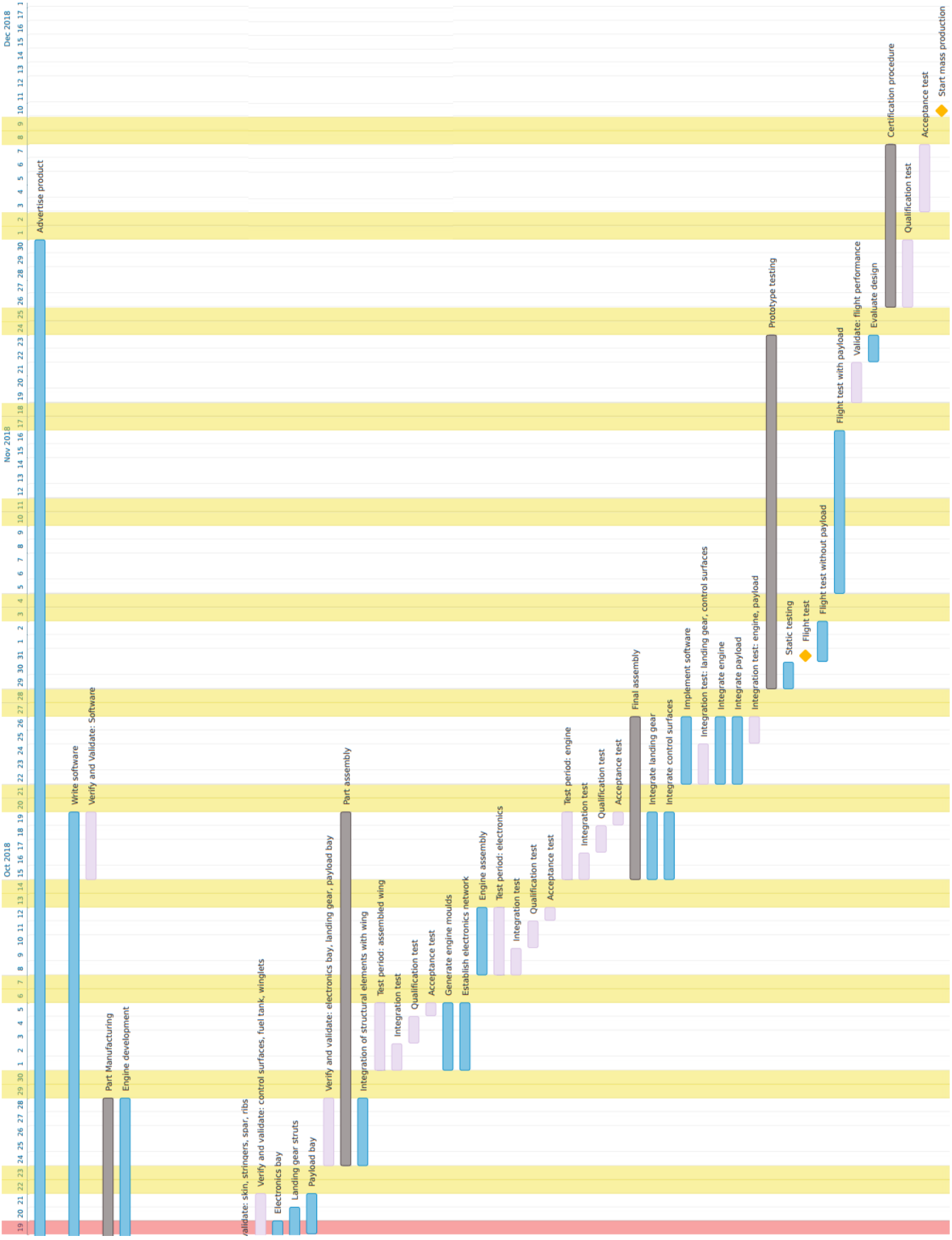

Figure 24.2: Phase 2 post DSE Gantt chart.

25
Discussion and Recommendations

To provide more clarity on the results that are displayed in this report, a discussion of the results is necessary which is done in section 25.1. This discussion also elaborates on the limitations of the design. The scope of the DSE project stretches to a preliminary design. However, more research has to be conducted to design a fully functioning system. Therefore, recommendations for future work are provided in section 25.2.

25.1. Discussion

The mission of this project was to design a UAV system capable of monitoring and inspecting gas pipelines, which is both economically and ecologically more attractive than current solutions. The degree in which the final design of MAINTAIN meets this goal is evaluated in this section.

First of all, MAINTAIN is capable of directly detecting gas leaks, but not corrosion. However, by implementing a LiDAR system, the environment of the pipeline can be mapped and these mappings can be compared every passage to identify vegetation differences and land movements. Furthermore, at locations where land movements occur, high stresses are induced on the pipeline which increases the probability of corrosion. Therefore, critical areas can be pinpointed for a more detailed inspection.

Economically, MAINTAIN proves to be significantly less expensive than manned inspection by a helicopter which uses a mid-infrared wavelength LiDAR system. However when comparing it to alternative UAVs which use thermal imagery to identify gas leaks, MAINTAIN is more expensive. This has to do with the well-considered decision to incorporate a more accurate and multi-functional, though heavier and more expensive payload in MAINTAIN. Therefore, MAINTAIN shall focus on replacing the manned-inspection by helicopter based on its lower operational costs. The uncertainty whether the increased accuracy using this type of LiDAR system exceeds the cheaper solution of a smaller drone, which uses a thermal camera to identify gas leakages and is propelled by a reciprocating engine, still remains.

The range of MAINTAIN exceeds 1000 km and that is due to the endurance requirement. Since the design is more efficient at a higher than required velocity for the range requirement, it logically follows that the covered distance is higher than required at an endurance of 20 hours. To be ecologically more attractive than its competitors MAINTAIN established recycle plans for its main components, produces less noise than inspection by helicopter, has a lower equivalent CO_2 emission and the micro gas turbine engine produces less vibrations than a reciprocating engine of the same size.

25.2. Recommendations for Future Work

This section elaborates on what steps to take in the post-DSE phase to further develop the MAINTAIN system. The recommendations can be split up into two categories; the recommendations that will facilitate in further design stages and recommendations for future research opportunities.

- **Propulsion**: The turbine and compressor can be further optimised using adjoint-based sensitivity analysis of the Navier-Stokes equations using SU2. The same holds for the inlet and outlet. This will increase their efficiency further. The combustor needs to be designed using a combination of computational fluid dynamics and experiment. Additionally, more investigation into the engine materials is required for better assessment of the maximum temperatures within the engine. Research into new manufacturing techniques may mitigate tip clearance losses. Small-scale wind tunnel testing to validate component design and a finite element analysis to validate engine vibrations needs to be performed as well.
- **Stability and Aerodynamics**: Small-scale wind tunnel testing to further validate the aerodynamic design and stability.
- **Payload**: Development of algorithms that extract the required information from the LiDAR mappings for detecting corrosion. A deep learning algorithm can be trained on existing examples of corrosion as collected by the manned helicopter inspection routines.

26 Conclusion

This report presented the preliminary design of the MAINTAIN system. The aim of this project was to design an unmanned aircraft vehicle propelled by a micro-turbine engine for remote monitoring of gas pipeline networks. The minimum range and endurance of the UAV are 1000 km and 20 hours respectively.

The final design of MAINTAIN has a range of 1645 km and an endurance of 20.4 hours. The key design characteristics necessary to achieve this range and endurance are summarised below:

- **Wing**: MAINTAIN has a span of 10.6 m, a wing area of 9.4 m^2 and a quarter chord sweep of 25 degrees.
- **Propulsion**: Micro gas turbine engine provides a maximum power of 3.75 kW at standard sea-level conditions with a SFC of 290 g/kWh.
- **Weight decomposition**: MTOW of 160.4 kg, OEW of 72.9 kg, payload weight of 68 kg and a fuel weight of 19.5 kg.
- **Materials**: Lightweight ribs and spars of carbon fibre reinforced polymer, a tough skin of GLARE and stringers made of 7075-T6 aluminium.
- **Stability**: Statically stable in all directions. All eigenmodes are stable, except for the the spiral mode. The onset of this mode is slow enough for the autopilot to correct. Stability is achieved by large winglets.
- **Cruise conditions**: Cruise velocity of 96 km/h and cruise height of 300 m above the surface of the earth. The cruise lift to drag ratio is 33.2.

The subsystems required to effectively control the UAV are:

- **Electrical Subsystems**: An Inertial Navigation System (INS), Global Positioning System (GPS) and altimeter for navigation, an Aviator UAV 200 communication system for communication, an Odroid XU4 1.4 - 2.0 GHz processor as CPU and a memory of 64 GB for storage.

Furthermore, to allow MAINTAIN to successfully monitor gas pipelines, the following operation specific elements are included:

- **Payload**: Mid-infrared wavelength (3-5μm) LiDAR system, weight of 68 kg, operable in light rain and at cruise conditions. Uses spectroscopy to identify methane and can map the ground to find corrosion threats by looking at land movements.
- **Ground Segment**: A pilot is available at any hour of the day for UAV control and up to two UAVs can be controlled simultaneously per pilot. Furthermore, pre-flight maintenance is performed by airport crew and specialised maintenance crew is present at 10 airports.

As sustainability, cost and risk have been the focus areas for MAINTAIN, analyses were performed to evaluate them. These are summarised below:

- **Sustainability**: The noise emission is estimated to be 65.2 dB at cruise altitude compared to 87 dB of current manned inspection solutions. Furthermore, all components of the UAV are recyclable and the CO2 equivalent emission is reduced by 97% compared to current manned inspections using helicopters.
- **Risk**: After mitigation, the risk of missing a gas leak is still evident due to inaccuracies in MAINTAIN's systems. Further mitigation will be done by developing deep learning algorithms that can accurately extract the minor shifts in monitored strain fields.
- **Cost**: A selling price of 2,000,000 USD is extracted from the market analysis at a cost price of 1,487,549 USD. The operational cost are estimated to be 1.62 USD per km compared to an operational cost of 83.33 USD per km for manned-inspection by helicopter. and the MAINTAIN is expected to be profitable after 3 years.
- **RAMS**: Based on the reliability, 8 failures are expected to occur every operational year per UAV. Maintenance occurs 66 days per year and together with the reliability this yields an availability of 80%. Furthermore, a reduction of 70% in fatal accidents compared to general aviation is achieved.

To conclude, the final design of MAINTAIN will be an economically and ecologically more attractive solution for inspecting gas pipelines. Furthermore, this report can be seen as a proof of concept that the implementation of a micro gas turbine engine on a UAV can yield impressive performance.

Bibliography

Books

[1] J. Gundlach. *Designing unmanned aircraft systems: a comprehensive approach*. AIAA, 2014.

[2] S. L. Dixon. *Fluid mechanics, thermodynamics of turbomachinery*. Elsevier-Butterworth-Heinemann, 2005.

[3] P. R. Roberge. *Handbook of corrosion engineering*. New York, 2012.

[4] M. E. Orazem. *Underground Pipeline Corrosion*. Woodhead Publishing, 2014.

[5] U.S. government. *Transportation, 49 C.F.R §192*. Legal Information Institute.

[6] P. R. Garvey. *Analytical Methods for Risk Management: A Systems Engineering Perspective*. Chapman-Hall/CRC-Press, Oct. 2008.

[7] D. P. Raymer. *Aircraft design: a conceptual approach*. American Institute of Aeronautics and Astronautics, 2012.

[8] W. Green. *The Observers Book of Aircraft*. Frederick Warne and Co., 1970.

[9] J. Roskam. *Airplane Design Part IV: Preliminary Calculation of Aerodynamic, Thrust and Power Characteristics*. DARcorporation, 2000.

[10] M. A. R. do Nascimento and E. C. dos Santos. *Biofuel and Gas Turbine Engines, Advances in Gas Turbine Technology*. Ed. by E. Benini. InTech, 2011.

[11] A. Demirbas. *Biodiesel: A Realistic Fuel Alternative for Diesel Engines*. 978-1-84628-994-1. Springer, 2008.

[12] R. J. Recks. *Building small gas blimps*. 1997 Edition. Recks publications, 1977.

[13] M. M. Steyn. *The Conceptual Design and Development of a Micro Gas Turbine Generator*. Ed. by B. Botha. North-West University, 2006.

[14] M. Olivero. *EVOLUTION OF A CENTRIFUGAL COMPRESSOR From turbocharger to micro gas turbine applications*. Ipskamp Drukkers, 2012.

[15] A. J. Glassman. *Computer program for preliminary design analysis of axial-flow turbines*. National Aeronautics and Space Administration, 1972.

[16] A. Whitfield and N. C. Baines. *Design of radial turbomachines*. Longman Scientific & Technical, 2002.

[17] C. N. Adkins and R. H. Liebeck. *Design of optimum propellers*. 1983.

[18] A. Betz. *Screw propellers with minimum energy loss*. NRC, Division of Mechanical Engineering, 1958.

[19] E. G. Reid. *The Influence of blade-width distribution on propeller characteristics*. National Advisory Committee for Aeronautics, 1949.

[20] J. D. Anderson. *Fundamentals of Aerodynamics*. 5th Edition. University of Maryland, 2010.

[21] E. Torenbeek. *Synthesis of Subsonic Airplane Design*. Delft University Press, 1982.

[22] K. Nickel and M. Wohlfahrt. *Tailless aircraft in theory and practice*. Ed. by E. Arnold. 1994. ISBN: 9781563470943.

[23] T.H.G. Megson. *Aircraft Structures*. Elsevier, 2007.

[24] W. Callister. *Materials Science and Engineering introduction*. 9th. John Wiley &Amp; Sons Inc, 1985.

[25] Y. C. Fung. *An introduction to the theory of aeroelasticity*. Dover, 2008.

[26] M. H. Sadreay. *Aircraft Design: A Systems Engineer Approach*. John Wiley & Sons, 2013.

[27] J.A. Mulder et al. *Lecture Notes AE3202 Flight Dynamics*. TU Delft, 2013.

[28] Federal Aviation Administration. *Airplane Flying Handbook*. U.S. Department of Transportation, 2016.

[29] W. Sun and Y. X. Yuan. *Optimization theory and methods: nonlinear programming*. Springer, 2006.

[30] J. Sobieszczanski-Sobieski, A. J. Morris, and M. J. L. van Tooren. *Multidisciplinary design optimization supported by knowledge based engineering*. John Wiley & Sons, 2015.

[31] S. Gudmundsson. *General Aviation Aircraft Design*. Butterworth-Heinemann, 2013.

[32] R.J. Hamann and M.J.L. van Tooren. *Lecture Notes AE3-S01 Systems Engineering & Technical Management Techniques*. TU Delft, 2006.

[33] J. Cherwonik. *Unmanned Aerial Vehicle System Acquisition Cost Estimating Methodology*. Deputy Assistant of the Army for Cost and Economics, 2003.

[34] J. E. Marte and D. W. Kurtz. *A review of aerodynamic noise from propellers, rotors, and lift fans*. Jet Propulsion Laboratory, California Institute of Technology, 1970.

[35] N. Reynolds and M. Pharaoh. *Management, Recycling and Reuse of Waste Composites*. Ed. by V. Goodship. Woodhead Publishing, 2010.

[36] RICS. *Contamination, the environment and sustainability*. 3rd. RICS Books Imprint, 2010.

Reports, Theses and Individual Papers

[37] A. Marcellan. “An exploration into the potential of microturbine based propulsion system for civil Unmanned Aerial Vehicles”. In: (2015).

[38] M. Parvini and E. Gharagouzlou. “Gas leakage consequence modeling for buried gas pipelines”. In: 37 (Sept. 2015), pp. 110–118.

[39] Y. C. Choung, J. H. Shin, and J. K. Paik. “Generalized image degradation model for removing motion blur in image sequence”. In: *Spie* (1998). DOI: 10.1117/12.298338.

[40] E. Bernard et al. “Active and thermal imaging performance under bad weather conditions.” In: *6th International Symposium on Optronics in Defence and Security* (Jan. 2014).

[41] O. Lemmers, R. Smit, and R. Wijnen. “Russian boycott will cost Dutch economy 300 million euros”. In: *CBS* (2014).

[42] B. van Beurden et al. “Midterm Report”. In: *TU Delft* (2018).

[43] C. E. Smith. “Near-term pipeline plans shrink, longer-term growth returns”. In: *Oil & Gas Jounral* (Feb. 2015).

[44] D. Hausamann, W. Zirnig, and G. Schreier. “Monitoring of gas transmission pipelines - a customer driven civil UAV application.” In: *German Aerospace Center* ().

[45] B. van Beurden et al. “Baseline Report”. In: *TU Delft* (2018).

[46] F. I. Romli. “Functional Analysis for Conceptual Aircraft Design”. In: *Journal of Advanced Management Science* 1.4 (Dec. 2013), pp. 349–353.

[47] B. Dehoff, D. J.H. Levack, and R. E. Rhodes. “The Functional Breakdown Structure (FBS) and Its Relationship to Life Cycle Cost”. In: *AIAA/ASME/SAE/ASEE Joint Propuslion Conference* (Aug. 2009).

[48] E. P. de Freitas et al. “Cooperation among Wirelessly Connected Static and Mobile Sensor Nodes for Surveillance Applications”. In: 13 (Oct. 2013), pp. 12903–28.

[49] C. Eriksen, K. Ming, and Z. Dodds. “Accessible Aerial Robotics”. In: 29 (Apr. 2014), pp. 218–227.

[50] J. Kamienski and J. Semanek. “ATC Perspectives of UAS Integration in Controlled Airspace”. In: *Procedia Manufacturing* 3 (2015). 6th International Conference on Applied Human Factors and Ergonomics (AHFE 2015) and the Affiliated Conferences, AHFE 2015, pp. 1046–1051. ISSN: 2351-9789. DOI: https://doi.org/10.1016/j.promfg.2015.07.169. URL: http://www.sciencedirect.com/science/article/pii/S2351978915001705.

[51] R.W. Saaty. “The analytic hierarchy process—what it is and how it is used”. In: *Mathematical Modelling* 9.3 (1987), pp. 161–176. DOI: https://doi.org/10.1016/0270-0255(87)90473-8. URL: http://www.sciencedirect.com/science/article/pii/0270025587904738.

[52] G. Whiley. “Flying the Fokker F27”. In: *Aussie Star Flight Simulation* (2016).

[53] E. Aro. “From first generation biofuels to advanced solar biofuels”. In: *Ambio* 45 (Jan. 2016), pp. 24–31.

[54] D. A. Heck et al. “Quantification of the Cold Flow Properties of Biodiesels Blended with ULSD”. In: *Iowa Biodiesel Board* ().

[55] T. J. Hilbers et al. “Green Diesel from Hydrotreated Vegetable Oil Process Design Study”. In: *Chemical Engineering & Technology* (Feb. 2015).

[56] H. Aatola, M. Larmi, and T. Sarjovaara. “Hydrotreated Vegetable Oil (HVO) as a Renewable Diesel Fuel: Trade-off between NOx, Particulate Emission, and Fuel Consumption of a Heavy Duty Engine”. In: *Helsinki University of Technolog* (2008).

[57] NESTE. “SAFETY DATA SHEET NEXBTL Renewable Diesel; Neste 100 % NEXBTL -diesel; Neste Green 100 -diesel”. In: (Feb. 2016).

[58] K. Sugiyama et al. “Effects of Hydrotreated Vegetable Oil (HVO) as Renewable Diesel Fuel on Combustion and Exhaust Emissions in Diesel Engine”. In: *ResearchGate* (2011).

[59] A. Kallenberg. “Liquid Bio Fuels for Gas Turbines”. In: *Department Of Energy Sciences Faculty Of Engineering* (2013).

[60] E. Bradley et al. “Technology and Benefits of Aircraft Counter Rotating Propellers”. In: *NASA* (Oct. 1982).

[61] J. Longbottom. “Investigation into the Reduction of the Drag Area of a Paramotor”. In: *University of South Wales* (Oct. 2006).

[62] J. S. Vanderover and K. D. Visser. “Analysis of a Contra-Rotating Propeller Driven Transport Aircraft”. In: *Clarkson University* (). American Institute of Aeronautics and Astronautics.

[63] T. Stefanov-Wagner. “Mechanical Design of a Contra-Rotating Propeller Assembly for a Small Underwater ROV”. In: *Massachusetts Institute of Technology* (June 2006).

[64] R. Mason. “EZ-VTOL”. In: *Mason Aviation Company, Inc* (2003).

[65] L. Mei and J. Zhou. “Effects of Blade Tip Foil Thickening on Tip Vortexes in Ducted Propeller”. In: *Harbin Institute of Technology in Weihai* (2015).

[66] I. Martinez. “Propellers”. In: (2018).

[67] M. A. R. do Nascimento, Lucilene de Oliveira Rodrigues, et al. “Micro Gas Turbine Engine: A Review”. In: *Progress in Gas Turbine Performance Ernesto Benini* (June 2013). DOI: DOI:10.5772/54444.

[68] W. P. J. Visser, S. A. Shakariyants, and M. Oostveen. “Development of a 3 kW Microturbine for CHP Applications”. In: *Journal of Engineering for Gas Turbines and Power* (Apr. 2011). DOI: DOI:10.1115/1.4002156.

[69] F. Oppung et al. “Micro Gas Turbine Performane Evaluation”. In: *Ghana Journal of Technology* 1.2 (2017), pp. 1–8.

[70] B. Allan, L. Owens, and B. Berrier. “Numerical Modeling of Active Flow Control in a Boundary Layer Ingesting Offset Inlet”. In: *2nd AIAA Flow Control Conference* (2004). DOI: 10.2514/6.2004-2318.

[71] A. G. Rao, A. Sharma, and R. van Dijk. “A CFD Based Parametric Analysis of S-Shaped Inlet for a Novel Blended Wing Body Aircraft”. In: *SSRN Electronic Journal* (2017). DOI: 10.2139/ssrn.3101299.

[72] C. A. M. Ventura et al. “Preliminary Design and Performance Estimation of Radial Inflow Turbines: An Automated Approach”. In: *Journal of Fluids Engineering* 134.3 (2012), p. 031102. DOI: 10.1115/1.4006174.

[73] K. Rahbar et al. “Parametric analysis and optimization of a small-scale radial turbine for Organic Rankine Cycle”. In: *Energy* 83 (2015), pp. 696–711. DOI: 10.1016/j.energy.2015.02.079.

[74] H. S. Ribner and S. P. Foster. “Ideal efficiency of propellers - Theodorsen revisited”. In: *Journal of Aircraft* 27.9 (1990), pp. 810–819. DOI: 10.2514/3.45941.

[75] M. Drela. “QPROP Formulation”. In: (June 2006).

[76] “Gas Turbine Engine Components”. In: *Gas Turbine Performance* (), pp. 159–291. DOI: 10.1002/9780470774533.ch5.

[77] A. C. Jones. “Design and Test of a Small, High Pressure Ratio Radial Turbine”. In: *Volume 1: Turbomachinery* (1994). DOI: 10.1115/94-gt-135.

[78] V. Jeevanantham, P. Vadivelu, and P. Manigandan. “Material Based Structural Analysis of a Typical Landing Gear”. In: *International Journal of Innovative Science, Engineering and Technology* 4.4 (2017), p. 297.

[79] R. Sanchez et al. “Assessment Of The Fluid-Structure Interaction Capabilities For Aeronautical Applications Of The Open-Source Solver Su2.” In: *Proceedings of the VII European Congress on Computational Methods in Applied Sciences and Engineering (ECCOMAS Congress 2016)* (2016). DOI: 10.7712/100016.1903.6597.

[80] T. Macdonald et al. “SUAVE: An Open-Source Environment Enabling Multi-Fidelity Vehicle Optimization”. In: *18th AIAA/ISSMO Multidisciplinary Analysis and Optimization Conference* (Feb. 2017). DOI: 10.2514/6.2017-4437.

[81] V. Sokolevic, G. Dikic, and R. Stancic. “Integration of INS, GPS, Magnetometer and Barometer for Improving Accuracy Navigation of the Vehicle”. In: *Defence Science Journal* 63.5 (2013), pp. 451–455. DOI: 10.14429/dsj.63.4534.

[82] Z. M. Kassas et al. “LTE Steers UAV”. In: *GPS World* 28.4 (2017), pp. 18–25.

[83] H. Skinnemoen. “UAV & satellite communications live mission-critical visual data”. In: *IEEE International Conference on Aerospace Electronics and Remote Sensing Technology* (Nov. 2014), pp. 12–19. DOI: 10.1109/ICARES.2014.7024391.

[84] D. Hulens, J. Verbeke, and T. Goedemé. “How to Choose the Best Embedded Processing Platform for on-Board UAV Image Processing ?” In: 3 (Mar. 2015).

[85] C. Heath and J. Gray. “OpenMDAO: Framework for Flexible Multidisciplinary Design, Analysis and Optimization Methods”. In: *53rd AIAA/ASME/ASCE/AHS/ASC Structures, Structural Dynamics and Materials Conference
20th AIAA/ASME/AHS Adaptive Structures Conference
14th AIAA* (2012). DOI: 10.2514/6.2012-1673.

[86] M. M. J. Opgenoord and K. E. Willcox. “Sensitivity Analysis Methods for Uncertainty Budgeting in System Design”. In: *AIAA Journal* 54.10 (2016), pp. 3134–3148. DOI: 10.2514/1.j054743.

[87] A. Head and W. J. Visser. “Scaling 3-36kW Microturbines”. In: *ASME* (2012).

[88] E. Petritoli, F. Leccese, and L. Ciani. “Reliability Assessment of UAV Systems”. In: *ResearchGate* (June 2017).

[89] E. Yu. “Peacetime Attrition Analysis of Selected Unmanned Aerial Vehicles”. In: *Centre for Operational Research & Analysis* (Dec. 2008).

[90] P. Gonçalves, J. Sobral, and L. Ferreira. “Reliability database for unmanned aerial vehicles based on morphological analysis”. In: *The Aeronautical Journal* 120.1230 (Aug. 2016), pp. 1262–1274.

[91] R. Clothier and R. Walker. “Determination and Evaluation of UAV Safety Objectives”. In: *Australian Research Centre for Aerospace Automation* (2006).

[92] D. W. King, A. Bertapelle, and Moses C. “UAV Failure Rate Criteria For Equivalent Level Of Safety”. In: *Bell Helicopter Textron, Inc.* (Sept. 2005).

[93] A. A. Yehia. “Recycling of Rubber Waste”. In: *Polymer-Plastics Technology and Engineering* 43.6 (Feb. 2007).

[94] J. Hopewell, R. Dvorak, and E. Kosior. “Plastics recycling: challenges and opportunities”. In: *Philos Trans R Soc Lond B Biol Sci* 364.2115–2126 (July 2009).

[95] N. Singh et al. “Recycling of plastic solid waste: A state of art review and future applications”. In: *Composites Part B Engineering* (Sept. 2016), pp. 1–14.

[96] S. Pimenta and S. T. Pinho. “Recycling carbon fibre reinforced polymers for structural applications: Technology review and market outlook”. In: *Elsevier* 31 (Oct. 2011), pp. 378–392.

[97] G. Oliveux, L. O. Dandy, and G. A. Leeke. “Current status of recycling of fibre reinforced polymers: Review of technologies, reuse and resulting properties”. In: *Elsevier* 72 (2015), pp. 61–99.

[98] G. Zhu. “Recycling of Glass Fibre Reinforced Aluminium Laminates and Silicon Removal from Aerospace Al Alloy”. In: *TU Delft* (Oct. 2012).

[99] B. Debnatha, P. Roychowdhury, and R. Kunduc. “Electronic Components (EC) Reuse and Recycling – A New Approach towards WEEE Management”. In: *Elsevier* 35 (2016), pp. 656–668.

[100] Neste Coperation. “Neste Renewable Diesel Handbook”. In: *Neste Proprietary publication* (May 2016).

[101] P. Jun, M. Gillenwater, and W. Barbour. “CO2 , CH4 , AND N2O EMISSIONS FROM TRANSPORTATION-WATER-BORNE NAVIGATION”. In: *Good Practice Guidance and Uncertainty Management in National Greenhouse Gas Inventories* ().

[102] A. L. Radle. “The Effect Of Noise On Wildlife: A Literature Review”. In: (Mar. 2007).
[103] B. O. Elton. “Mechanical Properties Characterisation of Fibre Metal Laminate GLARE-3”. In: (2010).
[104] J. Sinke. “Manufacturing of GLARE Parts and Structures”. In: *Applied Composite Materials* (2003), pp. 293–305.
[105] C. D. Rans et al. “Modelling of the Rivet Forming Process in Aluminium and GLARE for Design against Fatigue”. In: (2005).

Electronic Publications

[106] *2017 Commercial Drone Industry Trends*. URL: https://www.dronedeploy.com/resources/ebooks/commercial-drone-industry-trends-2017/.
[107] E. Sander. *Engineering Entrepreneurship EGN4641*. University of Florida.
[108] Global Market Insights. *Commercial Drone/Unmanned Aerial Vehicle (UAV) Market Size By Product, Mode of Operation, Application*. 2004. URL: https://www.gminsights.com/segmentation/detail/unmanned-aerial-vehicles-UAV-commercial-drone-market.
[109] Grand View Research. *Commercial Drone Market Analysis By Product (Fixed Wing, Rotary Blade, Nano, Hybrid), By Application (Agriculture, Energy, Government, Media & Entertainment) And Segment Forecasts To 2022*. 2016. URL: https://www.grandviewresearch.com/industry-analysis/global-commercial-drones-market.
[110] M. Ballve. *Commercial drones have leapt far ahead of regulators and are already entrenched in a handful of massive industries*. Feb. 2015. URL: https://www.businessinsider.com.au/uav-or-commercial-drone-market-forecast-2015-2.
[111] Bureau of European and Eurasian affairs. *U.S. Relations With the Netherlands*. Apr. 2018. URL: https://www.state.gov/r/pa/ei/bgn/3204.htm.
[112] LaSen. *Airborne Lidar Pipeline Inspection Service*. May 2007. URL: https://www.epa.gov/sites/production/files/2017-07/documents/lasen_april_2007_houston_2007.pdf.
[113] K. Mohammadian. *Estimation of Costs of Cars and Light Trucks Use per Vehicle-Kilometre in Canada*. Mar. 2006. URL: http://www.bv.transports.gouv.qc.ca/mono/0965382.pdf.
[114] R. Vos, J.A. Melkert, and B.T.C. Zandbergen. *AE1222-II Aerospace Design and Systems Engineering Elements I*. TU Delft. Mar. 2017.
[115] *Capstone Turbine Corporation*. https://www.capstoneturbine.com/products/c30. 2018.
[116] M. Pini. *Lecture 8 - Radial (Centrifugal) compressors*. TU Delft. 2018.
[117] *AutoDesk Inventor*. URL: https://www.autodesk.eu/products/inventor/overview.
[118] A. Elham. *Aerospace Design and Systems Engineering Elements II AE2111-II aircraft part: Aileron Design*. TU Delft. 2016.
[119] Airbus. *Marketing plan*. "www.marketingplannow.com/%5Cuserfiles%5Cmarketing%5CAircraft%20manufacturer%20marketing%20plan.pdf". 2010.
[120] Avjobs. *Aviation Sales and Marketing Salaries, Wages and Pay*. "https://www.avjobs.com/salaries-wages-pay/sales-marketing-pay.asp. 2018.
[121] FedEx. *Rate & Ship*. "https://www.fedex.com/en-us/home.html". 2018.
[122] NASA Exploration System Directorale. *Margins and Contingency*. 2008.
[123] W. Verhagen. *Systems Engineering and Aerospace Design - Risk Management & Reliability Engineering*. TU Delft.
[124] J. Sinke. *Processes for Thermoplastic(TP) and Thermoset (TS) Composites*. TU Delft.
[125] J. Sinke. *Adhesive bonding and Welding*. TU Delft.
[126] J. Sinke. *Assembly of aircraft*. TU Delft.
[127] J. Sinke. *Organisation of the production process*. TU Delft.